Tunable adhesion of hydrogels

Guillaume Sudre

THESE DE DOCTORAT DE
L'UNIVERSITE PIERRE ET MARIE CURIE

Spécialité

Chimie et Physico-Chimie des Polymères
(ED 397, Physique et Chimie des Matériaux)

Présentée par

M. Guillaume SUDRE

Pour obtenir le grade de

DOCTEUR DE L'UNIVERSITE PIERRE ET MARIE CURIE

Sujet de la thèse :

Adhésion stimulable d'hydrogels

Soutenue le 18/01/2011 devant le jury composé de :

Mme Françoise Brochard-Wyart	Professeur, UPMC-Institut Curie	Présidente
M. Mark Geoghegan	Professeur, Université de Sheffield	Rapporteur
M. Bruno Grassl	Maître de Conférences, Université de Pau et des Pays de l'Adour	Examinateur
M. Eric Papon	Professeur, Université Bordeaux 1-ENSCPB	Rapporteur
Mme Florence Petit-Agnély	Professeur, Université Paris-Sud 11	Examinateur
M. Costantino Creton	Directeur de Recherche, ESPCI Paristech	Directeur de thèse
M. Dominique Hourdet	Professeur, UPMC-ESPCI Paristech	Co-directeur de thèse
Mme Yvette Tran	Maître de Conférences, ESPCI Paristech	Co-directrice de thèse

Université Pierre & Marie Curie - Paris 6
Bureau d'accueil, inscription des doctorants
Esc G, 2ème étage
15 rue de l'école de médecine
75270-PARIS CEDEX 06

Tél. Secrétariat : 01 44 27 28 10
Fax : 01 44 27 23 95
Tél. pour les étudiants de A à EL : 01 44 27 28 07
Tél. pour les étudiants de EM à MON : 01 44 27 28 05
Tél. pour les étudiants de MOO à Z : 01 44 27 28 02
E-mail : scolarite.doctorat@upmc.fr

REMERCIEMENTS

Mon travail de thèse a été réalisé au sein du Laboratoire de Physico-chimie des Polymères et des Milieux Dispersés de l'ESPCI ParisTech. Je remercie François Lequeux et Christian Frétigny, ses directeurs successifs, d'avoir toujours su mettre à disposition tous les éléments nécessaires à mes travaux de recherche.

J'adresse aussi mes plus sincères remerciements à mes trois encadrants, Yvette, Dominique et Costantino, dont j'ai appris tellement et dont j'aurais pu apprendre bien davantage. J'espère avoir la chance de pouvoir travailler de nouveau avec des personnes d'une telle complémentarité, aussi riches de qualités personnelles et de compétences scientifiques (conditions qui seules peuvent rendre possible l'utilisation de deux mains par quatre cerveaux). J'ai grandement apprécié nos discussions et votre confiance de me laisser participer activement à la gestion de notre projet et de me permettre de voyager. Merci pour ces voyages tant en France (Saint-Pierre-des-Corps, Bordeaux, Presqu'île de Giens, Amnéville-les-Thermes et Saclay) qu'à l'étranger (Larnaca, Chypre ; Sheffield et Glasgow, Royaume-Uni ; Aix-la-Chapelle, Allemagne ; Daytona Beach, Floride, Etats-Unis) qui m'ont permis de communiquer et d'apprendre.

Je tiens à remercier chaleureusement les autres membres du jury. Plus particulièrement, merci à Mark Geoghegan et Eric Papon d'avoir accepté de rapporter mon travail de thèse. Merci à Florence Petit-Agnély et Bruno Grassl qui ont enrichi la discussion par la pertinence de leur lecture et de leurs questions ; et merci à Françoise Brochard-Wyart qui m'a fait l'honneur de présider ce très beau jury.

Je veux ensuite adresser ma reconnaissance à tous ceux qui ont contribué à apporter des résultats présents dans la suite du manuscrit, notamment les nombreux ITA du labo : Sandrine Mariot qui m'a formé à l'utilisation des machines thermiques, Linh pour ses synthèses de qualité, Agnès et Mohamed qui les ont caractérisées, Guylaine pour son expertise en rhéologie, Ludovic qui m'a aidé à concevoir cette fameuse boîte du chapitre 5. Mes pensées vont aussi à ceux dont l'apport, peut-être moins direct, est tout aussi indispensable : Isabelle, Annie, Flore, Gilles, Freddy et Armand, merci à vous. Je présente mes vifs remerciements à « mes » stagiaires : Stéphanie Génain et Claire Goldmann, deux « perles » qui ont fortement contribué au début du chapitre 4. Merci aux trois futurs ingénieurs ESPCI ParisTech, Clément Bottois qui a ajouté des résultats à ceux de Stéphanie, Florent Bories et David Kupiec, qui m'ont beaucoup aidé pour la mécanique des gels. Merci à Alicia pour ses synthèses de qualité. Etienne Ducrot mérite ma sincère gratitude pour son travail sur des interactions interfaciales électrostatiques, et sa joie de vivre communicative…

Je remercie avec déférence Fabrice Cousin du Laboratoire Léon Brillouin (CEA, Saclay), qui m'a chaleureusement accueilli en équipe à de très nombreuses reprises sur Eros, mon réflectomètre préféré, et sur PACE pour la diffusion aux petits angles. « Tout est bon dans le neutron ».

J'adresse ma sincère gratitude à Liliane Bokobza, Jean Louis Halary et Henri Van Damme qui m'ont fait l'honneur de me permettre d'enseigner pour eux à l'ESPCI ParisTech.

Merci à mon tuteur de monitorat à Paris Descartes, Gérard Louis. Je suis profondément reconnaissant envers Benoît Forget (et le chocolat des corrections des 2000 copies) et Marie-Claude Fauré qui a partagé le chocolat et les corrections, sa bonne humeur et ses avis éclairés et étendus sur la physique en PCEM 1 ; merci à Lincoln Travens, Stéphanie Moreau, Anne Baudot, Wladimir Urbach pour leurs explications, analyses et détails des enseignements et de l'enseignement. Une pensée pour mes étudiants de médecine, qui ont subi sans broncher et avec joie et enthousiasme (peut-être simulé) mes TD tyranniques où leur intérêt se traduisait par mon envie d'y aller enseigner. Merci enfin à Gérald Boéri, pour lequel j'ai collé en prépa en physique et chimie pendant de nombreuses années, à Fénelon puis à Janson de Sailly.

J'aimerais ensuite remercier tous ceux qui m'ont supporté à diverses échelles, et font que je ne peux partir sans un pincement au cœur. Je pense d'abord à ceux qui ont partagé mon bureau, avec par ordre d'apparition Stéphane et Elodie au thésarium, puis Armand, Maxime et Sarra en E0.10 ; et enfin en H2.07, ma dernière demeure au labo, de nouveau Elodie, et Séverine, Linn, Bétina et Clémence. Puis je pense à ceux qui ont partagé mes labos de chimie : Juliette, Elodie, Clémence et Clémence, Chau-Jean, Etienne…
Enfin, n'oublions pas les bons moments aux déjeuners et les bars du vendredi soir. Parmi les nombreux participants, j'aimerais citer Angélina, Ali, Caroline, Elise et Elise, Karine, Wei, François, Céline, Aurélie et Eric, Marie-Charlotte, Piero… Merci à vous tous !

J'ai aussi une pensée particulière pour Astrid qui a partagé une conf' de deux semaines à Aix-La-Chapelle et n'a pas hésité à m'accompagner de nouveau, avec Juliette, à Amnéville-les-Thermes pour un JEPO mémorable. Merci à David, Chau-Jean, et Elise pour les moments passés en Floride, à Chypre et à Bordeaux.

Un grand merci à tous les non-permanents – qui m'ont permis de les représenter au Conseil de Labo – et notamment ceux de l'équipe *Soft Polymer Networks*, avec qui il a toujours été facile d'échanger et d'apprendre ; Elodie, dont la rigueur au laboratoire de chimie m'a souvent fait regretter par la suite que tous au PPMD n'aient pas passé quelques jours sous son œil expert et reçu ses conseils avisés, Elise pour la méca et pour Igor, David pour ses trucs et astuces indispensables à la mise au point d'expériences utiles. Merci et bonne chance aux futurs docteurs !

Je remercie l'ensemble du laboratoire. Hélène et Laurence, merci pour votre bonne humeur et joie de vivre, pour les discussions et les pauses « goûter », pour avoir coupé des vacances en deux et me permettre d'avoir du café en plein mois d'août de rédaction…

Je remercie Pierre Muller et Olivier Théodoly qui ont écrit et co-écrit mon premier article.

Je remercie mes amis, les lecteurs ; et à tous ceux que j'ai oubliés mais qui devraient apparaître sur ces pages, je présente mes excuses les plus sincères et mes vifs remerciements.

Je tiens finalement à remercier mes parents et ma sœur, toujours encourageants et d'un soutien sans faille, un refuge dans mes tempêtes.

TABLE OF CONTENTS

LIST OF ABBREVIATIONS

AA	Acrylic acid
AFM	Atomic force microscope or microscopy
AM	Acrylamide
ATRP	Atom transfert radical polymerization
DMA	*N*,*N*-Dimethylacrylamide
DNA	Deoxyribonucleic acid
DOPA	3,4-Dihydroxy-L-phenylalanine
FTS	1H,1H,2H,2H-Perfluorodecyltrichlorosilane
GPS	γ-Glycidoxypropyltrimethoxysilane
HMDZ	Hexamethyldisilazane
IPC	Interpolymer complex
IR-ATR	Infrared spectroscopy by attenuated total reflectance
JKR	Johnson, Kendall and Roberts
KPS	Potassium persulfate
LCST	Lower critical solution temperature
MBA	*N*,*N'*-Methylene-bis-acrylamide
MeP4VP	Poly(*N*-methyl-4-vinylpyridinium iodide)
NMP	Nitroxide mediated polymerization

NMR	Nuclear magnetic resonance
OTS	Octadecyltrichlorosilane
P4VP	Poly(4-vinylpyridine)
PAA	Poly(acrylic acid)
PAM	Poly(acrylamide)
PDEA	Poly(*N*,*N*-diethylacrylamide)
PDI	Polydispersity index
PDMA	Poly(*N*,*N*-dimethylacrylamide)
PDMAEMA	Poly((2-dimethylamino)ethyl methacrylate)
PDMS	Poly(dimethylsiloxane)
PEO	Poly(ethylene oxide)
PMAA	Poly(methacrylic acid)
PMAETAC	Poly(2-(methacryloxy) ethyl trimethylammonium chloride)
PMMA	Poly(methyl methacrylate)
PNIPAM	Poly(*N*-isopropylacrylamide)
PP	Poly(propylene)
PtBuA	Poly(t-butylacrylate)
PVDF	Poly(vinylidene fluoride)
PVP	Poly(*N*-vinyl-2-pyrrolidone)
RAFT	Reversible addition-fragmentation chain transfer
SAM	Self-assembled monolayer
SANS	Small angle neutron scattering
SFA	Surface force apparatus
SMFS	Single-molecule force spectroscopy
TEMED	N,N,N',N'-Tetramethylethylenediamine
TGA	Thermogravimetric analysis
THF	Tetrahydrofuran
UCST	Upper critical solution temperature

INTRODUCTION GÉNÉRALE

De nombreux hydrogels, la plupart d'origine naturelle, sont utilisés dans l'alimentation, dans le domaine du vivant, et dans le domaine biomédical. En particulier, leur utilisation pour la vectorisation de principes actifs ou pour la construction de tissus artificiels se répand. Les hydrogels sont des matériaux qui présentent de nombreux attraits, notamment parce qu'ils sont en général biocompatibles, très déformables et aux propriétés adaptables à façon par la chimie. Cependant, comme ils contiennent de grandes quantités d'eau, ce sont aussi des matériaux fragiles et élastiques qui ne sont pas naturellement collants. Pourtant, leurs propriétés d'adhésion sont essentielles dans bien des applications et restent jusqu'alors peu étudiées et encore moins comprises.

Cependant, dans la nature, il existe des exemples d'hydrogels collants : en environnement marin, la patelle se colle au rocher par la sécrétion d'un hydrogel complexe de polysaccharides et de protéines. Afin de comprendre les mécanismes qui permettent de contrôler l'adhésion entre un hydrogel et une surface, l'utilisation de systèmes modèles simples a été privilégiée. Pour pouvoir modifier les propriétés adhésives des hydrogels sur des surfaces, deux démarches sont envisageables. La fonctionnalisation des hydrogels avec des motifs stimulables permettrait de changer leur affinité avec un substrat. Nous avons préféré la fonctionnalisation de la surface par des polymères associatifs au réseau polymère de l'hydrogel.
Prenant exemple sur les études menées en l'absence de solvant, des surfaces fonctionnalisées par des chaînes de polymère permettent de renforcer considérablement les phénomènes d'adhésion d'un réseau élastomère : lorsque la surface de l'élastomère est mise en contact avec la surface greffée, l'enchevêtrement des chaînes à l'intérieur du réseau élastomère est à l'origine d'un renforcement de l'adhésion entre les surfaces. Cette adhésion peut être aussi renforcée par la présence de liaisons spécifiques entre les greffons et le réseau. Dans le cas de réseaux dilués, l'effet des enchevêtrements est fortement réduit et les interactions spécifiques deviennent essentielles.

Ces interactions spécifiques et réversibles entre polymères ont été largement étudiées et de nombreux groupes ont conçu des systèmes macromoléculaires variés aux propriétés stimulables. Cette sensibilité des systèmes macromoléculaires est liée à leurs propriétés thermodynamiques, qui dans l'eau peuvent être modifiées en jouant sur une large gamme d'interactions. La variété des interactions permet d'envisager de nombreux stimuli (la lumière, les champs électrique ou magnétique, la température, l'acidité du milieu ou sa force

ionique) pour contrôler la formation spécifique de complexes interpolymères dans l'eau, dont la réversibilité constitue un atout supplémentaire pour adapter les propriétés d'adhésion d'hydrogels.

Dans le but de contrôler l'adhésion, ces associations spécifiques en solution sont transposables aux interfaces par l'utilisation d'un système macromoléculaire dont les interactions avec l'hydrogel peuvent être stimulables : une brosse de polymère (voir Figure 1). Notre choix s'est porté sur des brosses de polymères stimulables par le pH dont la synthèse est effectuée par greffage chimique sur un substrat, ce qui lui confère une grande stabilité. De même, des hydrogels modèles réticulés chimiquement, peu dissipatifs et peu sensibles aux conditions environnementales, ont été privilégiés.

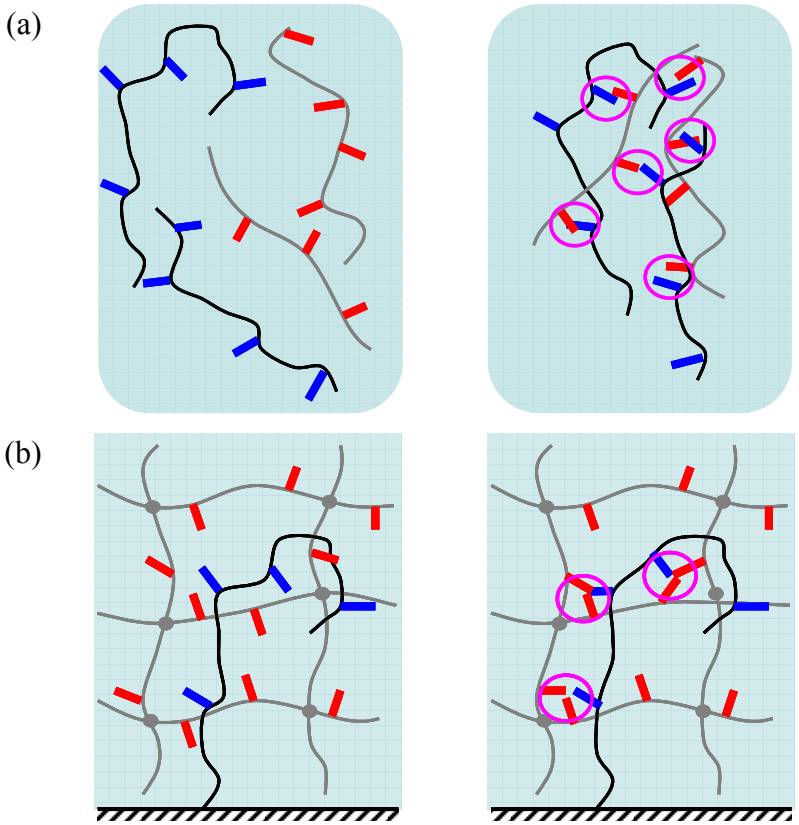

Figure 1 - Représentation des associations macromoléculaires stimulables en solution aqueuse (a) et transpose aux interfaces (b), où les chaînes noires sont celles de la brosse et les grises celles du gel.

Pour examiner les phénomènes qui peuvent piloter l'adhésion réversible d'hydrogels sur des surfaces fonctionnalisées, notre problème a été ramené à des systèmes modèles des plus simples d'homopolymères dont les interactions sont principalement stimulables par le pH. Cependant, si l'étude de ces interactions en solution reste relativement simple, la

compréhension des phénomènes d'adhésion d'hydrogels sur des brosses est un problème complexe qui nécessite l'intervention de compétences multiples :

- La modification de surface par greffage chimique de brosses de polymères stimulables ;
- La synthèse d'hydrogels à propriétés choisies et notamment capables d'interagir de façon réversible avec d'autres systèmes ;
- La caractérisation des propriétés adhésives de l'interface hydrogel/surface.

Cette multidisciplinarité se rencontre au sein de l'équipe *Soft Polymer Networks* du laboratoire *Science et Ingénierie de la Matière Molle*, ce qui en fait un environnement de choix pour traiter ce sujet.

Ce manuscrit est divisé en quatre parties et six chapitres.
La première partie (chapitre 1) est consacrée à une présentation générale de la problématique de l'adhésion dans l'eau, afin de rassembler les éléments essentiels à une bonne compréhension des phénomènes permettant le contrôle de l'adhésion immergée.
La seconde partie est dédiée à la synthèse et à la caractérisation des objets nécessaires à l'étude. Le deuxième chapitre se concentre sur l'élaboration et la structure de brosses de polymère sensible au pH, alors que le troisième chapitre porte sur la préparation d'hydrogels neutres et sur l'étude de leurs propriétés structurales, mécaniques et de gonflement.
Dans la troisième partie, les interactions spécifiques stimulables entre les polymères confectionnés dans la deuxième partie sont étudiées en solution. Les différents aspects de leur sensibilité aux modifications environnementales sont précisés et l'étude est transposée aux interfaces par une méthode de caractérisation structurale.
La dernière partie s'attache à la détermination des propriétés d'adhésion immergée des gels et des brosses décrits dans la seconde partie. Dans le chapitre 5, les difficultés liées à des mesures reproductibles de l'adhésion immergée sont mises en exergue et un nouveau montage expérimental est proposé en association aux protocoles de mesures adaptés. L'étude des propriétés d'adhésion entre les gels et les brosses est présentée dans le chapitre 6. Les effets des conditions environnementales et expérimentales sur les résultats sont soulignés afin de remonter aux paramètres caractéristiques des interactions.
Les apports de ce travail sont rappelés en conclusion et sont accompagnés de ses perspectives.

Finalement, il nous a semblé essentiel de rendre ce manuscrit accessible au plus grand nombre. En particulier, l'équipe *Soft Polymer Networks*, au sein du laboratoire *Science et*

Ingénierie de la Matière Molle, constitue en elle-même un environnement international. Nous avons aussi voulu valoriser au maximum l'exercice de rédaction qui participe à la formation du thésard pour le préparer au métier de docteur ; ces derniers, dans l'industrie comme dans le milieu académique, sont de plus en plus confrontés à l'écriture de rapports ou d'articles souvent diffusés dans de nombreux pays. Nous avons par conséquent choisi de rédiger la majeure partie de ce manuscrit en anglais, langue de la communication scientifique de fait. Pour en faciliter l'approche au lecteur français, cette introduction générale, la conclusion générale et un résumé substantiel sont rédigés en français.

GENERAL INTRODUCTION

Many hydrogels, mainly those that are natural, are being increasingly used in food science, in biology and biomedicine. In particular, their use for targeted drug delivery or for artificial tissue scaffolding spreads. Hydrogels are materials that are very attractive, especially because they are generally biocompatible, highly deformable and with adaptable properties by varying their chemistry. However, since they contain large amounts of water, they are also fragile and elastic materials and are not naturally sticky. Yet, their adhesive properties are essential in many applications and remain, until now, poorly studied and even less understood.

However, in nature, there are examples of sticky hydrogels: in marine environment, the limpet clings to the rock by the secretion of a complex hydrogel made of polysaccharides and proteins. To understand the mechanisms that control the adhesion between hydrogels and surfaces, we have favored the use of simple model systems. To modify the adhesive properties of the hydrogels on surfaces, two approaches can be distinguished. The functionalization of hydrogels with sensitive units could trigger a change of their affinity with a substrate. We preferred to functionalize the surface with polymers associative to the polymer constituting the hydrogel network.
Following the example from the studies performed in the absence of solvent, surface-functionalized polymer chains can greatly enhance the adhesion phenomena of an elastomeric network: when the surface of the elastomer is in contact with the grafted surface, the entanglement of the chains within the elastomer network is the cause of a strengthening of the adhesion between the surfaces. This adhesion can also be enhanced by the presence of specific interactions between the grafts and the network. In the case of diluted networks, the effect of entanglements is substantially reduced and the specific interactions become essential.

These specific and reversible interactions between polymers have been extensively studied and many groups have developed various macromolecular systems with responsive properties. This responsiveness of macromolecular systems is related to their thermodynamic properties, which in water can be tuned with a wide range of interactions. The variety of interactions allows many stimuli (light, electric or magnetic fields, temperature, acidity of the medium or its ionic strength) to control the specific formation of interpolymer complexes in water. The reversibility is an additional advantage to adapt the adhesive properties of hydrogels.
In order to control the adhesion of hydrogels, these specific associations in solution are adaptable to the interfaces by using a macromolecular system whose interactions with the hydrogel can be triggered: a polymer brush (see Figure 1). Our choice fell on pH-responsive

polymer brushes, the synthesis of which is performed by chemical grafting on a substrate, guaranteeing a great stability. Similarly, chemically cross-linked model hydrogels, weakly dissipative and insensitive to their environmental conditions, were selected.

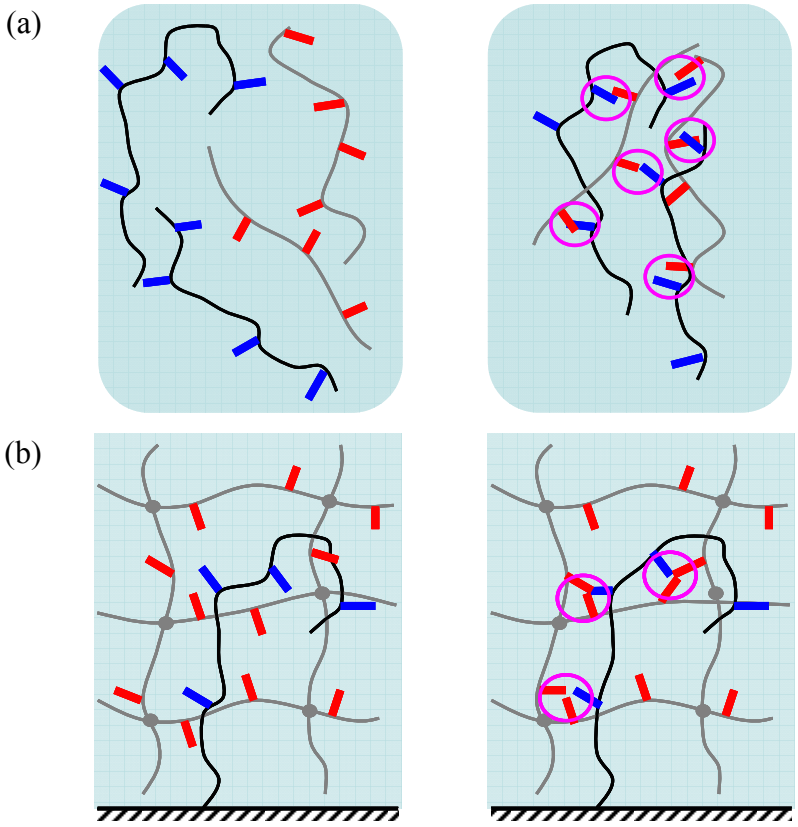

Figure 1 - Schematic representation of sensitive macromolecular associations in aqueous solution (a) and adapted at interfaces (b), where the black chains are those of the brush and the grey ones are those of the gel.

To determine the phenomena that can drive the reversible adhesion of hydrogels on functionalized surfaces, our problem has been simplified to model systems of homopolymers that are able to interact, their interaction being primarily driven by pH. However, if the study of these interactions in solution is relatively simple, the understanding of the adhesive phenomena of hydrogels on the brushes is a complex problem that requires the many different skills:

- The surface modification by chemical grafting of responsive polymer brushes;
- The synthesis of hydrogels with select properties, and in particular able to reversibly interact with other systems;
- The characterization of the adhesive properties of the hydrogel interface/surface.

This multidisciplinary can be found in the *Soft Polymer Networks* team of the *Soft Matter Science and Engineering* Laboratory. It makes this team an environment of choice for treating this subject.

This manuscript is divided into four parts and six chapters.
The first part (Chapter 1) is devoted to an overview of the issue of underwater adhesion with the purpose of gathering the elements essential to understand the phenomena which control immersed adhesion.
The second part is dedicated to the synthesis and characterization of the objects needed throughout the study. The second chapter focuses on the elaboration and the structure of pH-responsive polymer brushes, while the third chapter focuses on the preparation of neutral hydrogels and on the study of their structural, mechanical and swelling properties.
In the third part, the specific interactions between responsive polymers – synthesized in the second part – are studied in solution. The various aspects of their sensitivity to environmental changes are detailed and the study was implemented at interfaces by a method of structural characterization.
The last part deals with the determination of adhesive properties of immersed gels and brushes described in the second part. In Chapter 5, the difficulties associated with reproducible measurements of the underwater adhesion are highlighted and a new experimental setup is proposed in combination with adapted measurement protocols. The study of the adhesive properties between the gels and the brushes are presented in Chapter 6. The effects of the environmental conditions and the experimental results are highlighted in order to determine the characteristic parameters of the specific interactions.
The contributions of this work are recalled in conclusion, which comes with its outlook.

CHAPTER 1 - UNDERWATER INTERACTIONS AND ADHESION

Adhesion is a process found in Nature, mainly at small scales. For many applications, adapted adhesives have been engineered to answer technical issues and we are now surrounded by man-made adhesives. Nevertheless, the theories for in-air adhesion have been far more developed than those for underwater processes, the applications of which remaining somehow more restricted. As a consequence, underwater adhesion is an open field where one finds inspiration from technical solutions in Nature. As a matter of fact, many marine animals are able to get fixed on a substrate, either momentarily or for long periods of time. At the cellular level, the attachment between cells is at the origin of the multi-cellular organisms, defining their shape and most of their physiological functions.

So, how does adhesion work underwater? How can we create underwater adhesion? The answers obtained from the biological studies on animals such as mussels or barnacles are that they have been able to create adhesive bonds with many different substrates, using different technologies. Most of them consists in secretions of cement or concentrated polymeric adhesives, others are based on Van der Waals interactions between the substrate and the structured surface of the animal. A great number of studies focuses on this type of adhesion where polymers are largely involved. The main differences between these bioadhesives and the man-made ones for in-air applications are the chemical composition. Current technologies are based upon synthetic materials from petrochemical products whereas the polymers used for underwater adhesion are water-soluble and able to form various types of interactions. Basically polysaccharides or polydopamine, proteins such as adhesins or cadherins, are responsible for cell or animal adhesion. Then, the objective of many biomimicking studies is often to reproduce such interactions.

In this short introductive chapter, we briefly review the intermolecular interactions that are commonly present in condensed matter and we discuss their adaptability for surface interactions in underwater conditions. Keeping in mind that many answers can be found in Nature, we review the various attachment or holdfast systems that are used by marine animals such as mollusks or crustaceans and the methods used at the cellular scale to link cells together or to a substrate. Finally, the importance of polymers in biomedical adhesive applications is demonstrated and the further interests coming from these objects are developed.

1- Mechanisms and interactions involved in underwater adhesion

The central problem of this first part is to determine the types of interactions that can occur between elements, atoms or molecules, and to what extent they can be used to create, reinforce or tune underwater adhesion. A great number of intermolecular interactions [1-3] will be reviewed at first, from the strongest "chemical bonds" which are the *covalent* bonds to the weakest "physical bonds" that can definitely be screened in a medium such as water. Then, this review is extended to the inter-surface forces, considering larger effects and more complex mechanisms.

1-1- Intermolecular interactions

Strong intermolecular forces

Water is composed of two atoms of hydrogen which are tightly linked to an atom of oxygen via covalent bonds. In such a system, the atoms share some of their electrons so that their total number corresponds to a valency of high stability for each atom. These interactions are strong (100–300 kT[i]), very short-range and directional. In organic compounds, creating or breaking such interactions often requires drastic conditions or the addition of strong reagents which leads to partial modification of the starting molecules while the reverse reaction is not always possible. The covalent bonds are very similar to the metallic bonds.

The other electron pair sharing interactions are in the donor-acceptor category: in coordination chemistry, it corresponds to the bonds that form between a ligand and a central metal atom, but it also corresponds to the acid-base interactions. The acid-base interaction in the sense of Lewis[ii] involves an electron pair donor (the base), which shares a non-bonded electron pair with an acceptor (the acid), which is deficient in electrons and can accommodate the electron pair.

[i] That is to say in the order of magnitude of 100 to 300 times the energy from thermal agitation at the ambient temperature.

[ii] These acid-base interactions by electron pair sharing must be distinguished from the more common-place acid-base interactions in the sense of Brønsted-Lowry for which the characteristic reaction consists in an exchange of a hydrogen ion H^+ (or proton) between two species, the proton-donor being the acid and the proton-acceptor the base.

These interactions, that are often called “chemical interactions”, are formed when two species pool their molecular orbitals, their overlapping leading to common constructive occupied orbitals of lower energy.

It is distinguished from the “physical interactions”, the stronger one being the electrostatic or Coulombic interaction which corresponds to charge-charge interaction. It occurs when two species bear fixed charges. When the two charges have the same sign, they repel one another and when the charges have opposite signs, the interaction is attractive. It corresponds to a long-range interaction with an energy varying in r^{-1} (where r is the distance between the two charges). In vacuum and for two monovalent ions in contact (such as Na^+ and Cl^-), the energy of the interaction is about 200 *kT*. However, things are different in water, for at least three reasons:

- The permittivity of water is 80 times higher than the permittivity of vacuum and as a consequence, the forces and energies are 80 times weaker. For charged particles that are big enough, the water can be indeed considered a continuous medium, while for small ions, this simple approach does not fully describe the situation but predicts the right trend.
- In a medium, the ions are never isolated and positive ions are in the vicinity of negative ones, screening the effect of the former and leading to a variation of the interaction in r^{-3}, that is to say on shorter ranges.
- For ions of size about that of a water molecule, the polarity[iii] of the water molecules plays a role. In the case of an ion surrounded by water, the interaction corresponds to a charge-dipole interaction, which decreases with distance like that of the charge-charge interaction but which is less energetic (few tens of *kT* for molecule and ion in contact). Then, close to the ion where the electric field is important, the dipole moment of water tends to align in the field, modifying the local molecular ordering: this is called a solvation effect, or a hydration effect when the solvent is water.

As a consequence, the Coulombic interaction in water for small ions is of the order of a few *kT*. Adding many of them can be profitable to create a strong interaction at surfaces.

[iii] The polarity corresponds to the electric dipole created by the tendency of some atoms in the molecule to attract the bonding electron pair closer to them due to their higher electronegativity. The general result is an electric dipole with two opposite partial charges on different moieties of the molecule.

Van der Waals interactions

Van der Waals interactions are weaker interactions than the previous ones, but their source is – physically speaking – the same as the electrostatic interactions. However, for Van der Waals interactions, no fixed charge is involved but solely dipoles. In some cases, the dipole is permanent, that is to say, due to the arrangement of the atoms of different electronegativity in the molecule; or it is due to the polarizability of a molecule for which a dipole can be induced by an external electric field (caused by another dipole or a charge) which modifies the shape of the electronic cloud of a molecule. The variation of the energy of dipole interactions with the distance is in r^{-6}, which means that it is of shorter range than with fixed charges.

The strongest of the Van der Waals interaction is for permanent dipoles: the dipole–dipole interaction, or Keesom interaction. Then, the dipole–induced dipole interaction, also called Debye interaction, considers the interaction between a permanent dipole and a polarizable molecule. The induced dipole–induced dipole interaction (or London interaction) is the third one. It corresponds to the dispersion forces that can be observed between two molecules with electron clouds that can be polarized momentarily, since for a non polar molecule, there is a finite probability that it can show a polarization at one instant and then become an instantaneous dipole. An induced instantaneous dipole may interact with the first one.

As for Coulombic interactions, the weaker Van der Waals interactions are depending on the medium. Consequently, these interactions between solute species are much reduced in aqueous solutions and this disturbance is linked to the properties of water.

Water specific interactions: the hydrogen bond and the hydrophobic interaction

Our medium of interest, water, has proven to weaken the physical interactions presented above, but due to its strong unusual characteristics, two types of interactions are intimately linked to its properties. Put together, these interactions are responsible of many phenomena observed in living systems, from the lipid bilayers of cells to the double helix of DNA or the folding of proteins. One of them is the hydrogen bond and the other one is the hydrophobic effect. The latter is due to the tendency of the polar water molecules to exclude the non polar molecules and segregate them. This is often explained by the rupture of the highly dynamic lattice of the hydrogen bonds between water molecules in the vicinity of the apolar solute and by the entropically unfavorable immobilization of water molecules around the solute in what is called the hydration shell (or hydration cage). In some specific cases, the hydration shell can form at a given temperature, but being entropically unfavorable, it is eventually

destabilized upon heating and the solute becomes phase-separated at a lower critical solution temperature. It is the case of the poly(*N*-isopropylacrylamide) polymer which undergoes a phase separation in water at 32°C [4].

The hydrogen bond, which is at the centre of our interest, is a short ranged and directional interaction between an electronegative atom (such as oxygen, nitrogen or fluorine) and a hydrogen atom covalent to another electronegative atom. The hydrogen bond is commonly classified as an electrostatic effect since the hydrogen is partially positively charged when linked to a very electronegative atom which leads to strong local dipoles. The presence of another electronegative atom nearby is often the source of another dipole which strongly interacts with the first one. The two dipoles tend to align and get very close, which is possible due to the small size of the hydrogen atom. The shortness of the hydrogen bond and its directionality is similar to that of the covalent bonds, but its energy is far smaller, in a range of 4 to 20 kT.

Due to its structure, hydrogen bonds are everywhere in water, the molecules of which are able to form 4 hydrogen bonds (2 with the hydrogen atoms and 1 with each of the 2 lone pairs of electrons of the oxygen) with other ones. Then, when two species are able to form H-bonds with one another, their bridging in aqueous solution becomes less favorable since water is a competitor for the formation of H-bonds.

However, for macromolecules, H-bond interactions with long life-times are observed from nature: the pairing of DNA moieties and the structural folding of the proteins are well-known examples. In each case, the H-bond interactions can be broken upon heating. As a consequence, the formation of H-bonded complexes of macromolecules has attracted a lot of experimental work (see Chapter 4) and theoretical work. Tanaka *et al.* [5] and Dormidontova *et al.* [6] have focused their first studies on the H-bonding polymer association in bulk between a chain of one polymer and the tail of an oligomer. They propose a model to describe the H-bond formation and predict the phase diagram of the system (varying the fraction of both polymers and the temperature). They investigate the effects of chain length or H-bond strength. However, the addition a third component, the solvent, in such systems is particularly difficult. Dormidontova [7] discussed later the competition between the water–water or the poly(ethylene oxide)–water H-bonds to describe the properties of solutions of PEO by a mean-field approach. Li *et al.* [8] have performed an experimental determination of the various H-bond interactions that can be found in hydrated poly(acrylic acid). Ternary systems solvent/polymer 1/polymer 2 have been studied by Campos *et al.* very recently [9-11]. They use a thermodynamic approach to describe the interaction and thanks to experimental data,

they determine the interaction parameters in their systems. In all cases, they considered that only one of the polymers was proton-donor, which can not represent the case of aqueous solutions.

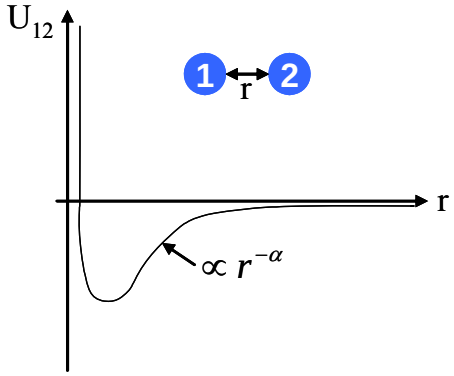

Figure 1 - Schematic representation of the typical interaction potential between two molecules. The exponent α depends on the type of force exerted between the two entities. For fixed charges: $\alpha = 1$; Charge-dipole: $\alpha = 2$ or 4; Van der Waals: $\alpha = 6$. For hydrophobic interactions, the variation looks similar but is exponential.

All together, these interactions are the most fundamental ones and they are the basis for the supramolecular chemistry (see Figure 1). Using the molecular self-assembly from hydrophobic interactions, H-bonds, electrostatic interactions (and the π–π interactions not described here), the supramolecular chemistry builds chemical structures of large dimensions by sticking together small units. In this part, we focus on the possibility for these interactions to be transferred to interfaces and give rise to tunable adhesive properties.

1-2- The inter-surface forces

Surface tension: a powerful tool

One of the approaches that can be used to evaluate the inter-surface forces consists in using the expression of the intermolecular interactions, particularly those from the electrostatic forces and the Van der Waals forces, and summing them on the totality of the materials. Fowler and Guggenheim have used this integration method to calculate the energy of interaction between two surfaces in vacuum when the potential interaction was of a Lennard-Jones type (with an attractive term of Van der Waals type and a very short-range repulsive term corresponding to the non-superposition of electronic clouds, with a variation expressed as $-Ar^{-6} + Br^{-12}$, with A and B positive constants). It is possible, using the same methodology, to produce results for other cases: the DLVO (for Derjaguin, Landau, Verwey

and Overbeek) theory describes the interactions between charged surfaces in a medium, taking into account the charge distribution of the ions in the medium.
However, Fowler and Guggenheim approach can be substituted by a much simpler approach that considers the global thermodynamics of the surface. Both methods give access to the role of surface tension in the inter-surface forces. Every day examples of the surface tensions are the wetting ability of liquid on a surface, the spherical shape of the rain droplets or the possibility to filling up a glass upper than its limit. To define the surface stress, we are giving two approaches. One is mechanical and the other one is thermodynamic.

One the one hand, liquids, contrary to vapor, do not spread in all the space available, and this is because the molecules are forced to stay close to each other, because of cohesion forces, mainly Van der Waals forces. These cohesion forces are attraction forces that are created by one molecule toward each of its neighbors. A general idea explaining the energy excess of molecules at surfaces compared to those in bulk consists in comparing those forces. For one bulk molecule in the middle of the liquid, the sum of the forces applied by all its neighbors is statistically equal to zero (left of Figure 2). On the contrary, for a molecule that is at the interface, the sum of attraction forces created by its neighbors is a force directed towards the interior of the liquid (right of Figure 2). Thermodynamically speaking, bringing a molecule from the inside of the liquid to the surface of the liquid (so, to increase the surface of the interface), a mechanical work has to be furnished to fight against a cohesion energy proportional to the area of the interface. We are talking about surface tension, and at the interface between A and B, it is labeled $\gamma_{A\text{-}B}$.

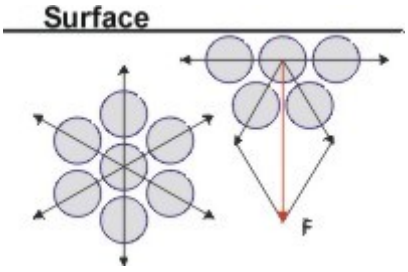

Figure 2 - Schematic view of the mechanical origin of surface tension.

This approach which is very intuitive for liquids is valid with solids and it can be used to determine the work of adhesion W_{adh}. For this calculation, two dissimilar and purely elastic materials A and B are in intimate contact. A tensile force is applied so that the two materials

are set apart. If the cross-section of the contact is of a unit area, the energy expansion corresponds to the two surface tensions created between the two materials and the immersing medium (IM), from which the surface tension between A and B has to be subtracted since this interface is broken:

$$W_{adh} = \gamma_{A-IM} + \gamma_{B-IM} - \gamma_{A-B} . \quad \textbf{Eq. 1}$$

Using water as immersing medium instead of air for classical adhesive joints is a source of many modifications in the strength and the stability of the adhesion.

Water: a contaminant in classical adhesive joints

All the classical pressure sensitive adhesives (adhesive tape for instance) do not typically work on wet surfaces. Furthermore, in classical adhesive joints, such as aluminum/epoxy joints, the presence of water is generally detrimental. Calculating the work of adhesion based on a surface energy method, Pocius [2] demonstrates that water tends to wet the aluminum surface, leading to an unstable aluminum/epoxy system in the presence of water. The first consequence is the surface preparation of the adherent whenever possible, to prevent these effects in industrial bonded products.

In the presence of water, the work of adhesion is modified compared to that in air and as a consequence, it is mandatory to reinforce the interactions at the molecular scale. One approach can be, for instance, to use covalent bonding: it is the methodology we have chosen to apply to irreversibly attach gels on glass slides and the process is presented in Chapter 4.

In a more general approach and targeting tunable and reversible adhesion, the surface can be modified with sticker molecules or adhesion promoters; obviously, they need to be tunable or deactivable.

Mechanisms favorable to adhesion

If the adhesion is possible in the presence of water between two materials, some mechanisms are favorable in establishing it quickly, or in reinforcing its strength. To facilitate the discussion, let us consider that one of the materials supposed to stick on the other one (or at least its surface) is swollen, that is to say contains a given amount of water that solvates its deformable structure [12]. If the swollen material was in its dry state, its ability to swell is essential to its adhesive properties, particularly in the case of mucoadhesives [13]. Related to the surface tension phenomena, the spreading of the soft material, that is to say its ability to

cover a maximum surface of the adherent by specific interactions that favor the wetting of one surface by the other, is essential to enhance the adhesion phenomenon. Joanny *et al.* [14] studied the spreading of gels at interfaces by balancing the effects of bulk elasticity of the gel and the spreading power of the swelling solvent on the substrate. However, when the substrate is immersed in the swelling solvent, such a spreading parameter no longer exists and the specific interactions between the polymer network and the substrate are essential.

A second major enhancement of the adhesive strength can rise from the ability of the interface to become diffuse. It means that the materials allow one another to interdiffuse and interpenetrate. Basically, it leads to an increased contact volume in which the number of specific interactions can be multiplied, which leads to an enhanced adhesion. These specific interactions can be due to the chemistry of the materials since electrostatic interactions can be added to H-bonding (as we will see at the end of Chapter 6). Or their structure can play a part, for instance by the possibility to form entanglements between the two materials. On dry elastomer networks, the effects of entanglements on the reinforcement of adhesion using connector molecules has been widely studied [15-19] on rubber-rubber or rubber-grafted solid systems. The theoretical and experimental work has been reviewed by Léger *et al.* [20]. The application of these connector molecules for the adhesion of hydrogels was first suggested in Peppas's group by DeAscentiis *et al.* [21] who added poly(ethylene glycol) to a hydrogel of poly(2-hydroxyethyl methacrylate) and reinforced its adhesion on mucosa. A similar study has been carried out on poly(methacrylic acid) gels [22] with mucosa before the gel-gel adhesion reinforced by connector molecules was theoretically studied by Huang *et al.* [23].
Finally, viscous dissipation in the bulk of the materials can only lead to a stronger practical work of adhesion since the larger the dissipation, the higher the energy of adhesion. This is a paradox of adhesion [24], which can not only be explained by interfacial properties but bulk dissipative effects have to be taken into account in the process of adhesion[iv].

To summarize this paragraph, here is a list of effects which can control the adhesive properties between two materials under water:

- The presence of specific interactions;

[iv] A vulgarized explanation of these bulk dissipative effects is given by Liliane Léger on the website of "l'Université de Tous les Savoirs": for French speaking people, see www.canal-u.tv.

- The interdiffusion and the interpenetration of the materials, to increase the density of interactions per unit of interfacial area;
- The addition of entanglements;
- The bulk dissipative effects that reinforce the work of adhesion by the irreversible energy loss.

All these effects are of interest in particular for soft matter physicists who performed some systematic investigations to elucidate interactions between surfaces. For instance, Israelachvili first proposed an experimental setup, the surface force apparatus, to measure Van der Waals or electrostatic forces between two surfaces separated by a liquid [25]. It has been applied to the determination of the size of hydration layers on charged substrate, etc. (see Chapter 5 for a more detailed discussion).

Very recently, Varenberg *et al.* [26] and Vajpayee *et al.* [27] have studied the adhesion of fibrillar structured materials on hydrophobic substrates. The interactions studied correspond to Van der Waals forces and they are at the base of the principle used by the gecko to climb walls. They have shown that these interactions were reinforced under water.

Most importantly, these interactions are at the basis of life, and the resulting adhesion is essential for the formation of multicellular organisms and the attachment of animals in many different ways, as developed in the next paragraph.

2- Adhesion in living matter

Bioadhesion is the process by which two surfaces can adhere through intermolecular interactions, one of the materials being of biological nature. Roughly, three cases can be distinguished in underwater bioadhesion: the adhesion of unicellular systems in multicellular ones, the formation of biofilm and the adhesion of animals in marine environment. The ways these systems stick usually involves of natural polymeric materials. A specific case of bioadhesion is when a synthetic or natural macromolecule sticks to a biological tissue. In this case, the phenomenon is called mucoadhesion. Bioadhesion and mucoadhesion are both phenomena of interest in the case of underwater adhesion or for the adhesion of swollen materials since life is composed of a great amount of water. This is why we are giving some chosen examples of bioadhesion.

2-1- Bioadhesion

The bioadhesion represents a wide range of natural processes visible in Nature. The spider catches the prey which is stuck on its web. Some insects and fishes attach their eggs at the surface of vegetation or rocks using adhesives based on proteins. Unicellular bacteria, algae or fungi colonize surfaces in air and under water.

As a consequence, focusing on underwater adhesion, it is possible to take examples from nature in all the phenomena involved in bioadhesion. We will distinguish two types of bioadhesion in this part, the adhesion of marine organisms in a first part, and the adhesion of cells.

Marine biology

In the marine environment, bioadhesion generally concerns the fixation of marine animals on any type of substrate from rock to the hull of ships. As a consequence, it is of prime interest to people trying to understand fouling and to design antifouling systems. There, the bio-fouling, which concerns the adhesion of living organisms, can be distinguished from the deposition of non-living substances. Both occur in the marine environment, but also in the piping or in the bathrooms.

Many biopolymers are involved in the underwater adhesion of marine animals and most studies on that topic focus on the compositional analysis of the materials involved and on their mode of attachment. The secretions of a few animals have been investigated; they are sea cucumbers, mussels, tubeworms, limpets and barnacles.

Depending on the animal, their attachment mode on the foreign substrate is different. The byssus of the mussel is a group of biological threads anchored inside the animal and linking it to a substrate by the formation of plaques [28]. As a comparison, to attach their calcareous shell to their substrates, barnacles secrete a cement that is made out of bio-molecules and that strongly sticks to the substrate [29]. A schematic representation of the attachment modes of some of these animals is given in Figure 3.

Despite the various attachment modes observed, the composition of the adhesive materials is somewhat similar and generally consists of concentrated natural polymers, often called cements. In Herbert Waite[v] group, many proteins constituting the adhesive secretions of

[v] For references on the marine adhesion, the Waite collection which represents 5 issues of the Journal of Adhesion can be consulted since it assembles articles focusing on marine bioadhesion.

mussels and of tube-building worms have been characterized. For instance, DOPA (3,4-dihydroxy-L-phenylalanine) which is a modified amino acid, had long been identified as a recurrent constituent of the adhesives from marine animals Recently, Flammang *et al.* [30] have demonstrated the importance of the phosphorilation of glycoproteins in the marine adhesion mechanisms and they have identified phosphoserine as another recurrent component of the adhesive material from three animals with no close link in their evolution (phylogenetically different). Kamino focused in a recent study [29] on the composition of the barnacle cement and its differences compared to that of the mussel and of the tubeworm. He concluded that this cement could be useful for many applications since it allows to bind different types of other materials in water [31].
The composition of the adhesive secreted by the limpet can be separated from that of the others previously cited since its natural nonpermanent adhesive involves a hydrogel made of polysaccharide and proteins [32].

In a few studies, force measurements have been carried out directly on the animals. In Flammang's group, the adhesion strength of the attachment of a sea cucumber was measured and an energy of adhesion ranging between 30 and 135 $N.m^{-2}$ [33] was found. Burkett *et al.* [34] have performed pull-off tests to characterize the strength of the attachment of the mussel on various surfaces such as glass, aluminum or poly(vinyl chloride) with the purpose of finding useful clues for the development of new anti-fouling surfaces. They found energies of adhesion in the range of 100-300 $N.m^{-2}$.

With completely different mechanisms involved, Lin *et al.* [35] demonstrated the effect of Van der Waals and capillary forces in the adhesion of abalone. Abalones stick to their substrate through a foot which has been analyzed and found to be constituted of a fibrillar structure, resembling the structure of the gecko foot (see Figure 4). Due to the multi-scale structure of the abalone foot, the fibrils are able to be in intimate contact with the substrate, and the relatively low strength of each bond can be cumulated to show a strong macroscopic effect.

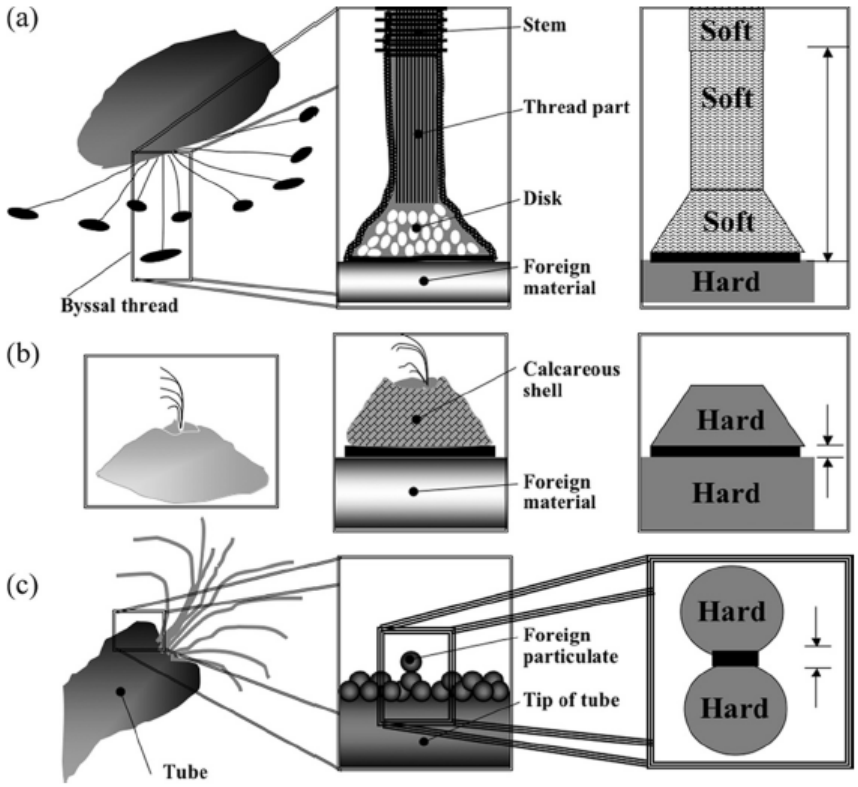

Figure 3 - Modes of attachment of mussel, barnacle, and tubeworm from [29]. Schematic illustrations of adhesive joints: (a) Mussel makes several tens of byssal threads that have macroscopically modular structures. The byssal thread as a whole functions as the holdfast of the animal, with a distance between the animal and foreign materials on the order of cm. The coupling layer at the tip of the byssal disk actually bonds hard matter (foreign materials) and soft matter (the mussel's own byssal thread). A simplified illustration is shown on the right side. (b) Barnacle attaches to foreign materials by secretion of the cement underneath their own calcareous base. The cement layer on natural or easy-to-attach surface usually has a thickness of a few mm. Thus, the barnacle bonds two hard materials, and the distance between the two hard materials is of the order of micrometers. (c) Tubeworm dwells in their inhabiting tube made of natural particulates. The particles are bonded together via tubeworm cement to construct the tube. In the process of construction, the animal picks an appropriate particulate, puts the cement onto it, and pushes it onto the edge of the building tube.

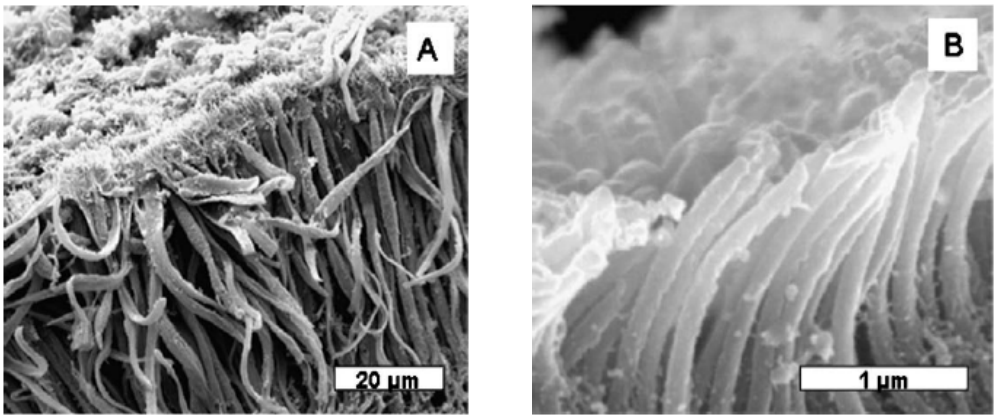

Figure 4 - SEM images from [35] showing detailed nature of foot surface with fibers terminating in nanofibrils: (A) ventral side of tissue consisting of fibers 100 µm in length and 2 µm in diameter, called setae and (B) nanofibrils with ~200 nm diameters.

Finally, the components of mussel adhesive secretion, in particular polydopamine, have been used by Ku *et al.* [36] to control the attachment of cells as discussed in the next paragraph. It should be clear from this short review that the interest for marine adhesion focuses on systems which are rather concentrated ones; they lead to strong and irreversible adhesive interactions. In fact, most of the reversible adhesion of marine animals is provided by suction.

Cell biology

The adhesion of the cells is essential in many steps of their lives (survival, proliferation, migration, differentiation, activation…) and is responsible of many pathological phenomena within an organism. Two situations can be distinguished: in the first one, two cells are stuck together, whereas in the other case, a cell is in contact with another non-living substrate. In both situations, their adhesion is regulated thanks to an extra-cellular polymeric layer called glycocalyx which is composed of proteins and polysaccharides. An equivalent material is found at the surface outside a fish or inside the digestive tract, playing a fundamental role in the absorption of substances.

In this extra-cellular layer, specific proteins such as cadherin or selectin [37,38] (represented on Figure 5) are known to form complexes of very high stability by the multiplication of H-bonds and hydrophobic interactions, leading to a specific molecular recognition for cell-cell binding. This step of attachment is essential for the reproduction of the cells to form a tissue. As a consequence, the optimization of synthetic substrates such as glass or various polymers to favor the binding of cells to grow tissues is essential [39]. Following the same idea, the adhesion of cells on synthetic materials is important for the design of smart scaffolds favoring the re-growth of bones or muscles after a surgery [40]. The absence of adhesion is also of vital issue, for instance in heart surgery: after the replacement of a deficient valve by a synthetic one, no cell should adhere on the new valve, risking to disturb its function and to release potentially harmful blood clots. For instance, Ku *et al.* [36] have used a mussel-inspired surface modification with polydopamine to selectively and locally attach and favor the growth of cells.

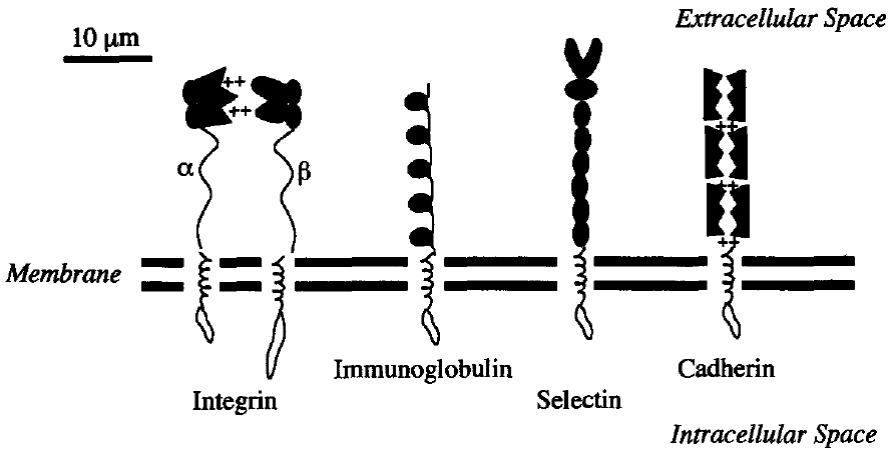

Figure 5 - Schematic diagram of four of the major classes of adhesion receptors, from [37].

Finally, controlling the adhesion of cells and tissue is highly linked to the optimization of the adhesion on the biological tissues, most of which concerns the mucoadhesion. Contrary to the irreversible non-swollen concentrated adhesive systems that were discussed in the case of the adhesive secretions from marine animals, the adhesion of cells involves more dilute materials and reversible interactions.

2-2- Mucoadhesion

The interest for mucoadhesion relies on its possibility to be used in pharmaceutical applications since it is fundamentally linked to the drug delivery issue [41,42]. The objectives of drug delivery are to specifically target the zone which is diseased, a primary objective being to adequately release the active ingredients while the container is attached within this zone for a given residence time. The administration routes can be various, and the localization of the drug deliverer adapted for the application, for instance on the skin (cutaneous or subcutaneous) or by a delivery that can be buccal, ocular, nasal, stomachic, rectal, etc. A lot of experimental data, which consists for instance in screening the optimal gel for optimizing the adhesion with a given mucosa [43], have been carried out, usually for immediate biopharmaceutical applications, but model systems and general features have rarely been studied.

Both water soluble and water insoluble polymers have been used in the first studies on mucoadhesives, either for the synthesis of polymer gels, or under dry forms. In particular, poly(acrylic acid) – that has been used to synthesize model surfaces in this thesis – has been

studied as a reference material in mucoadhesion for almost 30 years [44-46]. Other objects, such as specific proteins, have been used to reproduce the specific adhesion of cells. Their specificity is interesting in the targeting of epithelial tissues.

Taking nature as an inspiration, hydrogels are first-rate model materials for biological and biomedical applications. In-vivo, designed as mucoadhesives [42], both their ability to gradually release a substance by controlled deswelling and their barrier properties are of interest. This is why targeted drug delivery or the acceleration of the processes of burn or wound healing [47] are in the range of their applications. They can also be used for tissue scaffolding [48] or in the design of retinal implants [49]…

2-3- General methodologies for measuring adhesion

The measurement of adhesion or specific interactions between surfaces is classically measured with different normalized tests [2]. Particularly in the case of bioadhesion that mostly concerns soft materials and weak energies of adhesion, the usual tests can be classified into three types of tests. They can be distinguished by the debonding mode that is used to break apart the two materials. These three classes of tests are the peel tests, the shear tests and the tensile tests represented on Figure 6. The shear test is more commonly used to characterize the friction properties between two materials. And the main peel test application in the case of bioadhesion is for the characterization of the adhesion of patches. Then, the most used tests are the tensile tests.

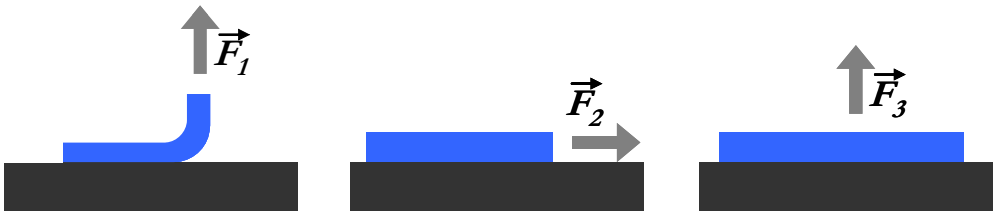

Figure 6 - Schematic representation of the peel (F_1), shear (F_2) and tensile (F_3) forces that can be measured during an adhesion test.

The tensile tests can be macroscopic, involving a standard force machine, or microscopic, using colloidal probe spectroscopy (by micropipette suction, optical tweezers or atomic force microscopy). Macroscopic measurements of the pull-off force have been performed to characterize the adhesion of mussels [34], or the adhesion of retinal implants on pig's

eyes [49]. Hägerström *et al.* [46] proposed flat-flat contact tests to measure the mucoadhesion of gels used in drug delivery systems. Specific measurement methods of tensile tests will be discussed in Chapter 5, the purpose of which is to propose a new macroscopic underwater adhesion test particularly adapted to probe bio- or muco-adhesion.

3- Polymeric systems for modeling underwater adhesion

Polymer layers for modeling cell contact

As already discussed, the external membranes of cells are coated with a layer of swollen polymeric material that contains specific proteins essential to adhesion. This layer, discovered in 1943 by Zobell [50], can be modeled by a polymeric layer. The specific complexation of different proteins at the surface of the cell has been identified and macromolecules such as integrins, cadherins, lectins, etc. are playing a part in the adhesive properties of the cells. When adhering to non-biological surfaces, cells form what is usually called a biofilm. It is usually made of bacteria, algae, fungi or protozoa. They symbiotically settle on the surface and secrete a relatively large amount of adhesive and extra-cellular polymeric matrix. Most of it consists of various polysaccharides (such as cellulose), proteins, lipids and a large amount of water.

This type of extra-cellular secretions can be modeled by simple and synthetic polymeric systems. By selecting the proper polymers, it must be possible to gain further knowledge about the physicochemical parameters that are implied in bioadhesion, in addition to the biological ones.

Targeted drug delivery

Such studies of model systems are fundamental for the improvement of targeted drug delivery. For the transport of classical drugs, the use of gels is common and generally coupled to other systems preventing a too fast diffusion of the active ingredient outside the carrier. In those systems, the drug can be formulated inside spheres, for instance liposomes or surfactant aggregates, or it can be maintained inside the gel by specific interaction with the polymer.

In these cases, the gel beads can be synthesized or coated with a swollen polymeric layer adapted to mucoadhesion [21], as shown on Figure 7. With the purpose of improving drug

delivery, the modeling of the polymeric layer should clarify the processes involved in the adhesion and the residence time of the gels used for targeted drug delivery.

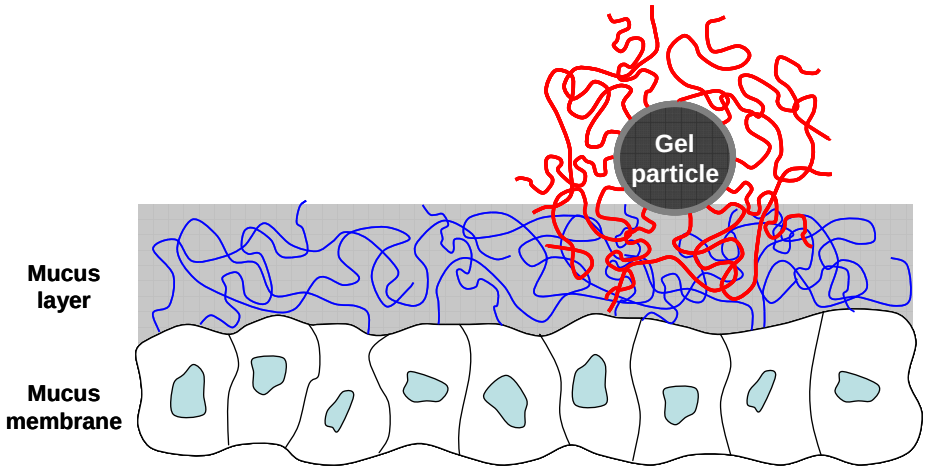

Figure 7 - Schematic diagram representing the interpenetration between tethered chains and mucus gel layer, from [22].

Huang *et al.* [22] in the group of Peppas reviewed the various adhesion theories that usually apply to mucoadhesive systems, that is to say electronic theory, wetting theory, adsorption theory and diffusion theory. They later discussed the theoretical impact of the presence of adhesion promoters, such as grafted polymer chains, for the reinforcement of the gel-gel adhesion [23]. Their goal however is purely qualitative since they aim at optimizing the mucoadhesive properties of their materials. This is why their experiments are carried out using various experimental conditions which make it difficult to give a quantitative interpretation and comparison between the different systems. For instance, some experiments were performed in-air with a 90% relative humidity, and the contact time used was about 15 min and a debonding velocity of 1 $mm.min^{-1}$, but they do not give quantitative measurements, but just variations [51] while quantitative but non-normalized values were given for experiments performed with a 5-min contact time and a debonding velocity of 100 $\mu m.s^{-1}$ [52].

Interactions between tethered polymers: the physicist's approach

Finally, beside their resemblance with biological systems and their use in the materials for drug delivery, the swollen polymers have other interesting features that make them a material of choice as model systems. One of these is the possibility for two polymers to form complexes depending on the solution characteristics. These tunable interactions between polymers have been used to synthesize various objects that usually present temperature or pH

sensitivity. These interactions, that are not strong enough to make complexes between the monomers, are stronger in the polymer systems since the number of interactions per molecule is increased and the translational entropy is lower for a macromolecule than for a small molecule. These interactions can be specifically transferred to interfaces within the purpose of tunable adhesion.

A second interesting point about polymers is their tendency to interact with the presence of secondary interactions. For instance, two polymers interacting primarily through H-bonding may have their complexes reinforced due to Van der Waals or hydrophobic interactions. The proximity of many similar bonds, such as in H-bonded complexes, is often called the "zipper effect". This name suggests that it is not possible to break one bond without breaking the others, which is very energetic. In addition and due to the conformation of polymers, entanglements are expected to occur in these systems.

Many polymer-polymer interaction measurements have been carried out in Klein's group. They use the surface force apparatus (SFA) developed by Israelachvili *et al.* [53] with well-defined polymer-grafted or bare mica surfaces with half-cylindrical shapes. Then, they measured with great accuracy the force and the displacement between the two surfaces schematically represented on Figure 8.

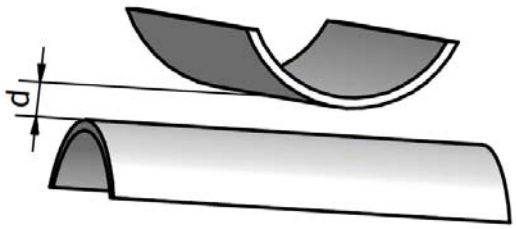

Figure 8 - Schematic representation of the two crossed cylinders of the SFA, and representation of the distance d between them.

In their studies on bare surfaces, they demonstrated that water keeps a high fluidity even when confined to subnanometer films between hard surfaces [54]. During their studies on brush-grafted surfaces, they preferably used the same polymer on both surfaces: the resulting normal interaction forces in good solvent have been found repulsive due to steric effects [55,56], and attractive in poor solvent, as summarized in Figure 9 (see [57] and references therein). In the case of water-soluble polymer, the results are similar, as recently shown by Malham *et al.* [58] on PNIPAM thermosensitive brushes.

The attractive interactions that can be tested in good solvent conditions are observed in sliding experiments when the two brushes are overlapping under compression. In this case, the brushes interpenetrate and the forces measured are mainly due to friction dissipation as they are dragged through the overlap region. For moderate compressions, the interpenetration zone keeps below the entanglement regime. With increasing compression, the overlapping region thickens up to a point where entanglements become predominant [57].

In the case of identical polyelectrolyte brushes in water, the interpenetration is measured and calculated as weak [59] which justifies the particularly low friction between them. Among others, Sokoloff theoretically explained the low friction between charged brushes [60] or charged hydrogels [61] by a mean field approach which emphasizes the role of the osmotic pressure of the counterions of the polyelectrolyte brushes or gels.

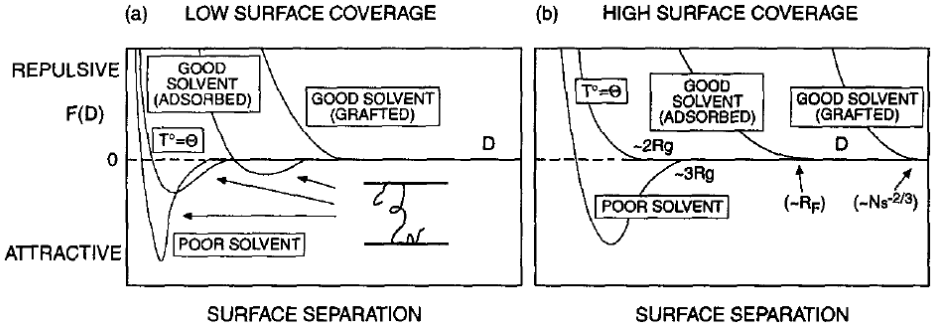

Figure 9 - Schematic summary of equilibrium normal forces between polymer-bearing surfaces as a function of surface separation schematized on Figure 8, from [57].

The SFA allows to perform well controlled experiments between thin grafted polymer layers. However, it remains far from the "real life" cases and, to our knowledge, no specific attractive interactions measurements have been performed between solvated polymeric systems.

However, attractive interactions have been investigated with other experimental setups. For instance in the case of oppositely charged gels, Gong *et al.* [62] performed underwater friction experiments with a rheometer. The adhesive forces between disk-shaped gels under compression submitted to shear were so high that the gels broke during the tests. Recently, La Spina *et al.* [63] performed an underwater JKR-type experiment (described in Chapter 5) to obtain quantitative values of energies of adhesion for a half-spherical lens made of a polyelectrolyte hydrogel put into contact with an oppositely charged planar brush. By using weak polyelectrolytes, that is to say pH-sensitive polymers, they were able to reversibly

change the adhesive properties between the gel and the brush by varying the pH of the immersing solution.

4- Objectives of the thesis

The results obtained from the mucoadhesion tests are disparate since no normalized test is being used. In general, their macroscopic tests of adhesion are pull-off tests that involve at least one gel-like material. One of our objectives is to propose a well-defined, simple and versatile test with a few specifications: the measurements should be performed on soft and swollen materials with an easy-access to the energies of adhesion with a reasonably wide range of magnitudes. To reach this goal, we designed a flat-flat contact test, which gives a simple way to control the contact area.

The polymers showing responsive properties in solution have a strong potential to be used to tune adhesive properties at interfaces. For instance, Malham *et al.* [58] used the reversible volume transition of PNIPAM to change the surface interactions between such brushes; and La Spina *et al.* [63] took advantage of the pH-sensitive electrostatic complexation between a weak polyacid gel and a weak polybase brush to tune their adhesive properties. In both cases, the modification of the adhesive properties is associated with a change in the degree of swelling of the polymer network. Such a change of degree of swelling also affects the mechanical properties of the gel and its dimensions. In the following study we take great care to use a gel which sees only small changes in mechanical and structural characteristics while tuning its adhesive properties.

We then investigate the possibility of synthetically creating tunable adhesion under water. Taking inspiration from the hydrogen bonding complexation of polymers in aqueous solutions, we study the same interactions at the interface between a hard surface, functionalized with a resistant polymeric brush, and a soft and neutral polymer gel.

The work produced in this manuscript can be divided into three parts:

1) Synthesis and characterization of the model systems to be used for the study of underwater adhesion, where the mains goals were:

- The synthesis of environmentally responsive polymeric layers on hard planar substrates, poly(acrylic acid) brushes here, and their structural characterization in various aqueous conditions (Chapter 2).
- The synthesis and characterization of the mechanical and swelling properties of neutral hydrogels; they are made of poly(acrylamide) and poly(*N*,*N*-dimethylacrylamide) (Chapter 3).

2) Characterization of the specific interactions between the chosen polymeric systems (Chapter 4), the study of which was divided into:

- The interactions between polymeric pairs investigated in solution at low concentration to determine the phase diagram of blends of poly(acrylic acid) and poly(acrylamide-*co*-*N*,*N*-dimethylacrylamide) diluted in aqueous solutions.
- The characterization of the sensitivity of the poly(acrylic acid) brush when facing a neutral hydrogel able to form interpolymer complexes.

3) Determination of the underwater adhesion of swollen polymeric objects: a brush and a gel, by the means of:

- The development and the adaptation of a new methodology to perform tensile flat-flat contact tests for the measurement of weak adhesive energies in underwater environments.
- The systematic investigation of the energy of adhesion between the planar poly(acrylic acid) brush and the neutral hydrogels as a function of the nature of the gel, contact time and debonding velocity: the quantitative and reproducible values obtained are then analyzed and some proposals of mechanisms are made.

5- References

[1] Israelachvili, J. N. *Intermolecular and Surface Forces*, 2nd Edition ed.; Academic Press: New York, **1992**.
[2] Pocius, A. V. *Adhesion and Adhesives Technology: an Introduction*, 2nd Edition ed.; Carl Hanser Verlag: Munich, **2002**.
[3] Kendall, K. *Molecular Adhesion and its Applications: the Sticky Universe*; Kluwer: New York, **2001**.
[4] Liu, H. Y.; Zhu, X. X. *Polymer* **1999**, *40*, 6985-6990.
[5] Tanaka, F.; Edwards, S. F. *Macromolecules* **1992**, *25*, 1516-1523.
[6] Dormidontova, E.; ten Brinke, G. *Macromolecules* **1998**, *31*, 2649-2660.
[7] Dormidontova, E. E. *Macromolecules* **2002**, *35*, 987-1001.
[8] Li, B.; Xu, L.; Wu, Q.; Chen, T.; Sun, P.; Jin, Q.; Ding, D.; Wang, X.; Xue, G.; Shi, A. C. *Macromolecules* **2007**, *40*, 5776-5786.
[9] Figueruelo, J. E.; Monzo, I. S.; Gomez, C. M.; Soria, V.; Abad, C.; Campos, A. *Macromolecular Theory and Simulations* **2007**, *16*, 62-76.
[10] Figueruelo, J. E.; Garcia-Lopera, R.; Monzo, I. S.; Abad, C.; Campos, A. *Express Polymer Letters* **2008**, *2*, 313-329.
[11] Soria, V.; Figueruelo, J. E.; Gomez, C. M.; Abad, C.; Campos, A. *Macromolecular Theory and Simulations* **2007**, *16*, 53-61.
[12] Leung, S. H. S.; Robinson, J. R. *Journal of Controlled Release* **1990**, *12*, 187-194.
[13] Hägerström, H. In *Comprehensive Summaries of Uppsala Dissertations from the Faculty of Pharmacy*: Uppsala, **2003**.
[14] Joanny, J. F.; Johner, A.; Vilgis, T. A. *European Physical Journal E* **2001**, *6*, 201-209.
[15] Raphael, E.; Degennes, P. G. *Journal of Physical Chemistry* **1992**, *96*, 4002-4007.
[16] Creton, C.; Kramer, E. J.; Hui, C. Y.; Brown, H. R. *Macromolecules* **1992**, *25*, 3075-3088.
[17] Brown, H. R. *Macromolecules* **1993**, *26*, 1666-1670.
[18] Brochard-Wyart, F.; De Gennes, P. G.; Leger, L.; Marciano, Y.; Raphael, E. *Journal of Physical Chemistry* **1994**, *98*, 9405-9410.
[19] Brochard-Wyart, F.; De Gennes, P. G. *Journal of Adhesion* **1996**, *57*, 21-30.
[20] Leger, L.; Raphael, E.; Hervet, H. *Polymers in Confined Environments* **1999**, *138*, 185-225.
[21] Deascentiis, A.; Degrazia, J. L.; Bowman, C. N.; Colombo, P.; Peppas, N. A. *Journal of Controlled Release* **1995**, *33*, 197-201.
[22] Huang, Y.; Leobandung, W.; Foss, A.; Peppas, N. A. *Journal of Controlled Release* **2000**, *65*, 63-71.
[23] Huang, Y. B.; Szleifer, I.; Peppas, N. A. *Journal of Chemical Physics* **2001**, *114*, 3809-3816.
[24] Leger, L.; Creton, C. *Philosophical Transactions of the Royal Society a-Mathematical Physical and Engineering Sciences* **2008**, *366*, 1425-1442.
[25] Israelachvili, J. N.; Adams, G. E. *Nature* **1976**, *262*, 773-776.
[26] Varenberg, M.; Gorb, S. *Journal of the Royal Society Interface* **2008**, *5*, 383-385.
[27] Vajpayee, S.; Jagota, A.; Hui, C. Y. *Journal of Adhesion* **2010**, *86*, 39-61.
[28] Vreeland, V.; Waite, J. H.; Epstein, L. *Journal of Phycology* **1998**, *34*, 1-8.
[29] Kamino, K. *Journal of Adhesion* **2010**, *86*, 96-110.
[30] Flammang, P.; Lambert, A.; Bailly, P.; Hennebert, E. *Journal of Adhesion* **2009**, *85*, 447-464.

[31] Khandeparker, L.; Anil, A. C. *International Journal of Adhesion and Adhesives* **2007**, *27*, 165-172.
[32] Santos, R.; da Costa, G.; Franco, C.; Gomes-Alves, P.; Flammang, P.; Coelho, A. V. *Marine Biotechnology* **2009**, *11*, 686-698.
[33] Flammang, P.; Ribesse, J.; Jangoux, M. *Integrative and Comparative Biology* **2002**, *42*, 1107-1115.
[34] Burkett, J. R.; Wojtas, J. L.; Cloud, J. L.; Wilker, J. J. *Journal of Adhesion* **2009**, *85*, 601-615.
[35] Lin, A. Y. M.; Brunner, R.; Chen, P. Y.; Talke, F. E.; Meyers, M. A. *Acta Materialia* **2009**, *57*, 4178-4185.
[36] Ku, S. H.; Lee, J. S.; Park, C. B. *Langmuir* **2010**, *26*, 15104-15108.
[37] Hammer, D. A.; Tirrell, M. *Annual Review of Materials Science* **1996**, *26*, 651-691.
[38] Leckband, D. *Cellular and Molecular Bioengineering* **2008**, *1*, 312-326.
[39] Olivieri, M. P.; Wollman, R. M.; Hurley, M. I.; Swartz, M. F. *Journal of Adhesion* **2010**, *86*, 111-130.
[40] Anamelechi, C. C.; Truskey, G. A.; Reichert, W. M. *Biomaterials* **2005**, *26*, 6887-6896.
[41] Leung, S. H. S.; Robinson, J. R. *Acs Symposium Series* **1991**, *467*, 350-366.
[42] Peppas, N. A.; Sahlin, J. J. *Biomaterials* **1996**, *17*, 1553-1561.
[43] Deascentiis, A.; Colombo, P.; Peppas, N. A. *European Journal of Pharmaceutics and Biopharmaceutics* **1995**, *41*, 229-234.
[44] Ishida, M.; Nambu, N.; Nagai, T. *Chemical & Pharmaceutical Bulletin* **1983**, *31*, 1010-1014.
[45] Hagerstrom, H.; Bergstrom, C. A. S.; Edsman, K. *Journal of Pharmacy and Pharmacology* **2004**, *56*, 161-168.
[46] Hagerstrom, H.; Edsman, K. *Journal of Pharmacy and Pharmacology* **2001**, *53*, 1589-1599.
[47] Sekine, T.; Nakamura, T.; Shimizu, Y.; Ueda, H.; Matsumoto, K.; Takimoto, Y.; Kiyotani, T. *Journal of Biomedical Materials Research* **2001**, *54*, 305-310.
[48] Drury, J. L.; Mooney, D. J. *Biomaterials* **2003**, *24*, 4337-4351.
[49] Tunc, M.; Cheng, X. H.; Ratner, B. D.; Meng, E.; Humayun, M. *Retina-the Journal of Retinal and Vitreous Diseases* **2007**, *27*, 938-942.
[50] Zobell, C. E. *Journal of Bacteriology* **1943**, *46*, 39-56.
[51] Peppas, N. A.; Keys, K. B.; Torres-Lugo, M.; Lowman, A. M. *Journal of Controlled Release* **1999**, *62*, 81-87.
[52] Thomas, J. B.; Tingsanchali, J. H.; Rosales, A. M.; Creecy, C. M.; McGinity, J. W.; Peppas, N. A. *Polymer* **2007**, *48*, 5042-5048.
[53] Israelachvili, J. N.; Adams, G. E. *Journal of the Chemical Society-Faraday Transactions I* **1978**, *74*, 975-&.
[54] Raviv, U.; Laurat, P.; Klein, J. *Nature* **2001**, *413*, 51-54.
[55] Taunton, H. J.; Toprakcioglu, C.; Fetters, L. J.; Klein, J. *Nature* **1988**, *332*, 712-714.
[56] Taunton, H. J.; Toprakcioglu, C.; Fetters, L. J.; Klein, J. *Macromolecules* **1990**, *23*, 571-580.
[57] Klein, J. *Annual Review of Materials Science* **1996**, *26*, 581-612.
[58] Malham, I. B.; Bureau, L. *Langmuir* **2010**, *26*, 4762-4768.
[59] Raviv, U.; Giasson, S.; Kampf, N.; Gohy, J. F.; Jerome, R.; Klein, J. *Langmuir* **2008**, *24*, 8678-8687.
[60] Sokoloff, J. B. *Journal of Chemical Physics* **2008**, *129*, -.
[61] Sokoloff, J. B. *Soft Matter* **2010**, *6*, 3856-3862.

[62] Gong, J. P.; Kagata, G.; Osada, Y. *Journal of Physical Chemistry B* **1999**, *103*, 6007-6014.
[63] La Spina, R.; Tomlinson, M. R.; Ruiz-Perez, L.; Chiche, A.; Langridge, S.; Geoghegan, M. *Angewandte Chemie-International Edition* **2007**, *46*, 6460-6463.

CHAPTER 2 – POLY(ACRYLIC ACID) BRUSHES: SYNTHESIS, CHARACTERIZATION AND STRUCTURE

This first experimental chapter focuses on the synthesis of pH-sensitive polymer brushes of poly(acrylic acid) (PAA) on hard silicon substrates. We use a “grafting onto” approach which allows the synthesis of polymer brushes of well-defined molecular weight and of varying grafting densities. This choice is motivated by the good reproducibility of this type of synthesis and by its simplicity. Then, we propose a handy brush synthesis method, which is based on the use of very small amounts of commercial end-functionalized polymer chains and which is easily implementable by the polymer physicist.

This synthesis is performed in three steps. The first one consists in the formation of a self-assembled monolayer of an epoxy-functionalized silane. Then, a protected version of the poly(acrylic acid) chains as poly(t-butyl acrylate) are anchored on the epoxydes by annealing. Finally, the conversion of the ester into the acid is performed *in situ* either by acid hydrolysis or pyrolysis. These steps have to be performed carefully and we have determined the best synthesis conditions to obtain PAA brushes. For instance, if the conversion is carried out by hydrolysis, it is responsible for a partial degrafting of the polymer chains and the pyrolysis must be performed on a passivated surface at the risk of prolonging the annealing step.

After the presentation of the optimization of this synthesis, we obtain different brushes made of short chains only, or bimodal brushes with short chains and long chains of varying grafting densities. The structure of these systems is investigated by neutron reflectivity to determine the structures of the synthesized systems through the polymer density profiles. Since PAA is a weak polyelectrolyte, the swelling behavior of the brushes is investigated at various pH and is compared with the scaling laws from the theoretical predictions corresponding to the adapted neutral and charged brush regimes.

Polymer layers have important applications in the modification of the physical and chemical properties of a substrate [1,2]. Grafted, adsorbed or coated, the polymer layer can provide a modification in interfacial properties such as wetting properties [3,4], lubrication [5], or adhesion [6,7]. They are also used to shield the surface from corrosion, to enhance the response of sensors or to stabilize colloidal dispersions.

A layer of polymer in which each chain is end-attached to a substrate is considered as a brush when the grafting density is high enough so that the chains are stretched away from the surface [8]. Then, the distance between contiguous grafting points D is smaller than the radius of gyration of the polymer chains R_G, as shown in Figure 1. At the opposite, when the chains can be considered as isolated from each other (for $D > 2R_G$), the polymer layer is in the mushroom regime.

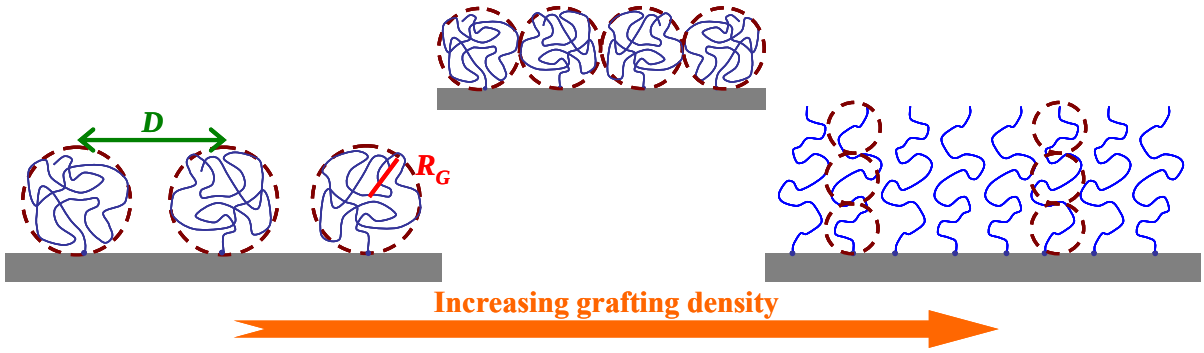

Figure 1 - Schematic representation of end-grafted polymer chains: from a low grafting density in the mushroom regime to a higher grafting density in the brush regime through the transition (for which $D = R_G$) mushroom to brush regime.

Two main routes are used to build these covalently end-attached polymer systems. We distinguish here physisorption, where the anchoring of the chains is physical, from chemical methods which lead to irreversible and resistant grafted layers.

For physical anchoring, polymers are adsorbed on a surface using a specific interaction with the substrate. A classic case is that of amphiphilic block copolymers [3,9]. The use of physisorption often leads to well-controlled systems but presenting a poor resistance toward the modification of environmental conditions (solvent vapors, heat…).

Far more robust, the covalent anchoring can be obtained by the “grafting onto” or by the “grafting from” method, represented on Figure 2. In the “grafting from” synthesis, the polymer chains are directly grown from the surface on which a monolayer of initiator has

been attached. In the “grafting onto” method, pre-formed polymer chains with a specific end-function are attached to a (modified) substrate through a chemical reaction. With this latter method, obtaining high grafting densities remains difficult since the diffusion of the whole polymer chains to the surface is concerned whereas in the “grafting from” method, only the diffusion of the monomers (small molecules) plays a part.

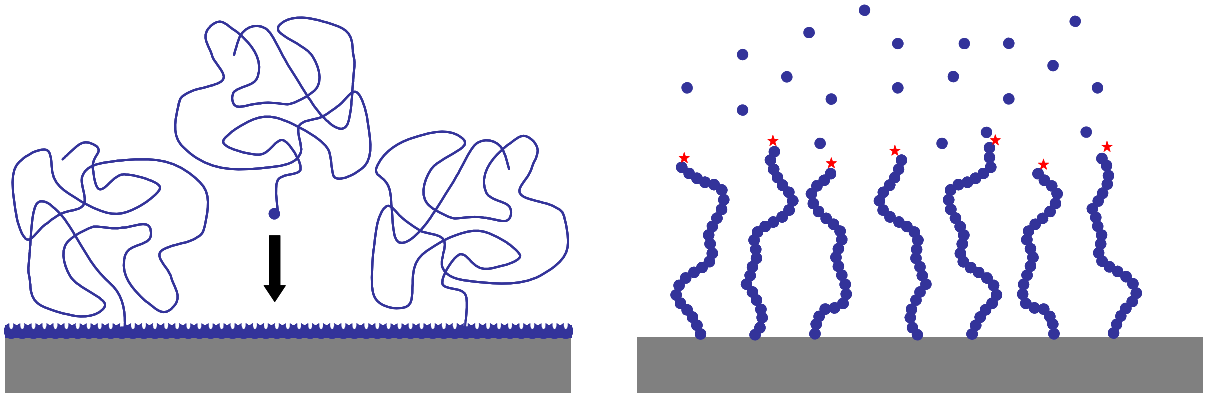

Figure 2 - Schematic representation of the two routes for the chemical anchoring of polymer brushes. On the left, the “grafting onto” technique and on the right, the “grafting from” technique are represented.

Among all sorts of coatings, the stability of end-grafted polymer systems and the responsiveness of adaptive and environment-sensitive macromolecules have attracted many studies [1,10-12]. The interest for tunable brushes has been granted in many areas, from biology to sensors [4,13-17]. For instance, poly(N-isopropylacrylamide) is a temperature-sensitive polymer, which undergoes a reversible lower critical solution temperature (LCST) phase transition around 32°C in water, from a swollen conformation at low temperature to a collapsed state at high temperature [18-23]. The conformation of weak polyelectrolytes is sensitive to the pH and to the ionic strength of the solution in which they are immersed. Poly(acrylic acid) focuses most experimental studies on weak polyacid brushes [3,9,24-34]. Their conformational behavior as a function of pH is expected to undergo a transition from a good solvent conformation when the chains are uncharged at low pH (pH<<pKa) to a stretched conformation at high pH (pH>>pKa), when the chains are completely ionized [35].

1- Synthesis of poly(acrylic acid) brushes: "grafting onto" method

In the present study, we have chosen to prepare poly(acrylic acid) grafted surfaces following a "grafting onto" method. This choice is motivated first by the good reproducibility of this type of synthesis, and by the possible characterization of the functionalized polymer chains before grafting. In addition, controlling a "grafting from" synthesis often requires an excellent background in polymerization techniques, while the purpose of this synthesis is to propose a handy brush synthesis method easily implementable by the polymer physicist. With the "grafting onto" method, starting from a substrate and end-functionalized polymer chains, we end up with a polymer grafted surface. Two different paths are possible to reach this objective.

Either the polymer chain is terminated with a chemical function able to react directly on the bare substrate. This is the case for thio-functionalized polymers on gold surfaces, or for chlorosilane-terminated polymers on mica or silicon substrates [36].

The polymer end-group may not be able to react directly on the bare substrate. Then, the chain ends can be modified to become reactive with the substrate. Or, the substrate can be coated with a self-assembled monolayer which modifies the chemical composition of the surface of the substrate in such a way that it can react with the end-function of the polymer.

In this work, a silicon substrate was modified with an epoxy-functionalized silane able to react with a carboxy-terminated poly(tert-butylacrylate) (PtBuA) chain [37-39]. The PtBuA-grafted surface is then converted in a PAA grafted surface after the removal of the *tert*-butyl group through acid hydrolysis [26,27,31,40,41] or pyrolysis [29,42-44]. This synthesis is described in details along the next paragraphs.

1-1- Choice of the substrate

For many reasons, we have chosen to work on silicon wafers as model substrates. Besides its relative low cost and its availability, the silicon wafer – made out of a monocrystal – is smooth at the atomic scale and bears at its surface a 15 Å-thick layer of native silica. On top of it, silanol functions are chemically reactive with different types of small molecules including some silanes with which they form covalent bonds.

The interaction between radiation and silicon are also very adapted for a wide range of characterizations. As the silicon wafers are atomically smooth and the interface air-silicon is

totally reflective for the UV-visible or the neutron wavelengths, a silicon monocrystal is perfectly adapted for characterization techniques of the interfacial structure such as ellipsometry or neutron reflectivity. As it is transparent for infrared wavelengths (from 1 500 cm^{-1} to 4 000 cm^{-1}) infrared spectroscopy in attenuated total reflectance (IR-ATR) gives access to the infrared spectrum (and possibly the chemical composition) of the first microns deposited on the silicon substrate. As it is also almost transparent for neutrons, reflectivity can also be used to characterize the interface between silicon and a liquid.

The geometry of the silicon monocrystals used for this study was strongly dependent on the characterization technique being used. Although ellipsometry can be carried out on any type of reflective and atomically smooth substrate, for IR-ATR we used silicon monocrystals shaped as Dove prisms and polished on all faces. A Dove prism is an isosceles right-angle prism where the zone containing the right-angle has been truncated parallel to the non-truncated face. The non-truncated face measures 70×10 mm^2 and the trapezoidal face has a base dimension of 70 mm and a height of 1.5 mm. For neutron reflectivity, we used silicon monocrystals, either shaped as rectangular parallelepiped (or cuboid) of dimensions 100×50×10 mm^3 polished on the largest faces or classical silicon wafers with a 2-inch diameter and a 3 to 5 mm thickness, polished on a single side.

Prior to any chemical modification of the silicon surface, it is necessary to activate the silanol functions of the native layer of silica. For this purpose, the substrates were cleaned in a freshly prepared “piranha” solution (70 vol% of sulfuric acid (>95%), 30 vol% of hydrogen peroxide (35%)) heated at 150°C. The silicon substrates were immersed in this very exothermic and oxidative solution until ebullition stopped (20 to 30 min). Piranha is supposed to remove all traces of pollutants. The substrates were then extensively rinsed in Milli-Q water and sonicated in Milli-Q water during 1 min and finally dried under nitrogen.
At this point, the thickness of the silica layer was measured by ellipsometry: different measurements performed on the same sample must give a thickness lower than 20 Å with a standard deviation lower than 10% of the mean thickness.

1-2- Formation of self-assembled monolayers

On their surface, silicon substrates bear specific and reactive functions, silanol sites naturally present at the surface of the wafer. Thanks to these sites, it is possible to synthesize a self-assembled monolayer (SAM) of small molecules. The molecules we have grafted on silicon are mono- or tri-functional silanes. They have two sides: the first one is able to react on the silanol function being on the silicon wafer, and the second side is the side of interest, either functionalized to extend the chemical modification, or of specific characteristics to modify the physical properties of the substrate. The chemistry of the silanes enables a wide range of chemical modifications.

In the presence of a small amount of water, silanes can react with each other. The use of mono-functional silanes leads to a better-defined SAM since the single function can either react on the surface or with another silane. Tri-functional silanes can cross-link together and react on the surface at the same time. However, in the right conditions, the SAM obtained with tri-functional silanes are tougher than the ones synthesized from mono-functional silanes [45,46].

The chlorosilane functions are more reactive than the methoxysilanes. These silanes react with the silanol function on the surface of the silicon wafer via hydrolysis of the chloro- or methoxy-silane to a silanol function, and then condensation of this silanol on a silanol on the surface: siloxane Si–O–Si bonds link the surface and the grafted molecules.

For the synthesis of the polymer brushes, we have chosen an epoxy-functionalized trimethoxysilane: the 3-glycidoxypropyltrimethoxysilane (GPS, Figure 3) [37,47].

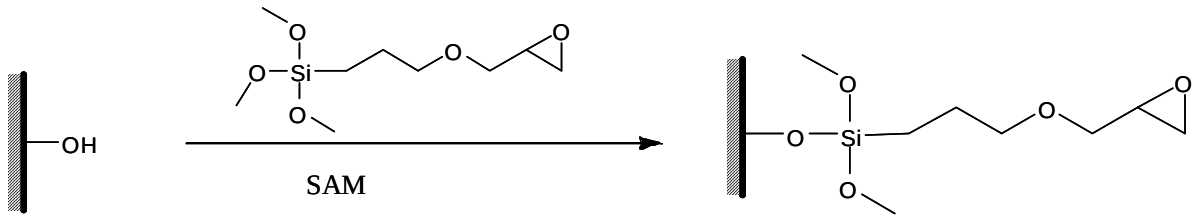

Figure 3 - Silanization of the surface with 3-glycidoxypropyltrimethoxysilane (GPS).

Clean and rejuvenated surfaces are stored in a reactor under nitrogen. A solution containing 2 vol% of GPS in extra-dry toluene is transferred in the reactor so that the wafer samples are immersed. The reaction is left to proceed at room temperature during 5 hours and then, the silicon samples are rinsed in two different baths of toluene, sonicated 30 seconds each time, and finally dried with a nitrogen flux.

The GPS layer grafted on the surface is quantified by ellipsometry. The measured thicknesses are 9 Å ± 2 Å. With the hypothesis that we obtain a dense SAM, it is possible to evaluate the theoretical thickness assuming that all bonds are carbon-carbon bonds, that is to say 8 bonds:

$$\gamma_{th} = 8 \times 1{,}5 \times \sin\left(\frac{110}{2}\right) \approx 10 \text{ Å}.$$

The experimental thicknesses are in good agreement with the predicted value.

1-3- Grafting of PtBuA and of PNIPAM chains

Once the SAM of epoxy-terminated silane has been synthesized, polymer chains can be grafted on the surface. To this purpose, the terminal carboxylic acid functions of polymer chains are used to react with the epoxy functions of the surface. We use a method combining spin-coating and annealing. The principle is represented Figure 4.

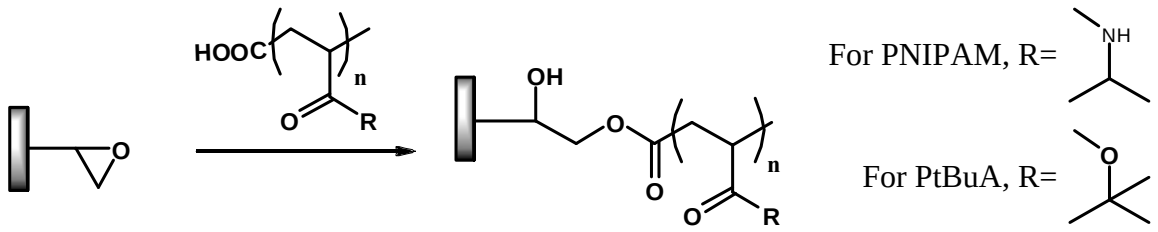

Figure 4 - Schematic of the synthesis of the end-grafting of PNIPAM or PtBuA chains on an epoxy-modified silicon wafer.

The polymer is dissolved at 1 wt% in filtered tetrahydrofurane (THF). A film is obtained either by spin-coating the solution on the wafer samples at 2 000 rpm during 30 seconds or by solvent evaporation. The thickness of this reservoir film is about 120 nm by spin-coating or higher than 700 nm by solvent evaporation.

To vary the grafting density, both the relative concentration between carboxy-terminated chains and inactive chains in the solution and the duration of the annealing have been adapted. Then, for the synthesis of PNIPAM brushes, the samples are heated in an oven under vacuum at 150°C during a predefined duration. During this step, it is necessary to heat enough so that the temperature of annealing is:

- higher than the glass transition temperature of the polymer (for PNIPAM, $T_g \approx 130°C$): the mobility of the chains is enhanced and the probability for a carboxylic acid termination to react with an epoxide on the surface increases;

- higher than the temperature needed to have the reaction occurring between the terminal carboxylic acid of the polymer chain and the epoxy of the pre-treated surface.
- lower than the temperature of degradation of the polymer.

PtBuA is susceptible to degradation at high temperature and the conversion of PtBuA in PAA can be carried out by pyrolysis as will be described later. However, if the PtBuA is degraded during the annealing step, the carboxylic acids formed along the polymer chain may be able to react on the still unoccupied epoxy functions at the surface, leading to the formation of loops. The temperature of annealing must be therefore chosen carefully: the highest possible to favor the grafting and low enough to prevent the degradation of PtBuA. To determine the best temperature of annealing, we have performed a thermo-gravimetric analysis (TGA) on a PtBuA sample. On the Figure 5 are represented both temperature and the normalized mass versus time. It clearly appears that PtBuA starts to degrade at 150°C (heating rate is equal to 5 K/min) and the weight loss corresponding to the full conversion of PtBuA into PAA can be reached at 200°C. The annealing temperature has been chosen above the glass transition temperature of PtBuA which was found to be 43°C by TGA and below 150°C, that is to say at 120°C for a predefined duration.

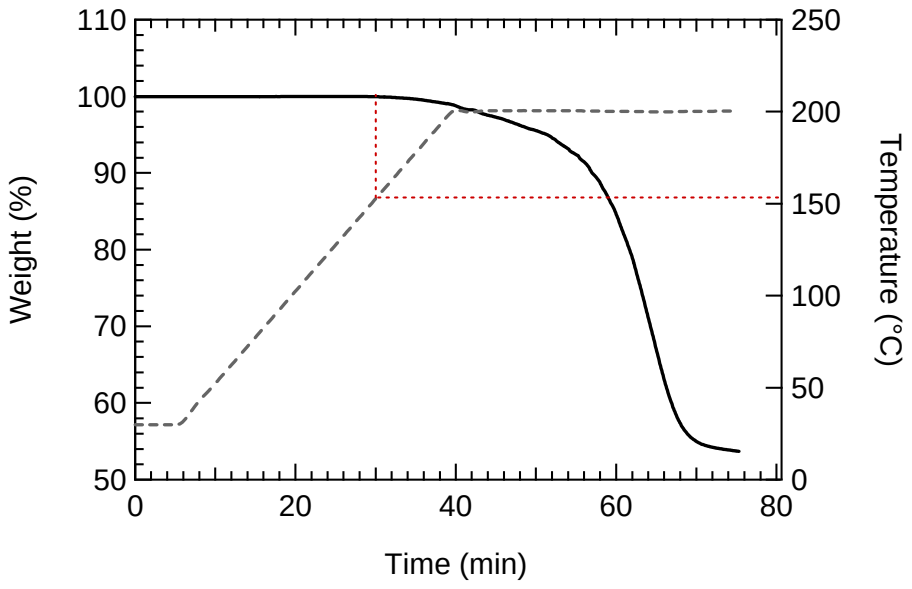

Figure 5 - Thermogravimetric analysis of a PtBuA sample.

The non-reacted polymer chains are removed from the surface: the samples are immersed in THF during one hour at least, sonicated and immersed in a second bath of THF. They are finally sonicated a second time and dried under nitrogen.

The dry thickness of the polymer layer γ is then measured by ellipsometry; the average distance between grafting points D and the density $\sigma = D^{-2}$ is deduced.

Average measurements obtained for PNIPAM- and PtBuA-coated surfaces are detailed in Table 1.

Polymer	M_n (kg.mol^{-1})	% COOH-terminated	Annealing duration	γ (Å)	σ (nm^{-2})	D (Å)
PNIPAM	96	100	24 h	103	0.090	33
PtBuA	6.5	100	24 h	45	0.450	15
	42	100	24 h	93	0.140	26
	42	10	1 h	40	0.062	40

Table 1 - Synthesis conditions and characteristics of the polymer layers: the dry thickness γ, the grafting density σ and the average distance between grafting points D.

From the thickness of the dry grafted layers it is possible to deduce the grafting density σ. Let D be the average distance between two grafting points; it is also the average cross-length occupied by a chain on the surface and it is related to the grafting density by $\sigma = D^{-2}$. For one single chain, it is then possible to express the density as:

$$\rho = \frac{M}{N_A \gamma . D^2} \qquad \textbf{Eq. 1}$$

where N_A is the Avogadro's number and M is the molar mass of the polymer. Hence, we obtain:

$$\sigma = \frac{1}{D^2} = N_A \frac{\gamma\rho}{M} \text{ or } D = \sqrt{\frac{M}{N_A . \gamma\rho}} \text{ or } \sigma(nm^{-2}) = 60.2 \frac{\gamma(\text{Å}) \times \rho(kg.L^{-1})}{M(g.mol^{-1})}.$$

We take from the literature $\rho_{PNIPAM} = 1.17 g/cm^3$ [48] and $\rho_{PtBuA} = 1.08 g/cm^3$.

The distance D can be then compared with the radius of gyration of the chain R_G:

$$R_G = \left(\frac{C_\infty n l^2}{6} \right)^{1/2} \qquad \textbf{Eq. 2}$$

where $n = 2N$ is twice the number of monomers in the chain and $l = 1.54\,\text{Å}$ is the carbon-to-carbon distance. For both polymers, the value of C_∞ can be found in the literature [49]: it is equal to $C_\infty = 9.9$ for PtBuA and $C_\infty = 10.6$ for PNIPAM.

Comparing the radius of gyration (Table 2) and the distance between contiguous grafting points (Table 1), it appears that in each case, the grafted layer is in the brush regime ($D < R_G$). But for low grafting densities of long chains PtBuA-42k, the transition to the mushroom regime is close.

Name	Polymer	M_n (kg.mol^{-1})	N	R_G (Å)
PNIPAM	PNIPAM	96	848	84
PtBuA-6.5k	PtBuA	6.5	51	20
PtBuA-42k		42	328	51

Table 2 - Radius of gyration of the PtBuA and PNIPAM chains.

Finally, we can determine the structure of PtBuA-grafted chains using neutron reflectivity. This technique (depicted in Annex), allows the determination of the structure of polymeric brushes at the solvent-silicon interface. The structure obtained from reflectivity can then be used to determine the behavior of the brush in a solvent. In fact, because of the sensitive behavior of PtBuA to exposure to high temperature, we make sure that the PtBuA is not degraded in PAA during the pyrolysis and that multi-points anchoring and loops are not present.

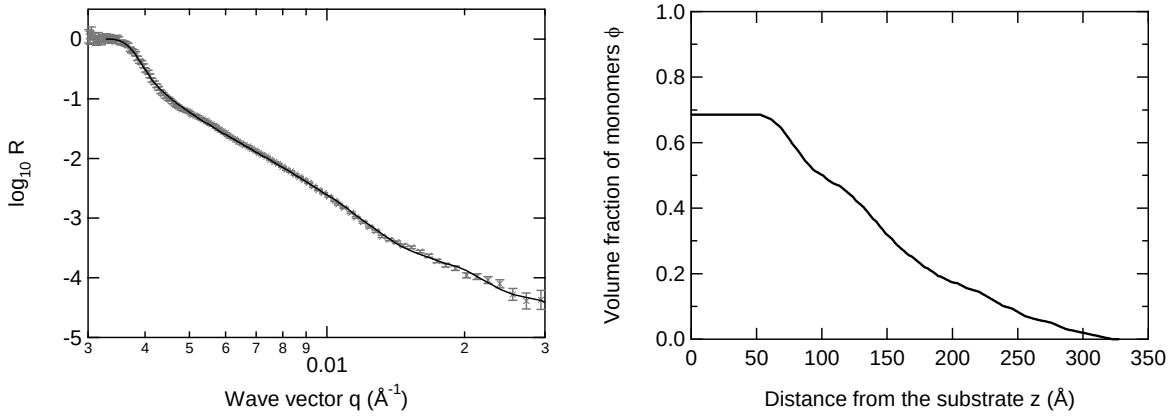

Figure 6 - Experimental and fitted neutron reflectivity data (left) and density profile of the grafted PtBuA layer immersed in $CDCl_3$ (right).

Figure 6 shows the neutron reflectivity curve obtained for the PtBuA-42k grafted layer (γ = 93 Å, σ = 0.140 nm^{-2}) immersed in a good solvent: the deuterated chloroform $CDCl_3$. The best fit plotted leads to a density profile of monomer which is soft and typical of a profile of a polymer brush. The mean swollen thickness h is about 180 Å and the brush is stretched up to 250 Å. It corresponds to a swelling ratio h/γ in deuterated chloroform $CDCl_3$ around 2 (see 2-5-).

The whole profile can be associated with a PtBuA brush in good solvent.

1-4- Conversion of PtBuA brushes into PAA brushes via acidic hydrolysis

After the first step consisting in the synthesis of PtBuA brushes, the PtBuA chains are converted in PAA by the de-protection of the t-butyl ester group. This last step can be realized either by hydrolysis or by pyrolysis.

The hydrolysis is a classical step in the synthesis of free chains of PAA in solution, even if PAA can be directly synthesized by some controlled radical polymerization such as NMP, or RAFT – or ATRP if synthesized in its ionized poly(sodium acrylate) form. Performed at the surface, the hydrolysis is a bit trickier.

The hydrolysis of PAA can be carried out either in acidic or basic conditions, but as silica starts to dissolve in basic conditions (pH > 10), the acidic conditions are preferred. Unfortunately, even if silica is preserved, other side reactions are possible:

1) Siloxane Si–O–Si bonds can be weakened, which means that PtBuA hydrolysis can be accompanied by a degrafting of the chains.

The best conditions for a total hydrolysis and a minimal degrafting have been determined in previous studies: the hydrolysis of poly(t-butylmethacrylate) has been widely studied by Sarah Sanjuan [50], and completely validated by Elodie Siband [51] for the hydrolysis of PtBuA brushes. Based on their work, the procedure can be briefly summarized as follows. For a PtBuA brush made of long chains (M_n = 42 000 g/mol) with a grafting density of 0.14 chains.nm^{-2} (γ = 80 Å), it has been shown that the hydrolysis in an aqueous solution of trifluoroacetic acid (concentration: 1.30 mol.L^{-1}) at 60°C during 130 hours was total [51]. The resistance ratio can then be evaluated at 48%, which corresponds to a resulting grafting density of PAA of about 0.07 chains.nm^{-2} (γ = 25 Å).

2) When formed during the hydrolysis, acrylic acid units can in principle react on the still present epoxy functions of the surface, leading to the formation of loops.
However, this hypothesis is unlikely since the reaction between carboxylic acids and epoxides must be thermally activated. In addition, the presence at high concentration levels of trifluoroacetic acid suggests that if this reaction took place, epoxide groups would react preferentially with trifluoroacetic acid instead of acrylic acid units.
The fact remains that this process must be adapted for each grafting density as the accessibility of t-butyl groups and of siloxane bonds becomes easier as the grafting density decreases. For instance, when applied to a PtBuA brush with a grafting density equal to 0.07 chains.nm^{-2}, the same procedure has led to a total degrafting of the chains.
Very recently, Lego et al. [41] proposed a new hydrolysis process. They claimed that no weakening of the siloxane bonds (on mica) happened during the immersion of the PtBuA brushes in a solution of trifluoroacetic acid in dichloromethane at 8.9 vol% during 12 hours at room temperature.

1-5- Conversion of PtBuA brushes into PAA brushes via pyrolysis

This procedure has been first proposed by Treat *et al.* [42] in Brittain's group. Starting from PtBuA brushes synthesized by ATRP, they converted PtBuA in PAA by heating the samples at 190-200°C during 30-90 min under vacuum, and by immersing them in Milli-Q water.
The main difference between their procedure and ours is the way the brush was synthesized as we used a "grafting onto" technique.
In our case, the PtBuA-grafted surfaces were put in the oven under vacuum at 200°C during a set reaction time, then removed, rinsed with Milli-Q water and dried under nitrogen. The duration of the pyrolysis treatment is a critical parameter and we have performed preliminary tests, during either 2 or 24 hours, on long PtBuA brushes (M_n = 42 kg.mol^{-1}). The samples have been characterized by neutron reflectivity.
Starting from PtBuA brushes with average thicknesses of 70 and 75 Å, we finally got PAA layers with very different sizes: 30 Å and 59 Å after a 2 h and a 24 h pyrolysis, respectively. The neutron reflectivity curves obtained with these samples immersed in heavy water equilibrated at pH 9 are given Figure 7, with the volume fraction of monomers corresponding to the best fit of experimental data. The latter is represented as a function of the distance from

the substrate z. In order to make the comparison easier, the volume fraction of monomers has also been plotted as a function of the swelling ratio z/γ. Actually, the layers obtained after pyrolysis have very different thicknesses, even if the initial PtBuA thicknesses were very close.

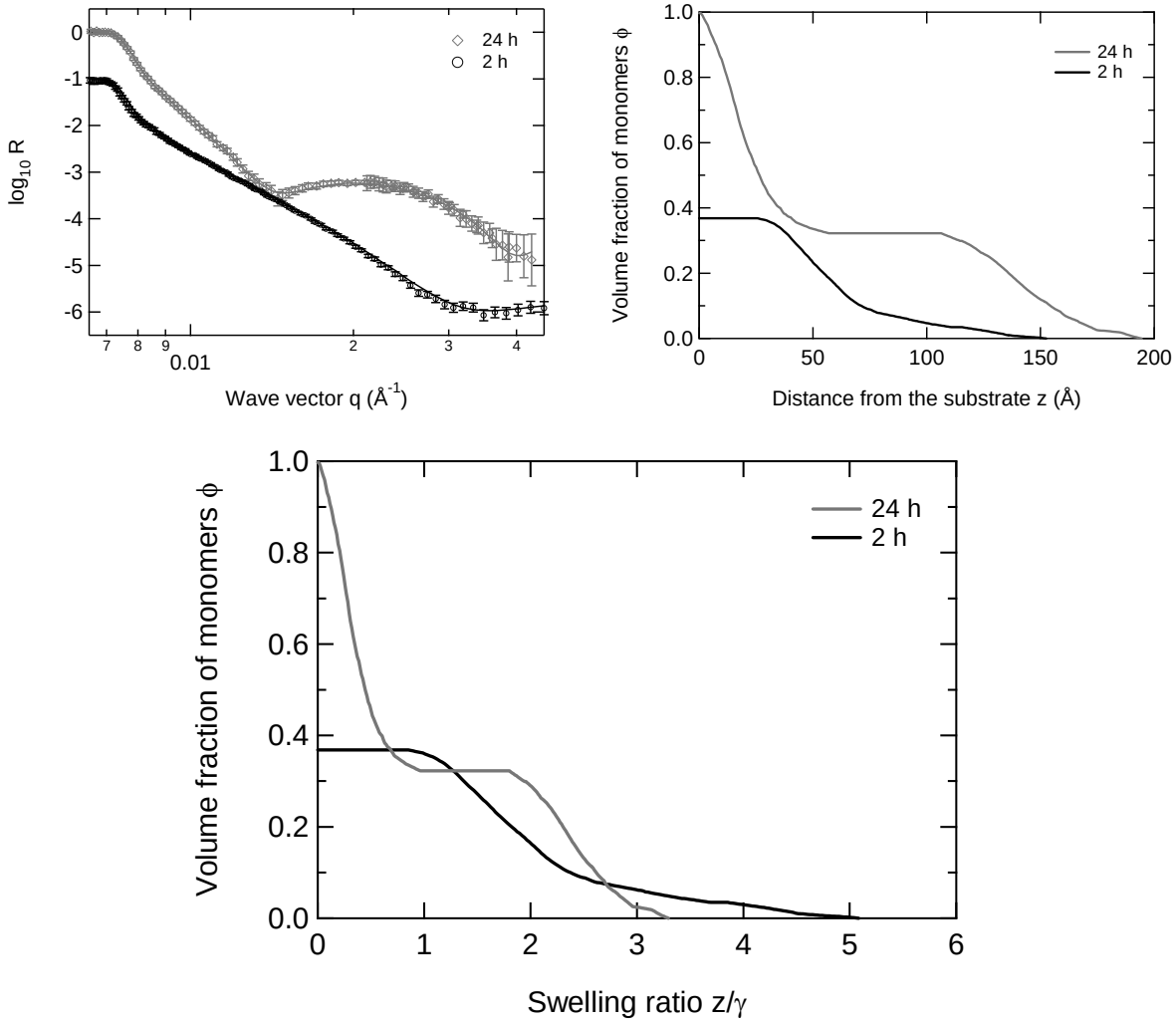

Figure 7 - Neutron reflectivity curves of pyrolyzed layers of PtBuA (left). Corresponding profiles of the volume fraction of monomers (right). The profiles are plotted as a function of swelling ratio to facilitate the comparison between them (bottom). The grey curves are obtained after a 24 h pyrolysis and the black curves after a 2 h pyrolysis.

The density profile of the sample which has undergone a 2 h pyrolysis is very stretched away from the substrate. At the surface, the volume fraction of monomer is equal to 0.37, which means that the polymer is highly swollen. The swelling ratio is equal to 2.5. Comparatively, the sample obtained after a 24 h pyrolysis shows a non-swollen layer close to the substrate with a very high monomer concentration, and the swelling ratio of the polymer layer is equal to 2. It has to be noted that an incomplete conversion from PtBuA to PAA is not a possibility since in this case the density profile at the surface would be at a higher volume fraction of

monomers than 1 since the neutron scattering density of acrylic acid was used for the calculation of the profile density[i]. Moreover, on top of the dense layer of the 24 h-pyrolyzed sample, one can observe a swollen layer that is stretched away from the surface but which remains quantitatively less extended than the polymer layer obtained after a 2 h pyrolysis.

The conclusion is that the measured monomer density profile of the sample pyrolyzed during 24 h is incompatible with the formation of PAA brushes and we propose two side-reactions which could lead to the formation of the dense zone near the surface:
1) The acrylic acids units formed along the chain are able to react with the remaining epoxide functions still present at the surface and may lead to the formation of loops instead of linear extended chains,
2) Neighboring carboxylic acid functions can dehydrate and form anhydride bridges, leading to the formation of a chemically cross-linked network with a lower swelling ability.

To avoid the "back-biting" of the PtBuA chains on the surface during the pyrolysis at 200°C, we have chosen to carpet the epoxy-functionalized surface by adding small reactive chains (M_n ~ 4 200 g/mol, N = 28) after the grafting of the long chains, to hinder the access to the surface for the long chains [36]. For the grafting of the short chains, we follow the same preparation method. After spin-coating of a reservoir film of PtBuA short chains, the wafer is let 24 to 48 hours in an oven under vacuum at 120°C, and after removal, the sample is rinsed thoroughly and dried under nitrogen.
The new PtBuA thickness is measured by ellipsometry.

After each step, the polymer layer obtained at the surface of the silicon wafer was characterized using ellipsometry, neutron reflectivity and IR-ATR. The results obtained by neutron reflectivity are widely presented in 2-.

On Figure 8 are represented the IR spectra of the polymer grafted layer after each step of the conversion of PtBuA brushes into PAA brushes, between 1 500 and 3 500 cm^{-1}.

[i] PtBuA has a lower neutron scattering density than PAA, a collapsed PtBuA layer would lead to a volume fraction of monomer equal to 1.45.

PtBuA corresponds to curve (a); we emphasize the presence of a thin strong peak at 1 728 cm^{-1} characteristic of the stretching of the C=O double bond of the ester group, and the importance of the peak of the asymmetric stretching of CH_3 at 2 980 cm^{-1}.

After pyrolysis, we obtained the spectrum (b) consistent with a great amount of PAA. However, the small peak at 1 802 cm^{-1}, next to the broader peak at 1 757 cm^{-1} corresponding to the stretching of the C=O double bond of the acid function, can be attributed to the stretching of the C=O double bond of anhydrides.

To perform the hydrolysis of anhydrides, we have chosen to immerse the sample in water equilibrated at pH 2 to favor the acidic mechanism of the hydrolysis of anhydrides. The immersion in water at pH 2 overnight led to the spectrum (c). In addition to the disappearance of the peak at 1 802 cm^{-1}, the peak at 1 757 cm^{-1} is shifted at 1 740 cm^{-1}, and the signal of the O–H stretching is intensified due to the inter-acid bonding.

We finally checked that we obtained tunable brushes by changing the pH. After an overnight immersion at pH 9, we obtained the spectrum (d) corresponding to the spectrum of poly(sodium acrylate): the two CO bonds of the COO- functions are equivalent, excited at the same frequency leading to a Fermi resonance and a doubling of the C=O bands with the presence of a peak at 1 572 cm^{-1}. As the labile acid hydrogen does not remain present in the basic form of PAA, the O–H stretching is no longer visible.

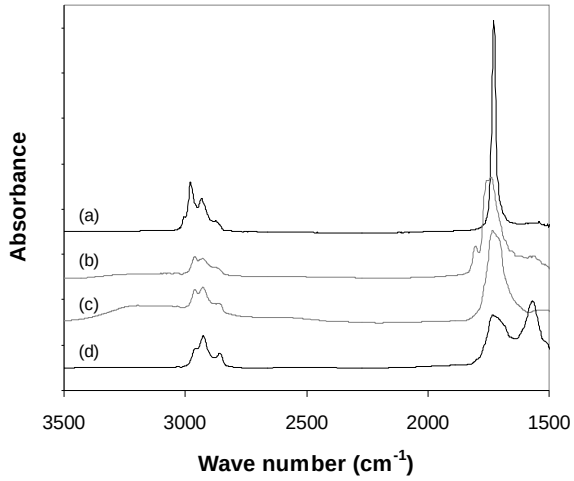

Figure 8 - FTIR-ATR spectra of the PtBuA brush (a) and the PAA brush obtained by the pyrolysis reaction (b). The PAA brush was then put in an aqueous solution at pH 2 (c) and pH 9 (d).

The hydrolysis has many disadvantages: the process is long (130 h) and must be adapted for each grafting density since a degrafting of the chains occurs as a side-reaction of the conversion of PtBuA into PAA. On the contrary, the pyrolysis method lasts only 2 h, can be

performed on any type of system as long as the access of the longer chains to the surface is hindered by a carpeting of short chains. Therefore, we choose the pyrolysis method for the conversion of PtBuA brushes into PAA brushes.

1-6- Conclusion: a "grafting onto" synthesis route for PAA brushes

In this part, we have described and studied the formation of PNIPAM, PtBuA and PAA brushes. The carboxylic acid termination of polymer chains has been successfully used to form end-tethered polymeric layers on silicon substrate. Since the synthesis of PAA brushes has proven to be particularly delicate, we focus our conclusion on the following steps that describe it. Some of them are summarized on Figure 9:

- The formation of a self-assembled monolayer of GPS is carried out on the silicon substrate.
- A micron-thick polymer film acting as a reservoir with a thickness of about a micron was deposited on the modified silicon wafer.
- The brush was then easily obtained by a thermal treatment with a temperature adapted to the specific polymer brush being prepared. It is equal to 120°C for PtBuA which is thermally sensitive.

To obtain a PAA brush from a PtBuA brush, the usual acidic hydrolysis reaction is not the best way since a partial degrafting occurs concurrently to the main de-esterification process. On the contrary, the pyrolysis reaction has proven to be more efficient and far easier to carry out. However, the pyrolysis being a second thermal treatment, at a higher temperature than the annealing step leading to the PtBuA grafting, it can lead to the formation of new carboxylic acid groups. Therefore, a prior deactivation of the epoxy-functionalized surface with very short PtBuA chains is recommended.

- The substrate is carpeted by these short reactive PtBuA chains following the same procedure as used for the long ones. They sterically hinder the surface from the formation of loops by stretching the long chains away from the surface.
- Finally, a pyrolysis at 200°C under vacuum can be performed to convert the PtBuA long and short chains into a PAA brush, with the shortest duration possible, evaluated around 2 h.

- Then, an overnight immersion of the brushes in water equilibrated at pH 2 removes the anhydrides formed during the pyrolysis.

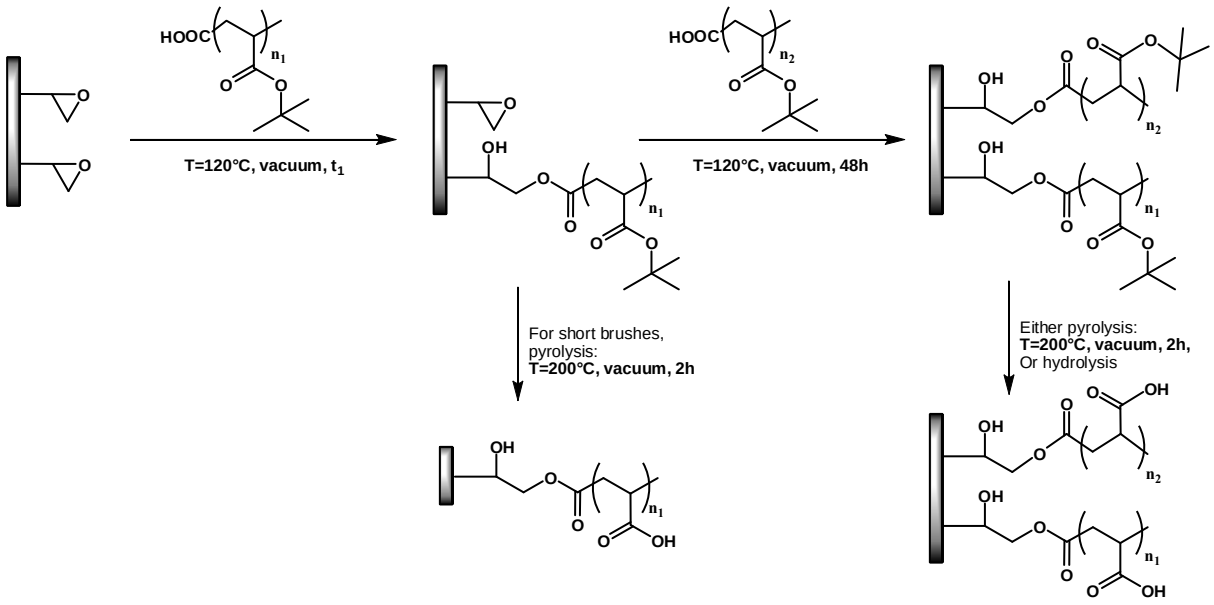

Figure 9 - Synthesis of the PAA brushes. On the epoxy-functionalized silicon wafers, the grafting of the long carboxy-terminated PtBuA (degree of polymerization DP equal to n_1) is first realized by a thermal annealing of duration t_1. If shorter chains are to be grafted, a second identical step is performed (DP n_2 = 33, duration t_2 = 48 h). Finally, the PtBuA brush is converted into a PAA brush by an acid hydrolysis (130 h) or a pyrolysis (2 h) reaction, followed by a soft hydrolysis consisting of an immersion in an aqueous solution at pH 2.

We give in the following Table 3 the characteristics of the brushes synthesized during this study. One was a PNIPAM brush, and we distinguish 5 types of PAA brushes: the first one is made of PAA chains with a molar mass of 3650 g.mol^{-1}, that we call short chains; the others are bimodal brushes composed of long chains of molar mass 23 610 g.mol^{-1} and of short chains 10 times smaller (M_n = 2 360 g.mol^{-1}). For one sample, the conversion of PtBuA into PAA was realized by hydrolysis instead of pyrolysis.

The brush samples were given names containing the polymer name. For PAA, the sample converted by hydrolysis was denominated PAA-h. For the other samples, PAA is followed by two letters: the first one accounts for the presence of short chains only (s) or the presence of short and long chains (l); the second one indicates the grafting density of the longest chains (with d for dense, m for medium and s for sparse).

These samples will be further used in the next section of this Chapter for their swollen behavior in aqueous solutions, in Chapter 4 for the study of interfacial interactions of gels on brushes, and in Chapter 6 for the measurement and characterization of macroscopic adhesion.

Brush obtained	Sample name	M_{n1} (g.mol^{-1}), t_1	γ_1 (Å)	γ_2 (Å)	$\gamma_{tot} = \gamma_1 + \gamma_2$ (Å)
PNIPAM	PNIPAM	96 000, 24 h	103 ± 5	-	103 ± 5
PAA-short	PAA-s,d	3 650, 24 h	20 ± 2	-	20 ± 2
PAA-hydrolyzed	PAA-h	23 610, 24 h	19	2	21
PAA-sparse	PAA-l,s	23 610*, 0.5 h	8 ± 1	14 ± 1	23 ± 2
PAA-medium	PAA-l,m	23 610*, 1 h	25 ± 2	8 ± 1	33 ± 2
PAA-dense	PAA-l,d	23 610,24 h	44 ± 5	4 ± 2	45 ± 5

Table 3 - Synthesis conditions and thicknesses of polymer brushes.

(*): 10% only of the PtBuA chains grafted by thermal treatment are carboxy-terminated.

2- Structure of the brushes

When end-tethered to a surface, polymer chains exhibit a different conformation from the one they have in solution or adsorbed at interfaces. When a hydrogel is put in contact with an interacting polymer brush, it may have a structural influence on the conformation of the brush. So, as a prerequisite to the study (at a molecular level) of the effect of a hydrogel adhering on the PAA brushes synthesized during the first part of this chapter, knowing the structure of the brushes in water is essential to our study.

Depending on the characteristics of the polymer brush and on its environment, the brush has a different conformation [52], which is given by the polymer density profile $\phi(z)$ normal to the interface between the solid surface and the solvent. It corresponds to the local monomer concentration in a layer at a distance z from the interface. From the profile, one can calculate the dry thickness γ of the polymer layer, equal to the zero-th order moment of $\phi(z)$ (or the integral of the profile), and the mean height of the brush h proportional to the normalized first order moment of $\phi(z)$:

$$\gamma = \int_0^{+\infty} \phi(z).dz \,, \qquad \textbf{Eq. 3}$$

$$h = 2\frac{\int_0^{+\infty} z.\phi(z).dz}{\int_0^{+\infty} \phi(z).dz} \,. \qquad \textbf{Eq. 4}$$

Moreover, h can be directly measured or determined using a surface force apparatus (SFA) or a multi-wavelength ellipsometer. As a consequence, the specific swelling properties of polymer brushes, given by h/γ, can be studied without the determination of the polymer density profile $\phi(z)$.

To investigate the conformation of the brushes, neutron reflectivity is certainly the best technique as it probes the polymer density profile $\phi(z)$ at the solid-liquid interface. Many theoretical papers have been published predicting the form of the density profile (and the mean height of the brush), starting with scaling approaches [53-55], self-consistent field [56,57] or classical theory [58-61], Monte Carlo [62,63] or Molecular Dynamics [64] simulations, for a large number of interfacial polymeric systems. Here, we limit our presentation to the different regimes that can be found, working with end-attached PAA chains.

In the following discussion, we first give a brief reminder of the predicted behavior of neutral polymer and polyelectrolyte chains end-attached to a flat substrate and immersed in a good solvent. These two different states can be readily observed with poly(acrylic acid) brushes which are widely used for their tunable properties in water. At high pH, the monomer units are ionized and the PAA chain behaves as a polyelectrolyte; while at low pH, the protonated carboxylic acids are uncharged and PAA behaves as a neutral chain in good solvent [27,30].
After this short introduction, we will briefly describe the basics of neutron reflectivity for polymeric systems at the solid-liquid interface and we will apply this technique to probe the structure of different systems based on end-grafted pH-sensitive PAA chains and to determine their density profiles. Different types of PAA grafted surfaces were synthesized: we can distinguish the one made of short chains with a high grafting density from those with longer chains on top of a carpet of short chains. Various grafting densities of long chains are studied, from a low grafting density giving an access to clear bimodal profiles to higher grafting densities where the influence of the short chains becomes negligible. These different brushes are detailed in Table 3, page 58.

2-1- Theoretical predictions for neutral polymer and polyelectrolyte planar end-attached systems

Neutral end-attached polymers

For end-attached polymeric chains, scaling arguments early distinguished two regimes, presented on Figure 1: mushroom or brush, depending on the grafting density σ.
In the mushroom regime, the chains are grafted at low density and are isolated. As the neighboring chains do not overlap, the polymer adopts a coil conformation, similar to the macromolecular conformation in good solvent and characterized by its Flory [65] radius:

$$R_G \propto bN^{3/5} \qquad \textbf{Eq. 5}$$

with b the Kuhn segment length and N the polymerization degree of the chain. In this situation, the distance between two grafting sites D is higher than $2R_G$ and as a consequence the grafting density is lower than the critical grafting density:

$$\sigma^* \propto \frac{N^{-6/5}}{b^2} \qquad \textbf{Eq. 6}$$

In the brush regime for $\sigma > \sigma^*$, polymer chains are closer to one another so that they overlap but for excluded volume reason, they tend to organize by stretching away from the surface. Their conformation results from a competition between the monomer-monomer interaction and the entropic elasticity of the polymer chain.

A third regime, which will not be described much here, arises when the polymer has a grafting density in the range of the mushroom regime and a strong affinity to the surface so that the chain has a great tendency to adsorbing on it: this regime is called the pancake regime and the polymer chains lie flat on the surface with an extension parallel to the surface comparable to that of the lateral extension of the coil in the mushroom regime $2R_G$ [12,66].

De Gennes [55] first proposed a scaling approach to predict the profile of the neutral end-attached polymer chains. Some of these results can be obtained by a Flory approach, which is described below. Following Alexander's hypotheses, assuming that the polymer density profile ϕ is constant inside the brush:

$$\phi = \frac{N}{h.D^2} = \frac{N\sigma}{h}, \qquad \textbf{Eq. 7}$$

and that the chain-ends are located at the distance h from the surface, we can write the free energy of a chain by summing two terms: the entropic loss due to stretching and the repulsive density energy due to monomer-monomer interactions. The first term is proportional to $(h/R_0)^2$, with $R_0^2 = Nb^2$ the mean square end-to-end distance of the coil and the second term scales like the squared monomer density ϕ times the excluded volume parameter ν_2 integrated on the volume of a chain $hD^2 = h\sigma^{-1}$. Flory's approximation then leads to the free energy per chain [65]:

$$\frac{F}{kT} = \frac{h^2}{Nb^2} + \nu_2 \left(\frac{N\sigma}{h}\right)^2 h\sigma^{-1}. \qquad \textbf{Eq. 8}$$

The minimization of the free energy with respect to h gives the equilibrium height which scales as:

$$h \propto Nb.\left(b^2\sigma\right)^{1/3}. \qquad \textbf{Eq. 9}$$

Then, for overlapping chains, the mean height varies linearly with the polymerization degree, which emphasizes the clear stretching of the chains. At the critical grafting density σ^* for which the chains are unperturbed by their neighbors, we find that $h \propto R_G$ by inserting Eq. 6 in Eq. 9, as it is expected.

From Eq. 9 and the expression of the volume of a chain in the brush in dry conditions ($Nb^3 \propto \gamma D^2 = \gamma\sigma^{-1}$), it is possible to obtain a variation of the swelling ratio of the brush h/γ which allows quantifying the stretching of the chains in a solvent. It is found independent of the polymerization degree and its expression emphasizes the importance of the grafting density:

$$\frac{h}{\gamma} \propto N^0 \left(b^2\sigma\right)^{-2/3}. \qquad \textbf{Eq. 10}$$

This scaling approach is a start for predicting the mean height of the brush h and its swelling ratio as it has been confirmed by experiments, self-consistent field theory and simulations.

However, the Alexander-De Gennes scaling approach cannot describe precisely the polymer density profile, since it is assumed to be constant in the starting hypothesis.
For the brush regime, the full mean-field calculation from Netz and Schick [58,59] gives results which expand the previous works by Milner *et al.* [56,67] or Skvortsov, Zhulina *et al.* [60,61,68] who have found that the density profile for a polymer planar brush in good solvent should be parabolic, with a form:

$$\phi(z) = \phi_0\left(1-\left(\frac{z}{l}\right)^2\right) \text{ for } z \le l, \qquad \textbf{Eq. 11}$$

where ϕ_0 is the density at the surface and l is the maximum extension of the brush. Different modifications of the first model have been brought to modify the end of the profile, adding for instance a short Gaussian tail to the parabolic profile, positively supported by Monte Carlo and Molecular Dynamics simulations, self-consistent field theory and experiments. For instance, Shull [69] proposed an analytical form from self-consistent field calculation which takes into account the dispersion of chain-ends by using a hyperbolic tangent:

$$\phi(z) = \frac{\phi_0}{2}\left(1+\tanh\left(2\frac{z_0-z}{\psi}\right)\right), \qquad \textbf{Eq. 12}$$

where ϕ_0 is the density at the surface, z_0 is the height verifying $\phi(z_0) = \phi_0/2$ and ψ is linked to the width of the profile. A comparison between this profile and the parabolic profiles can be observed on Figure 10.

To describe mushroom regime, De Gennes approach focuses on the region $b \le z \le R_G$. The value of the profile starts from the fraction of grafting points at the lower limit

($\phi(z=b)=b^2.\sigma$). The monomer volume concentration at $z=R_G$ is equal to the one inside a single coil b^3N/R_G^3 weighted by the surface fraction of the wall covered by polymer coils $R_G^2/D^2=\sigma R_G^2$, hence:

$$\phi(z=R_G)=b^2.\sigma.N^{2/5}. \qquad \textbf{Eq. 13}$$

A scaling law for $\phi(z)$ can be proposed with the generic form:

$$\phi(z)=b^2.\sigma.\left(\frac{z}{b}\right)^m. \qquad \textbf{Eq. 14}$$

The unknown exponent m can be determined as $m=2/3$ using both Eq. 13 and Eq. 14. Then, for $z>R_G$, the concentration profile drops down rapidly and Field *et al.* [70] have proposed to keep the scaling law proposed by De Gennes and to add a decreasing exponential factor as:

$$\phi(z)=A.\left(\frac{z}{b}\right)^{2/3}\exp(-\alpha.z), \qquad \textbf{Eq. 15}$$

where A and α are parameters that can be determined experimentally by fitting neutron reflectivity data with this type of profile. Here, the proposed profile clearly shows a depleted layer at the surface, directly coming from the hypothetic concentrations at the limits $z=b$ and $z=R_G$. However, this type of profiles obtained by scaling arguments is not supported by the full mean-field calculation [58,59] which gives a decreased importance to the depleted layer, which is often highly diminished or even removed.

Charged end-attached polymers

Numerous theoretical studies have been developed concerning the structure of charged end-attached brushes in the last 20 years (see [52,66,71] and references therein). Here, we focus on the theoretical background needed to fully interpret the results that can be obtained for PAA brushes immersed in water at pH 9 with no added salt. Since pH 9 is very superior to the pK_a of the PAA brush, it can be considered as a strong polyelectrolyte brush of poly(sodium acrylate) swollen in water at low ionic strength.

The first theoretical predictions were conducted using a Flory-type approach [65], using simplifying hypotheses. They give relationships between the mean height of the brush and its chemical characteristics (polymerization degree, charge density of the chains, grafting density of the brush) and environment (e.g. ionic strength). If for neutral brushes, only two terms are

taken into account (entropic loss due to stretching and the repulsive energy due to monomer-monomer interactions), in the case of polyelectrolyte brushes, the long-ranged Coulomb electrostatic interactions and the distribution of counter-ions play additional roles. Depending on the conditions, Pincus [72] proposed different scaling laws for the behavior of polyelectrolyte brushes by distinguishing different regimes by their counter-ions distribution. With Borisov *et al.* [73], Pincus [72] proposed a scaling law for the mean height h of the brush in the "osmotic regime", where the attractive chain elasticity is balanced by the repulsive osmotic counter-ion pressure (which is far higher than the negligible monomer-monomer exclusion). It corresponds to a polyelectrolyte brush with a high grafting density for which the counter-ions are located inside the brush to satisfy the local electroneutrality. In particular, it corresponds to the case of our concern. The osmotic pressure Π_{osm} due to the distribution of counter-ions confined inside the brush is proportional to the number density of charges on the polymeric chains (supposed equal to the number of polymerization degree N here) and we can write:

$$\Pi_{osm} \propto kT \times \frac{N}{hD^2}, \qquad \textbf{Eq. 16}$$

with D the distance between two grafting sites.

The pressure due to the elasticity of the chains Π_{el} can be deduced from the first term of Eq. 8 which corresponds to the free energy due to elasticity. Once normalized by the volume of a chain, the following expression is obtained:

$$\Pi_{el} \propto \frac{kT}{hD^2} \times \frac{h^2}{Nb^2}, \qquad \textbf{Eq. 17}$$

with b the monomer size.

The balance of the two effects leads to a mean height which varies as follows:

$$h \propto Nb. \qquad \textbf{Eq. 18}$$

The linear variation with the polymerization degree is identical to the variation obtained for neutral brushes. However, the mean height is independent of the grafting density: each chain is stretched by the osmotic pressure of its counter-ions and remains unperturbed by the neighboring chains.

From Eq. 18 and the expression of the volume of a chain in the brush in dry conditions ($Nb^3 \propto \gamma D^2 = \gamma\sigma^{-1}$), the variation of the swelling ratio of the polyelectrolyte brush is found independent of the polymerization degree with the form:

$$\frac{h}{\gamma} \propto N^0 \left(b^2 \sigma\right)^{-1}. \qquad \textbf{Eq. 19}$$

The scaling approach developed here is limited to our case and, as a consequence, very simplistic: it does not account for very low grafting densities, it assumes that all monomers are ionized and it considers that no salt is added to the immersing aqueous solution.

These results have been confirmed by Wittmer *et al.* [74]: they used the Flory approach (developed earlier for neutral brushes) with a box-model and minimized the total free energy as a function of the mean height, taking into account the electrostatic force.

Self-consistent field theories developed by Zhulina *et al.* [73,75,76] and simulations [77-79] confirmed the scaling laws previously obtained and gave access to the analytical form of the monomer density profile of the polyelectrolyte brushes. It is well described by a Gaussian function over a wide range of solvent quality:

$$\phi(z) = \phi_0 \exp\left(-\frac{z^2}{l^2}\right), \qquad \textbf{Eq. 20}$$

where ϕ_0 is the density at the surface and l is a specific length of the profile. Figure 10 shows a typical representation of this profile.

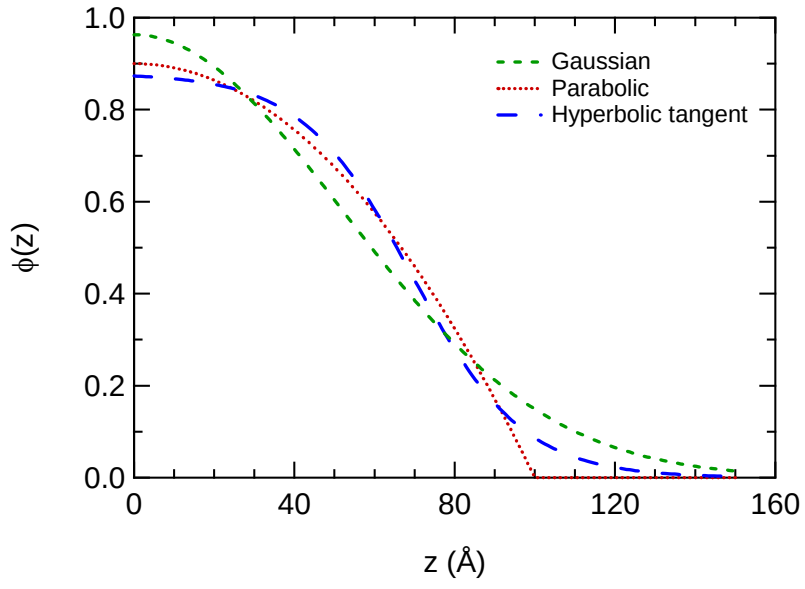

Figure 10 - Theoretical profiles of polymer brushes: for polyelectrolytes, the Gaussian profile is plotted; for neutral brushes, parabolic profile and hyperbolic tangent based profile are compared.

Determination of the mean height and thickness of the brush for theoretical profiles

The polymer fraction profile obtained from the neutron reflectivity experiments $\phi(z)$ can be fitted by using the theoretically expected profile, that is to say a parabolic profile or a tanh-derived profile for a neutral brush, and a Gaussian profile for an ionized brush. The equations and the fitting parameters are given in Eq. 11, Eq. 12 and Eq. 20. From the expression of the profile, it is possible to calculate the thickness of the dry brush γ from Eq. 3 and its mean height from Eq. 4. In the Table 4 below, we recall the expression of the profiles and give the expressions of the corresponding dry thickness and of the mean height, which will be further used for the deconvolution of the profiles of bimodal brushes.

Type	Expression	γ (Å)	h (Å)	
Parabolic	$\phi(z)=\phi_0\left(1-\left(\frac{z}{l}\right)^2\right)$ for $z \le l$	$\gamma=\frac{2}{3}\phi_0 l$	$h=\frac{3}{4}l$	**Eq. 21**
Tanh-derived	$\phi(z)=\frac{\phi_0}{2}\left(1+\tanh\left(2\frac{z_0-z}{\psi}\right)\right)$	$\gamma=\phi_0 z_0$	$h=z_0\cosh\left(\frac{2}{\pi}\frac{\psi}{z_0}\right)$ [ii]	**Eq. 22**
Gaussian	$\phi(z)=\phi_0\exp\left(-\frac{z^2}{l^2}\right)$	$\gamma=\frac{\sqrt{\pi}}{2}\phi_0 l$	$h=\frac{2}{\sqrt{\pi}}l$	**Eq. 23**

Table 4 - Theoretical profiles obtained for neutral (parabolic and tanh-derived) and ionized (Gaussian) brushes. They are associated with the expressions of the dry thickness of the brush and of the mean height.

2-2- Short brushes

For this section, short PAA brushes (PAA-s,d in Table 3) have been synthesized as described in the first part of this chapter. During the synthesis, the PtBuA dry thickness was measured by ellipsometry and the grafting density was calculated. The PAA dry thickness was measured at the end of the synthesis. We give in Table 5 the characteristics of these brushes. They consist of short PAA chains grafted with a rather high density.

[ii] The mean height for the tanh-derived profile is an approximation for $2\psi \le z_0$, otherwise, numerical calculation is carried out.

pH	M_n (g.mol^{-1})	γ (Å)	σ (nm^{-2})	D (Å)
2	3650	19	0.422	15
9				

Table 5 - Characteristics of the poly(acrylic acid) brush made of short chains: molar mass M_n, dry thickness γ, grafting density σ and mean distance between grafting points D.

The reflectivity data obtained on these systems are presented on Figure 11-left with their best fits. The absence of pronounced Kiessig fringes in the reflectivity data suggests that the corresponding polymer density profiles are soft. They are shown in Figure 11-right.

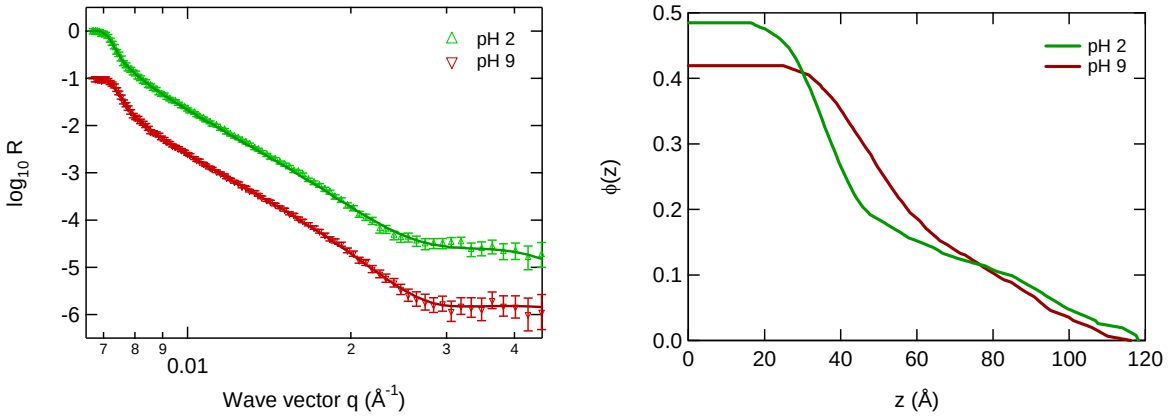

Figure 11 - Neutron reflectivity curves (left) and profiles of volume fraction of monomers (right) corresponding to the best fit of the reflectivity data. The samples are described in Table 5.

From the profile, the mean height h of the swollen brush has been calculated and found equal to 66 Å at pH 2 and 70 Å at pH 9. It is then possible to deduce the mean volume fraction inside the brush $\bar{\phi}$ as $\bar{\phi}.h = \gamma$ and the swelling ratio of the brush h/γ, which are in Table 6. The swelling behavior found experimentally is in good agreement with what we expected.

At pH 2 in deuterium oxide, the PAA chains are expected to be uncharged and in good solvent. At pH 9, the PAA chains are totally ionized and then its profile is expected to be more stretched.

The swelling ratio obtained at pH 9 (equal to 3) is in good agreement with the values expected from previous work on PMAA brushes performed by Sarah Sanjuan [50]. She effectively found that the swelling ratio of ionized PMAA brushes at pH 9 followed a single scaling law independent of the molar masses, which should give an expected swelling ratio equal to 2.5 for the brushes studied here.

The swelling ratios obtained at pH 2 and at pH 9 are close, which is expected at high grafting density when the scaling variation of the swelling ratio of the brush in good solvent (in $\sigma^{-2/3}$) crosses the one of the polyelectrolyte brush in water (in σ^{-1}), which will be discussed in 2-5-, page 75.

pH	h	$\bar{\phi}$	h/γ
2	66	0.35	2.87
9	70	0.33	3.04

Table 6 - Mean characteristics deduced from the poly(acrylic acid) brush density profile: mean height of the brush h, mean volume fraction $\bar{\phi}$ and swelling ratio h/γ.

2-3- Long chains on top of short brushes

As previously discussed concerning the carpeting of the surface with short PAA chains, we have synthesized PAA layers with very low grafting densities for the long chains, on top of a dense carpet of short chains, the PAA-l,s brushes (see Table 3).

pH	M_n (g.mol^{-1})	γ (Å)	σ (nm^{-2})	σ^{tot} (nm^{-2})	D (Å)	γ^{tot} (Å)
2	2360	14	0.456	0.48	14	22
	23610	8	0.024			
9	2360	13	0.422	0.45	15	22
	23610	9	0.029			

Table 7 - Characteristics of the poly(acrylic acid) brushes. For each molar mass M_n are given the corresponding thickness γ and the grafting density σ. Then, the total grafting density σ^{tot}, the mean distance between two grafting points D and the total thickness γ^{tot} are listed.

The neutron reflectivity data obtained at pH 2 and 9, and the corresponding polymer density profiles are shown in Figure 12, while the characteristics of the sample are listed in Table 7. For the PAA-l,s brushes, the grafting density of the long chains represents about 5-7% of the total grafting density and their dry thickness is equal to one third of the total dry thickness. Due to the relatively large amount of short chains at the surface, a two-step profile is expected. Close to the surface, an extensively stretched profile is expected for both long and short chains on a distance corresponding to the mean height of the short chains h_S. For

distances higher than h_S, only the long chains are playing a role and as a consequence, an adapted profile at low concentration has to be found (see Figure 12-right). It first can be noticed, on Figure 12-left, that the two reflectivity data collected at pH 2 and at pH 9 are not that different, so the profiles expected must be similar. The best profiles fitting the data (Figure 12-right) are in agreement.

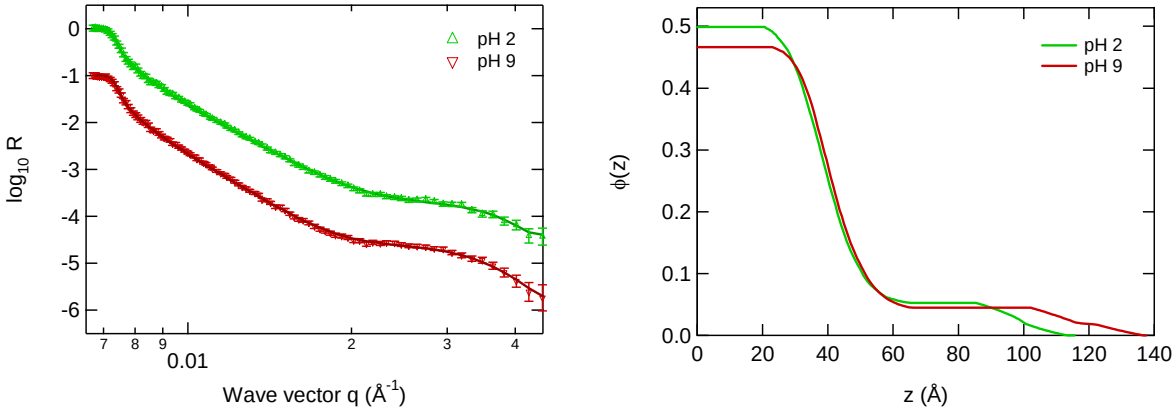

Figure 12 - Neutron reflectivity curves (left) and polymer density profile (right) corresponding to the best fit of the reflectivity data. The samples are described in Table 7.

The profile obtained at pH 2 was fitted successfully with a double-tanh-derived form:

$$\phi(z) = \frac{\phi_{0S}}{2}\left(1+\tanh\left(2\frac{z_S - z}{\psi_S}\right)\right) + \frac{\phi_{0L}}{2}\left(1+\tanh\left(2\frac{z_L - z}{\psi_L}\right)\right), \qquad \textbf{Eq. 24}$$

where ϕ_{0S}, ϕ_{0L}, z_S, z_L, ψ_S and ψ_L are the parameters to be determined. The profile and the fits are shown on Figure 13 where the part of the profile attributed to the short chains has been separated from the one due to the long chains. Here, the profile of the long chains is assumed to be unperturbed by the presence of the short chains.

It is possible to evaluate the quality of the fit by comparing – for both the long chains and the short chains – the dry thicknesses obtained from the tanh-derived fits using Eq. 22 and the dry thicknesses measured by ellipsometry. With this simple deconvolution, the integral of the short chains gives a dry thickness a bit overestimated at 17 Å and the one of the long chains is underestimated at 5 Å. Then the average characteristics of the profile (average heights h, volume fractions $\bar{\phi}$ and the swelling ratio h/γ) can be deduced for both chain lengths.

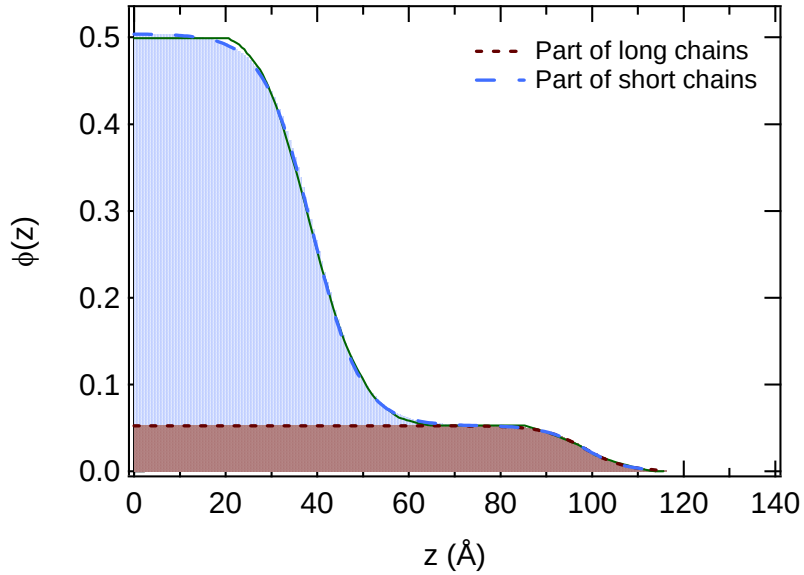

Figure 13 - Density profile of the PAA-l,s brush immersed at pH 2 and described in Table 7. The curve is fitted with Eq. 24 and the contribution of the long chains is distinguishes from the short chains. The filled areas correspond to the thicknesses of each contribution.

So, to go deeper in the analysis, the mean heights of the short chains $h_S = 41$ Å and of the long chains $h_L = 99$ Å have been calculated. The deduced swelling ratio for the short chains is equal to 2.86, which corresponds exactly to what was found for the short chains grafted with a similar density in the PAA-s,d brushes in the previous paragraph. For the long chains, the swelling ratio is equal to 13.0 which is consistent with theoretical expectations.

The same approach is doable at pH 9. Due to the form of the profile, we have not used a Gaussian function to fit the part of the profile attributable to the short chains, but the tanh-derived function was preferred. This choice is first motivated by the shape of the obtained profile, and then because of the high grafting density and the shortness of the chains, which do not allow to make a strong difference between neutral and charged brushes as previously shown in 2-2- and further discussed in 2-5-. For the long chains however, the common hypothesis for bimodal brushes [63,80-83] consists of considering that the presence of the short chains is at the origin of an additional stretching of the long chains, the profile of which is related to the distribution of chain-ends of the short chains. Here, we make the very simplified hypotheses that for distances where the short chains are not negligible, the profile of the long chains is constant due to the high density of monomers close to the surface and then decreases following a Gaussian shape. This hypothesis is summed up in Eq. 25, and the profile and its fits are represented on Figure 14.

$$\phi(z) = \frac{\phi_{0S}}{2}\left(1+\tanh\left(2\frac{z_S - z}{\psi_S}\right)\right) + \begin{cases} \phi_{0L} \text{ for } z \le z_S \\ \phi_{0L}\exp\left(-\frac{(z-z_S)^2}{l_l^2}\right) \text{ for } z \ge z_S \end{cases} \cdot \qquad \textbf{Eq. 25}$$

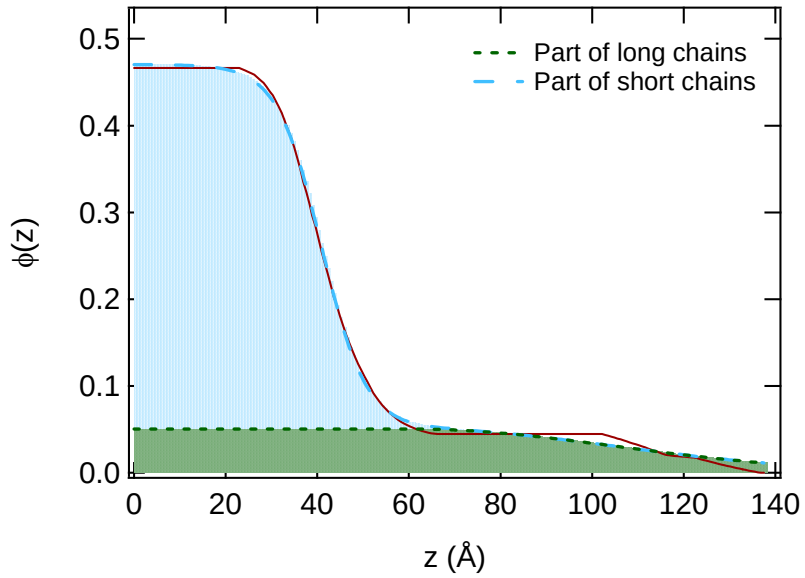

Figure 14 - Neutron reflectivity curves (left) and polymer density profile (right) corresponding to the best fit of the reflectivity data. The samples are described in Table 7.

As we previously did for the profile obtained at pH 2, the dry thicknesses are checked and found equal to 17 Å and 6 Å for short and long chains respectively. These results at pH 9 are equivalently consistent with the results from pH 2. The average characteristics are calculated by using the results obtained from the fitting parameters of Eq. 25. We find the mean height for the short chains equal to $h_S = 43$ Å which corresponds to a swelling ratio equal to 3.25 for short chain. This result is consistent with the results of the previous section. Using the parameters obtained from the Gaussian fit for the long chains, the dry thickness is corrected at 8.0 Å and their mean height is equal to $h_L = 169$ Å. The corresponding swelling ratio is equal to 19.2, which is consistent with the theory.

The main conclusion of this part is that it is possible to decorrelate the profiles obtained from bimodal brushes when the grafting density of the short chains is one order of magnitude higher than that of the long chains.

2-4- Long and dense brushes

The last two systems that were studied are long chains with a rather high grafting density, consolidated by the presence of short brushes, and are the PAA-l,m (that resemble PAA-h) and PAA-l,d samples (see Table 3). Apart from the sample with the lowest grafting density where the formation of PAA was carried out by hydrolysis (for PAA-h), all the other samples (PAA-l,d and PAA-l,m) were synthesized as previously described using the pyrolysis for the conversion step. The samples studied in this part are described in Table 8: the samples studied at pH 2 are presented first and then the samples studied at pH 9 are presented.

pH	Mn (g/mol)	γ (Å)	σ (nm^{-2})	σ^{tot} (nm^{-2})	D (Å)	γ^{tot} (Å)
PAA-l,m pH 2-33 Å	2360	8.5	$2.53\ 10^{-1}$	$3.26\ 10^{-1}$	17.5	33.1
	23610	24.6	$7.35\ 10^{-2}$			
PAA-l,d pH 2-42 Å	2360	2.4	$8.05\ 10^{-2}$	$2.14\ 10^{-1}$	21.6	41.7
	23610	39.3	$1.33\ 10^{-1}$			
PAA-l,d pH 2-48 Å	2360	5.3	$1.69\ 10^{-1}$	$3.06\ 10^{-1}$	18.3	48.0
	23610	42.7	$1.36\ 10^{-1}$			
PAA-h pH 9-21 Å	2360	1.5	$3.95\ 10^{-2}$	$0.97\ 10^{-1}$	32.1	20.8
	23610	19.3	$5.77\ 10^{-2}$			
PAA-l,d pH 9-44 Å	2360	1.9	$6.17\ 10^{-2}$	$1.97\ 10^{-1}$	22.5	44.1
	23610	42.2	$1.35\ 10^{-1}$			
PAA-l,d pH 9-50 Å	2360	1.8	$4.74\ 10^{-2}$	$2.00\ 10^{-1}$	22.3	49.6
	23610	47.8	$1.53\ 10^{-1}$			

Table 8 - Characteristics of the poly(acrylic acid) brushes: molar mass M_n of the grafted chains, thickness γ and grafting density σ. The total grafting density σ^{tot}, the mean distance between grafting points D and the total thickness γ^{tot} are also listed.

The lower grafting density of long chains ($5.8\ 10^{-2}$ nm^{-2}), obtained on the sample PAA-h at pH 9 is about two times higher than the grafting density of the samples detailed previously in Table 7. For the long chains, we got grafting densities around 0.15 chains.nm^{-2}. The grafting densities of the short chains are very low comparatively to the samples of the previous section.

As shown in Figure 15, the neutron reflectivity data obtained on these systems at pH 2 and 9 are all different. What can be noted first is that even if the short chains are present on all the samples, we were not able to distinguish them on all the profiles and they do not mainly affect the density profiles.

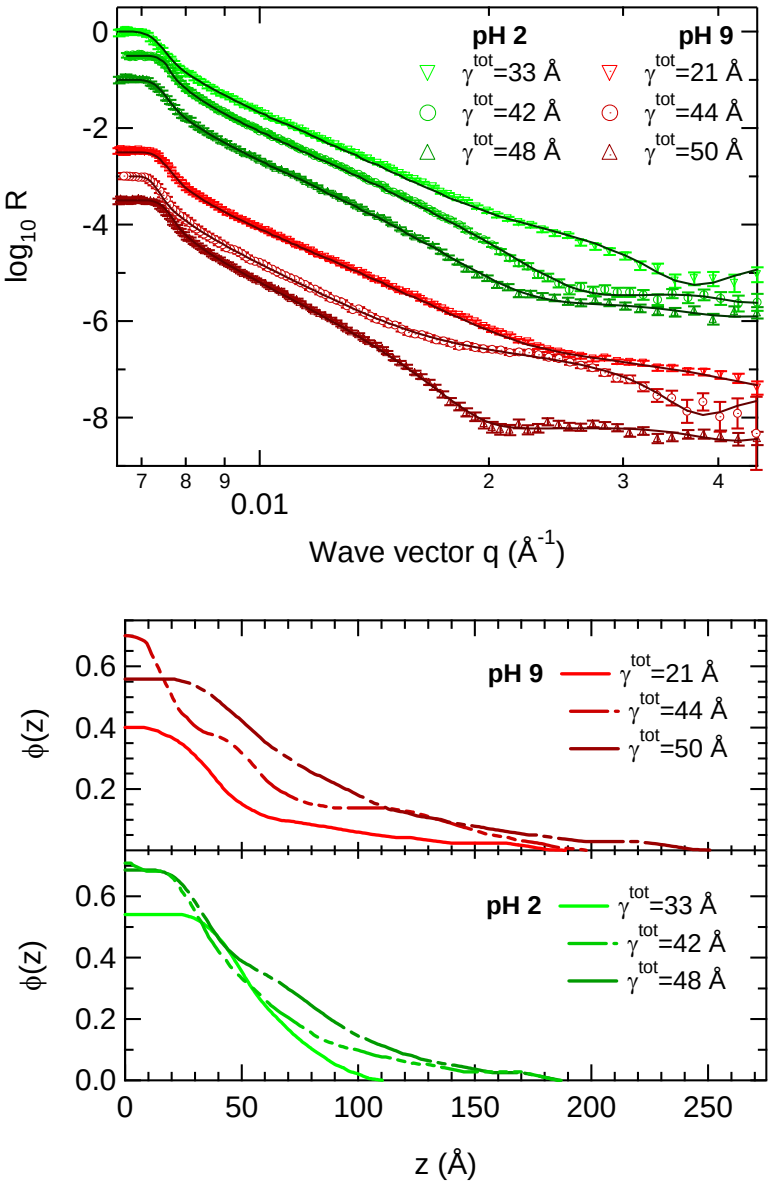

Figure 15 - Neutron reflectivity curves (top) and polymer density profiles (bottom) corresponding to the best fit of the reflectivity data. The samples are described in Table 8.

At pH 2, when the PAA brushes are neutral in good solvent, the measured polymer density profile is generally as expected, with a parabolic form. For instance, the parabolic shape for the sample PAA-l,m on Figure 16-left clearly demonstrates the very good agreement with theoretical predictions. By using the analytical form proposed by Shull (Eq. 12), the tails of

the brushes are taken into account and the agreement is particularly good (it is to be noted that one fitting parameter is added, compared to the parabolic fit). The dispersity of the polymer chains and the roughness of the surface could be the reason for the tail visible at pH 2. The density profile of the sample PAA-l,d (pH 2-48 Å) has been fitted with a double-parabolic function as in Eq. 24, and shows a relatively good agreement.

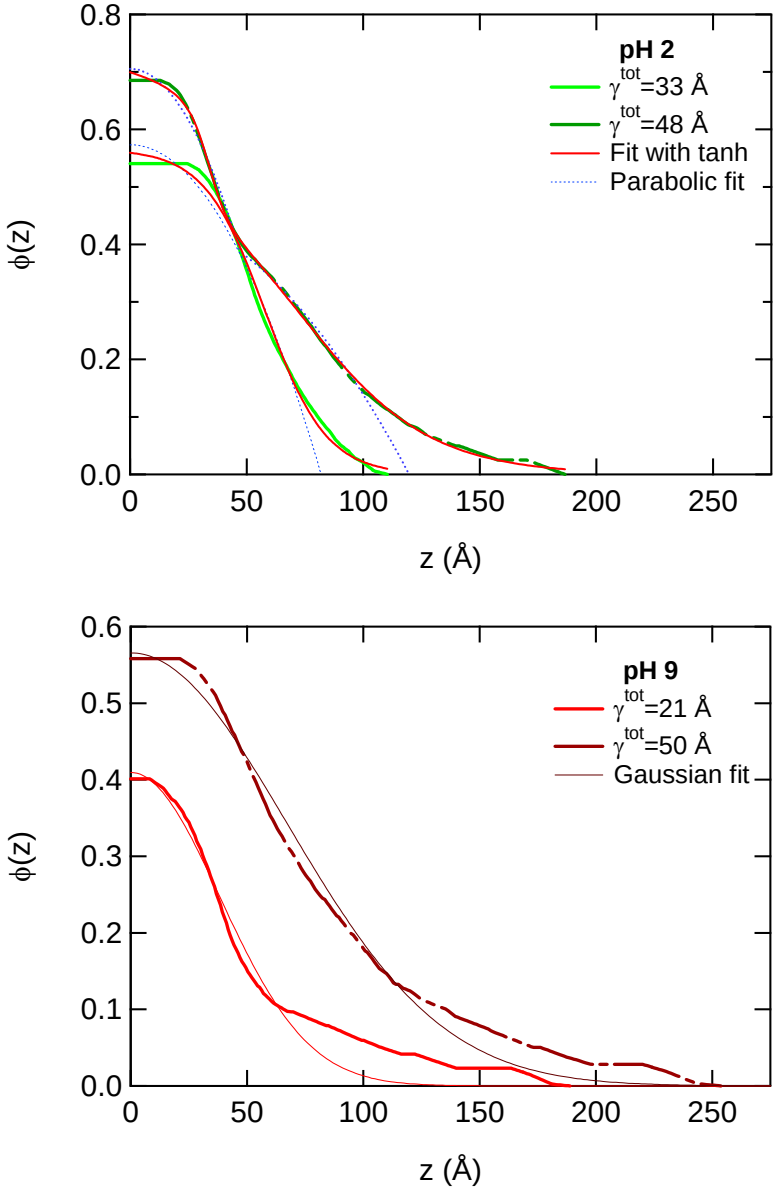

Figure 16 - Polymer density profiles corresponding to the best fit of the reflectivity data for the samples described in Table 8. At pH 2 (top), the polymer density profiles of PAA-l,m have been fitted with Eq. 11 (parabolic profile) and Eq. 12 (hyperbolic tangent based profile), and PAA-l,d (pH 2-48 Å) with a double parabolic function (Eq. 11) and a double hyperbolic tangent function (Eq. 12). At pH 9 (bottom), PAA-h and PAA-l,d (pH 9-50) have been fitted with Gaussian functions.

At pH 9, where the PAA brush is completely ionized, the polymer density profiles obtained from the fits of the reflectivity data have roughly Gaussian forms. The Gaussian fitting is specially very satisfying for samples PAA-h and PAA-l,d (pH 9-50 Å, see Figure 16).

In Table 9 are listed the swelling ratios of the brushes for each sample. These swelling ratios are deduced from the polymer density profiles. For the range of grafting densities explored here at pH 2, the swelling ratio is about 2 which means that the mean extension of the PAA brush in good solvent is twice the dry thickness.
At pH 9, for high grafting densities, the swelling ratio is a bit higher, around 2.40, which is a bit undervalued compared to the results obtained with the short brushes (where $h/\gamma = 3.04$ for $\sigma = 0.42$ nm^{-2}). At low grafting densities, we reach a swelling ratio around 3.

pH- γ^{tot}	h	$\bar{\phi}$	h/γ
PAA-l,m: pH 2-33 Å	66	0.50	2.00
PAA-l,d: pH 2-42 Å	82	0.49	1.95
PAA-l,d: pH 2-48 Å	93	0.48	1.94
PAA-h: pH 9-21 Å	62	0.33	2.96
PAA-l,d: pH 9-44 Å	108	0.41	2.46
PAA-l,d: pH 9-50 Å	120	0.42	2.40

Table 9 - Characteristics deduced from the poly(acrylic acid) brush density profile: mean height of the brush *h*, mean volume fraction $\bar{\phi}$ and swelling ratio *h/γ*.

2-5- Agreement with the scaling laws?

The swelling behavior of PAA brushes was investigated by neutron reflectivity. The brushes were immersed in water at two different pH. Sanjuan *et al.* [50] have worked on poly(methacrylic acid) (PMAA) brushes with DP ~ 300 and different grafting densities (σ = 0.40 nm^{-2} and σ = 0.29 nm^{-2}). In solvent, these brushes were found by at least twice more swollen than the dry brushes and tends to be more swollen in water (whatever the pH) than in methanol.

At pH 9, the PAA brush can be considered as completely ionized, as suggested by other groups. Dong *et al.* [30] have investigated the dissociation behavior of PAA and PMAA

brushes. They have shown that almost all the monomer units are ionized above pH 8, which was confirmed by Sanjuan *et al.* [50]. Wu *et al.* [27] have demonstrated by spectroscopic ellipsometry that the PAA brushes behaves as a strong polyelectrolyte at high pH since their swelling behavior follows the corresponding scaling models. The theoretical expectation for polyelectrolyte brushes in the osmotic regime [72] is given in Eq. 19, which is reminded here:

$$\frac{h}{\gamma} \propto N^0 \left(b^2 \sigma\right)^{-1} . \qquad \textbf{Eq. 19}$$

It is then independent of the chain length and follows a power law of the grafting density with an exponent of -1. Then, the swelling ratio of polymer brushes with different degree of polymerizations can be compared.

Previous data reported on polyelectrolyte brushes are plotted together on Figure 17 where swelling ratios obtained for ionized poly((2-dimethylamino)ethyl methacrylate) (PDMAEMA) brushes at pH 2 [84], poly(2-(methacryloxy) ethyl trimethylammonium chloride) (PMAETAC) in water [84], and poly(N-methyl-4-vinylpyridinium iodide) (MeP4VP) brushes in water [85]. For this combination of results obtained with all these brushes, the fit of the swelling ratio as a function of the grafting density on more than two decades gives a power law with an exponent of -0.97 in good agreement with theoretical expectations.

The scaling model for the variation of the swelling ratio of neutral brushes in good solvent is expressed in Eq. 10, which is recalled:

$$\frac{h}{\gamma} \propto N^0 \left(b^2 \sigma\right)^{-2/3} . \qquad \textbf{Eq. 10}$$

Accordingly, data obtained with polymer brushes of different degrees of polymerization can be compared in the same plot (see Figure 17). Then, the data obtained by Sanjuan *et al.* [50,84] on PMAA brushes in methanol are plotted together with their results on neutral poly((2-dimethylamino)ethyl methacrylate) (PDMAEMA) brushes in methanol and in water at pH 10 [84] and the results obtained by Biesalski *et al.* [86,87] with poly(4-vinylpyridine) (P4VP) brushes. The swelling behavior of all these brushes follows the same scaling prediction: it is a power law with an exponent of -0.67 consistent with the theoretical expectations.

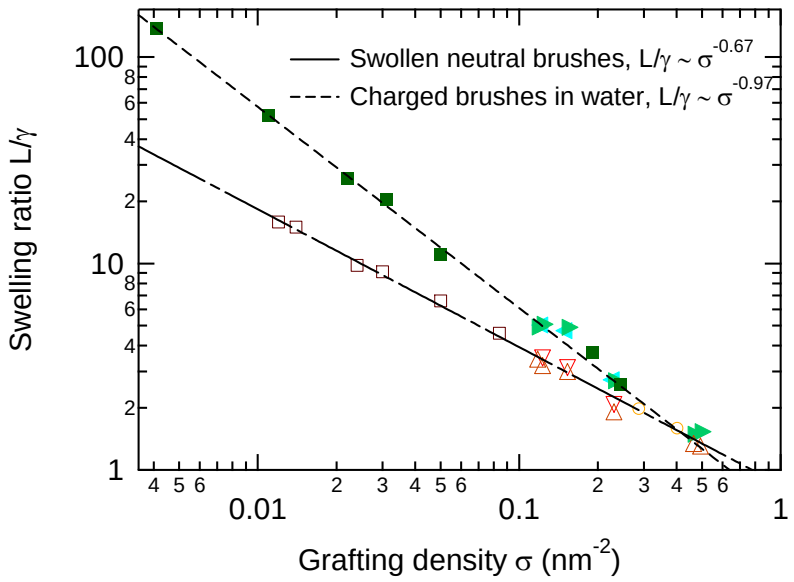

Figure 17 - Swelling ratios for charged and neutral brushes in good solvent, collecting results from various systems.

Neutral brushes swollen:

- in methanol: PMAA (○) [50], PDMAEMA (Δ) [88] and P4VP (□) [85] brushes

- in water at pH 10, PDMAEMA (▽) brushes [88].

Charged brushes: PDMAEMA brushes in water at pH 2 (◀) [88], PMAETAC (▶) [88] and MeP4VP (■) [85] brushes in water.

The two power laws have a cross-over at a grafting density equal to $\sigma = 0.42$ nm^{-2}.

Moreover, the alignment of all the data on the same master curves demonstrates that the ratio of the monomer size in the swollen state to that in the dry state is similar for the reported neutral brushes, and the ratio of the ionized monomer size in water to that in the dry state are close. Nevertheless, Eq. 10 and Eq. 19 can adequately describe the swelling behavior of a brush if the ratio of the monomer size in the swollen brush to that in the dry brush is independent of the grafting density.

Finally, it is to be noticed that the master curves of neutral brushes and charged brushes have a cross-over grafting density for which the swelling ratios are equal. It means that at a very high grafting density ($\sigma = 0.42$ nm^{-2}), the charged brushes have the same swelling ratio as the neutral brushes.

Besides, when working in water at pH 2, Sanjuan *et al.* [50] found that the swelling behavior of PMAA was that of a neutral brush in good solvent as its swelling ratio follows the appropriate scaling law. The swelling ratio of PMAA brushes at pH 2 is higher than in methanol, proving that PMAA brushes in water at pH 2 are in better solvent conditions than in methanol.

Our work is compared to the variations that have been found with the previous systems in the following Figure 18.

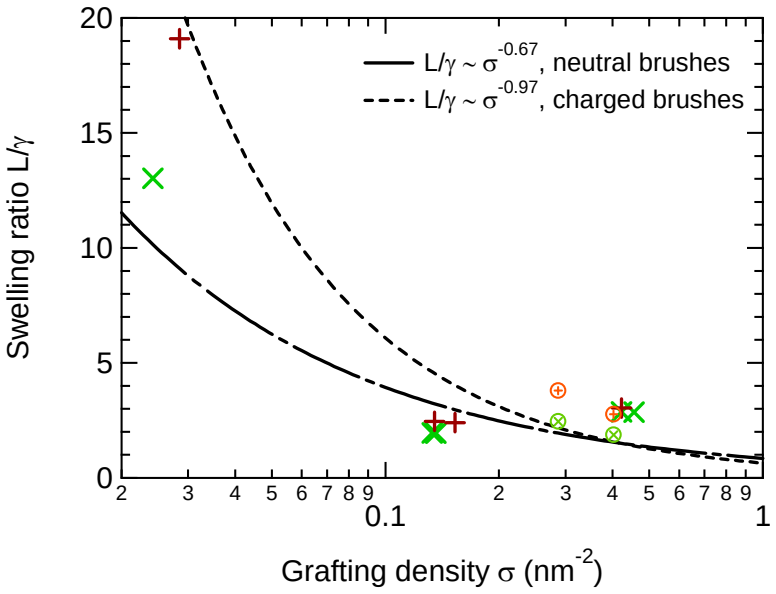

Figure 18 - Swelling ratios of neutral PAA brushes in water at pH 2 (×), and ionized PAA brushes in water at pH 9 (+). At high grafting densities, the data are obtained with short chains; the other data are obtained with chains of M_n = 23610 g.mol^{-1}. The two power laws are from Figure 17 and have a cross-over at a grafting density equal to $\sigma = 0.42$ nm^{-2}. Results obtained with PMAA brushes by Sanjuan *et al.* [50] at pH 2 (⊗) and pH 9 (⊕) have been added.

At very high grafting densities, the results are those obtained with the short brushes system (M_n = 3650 g.mol^{-1}) or with the short chains of the bimodal system (M_n = 2360 g.mol^{-1}). The stretching is found approximately equal to 3 and is almost similar at pH 2 and at pH 9, when the brush is neutral and charged, respectively. This value seems a bit overvalued compared to the theoretical expectation but the absence of noticeable variation between pH 2 and pH 9 is very consistent with the fact that the grafting density of these brushes corresponds to the cross-over of the scaling laws for neutral and charged brushes.

At very low grafting densities, the results were obtained with the bimodal brushes of 2-3-. Their structures are in agreement with what is expected from the theory. At intermediate grafting densities, the swelling ratio is a bit underestimated compared to what was previously obtained with other polymer brushes. However, the swelling behavior remains higher at pH 9. And the shape of the profiles allows the discrimination between the structure at pH 2 and at pH 9: the neutral brushes exhibit a hyperbolic-tangent based profile whereas the ionized profiles are rather Gaussian.

3- Conclusion

In the first part of this chapter, we have extensively described the synthesis of polymer brushes following a “grafting onto” route.

The PNIPAM brush, used as a reference in Chapter 4, has been obtained by a two-step process. After the substrate is covered by a SAM of epoxides, carboxy-terminated PNIPAM chains are grafted by annealing.

PAA brushes of varying grafting densities have been synthesized using a procedure which is similar but a bit more complex due to the presence of acidic functions. During the grafting process by annealing, the acid functions of PAA have to be protected by t-butyl groups. Thus, once the substrate was adequately modified, carboxy-terminated PtBuA chains have been first grafted and the surface was then passivated by the carpeting PtBuA short chains. The final step is the conversion into PAA brushes: the deprotection of the t-butyl groups can be realized by hydrolysis or pyrolysis. We have shown that the pyrolysis process has much more advantages than the hydrolysis reaction: it is simpler (it only requires an oven), faster (it lasts 2 h instead of 130 h for the hydrolysis), it is adapted to all grafting densities and no degrafting occurs during pyrolysis. It led to bimodal PAA brushes. Each step of the synthesis has been carefully characterized by ellipsometry, infrared spectroscopy and neutron reflectivity which ensured the formation of real brushes during synthesis.

The structures of these systems made of PAA brushes have been characterized by neutron reflectivity. We obtained the density profiles of the polymer brushes in the direction normal to the interface. The stretching of the brushes depends on the pH and is found in good agreement with the scaling laws. At high pH when PAA is ionized, the brush adopts the structure of a strong polyelectrolyte brush and its profile is Gaussian. At low pH, the PAA chains are neutral. Less extended than at pH 9, the brush is in good solvent, follows a hyperbolic tangent based profile.

At very high grafting densities for short brushes, the swelling of the neutral brush was found comparable to that of the polyelectrolyte brush, as predicted. Various grafting densities of long chains have been studied, from a low grafting density that gives access to clear bimodal profiles, to higher grafting densities where the influence of the short chains is negligible. The structure of bimodal brushes has been deconvoluted and the swelling behavior of each moiety could be extrapolated and compared to theoretical predictions.

The experimental results gave swelling ratios always higher than 2 and are in good agreement with what is predicted by the scaling laws. It emphasizes the very high stretching of the charged brushes at low grafting density.

4- References

[1] Zhang, J. L.; Han, Y. C. *Chem Soc Rev* **2010**, *39*, 676-693.
[2] Joanny, J. F. *Interface Sci* **2003**, *11*, 157-158.
[3] Muller, P.; Sudre, G.; Theodoly, O. *Langmuir* **2008**, *24*, 9541-9550.
[4] Howarter, J. A.; Youngblood, J. P. *Adv Mater* **2007**, *19*, 3838-+.
[5] Raviv, U.; Giasson, S.; Kampf, N.; Gohy, J. F.; Jerome, R.; Klein, J. *Langmuir* **2008**, *24*, 8678-8687.
[6] Maeda, N.; Chen, N. H.; Tirrell, M.; Israelachvili, J. N. *Science* **2002**, *297*, 379-382.
[7] Leger, L.; Raphael, E.; Hervet, H. *Adv Polym Sci* **1999**, *138*, 185-225.
[8] Milner, S. T. *Science* **1991**, *251*, 905-914.
[9] Currie, E. P. K.; Sieval, A. B.; Fleer, G. J.; Stuart, M. A. C. *Langmuir* **2000**, *16*, 8324-8333.
[10] Tokarev, I.; Motornov, M.; Minko, S. *J Mater Chem* **2009**, *19*, 6932-6948.
[11] Tokarev, I.; Minko, S. *Soft Matter* **2009**, *5*, 511-524.
[12] Papaefthimiou, V.; Steitz, R.; Findenegg, G. H. *Chem Unserer Zeit* **2008**, *42*, 102-115.
[13] Chen, T.; Ferris, R.; Zhang, J. M.; Ducker, R.; Zauscher, S. *Prog Polym Sci* **2010**, *35*, 94-112.
[14] Lee, H. I.; Pietrasik, J.; Sheiko, S. S.; Matyjaszewski, K. *Prog Polym Sci* **2010**, *35*, 24-44.
[15] Zdyrko, B.; Klep, V.; Li, X. W.; Kang, Q.; Minko, S.; Wen, X. J.; Luzinov, I. *Mat Sci Eng C-Bio S* **2009**, *29*, 680-684.
[16] Iwata, R.; Satoh, R.; Iwasaki, Y.; Akiyoshi, K. *Colloid Surface B* **2008**, *62*, 288-298.
[17] Motornov, M.; Sheparovych, R.; Katz, E.; Minko, S. *Acs Nano* **2008**, *2*, 41-52.
[18] Laloyaux, X.; Mathy, B.; Nysten, B.; Jonas, A. M. *Langmuir* **2010**, *26*, 838-847.
[19] Yim, H.; Kent, M. S.; Huber, D. L.; Satija, S.; Majewski, J.; Smith, G. S. *Macromolecules* **2003**, *36*, 5244-5251.
[20] Cooperstein, M. A.; Canavan, H. E. *Langmuir* **2010**, *26*, 7695-7707.
[21] Malham, I. B.; Bureau, L. *Langmuir* **2010**, *26*, 4762-4768.
[22] Wang, S. Q.; Zhu, Y. X. *Langmuir* **2009**, *25*, 13448-13455.
[23] Zhu, X.; Yan, C.; Winnik, F. M.; Leckband, D. *Langmuir* **2007**, *23*, 162-169.
[24] Sonnenberg, L.; Parvole, J.; Borisov, O.; Billon, L.; Gaub, H. E.; Seitz, M. *Macromolecules* **2006**, *39*, 281-288.
[25] Hollmann, O.; Gutberlet, T.; Czeslik, C. *Langmuir* **2007**, *23*, 1347-1353.
[26] Retsch, M.; Walther, A.; Loos, K.; Muller, A. H. E. *Langmuir* **2008**, *24*, 9421-9429.
[27] Wu, T.; Gong, P.; Szleifer, I.; Vlcek, P.; Subr, V.; Genzer, J. *Macromolecules* **2007**, *40*, 8756-8764.
[28] Rowe, M. A.; Hammer, B. A. G.; Boyes, S. G. *Macromolecules* **2008**, *41*, 4147-4157.
[29] Cullen, S. P.; Liu, X.; Mandel, I. C.; Himpsel, F. J.; Gopalan, P. *Langmuir* **2008**, *24*, 913-920.
[30] Dong, R.; Lindau, M.; Ober, C. K. *Langmuir* **2009**, *25*, 4774-4779.
[31] Roodenko, K.; Mikhaylova, Y.; Ionov, L.; Gensch, M.; Stamm, M.; Minko, S.; Schade, U.; Eichhorn, K. J.; Esser, N.; Hinrichs, K. *Appl Phys Lett* **2008**, *92*, -.
[32] Liu, G. M.; Zhang, G. Z. *J. Phys. Chem. B* **2008**, *112*, 10137-10141.
[33] Dominguez-Espinosa, G.; Synytska, A.; Drechsler, A.; Gutsche, C.; Kegler, K.; Uhlmann, P.; Stamm, M.; Kremer, F. *Polymer* **2008**, *49*, 4802-4807.
[34] Czeslik, C.; Jackler, G.; Hazlett, T.; Gratton, E.; Steitz, R.; Wittemann, A.; Ballauff, M. *Phys Chem Chem Phys* **2004**, *6*, 5557-5563.
[35] Zhulina, E. B.; Birshtein, T. M.; Borisov, O. V. *Macromolecules* **1995**, *28*, 1491-1499.

[36] Tran, Y.; Auroy, P. *J Am Chem Soc* **2001**, *123*, 3644-3654.
[37] Luzinov, I.; Julthongpiput, D.; Liebmann-Vinson, A.; Cregger, T.; Foster, M. D.; Tsukruk, V. V. *Langmuir* **2000**, *16*, 504-516.
[38] Luzinov, I.; Julthongpiput, D.; Malz, H.; Pionteck, J.; Tsukruk, V. V. *Macromolecules* **2000**, *33*, 1043-1048.
[39] Minko, S.; Patil, S.; Datsyuk, V.; Simon, F.; Eichhorn, K. J.; Motornov, M.; Usov, D.; Tokarev, I.; Stamm, M. *Langmuir* **2002**, *18*, 289-296.
[40] Sanjuan, S.; Tran, Y. *J Polym Sci Pol Chem* **2008**, *46*, 4305-4319.
[41] Lego, B.; Skene, W. G.; Giasson, S. *Macromolecules* **2010**, *43*, 4384-4393.
[42] Treat, N. D.; Ayres, N.; Boyes, S. G.; Brittain, W. J. *Macromolecules* **2006**, *39*, 26-29.
[43] Ayres, N.; Boyes, S. G.; Brittain, W. J. *Langmuir* **2007**, *23*, 182-189.
[44] Ayres, N.; Cyrus, C. D.; Brittain, W. J. *Langmuir* **2007**, *23*, 3744-3749.
[45] Silberzan, P.; Leger, L.; Ausserre, D.; Benattar, J. J. *Langmuir* **1991**, *7*, 1647-1651.
[46] Advincula, R. C.; Brittain, W. J.; Caster, K. C.; Rühe, J. *Polymer Brushes*; Wiley-VCH: Weinheim (Allemagne), **2004**.
[47] De Buyl, F.; Kretschmer, A. *J Adhesion* **2008**, *84*, 125-142.
[48] Arleth, L.; Xia, X. H.; Hjelm, R. P.; Wu, J. Z.; Hu, Z. B. *J Polym Sci Pol Phys* **2005**, *43*, 849-860.
[49] Brandrup, J.; Immergut, E. H.; Grulke, E. A.; Kurata, M.; Tsunashima, Y. *Polymer Handbook*, 4th ed.; Wiley Interscience: New York, **1999**; Vol. Viscosity - Molecular Weight Relationships and Unperturbed Dimensions of Linear Chain Molecules.
[50] Sanjuan, S. In *Thèse de Doctorat*: Paris VI, **2007**.
[51] Siband, E. In *Thèse de Doctorat*: Paris VI, **2009**.
[52] Toomey, R.; Tirrell, M. *Annu Rev Phys Chem* **2008**, *59*, 493-517.
[53] Alexander, S. *J Phys-Paris* **1977**, *38*, 983-987.
[54] De Gennes, P. G. *J Phys-Paris* **1976**, *37*, 1445-1452.
[55] De Gennes, P. G. *Macromolecules* **1980**, *13*, 1069-1075.
[56] Milner, S. T.; Witten, T. A.; Cates, M. E. *Europhys Lett* **1988**, *5*, 413-418.
[57] Milner, S. T.; Witten, T. A.; Cates, M. E. *Macromolecules* **1989**, *22*, 853-861.
[58] Netz, R. R.; Schick, M. *Macromolecules* **1998**, *31*, 5105-5122.
[59] Netz, R. R.; Schick, M. *Europhys Lett* **1997**, *38*, 37-42.
[60] Skvortsov, A. M.; Pavlushkov, I. V.; Gorbunov, A. A. *Vysokomolekulyarnye Soedineniya Seriya A* **1988**, *30*, 503-508.
[61] Skvortsov, A. M.; Pavlushkov, I. V.; Gorbunov, A. A.; Zhulina, Y. B.; Borisov, O. V.; Pryamitsyn, V. A. *Vysokomolekulyarnye Soedineniya Seriya A* **1988**, *30*, 1615-1622.
[62] Lai, P. Y.; Binder, K. *J Chem Phys* **1992**, *97*, 586-595.
[63] Lai, P. Y.; Zhulina, E. B. *Macromolecules* **1992**, *25*, 5201-5207.
[64] Murat, M.; Grest, G. S. *Phys Rev Lett* **1989**, *63*, 1074-1077.
[65] Flory, P. J. *Principles of Polymer Chemistry*; Cornell University Press, **1971**.
[66] Ruhe, J.; Ballauff, M.; Biesalski, M.; Dziezok, P.; Grohn, F.; Johannsmann, D.; Houbenov, N.; Hugenberg, N.; Konradi, R.; Minko, S.; Motornov, M.; Netz, R. R.; Schmidt, M.; Seidel, C.; Stamm, M.; Stephan, T.; Usov, D.; Zhang, H. N. *Polyelectrolytes with Defined Molecular Architecture I* **2004**, *165*, 79-150.
[67] Milner, S. T.; Witten, T. A.; Cates, M. E. *Macromolecules* **1988**, *21*, 2610-2619.
[68] Zhulina, E. B.; Borisov, O. V.; Brombacher, L. *Macromolecules* **1991**, *24*, 4679-4690.
[69] Shull, K. R. *J Chem Phys* **1991**, *94*, 5723-5738.
[70] Field, J. B.; Toprakcioglu, C.; Dai, L.; Hadziioannou, G.; Smith, G.; Hamilton, W. *J Phys Ii* **1992**, *2*, 2221-2235.
[71] Naji, A.; Seidel, C.; Netz, R. R. *Surface- Initiated Polymerization Ii* **2006**, *198*, 149-183.

[72] Pincus, P. *Macromolecules* **1991**, *24*, 2912-2919.
[73] Borisov, O. V.; Birshtein, T. M.; Zhulina, E. B. *J Phys Ii* **1991**, *1*, 521-526.
[74] Wittmer, J.; Joanny, J. F. *Macromolecules* **1993**, *26*, 2691-2697.
[75] Zhulina, E. B.; Borisov, O. V.; Priamitsyn, V. A. *J Colloid Interf Sci* **1990**, *137*, 495-511.
[76] Zhulina, E. B.; Borisov, O. V.; Birshtein, T. M. *J Phys Ii* **1992**, *2*, 63-74.
[77] Chen, H.; Zajac, R.; Chakrabarti, A. *J Chem Phys* **1996**, *104*, 1579-1588.
[78] Granfeldt, M. K.; Miklavic, S. J.; Marcelja, S.; Woodward, C. E. *Macromolecules* **1990**, *23*, 4760-4768.
[79] Seidel, C. *Macromolecules* **2003**, *36*, 2536-2543.
[80] Currie, E. P. K.; Wagemaker, M.; Stuart, M. A. C.; van Well, A. A. *Macromolecules* **1999**, *32*, 9041-9050.
[81] Levicky, R.; Koneripalli, N.; Tirrell, M.; Satija, S. K. *Macromolecules* **1998**, *31*, 2616-2621.
[82] Dan, N.; Tirrell, M. *Macromolecules* **1993**, *26*, 6467-6473.
[83] Kent, M. S.; Factor, B. J.; Satija, S.; Gallagher, P.; Smith, G. S. *Macromolecules* **1996**, *29*, 2843-2849.
[84] Sanjuan, S.; Perrin, P.; Pantoustier, N.; Tran, Y. *Langmuir* **2007**, *23*, 5769-5778.
[85] Biesalski, M.; Johannsmann, D.; Ruhe, J. *J Chem Phys* **2002**, *117*, 4988-4994.
[86] Biesalski, M.; Ruhe, J. *Macromolecules* **2002**, *35*, 499-507.
[87] Biesalski, M.; Ruhe, J. *Macromolecules* **2004**, *37*, 1166-1166.
[88] Sanjuan, S.; Tran, Y. *Macromolecules* **2008**, *41*, 8721-8728.

CHAPTER 3 – NEUTRAL POLY(ACRYLAMIDE) & POLY(*N,N*-DIMETHYLACRYLAMIDE) HYDROGELS

This second experimental chapter focuses on the synthesis of neutral hydrogels and on the consequent mechanical and structural properties. Above all, the goal of this study is to optimize the synthesis of neutral hydrogels to perform adhesion tests and to determine their essential characteristics needed to analyze these tests. Their ideal characteristics would be an insensitivity of the mechanical properties to environmental changes in the aqueous solution characteristics (pH, ionic strength) and a negligible viscous dissipation – that is to say a high entropic elasticity – when deformed.

We use a one-pot conventional radical polymerization for the synthesis of poly(acrylamide) and poly(*N,N*-dimethylacrylamide) gels. Their cross-linking is obtained by the presence of a tetra-functional cross-linker, methylene-*bis*-acrylamide. This choice is motivated by the very simple synthesis of such gels the properties of which are reproducible. However, since cross-linking and polymerization occur at the same time, this type of synthesis often leads to a heterogeneous structure.

The structure of the poly(*N,N*-dimethylacrylamide) gels is thoroughly investigated using different characterization techniques. While varying monomer and cross-linker concentrations at the synthesis stage, a simple swelling study has been performed and coupled with mechanical compression tests at equilibrium swelling. Put together, these two techniques give some access to the structure of the polymer network, being the backbone of the gel: information such as the average number of monomer between cross-links or the interaction parameter of PDMA in water can be determined. Adding a titration of the dangling double-bonds, it is possible to evaluate the proportion of inhomogenities in the network. Other structural information is obtained by Small Angle Neutron Scattering: we determine the size of the thermal blob of the system depending on its characteristics at the synthesis and the presence of another structure in the network.
A more detailed analysis of the mechanical compression tests gives access to other information on the characteristics of the network such as the chain extensibility, the energy loss per cycle, the presence of entanglements or the damages inflicted to the network after a first compression. Complementary information on the network mechanics can be obtained by rheology.

A gel (cf. Figure 1) is a soft material mainly composed of liquid but consisting of interconnected monomers, which could be molecules or colloids [1]. This molecular percolation dramatically enhances the resistance of the gel to flow and most often gels behave as soft solids with swelling and deswelling properties. Chemical gels which are covalently cross-linked polymer networks swollen in a solvent, are classically distinguished from physical gels. In the latter, cross-links are provided by reversible interactions [2], commonly Van der Waals interactions and their derivatives, such as hydrogen bonding, hydrophobic or ionic interactions, etc.

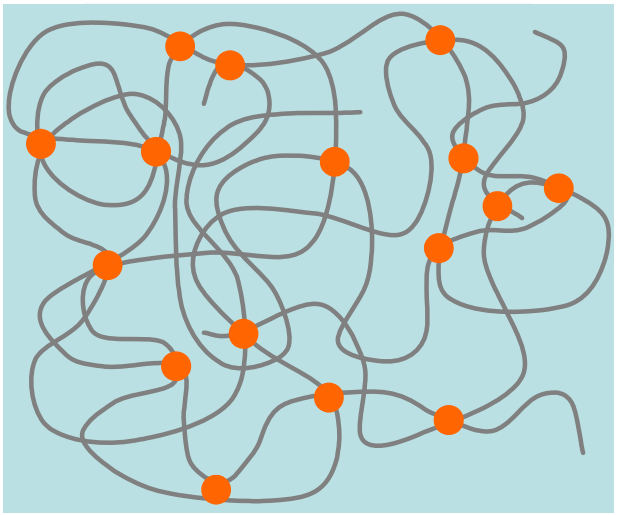

Figure 1 - Schematic structure of a gel: the grey polymer network with orange cross-links is swollen in a sea of blue solvent.

For their numerous applications in the life sciences, water-swollen polymer networks, which are called hydrogels, are widely studied and developed [3-5]. In many cases hydrogels are seen as aqueous reservoirs in which a water-soluble active ingredient can potentially be included so that it can diffuse out of the gel afterwards. Furthermore, the interactions of the polymer with water can present a strong responsiveness towards different environmental stimuli: mechanical stress, temperature, pH or ionic strength, light, etc. resulting in changes in swelling properties of the hydrogel [6].

From their macromolecular swollen structure, gels get their jelly-like behavior, ranging from soft to hard and from brittle to tough. The mechanical and swelling properties depend both on the lifetime of the cross-links (infinite in the case of chemical gels and temporary with a specific rearrangement kinetics in the case of physical gels), and on the characteristics of the polymer network (mesh size, inhomogeneities…).

In the case of covalent hydrogels, the swelling and mechanical properties also strongly depend on the presence of electric charges inside the network. When monomer units are ionized, the polyelectrolyte chains have the ability to be extremely stretched, due to electrostatic repulsion and to a tremendous osmotic contribution of the confined counter-ions to the swelling behavior of the network. The corresponding material has a tendency to be highly swollen, and is a prime choice material as super-absorbent since these networks can contain up to 99.9wt% of water. When monomer units are uncharged, as it is the case with both acrylamide (AM) and *N,N*-dimethylacrylamide (DMA), the water-soluble polymer usually adopts a less extended random coil conformation, which often leads to less swollen and less stiff materials. Their swelling behavior is also less sensitive to the ionic strength

Two main routes are generally used to build covalent networks. The first method consists of the synthesis of linear polymer chains from di-functional monomers. The cross-linking is then carried out in a second stage, thanks to the end-groups of the chains or to the presence in the backbone of reactive groups able to be cross-linked afterwards. In the second method, the network is synthesized in one step by mixing in the presence of solvent a di-functional monomer and a co-monomer, usually in a lower quantity, but with a higher functionality. This last method often leads to heterogeneous structures with a broad size distribution of the elastic chains [7].

Based on the principles of rubber elasticity – which compares the entropy of the network in the original unconstrained state to its entropy in the stressed state – chemical hydrogels are usually highly elastic [8], with a storage modulus in the range of 10^3-10^5 Pa [9]. Besides this modulus – weak compared to an equivalently crosslinked elastomer – the dilution of the polymeric material in the system is responsible for the fragility of the gels.

To fill the specifications of this PhD project, the model hydrogels need to meet many conditions. They should not flow and not change much their degree of swelling when submitted to environmental modifications like ionic strength, pH, or temperature, and they must be able to develop specific and tunable interactions with other polymers.

In the following, we report the synthesis of poly(acrylamide) and poly(*N,N*-dimethylacrylamide) hydrogels via a conventional radical polymerization. For each type of gel, the monomer concentration and/or the relative amount of cross-linker have been tuned to control the structure and the properties of the networks. A detailed study, based on swelling experiments and mechanical analysis, is reported on PDMA hydrogels.

1- Synthesis of hydrogels and characterization methods

1-1- Synthesis

The syntheses of poly(acrylamide) and poly(*N,N*-dimethylacrylamide) hydrogels have been carried out by free radical polymerization using *N,N'*-methylene-bis-acrylamide (MBA) as cross-linker (f=4). After dissolution of DMA, MBA and potassium persulfate in water, the solution is deoxygenated with a bubbling of nitrogen during 30 min. After a rapid addition of N,N,N',N'-tetramethylethylenediamine (TEMED) under stirring, the solution is then transferred in a mold initially placed under nitrogen atmosphere. The red-ox initiation rapidly takes place [10] and the polymerization is let to proceed during 4 h. As the gel formation is too fast when DMA is replaced by acrylamide, we do not use TEMED but simply initiate the reaction by thermal decomposition of KPS setting the system at 40°C during 4 h.Then, the mold is opened and the gel is immersed in Milli-Q water for dialysis. Water is changed twice a day during one week and the hydrogel is finally stored in its swollen state until final use.

During this study, we have chosen to work with normalized gels. The mass ratio of monomer (DMA or AM) in water is either 5, 10, 15 or 20 wt%. The molar ratio of cross-linker (MBA) to monomer varies from 0.2 to 10 mol%. The quantity of initiator (KPS and TEMED) has been set to 1 mol% of the monomer quantity.

In Table 1 and Table 2 are reported the different syntheses that have been carried out for PDMA and PAM gels, respectively.

In the following, the gels will be named according to the weight monomer concentration (m:w) and the molar cross-linker ratio (x:m) that are defined in the preparation state:

$$(\mathrm{m:w}) = 100\frac{m_{mono}}{m_{mono}+m_w};\ (\mathrm{x:m}) = 100\frac{[MBA]}{[monomer]}. \qquad \textbf{Eq. 1}$$

For example, PDMA-10x2 and PAM-10x2 are hydrogels prepared with (m:w) = 10 wt% and (x:m) = 2 mol%.

Sample	$100\frac{[MBA]}{[DMA]}$	$\frac{100.m_{DMA}}{m_{DMA}+m_w}$	DMA (g)	MBA (mg)	KPS (mg)	TMED (µL)	Water (g)
PDMA-10x0.2	0.2	10	2	6.2	54.6	30	18
PDMA-10x0.5	0.5	10	1	7.8	27.3	15	9
PDMA-15x0.5	0.5	15	1.5	11.7	41.0	22.5	8.5
PDMA-10x0.8	0.8	10	1	12.4	27.3	15	9
PDMA-5x1	1	5	0.5	7.8	13.6	7.5	9.5
PDMA-10x1	1	10	1	15.6	27.3	15	9
PDMA-15x1	1	15	1.5	23.3	41.0	22.5	8.5
PDMA-5x2	2	5	0.5	14.6	13.6	7.5	9.5
PDMA-10x2	2	10	1	31.1	27.3	15	9
PDMA-15x2	2	15	1.5	46.7	41.0	22.5	8.5
PDMA-20x0.5	0.5	20	2	14.6	54.6	30	8
PDMA-20x1	1	20	2	31.1	54.6	30	8
PDMA-20x2	2	20	2	62.3	54.6	30	8
PDMA-10x10	10	10	2	311.4	54.6	30	18
PDMA-20x10	10	20	2	311.4	54.6	30	8

Table 1 - Formulation of PDMA hydrogels.

Sample	$100\frac{[MBA]}{[AM]}$	$\frac{100.m_{AM}}{m_{AM}+m_w}$	AM (g)	MBA (mg)	KPS (mg)	Water (g)
PAM-10x0.5	0.5	10	1	11.0	38.0	9
PAM-15x0.5	0.5	15	1.5	16.5	57.0	8.5
PAM-5x1	1	5	0.5	11.0	19.0	9.5
PAM-10x1	1	10	1	22.0	38.0	9
PAM-15x1	1	15	1.5	33.0	57.0	8.5
PAM-5x2	2	5	0.5	22.0	19.0	9.5
PAM-10x2	2	10	1	44.0	38.0	9
PAM-15x2	2	15	1.5	154.0	57.0	8.5

Table 2 - Formulation of PAM hydrogels.

The analysis of extractible was not systematic, but no residual monomer was detected by size-exclusion chromatography (SEC) after extraction in the standard case of PDMA-10x1 and the sol fraction was not measurable in that case, or below 2 wt% of the total network. This result is consistent with the work of Gundogan *et al.* [11].

1-2- Titration of dangling double bonds

During the synthesis of the gel, part of the cross-linker MBA is expected to react only at one end, like a monomer of functionality 2. At the end of the synthesis, this results in the presence of dangling double bonds. This incomplete reaction of the cross-linker is responsible for the weakening of mechanical properties of the hydrogel and it is important to characterize the extent of unreacted double bonds.

The principle of this titration is to use the electrophilic addition reaction of iodine I_2 on the carbon-carbon double bond. However, performing such titration within a gel has some limitations; the main one being that the reaction will be slowed down by the diffusion of the species inside the gel.

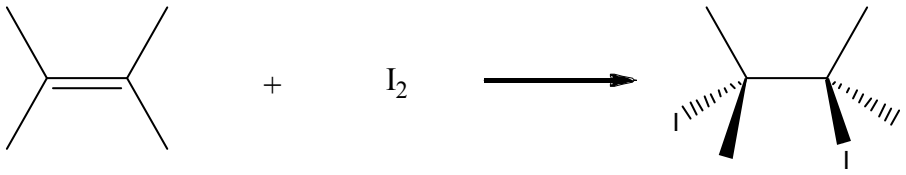

A given quantity of hydrogel previously dialyzed with Milli-Q water was introduced in an adequate volume of saturated solution of iodine (0.34 g/kg @ 25°C, 1.34 10^{-3} mol/L) during one week. The remaining iodine I_2 of the solution was then titrated with a solution of sodium thiosulfate at 10^{-3} mol/L with a few droplets of starch indicator. The equivalence point is observed when the titrated solution turns from dark blue to white and turbid. A control sample was titrated following the same protocol. The reduction-oxidation reaction is as follows:

$$I_2 + 2\,S_2O_3^{2-} \longrightarrow 2\,I^- + S_4O_6^{2-}$$

Finally, three parameters are to be taken into account when analyzing the titration:

- the dilution brought to the iodine solution in which the gel is immersed: the water contained inside the hydrogel is exchanged with the iodine solution, it is then necessary to know the water content of the gel, that is to say its swelling;
- the reaction of iodine on the dangling double bonds;
- the sensitivity of iodine towards external environment, which means that it is essential to use a control sample kept during the same time in the same conditions.

1-3- Structure: study by SANS

Small angle neutron scattering experiments have been carried out at the Laboratoire Léon Brillouin, CEA, Saclay. We used a small angle neutron spectrometer for isotropic scattering: PACE (Petits Angles CEntral). Samples of gel were prepared and dialyzed prior to the measurement: the hydrogenated polymer was swollen in deuterated water so that the difference in the coherent neutron scattering length densities between the solute and the solvent gave rise to an enhanced scattering.

In principle, an incident radiation of wave vector $\vec{k_0}$ is sent through a sample which induces a scattered radiation, the intensity of which is measured as a function of the scattered wave vector $\vec{k}$. After a treatment of the measured signal, the intensity $I(q)$ of elastically scattered neutrons is finally obtained as a function of the modulus of the transfer wave vector $\vec{q}$ which can be written as: $\vec{q} = \vec{k} - \vec{k_0}$ with a modulus equal to $q = \left\| \vec{q} \right\| = \frac{4\pi}{\lambda} \sin\theta$, for a wavelength λ and a scattering angle θ. This intensity $I(q)$, named absolute intensity, is obtained after taking into account the incoherent scattering due to the solvent and the sample cell. It is proportional to the probability of finding a characteristic distance q^{-1} in the spatial distribution of the different constituents of the sample.

For a gel, the theoretical expression of $I(q)$ is generally calculated from the addition of two essential components [12]: a gel is a semi-dilute solution in which the spatial distribution of the polymer segments is partially inhomogeneous (i) and static due to the presence of cross-links which hinder the amplitude of the movements of the polymer segments (ii).

For semi-dilute solutions of neutral polymers (i), the structure factor can be described as a Lorentzian function in the region where $q\xi \leq 1$, with ξ the polymer-polymer correlation distance in the solution.

$$I_{(i)}(q) = I_L(0) \frac{1}{1 + \xi^2 q^2}, \qquad \textbf{Eq. 2}$$

Due to the presence of covalent cross-links in the system (ii), a second term has to be introduced in the expression of $I(q)$. Three main functional forms of this second term have been proposed in the literature. Briefly, assuming that the gel has another correlation length Ξ, a second Lorentzian form has been suggested [13]:

$$I_{(ii)}(q) = I_{LL}(0)\frac{1}{1+\Xi^2 q^2}, (\Xi >> \xi). \qquad \textbf{Eq. 3}$$

Alternatively, Geissler *et al.* [14,15] used an extended form of the Guinier expression, supposing that non-interacting domains with various monomer concentrations are randomly distributed in the sample:

$$I_{(ii)}(q) = I_G(0)\exp\left(-(\Xi q)^{\alpha}\right),\ 0.5 > \alpha \geq 2\,. \qquad \textbf{Eq. 4}$$

Finally, Panyukov and Rabin [16] have proposed their own squared-Lorentzian function, representing a two phase system with sharp boundaries:

$$I_{(ii)}(q) = I_{SL}(0)\frac{1}{\left(1+\Xi^2 q^2\right)^2}\,. \qquad \textbf{Eq. 5}$$

Therefore, the absolute intensity scattered by a gel can be expressed as the sum of a Lorentzian and a second term:

$$I(q) = I_L(0)\frac{1}{1+\xi^2 q^2} + I_{(ii)}(q)\,. \qquad \textbf{Eq. 6}$$

In the case of non-charged gels, the most appropriate theory seems to be the Panyukov-Rabin theory as discussed by Shibayama [12]. The absolute intensity can be written as:

$$I(q) = I_L(0)\frac{1}{1+\xi^2 q^2} + I_{SL}(0)\frac{1}{\left(1+\Xi^2 q^2\right)^2}\,, \qquad \textbf{Eq. 7}$$

where Ξ is the characteristic correlation length of the solid-like inhomogeneities (ii).

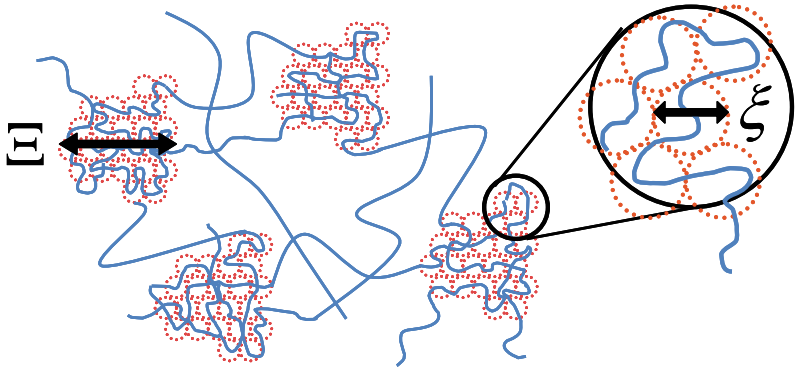

Figure 2 - Schematic representation of the structure of the gel, in the case where highly concentrated domains with a characteristic size Ξ distributed in a low concentration medium. In both domains, the polymer-polymer correlation distance ξ, corresponding to the thermal blob, is unchanged.

The SANS experiments were carried out either at 20°C or at 60°C. We used two configurations with a fixed sample-to-detector distance $D = 4.7$ m and two neutron beam

wavelengths $\lambda = 4.8$ Å and 12 Å which allow to explore the q-range between 8 10^{-3} and 1 10^{-1} Å^{-1}. The gels swollen in an excess of deuterium oxide were placed between two 1-mm-thick quartz slides hermetically sealed and separated by a distance of 2 mm. The raw data sets obtained for the two different configurations were then transformed into absolute intensities and combined, increasing in this way the range of wave vectors and the number of points in the intermediate q region.

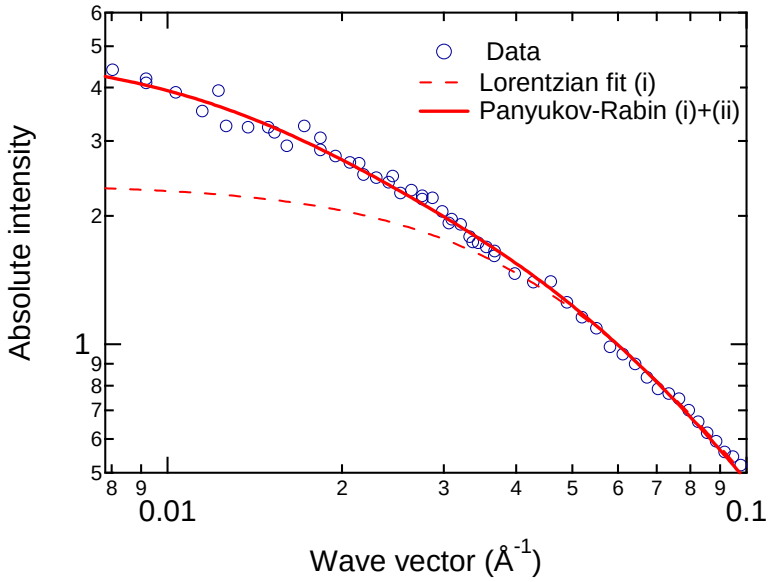

Figure 3 - Data and fits for the SANS measurement of a PDMA-10x2. The Lorentzian fit corresponds to the expected functional form of the high q region. The Panyukov-Rabin fit is the general form for the total range of wave vectors, from which the squared-Lorentzian fit and its fitting parameters (intensity and characteristic size Ξ) are extractible.

A typical neutron scattering curve is shown on Figure 3. Then the curves are fitted to obtain the structural characteristics of the gel. To avoid a large discrepancy on the fit for the weak intensity values at high q, the fits are weighed by the intensity values themselves and the fit is broken up in two parts since the theoretical models propose functional forms for the scattered intensity of gels at low q (ii) and at high q (i).

- First, the high q region is fitted with the Lorentzian form of equation Eq. 2, which gives the values of the intensity $I_L(0)$ due to the polymer solution behavior of the gel (i), and the characteristic size of the thermal blob ξ.
- Then, the whole data range is fitted with equation Eq. 7, imposing the values of $I_L(0)$ and ξ, and weighing the fit with the intensity values to moderate the influence of the intermediate region of wave vectors.

On Figure 3 are represented the fits carried out on the absolute intensity data. It is clearly visible that the model for scattered intensity at low q does not influence the high q region, since the Lorentzian fit (i) on Figure 3 merges perfectly with the Panyukov-Rabin fit. From the Panyukov-Rabin fit, we obtain characteristic values for the low q region, namely $I_{SL}(0)$ and Ξ.

The neutron scattering study is the method that has been used to directly evaluate the sizes of the thermal blob and of the solid-like inhomogeneities in the hydrogels of PDMA and PAM.

1-4- Mechanics: compression test

The first step of the adhesion test consists in a light compression of the hydrogel. For this reason, its mechanical response to compression is important. Furthermore, these tests are also a way to investigate the network architecture of the material. As a consequence, the objectives of this part are to study the mechanical response of hydrogels when subjected to compression tests in order to get an insight of their elastic properties and their macromolecular structure. These tests have been carried out on a home-made force apparatus. During the experiment, force and displacement are measured as a function of time, with a resolution of 0.001 N and 0.1 µm respectively. From this measurement, Young's modulus can be obtained.

The gel samples used for these tests are synthesized in PDMS cylindrical molds. The samples have a diameter of 7 to 8 mm from which can be calculated the cross-section S_0 and a height h_0 of at least 5 mm. The flat faces of the cylinders are cut if needed to have the most flat and regular possible faces perpendicular to the axis of compression. The height and diameter of the sample are then measured within a precision of 0.1 mm. The compression test is realized with the sample placed between two glass slides. The gel is covered with dodecane to limit the evaporation of water and to ensure perfect lubrication at the contact and to prevent the cylinder from barrelling, which is essential to have an ideal uniaxial compression [17,18].

At the beginning of each experiment, the cylinder faces are put in contact with the two glass slides, applying a pre-loading of 30 mN. Then, the compression test is carried out. The raw data obtained from these tests are plotted on Figure 4. Although generally, for compression tests, both the measured force F and the displacement δ are defined as negative, we have taken the opposite convention for this set of experiments.

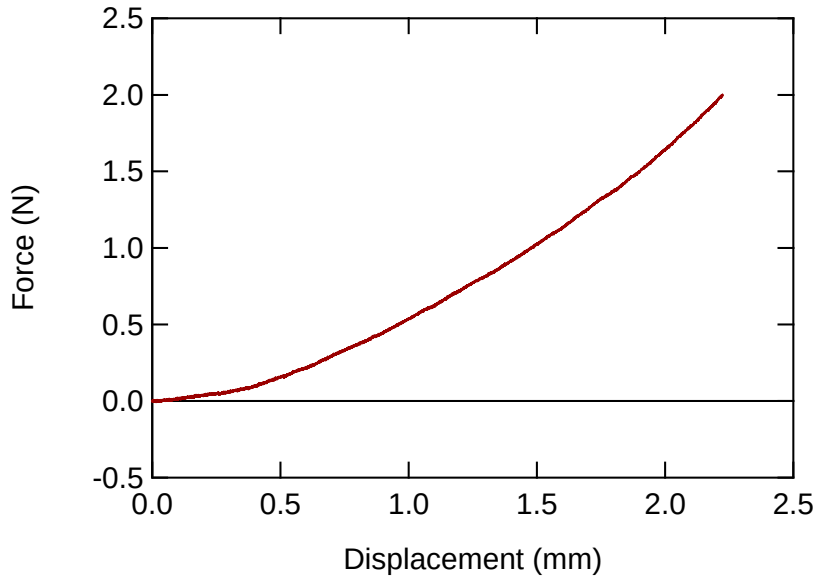

Figure 4 - Raw data: force versus displacement, obtained after a compression test on a cylindrical PDMA-10x2 gel sample. Diameter is equal to 7.5 mm and height to 6.1 mm.

Knowing the dimensions of the sample tested, it is then possible to obtain the nominal stress (also called engineering stress) and the true stress that are defined as:

$$\sigma_{nom} = \frac{F}{S_0}; \qquad \textbf{Eq. 8}$$

$$\sigma_{true} = \frac{F}{S_0}\lambda; \qquad \textbf{Eq. 9}$$

where

$$\lambda = \frac{h_0 + \delta}{h_0}. \qquad \textbf{Eq. 10}$$

The nominal and true stresses are plotted as a function of the strain $\varepsilon = -\frac{\delta}{h_0}$ (considered positive here), focusing on the linear region of Figure 4, as shown on Figure 5. We can then note that the linear domain is much more extended for the true stress compared to the nominal one. The affine fit for the true stress is then more reliable on a deformation domain close to 20%. It gives a value of the Young's modulus of the sample (E = 93.5 kPa in the example shown here).

However, due to experimental problems – such as capillary forces or the possible irregularity of one of the two bases of the cylinder – it is almost impossible to associate a force equal to zero with a total contact. To this end, a regression of the linear domain is performed to determine the proper elongation of the cylinder: a shift of the displacement is made to obtain a force equal to zero for a displacement nil, considered in the linear domain. The accuracy of

this calculation can be checked on plots such as Figure 6 which show the true stress σ_{true} as a function of the elongation λ. As a consequence, the Young's modulus slightly changes (in the example shown here, it is revaluated and found equal to E = 94.3 kPa). Moreover, the latter shift is a necessity prior to an analysis of the data using the Mooney-Rivlin approach.

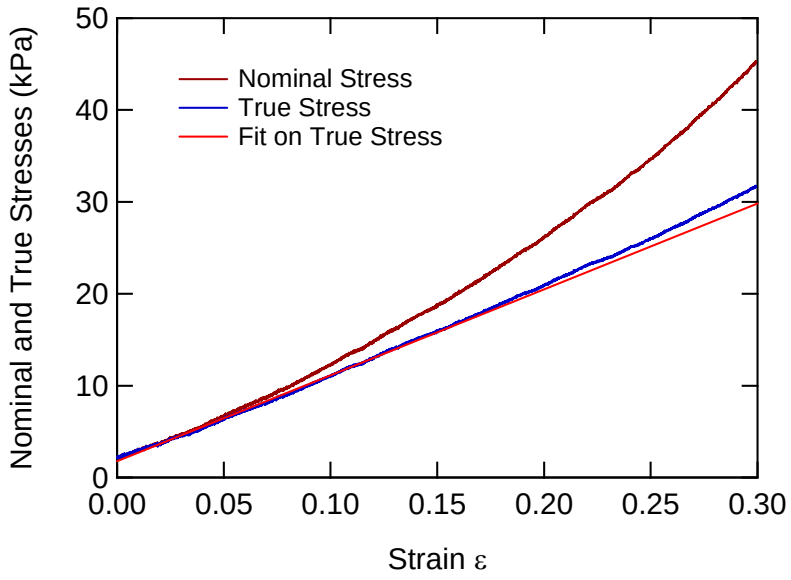

Figure 5 - Nominal and true stresses as a function of strain from the compression test presented on Figure 4. The fit gives a Young's modulus equal to 93.5 kPa.

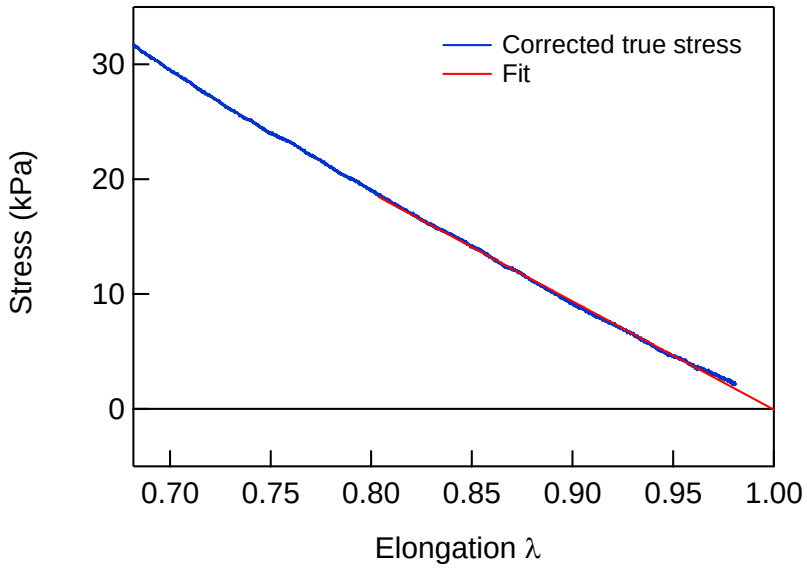

Figure 6 - True stress as a function of elongation from the compression test presented on Figure 4. The fit gives a Young's modulus equal to 94.3 kPa.

Finally, we obtain the Mooney-Rivlin plot (cf. Figure 7) in which a normalized form of the stress called the Mooney stress σ_{Mooney} is plotted as a function of the inverse of the elongation

λ^{-1}; the Mooney-Rivlin model predicts an affine variation written as follows for uniaxial compression:

$$\sigma_{Mooney} = \frac{\sigma_{true}}{\lambda^2 - \lambda^{-1}} = -\left(2C_1 + 2C_2\lambda^{-1}\right). \qquad \textbf{Eq. 11}$$

The Mooney reduced stress σ_{Mooney} diverges for $\lambda = 1$ but the extrapolation corresponding to the undeformed state gives the shear modulus $G = -\left(2C_1 + 2C_2\right)$ (see the red dot on Figure 7).

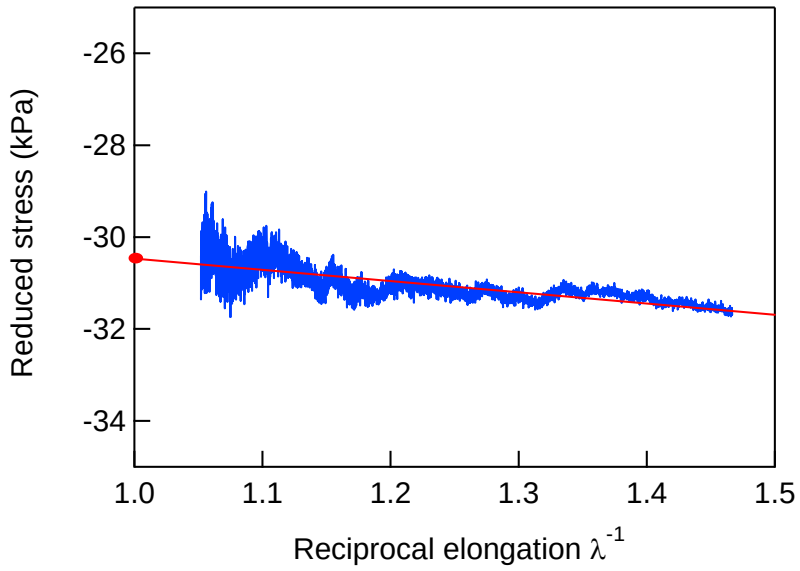

Figure 7 - Mooney plot for the uniaxial compression test presented on Figure 4. The fit gives $\begin{cases} -2C_1 = 29.80 \pm 5.9\,10^{-2}\ \text{kPa} \\ -2C_2 = 1.08 \pm 4.6\,10^{-2}\ \text{kPa} \end{cases}$ **, hence,** $G \approx 30.9\ \text{kPa}$ **.**

Writing the relation between Young's modulus and the shear modulus $E = 2G(1+\nu)$, with ν the Poisson coefficient, and making the incompressibility hypothesis for our experiments ($\nu = 0.5$), we find $E = 3G$, which leads to a Young's modulus found with the Mooney-Rivlin approach equal to 92.6 kPa.

In the case of classical elastic models (phantom or affine for instance), $C_2 = 0$ and $G = 2C_1$, and the Mooney-Rivlin plot corresponds to a horizontal line. The first coefficient C_1 is then related to the permanent entropic forces in the network, and C_2 is usually attributed to non-bonded interactions which are able to relax or reorient with strain; or in a more direct way, C_1 is the term due to cross-links and C_2 comes from entanglements or network defects.

Whatever the approach used to find Young's modulus or the shear modulus of the material, we find accuracy within a few percents.

1-5- Mechanics: rheology

The dissipative behavior of the hydrogels is important since the energy of adhesion is due to interfacial phenomena and bulk dissipation. To investigate the dissipative properties of the hydrogels, their linear viscoelastic properties have been studied on a strain-controlled rheometer Rheometrics RFSII. A sinusoidal strain (γ^*) of very low amplitude γ_0 is applied and the response of the material in producing a resulting sinusoidal stress (σ^*) of amplitude σ_0 is recorded.The phase of the strain is shifted by δ for the stress. The phase difference between the stress and the strain δ (from 0 to $\pi/2$) is characteristic of the dissipative properties of the constrained material: a strictly elastic material will have no phase difference whereas a purely viscous material will have a phase difference equal to $\pi/2$.

A way of writing Hooke's law for viscoelastic materials and for shear strains corresponds to the following expression $\sigma^* = G^* \cdot \gamma^*$, where G^* is the complex shear elastic modulus which is defined as: $G^* = G' + iG''$.

$G' = \frac{\sigma_0}{\gamma_0}\cos\delta$ is the elastic component of the modulus and is characteristic of the elasticity of the material and of the energy fraction which is stored per cycle.

$G'' = \frac{\sigma_0}{\gamma_0}\sin\delta$ is the loss component of the modulus: it is representative of the internal friction of the material due to viscosity, which is the source of a loss of energy.

We used a parallel-plate geometry with a 25 mm diameter. Both plates were roughened to avoid any slipping of the gels at the contact with the rheometer tools. For that purpose, gel plates are synthesized between two glass slides treated to be hydrophobic with octadecyltricholorosilane (see Chapter 3). The thickness of the plates does not exceed 1.7 mm. Discs of diameter 28 mm are cut out of the plate with a punch and are dialyzed against pure water. The gel sample is carefully deposited on the bottom plate of the rheometer and the top plate of the rheometer is moved down and put in contact with the gel to read a normal force of 10% (of the total normal force scale of the rheometer). Then, the samples are immersed in water to avoid drying. The immersion was carried out in paraffin oil for the samples with a monomer mass concentration (m:w) = 20 wt% since it minimizes the possibility of slippage.

Two types of measurements have been carried out: the first one is a strain sweep from 0.045% to 10% with a frequency equal to 1 Hz; the second one is a frequency sweep between 0.1 Hz and 20 Hz, with a low controlled strain (0.1%).

The strain sweep assures that the frequency sweep is performed in the region of strain where the response of the material is linear, and that there is no slipping at the interface between the gel and the plates of the rheometer. A second strain sweep is realized over a shorter range to make sure that the first measure did not alter the gel sample. Typical curves obtained are represented on Figure 8 and show the evolution of the moduli as a function of strain. For a strain lower than a few percents, the storage modulus remains constant, and decreases only for a higher strain value; this is usually the signature of flow or fracture that occurs in these conditions. With the second measurement, we make sure the system has not been damaged by the first measurement since no significant variation of the moduli could be observed. However, at larger strains, the possibility to break the gel sample becomes higher.

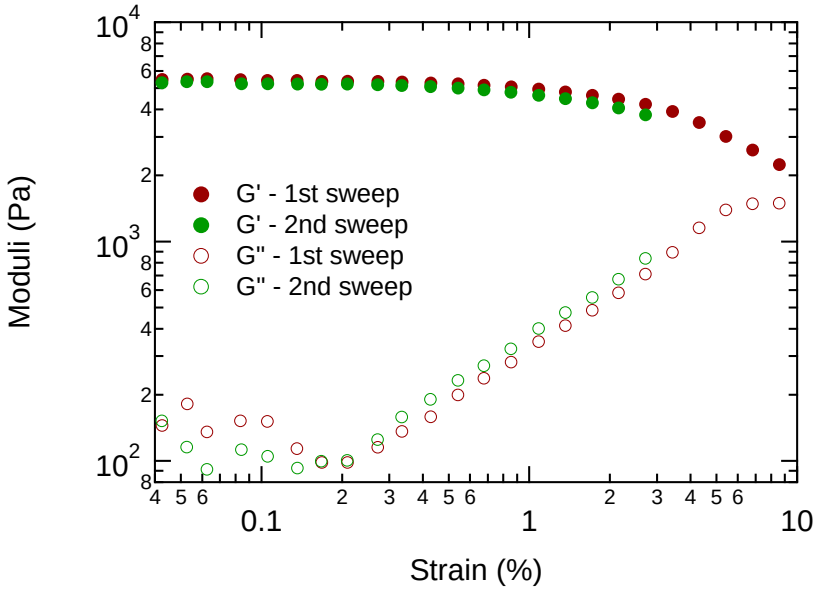

Figure 8 - Strain sweep at 1 Hz with a 10% normal force: storage and loss moduli as a function of strain for dialyzed PDMA-10x2 hydrogel.

The frequency sweeps are then performed in the linear strain regime of the material. The results shown in Figure 9 are typical for chemical gels with an elastic plateau (G_0)independent of the frequency and a viscous plateau at least one order of magnitude lower than the elastic one. The measure of the viscous modulus is then less accurate as the phase difference δ is low and the uncertainty of its measure becomes relatively high.

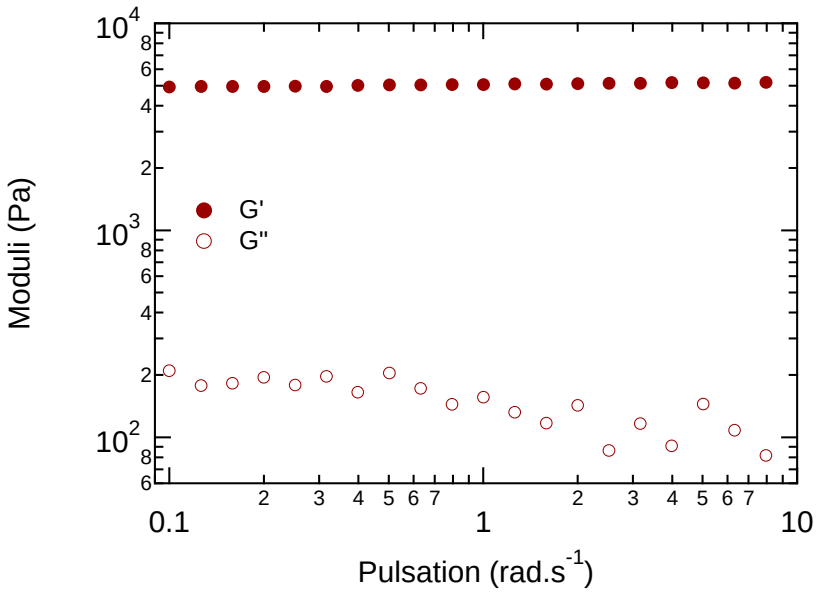

Figure 9 - Frequency sweep with a 10% normal force and a 0.1% strain: storage and loss moduli as a function of pulsation for dialyzed PDMA-10x2 hydrogel.

2- Characterization of PDMA hydrogels

2-1- Swelling behavior

Theoretical background

The swelling of a network in equilibrium with its environment (Q_e), or its volume fraction ($\phi_2 = 1/Q_e$), are very simple but important parameters that characterize the macromolecular architecture frozen during the synthesis (depending on initial concentration of monomers and relative concentration of cross-linkers) as well as the affinity of the polymer for its surrounding.

According to the theory, the swelling equilibrium arises from the competition between entropy of mixing and elasticity in the change of Gibbs free energy density: $\Delta g = \Delta g_m + \Delta g_{el}$.

The mixing term arises from the theory of Flory and can be written as:

$$\Delta g_m = \frac{RT}{V_1}\left(\phi_1 . \ln \phi_1 + \chi_{12}\phi_1\phi_2\right) \qquad \textbf{Eq. 12}$$

where we have the classical notations: V_1 the molar volume of the solvent, R the universal gas constant, T the temperature, ϕ_1 and ϕ_2 the solvent and polymer volume fractions in the gel ($\phi_1 + \phi_2 = 1$) and χ_{12} the Flory interaction parameter of the binary system.

Two main models describe the elasticity term: the so-called affine and phantom network models [19]. In the affine network model (Flory 1953), the points of cross-linking are supposed to be embedded in the network of volume *V* and as a consequence, the deformation of each elastic chain (v_e per volume unit) is homothetic to the macroscopic deformation. In the phantom network model (James and Guth 1947), the junction points are not constrained by the neighboring chains and are free to fluctuate over time on a range which is not affected by the macroscopic deformation.

Using the phantom theory, with the hypothesis that the deformation is isotropic, the density of Gibbs free energy is:

$$\Delta g_{el} = \left(1 - \frac{2}{f}\right)\frac{3kT\nu_e}{2V}\left(\alpha^2 - 1\right) \qquad \textbf{Eq. 13}$$

where α is the isotropic extension ratio $\alpha = \left(\phi_0/\phi_2\right)^{1/3}$, with ϕ_0 the polymer volume fraction in the preparation state, and f the functionality of the junction points.

For an ideal network, the concentration of elastically active chains (v_e / V) can be written as follows:

$$\frac{\nu_e}{V} = \frac{\phi_2 N_A}{v_{pol}^{spe} M_C} = \frac{N_A \phi_2}{N V_1} \qquad \textbf{Eq. 14}$$

where v_{pol}^{spe} is the specific volume of the dry polymer, N_A is Avogadro's number, N is the mean number of "equivalent" units between junction points.

In a good solvent, when the interactions between the polymer and the solvent are favorable (which corresponds to $\chi_{12} \leq 1/2$), the gel tends to swell and entropic effects of elasticity resist to this swelling. At the equilibrium, the osmotic pressures inside and outside the gel are equal, and $\Pi = 0$ outside the gel in the case of a pure solvent.

With:

$$\Pi_{gel} = \Pi_m + \Pi_{el} = \phi_2^2 \cdot \frac{\partial}{\partial \phi_2}\left(\frac{\Delta g_m + \Delta g_{el}}{\phi_2} \right) = 0 \qquad \textbf{Eq. 15}$$

and using the previous equations, we finally obtain:

$$\Pi_{gel} = -\frac{RT}{V_1}\left(\ln(1-\phi_2) + \phi_2 + \chi_{12}\phi_2^2 + \left(1 - \frac{2}{f}\right)\frac{\phi_0^{2/3}\phi_2^{1/3}}{N} \right) = 0 . \qquad \textbf{Eq. 16}$$

From this last expression, it is possible to predict the volume swelling at equilibrium ($Q_e = 1/\phi_2$), taking into account the solvent quality (χ_{12}), the volume swelling at synthesis ($Q_0 = 1/\phi_0$) and the proportion of cross-linkers through the average number of monomers between cross-links, proportional to N. N can be expressed as

$$N = \frac{M_X . v_{pol}^{spe}}{V_1}, \qquad \textbf{Eq. 17}$$

where M_X is the mean molar mass of the strand between cross-links, $v_{pol}^{spe} = 0.95\,\mathrm{cm^3.g^{-1}}$ in the case of PDMA and $V_1 = 18\,\mathrm{cm^3.mol^{-1}}$ is the molar volume of water. Q_0 can be calculated according to the following equation :

$$Q_0 = 1 + \frac{v_w^{spe}}{v_{pol}^{spe}}\left(\frac{m_{tot}}{m_{pol}} - 1 \right), \qquad \textbf{Eq. 18}$$

where $v_w^{spe} = 1\,\mathrm{cm^3.g^{-1}}$ is the specific volume of water, m_{tot} is the total mass of the gel formulation during synthesis and m_{pol} is the mass of polymer in the formulation.

Experimental results

Swelling experiments were carried out on PDMA hydrogels after equilibrium in milli-Q water and the results are reported in Figure 10.

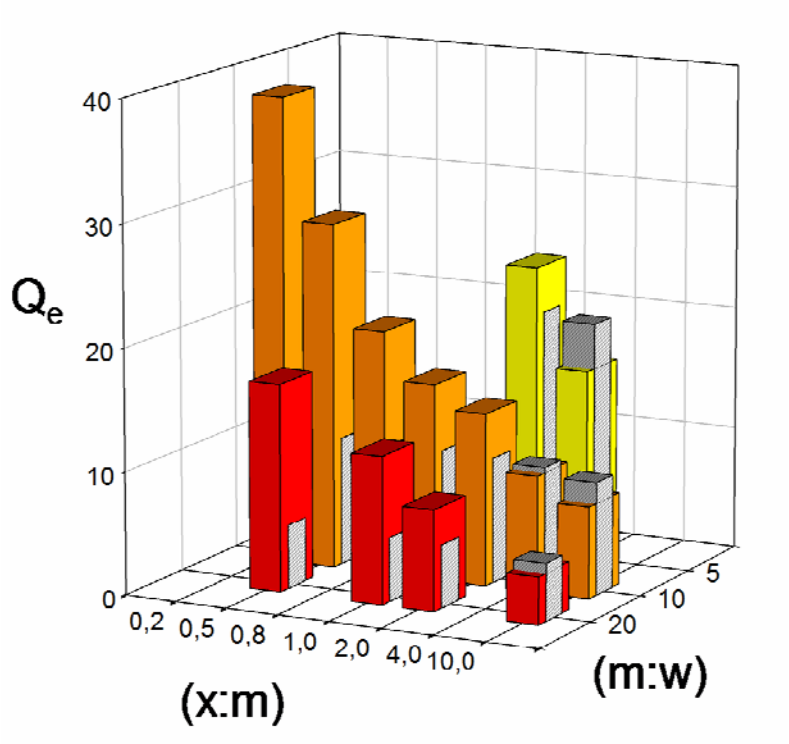

Figure 10 - Swelling behavior of PDMA gels in pure water (Q_e) as a function of the monomer mass concentration (m:w) and cross-linker molar ratio (x:m). For each gel, the initial swelling (Q_0) has been superposed in grey.

This representation is quite interesting as it easily captures the main effect of the parameters used in the formulation of hydrogels and more specifically their impact on the elastic contribution. For instance we can see that an increase of the cross-linker ratio (x:m), *i.e.* a decrease of N, immediately gives rise to a lower swelling ability of the network that can be physically correlated with the lower extensibility of shorter elastic chains (see Figure 11).

Similarly, working at a fixed (x:m) value, the decrease of monomer concentration during the synthesis (ϕ_0), *i.e.* an increase of the swelling in the reference state (Q_0), provides a higher swelling of the gel at equilibrium Nevertheless, if one compares Q_e and Q_0 at a given crosslinker ratio (see (x:m)=1, 2, 4 and 10 mol% in Figure 10), we can see that their ratio ($Q_e/Q_0 = \alpha^3$) decreases with decreasing concentration. In some cases, the swelling at equilibrium Q_e can be lower than Q_0 demonstrating syneresis during preparation.

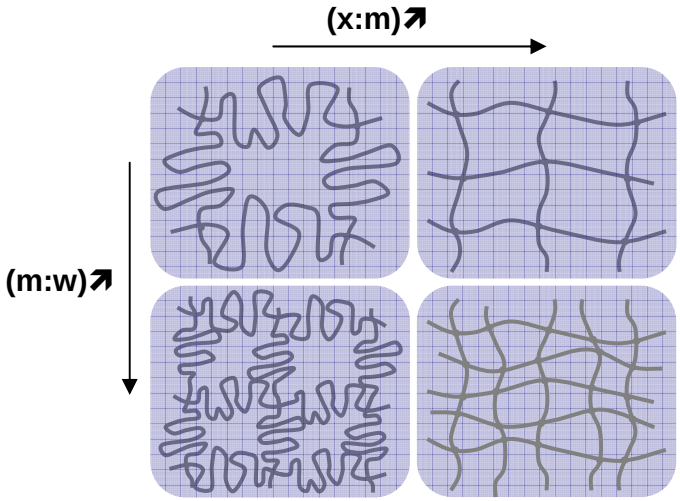

Figure 11 - Schematic representation of different hydrogels prepared by varying the cross-linking ratio (x:m) and/or the monomer concentration (m:w).

This behavior is emphasized in Figure 12 where the expansion ratio α is plotted versus the cross-linker fraction.

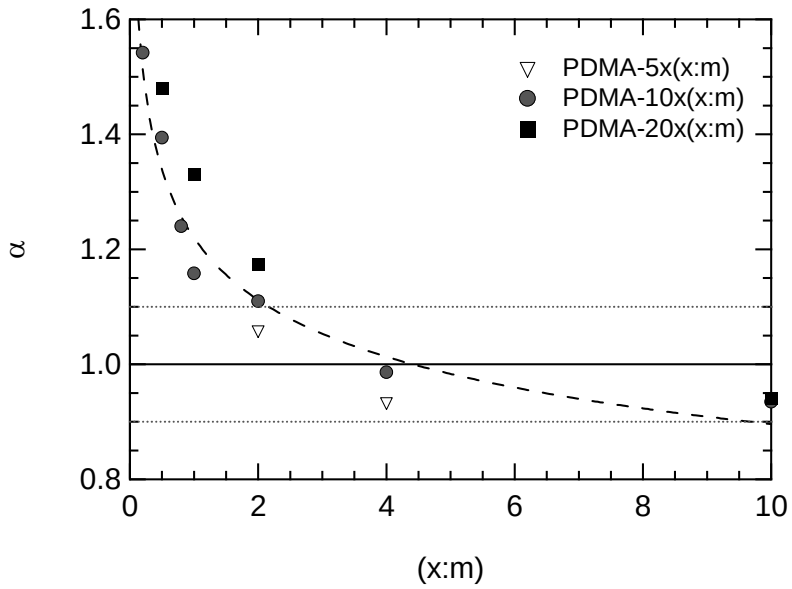

Figure 12 - Variation of the expansion ratio versus the cross-linker fraction for PDMA hydrogels prepared at different monomer concentrations. The dashed line is a guide for the eyes for the series PDMA-10.

It appears clearly that, for a given monomer concentration, the network must be sufficiently cross-linked, but not too much, if the objective is to get swelling values at equilibrium as close as possible to the preparation state. As it will be discussed in Chapter 5, this is a very

important feature to avoid large dimensional changes of gel samples that will be covalently attached to glass plates and placed in various aqueous environments (pH, ionic strength or temperature). During the experimental part on soft adhesion, we will set the swelling limits of our hydrogels to $\alpha = 1 \pm 0.1$, *i.e.* a maximum variation of 10% in one direction.

2-2- Mechanics: compression test

In order to investigate the mechanical properties and to characterize the macroscopic architecture of hydrogels, compression tests have been performed on various PDMA samples at their equilibrium swelling. A typical test and its level of reproducibility is shown in Figure 13 for the sample PDMA-10x1 and a general overview of the PDMA series is given in Figure 14.

The shear moduli (G), extrapolated from these compression tests, are gathered in Table 3 with the swelling data. From a qualitative point of view, we can verify that the mechanical stiffness of the hydrogels increases with the degree of cross-linking and/or the polymer concentration in the preparation state.

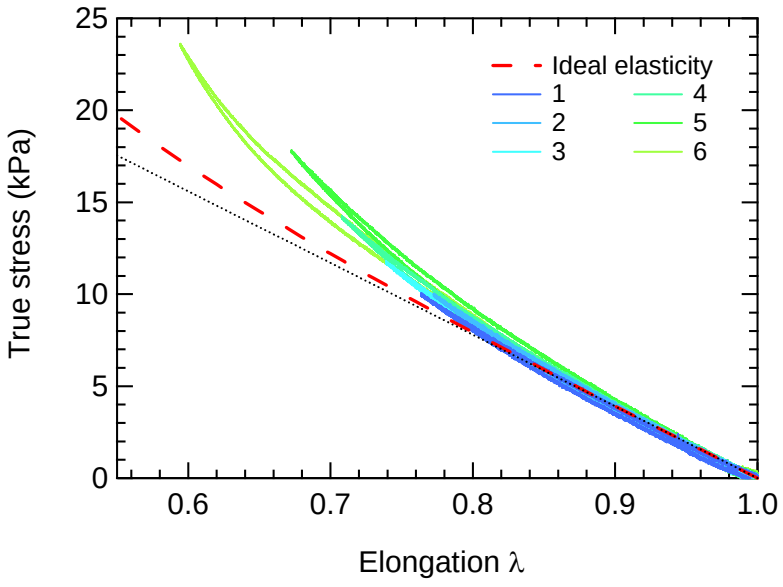

Figure 13 - Reproducibility of compression tests with the gel sample PDMA-10x1. The maximal stress increases with the experiment number. In red dashes is plotted the ideal entropic elasticity and in black the linear elasticity.

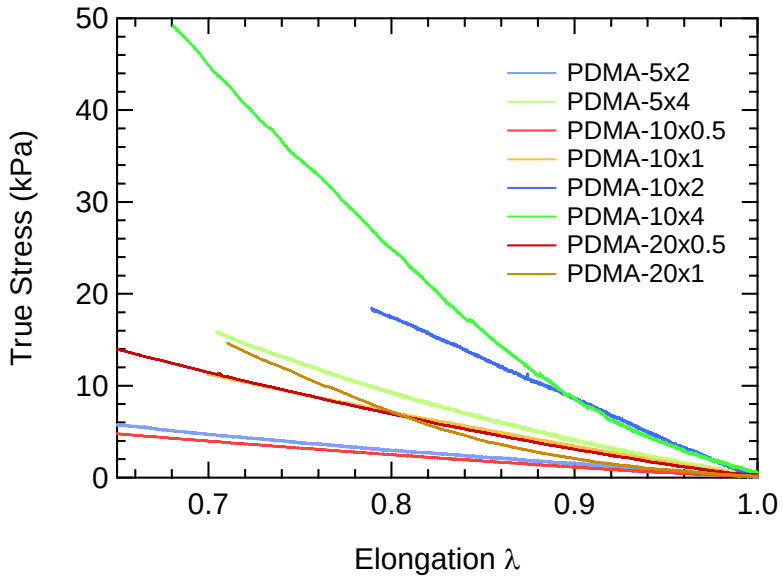

Figure 14 - Compression tests on PDMA gels.

Sample	Q_0	Q_e	G (kPa)	$M_{X,exp}$ (kg/mol)	$M_{X,th}$ (kg/mol)	$100\frac{M_{X,th}}{M_{X,exp}}$	$(x:m)_e$ mol%
PDMA-5x2	20.4	24.3	4.7	12.6	2.5	20	0.39
PDMA-5x4	19.8	16.2	14.1	4.9	1.2	25	1.00
PDMA-10x0.5	10.4	28,2	3.9	22.5	9.9	44	0.22
PDMA-10x1	10.3	16.0	11	9.8	5.0	51	0.51
PDMA-10x2	10.2	14.0	29	3.9	2.5	63	1.27
PDMA-10x4	9.9	9.5	78	1.7	1.2	72	2.87
PDMA-20x0.5	5.2	16.9	11	15.1	9.9	65	0.33
PDMA-20x1	5.1	12.0	28.2	6.7	5.0	74	0.74

Table 3 - Swelling and mechanical data of PDMA series.

A more quantitative picture of the network architecture can be obtained taking into account that the shear modulus is proportional to the concentration of elastically active chains or inversely proportional to the average molar mass between cross-links ($M_{X,exp}$). Using the phantom network model, the shear modulus is explicitly correlated to $M_{X,exp}$ by the following relation [8]:

$$G = \left(1 - \frac{2}{f}\right)\frac{RT}{v_{pol}^{spe} M_{X,exp}} Q_0^{-2/3} Q_e^{-1/3}. \qquad \textbf{Eq. 19}$$

The experimental $M_{X,exp}$ values calculated from Eq. 19 are given in Table 3 where they are compared with the theoretical molar masses ($M_{X,th}$) that can be obtained from the initial monomer composition and cross-linker functionality:

$$M_{X,th} = \frac{2M_0}{f}\frac{[DMA]}{[MBA]} = \frac{2M_0}{f}\frac{100}{(x:m)}. \qquad \textbf{Eq. 20}$$

with [DMA] and [MBA] the molar composition of monomer and cross-linker and M_0 the average molar mass of monomer units inside the network ($M_0 \cong 99$ g.mol^{-1}).

As we can see, the experimental molar masses obtained from compression tests ($M_{X,exp}$) are systematically higher than the theoretical ones, a signature of the presence of defects inside the network. Several reasons can be invoked to justify the presence of these defects or irregularities and particularly the copolymerization process itself that, carried out in batch conditions, makes the incorporation of monomers and cross-linkers statistic and not random with a drift of M_X along the conversion of the reaction. In other words, we expect a large distribution of molar masses between cross-links with heterogeneities at the local scale between soft lightly cross-linked domains alternating with more cross-linked ones.

Another important point is the conversion of the polymerization process. As previously mentioned, SEC analysis has shown the absence of residual free monomers at the end of the reaction. Nevertheless, from double bond titration performed on sample PDMA-10x2, we found that while approximately 90 mol% of the MBA cross-linkers have effectively reacted by their two ends, 10 mol% of MBA are just attached by one end and exhibit a free double bond at the other end. The presence of reactive double bonds embedded inside the network is an important feature that strongly impacts the formation, the architecture and the properties of interpenetrating networks or "double networks" as it has been discussed by Gong *et al.* [20].

Finally, regardless of the previous problems, we have also to take into account that all cross-links (f = 4) do not give rise to elastically active chains, *i.e.* bridges, and that inactive chains like dangling chains or loops are also formed during the polymerization/gelation process.

Assuming that mechanical tests provide the right concentration of elastically active chains and consequently the right average molar mass between cross-links, the ratio between theoretical and experimental M_X values ($M_{X,th}/M_{X,exp}$) allows to assess the efficiency of bridge formation. Similarly, we can recalculate the "effective" cross-linker/monomer ratio $(x:m)_e$, taking into account only MBA units that really participate to the formation of elastic bridges. As we can see in Table 12, there is a strong impact of both monomer and cross-linker concentrations over the efficiency of bridges formation. Obviously, the efficiency increases

with increasing monomer concentration, from 25 to 72% for samples PDMA-5x4 and PDMA-10x4, respectively, and with increasing MBA amount, from 44 to 72% with samples PDMA-10x0.5 and PDMA-10x4.

Using the series of hydrogels reported in Table 3, we have tried to fit their swelling behavior at equilibrium (Q_e) with Eq. 16 using the experimental average molar mass between cross-links ($M_{X,exp}$) to calculate N the mean number of "equivalent" units between cross-links (Eq. 17). As shown in Figure 15, a rather good agreement is obtained by plotting Q_e *versus* the effective degree of cross-linking $(x:m)_e$ by setting the Flory parameter at $\chi_{12} = 0.498$, *i.e.* close to the Θ-conditions ($\chi_{12} = 0.5$).

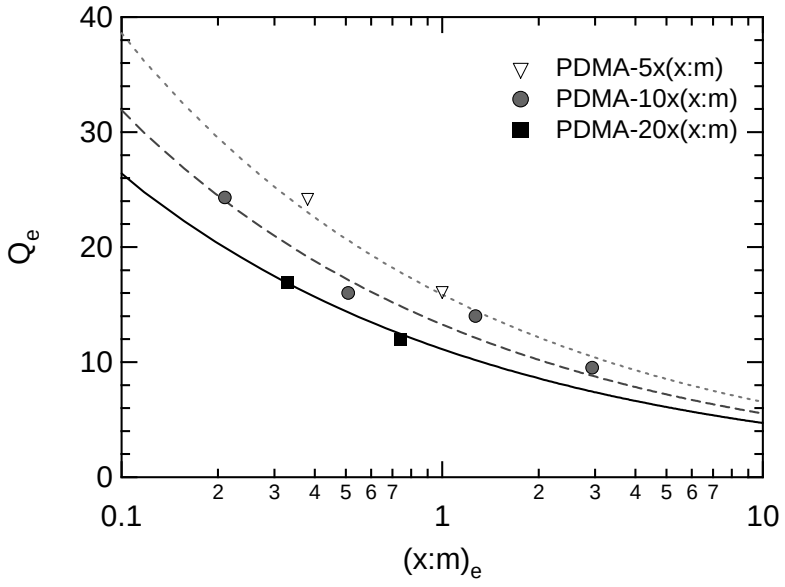

Figure 15 - Swelling behavior of hydrogels versus their effective degree of cross-linking. The lines have been calculated for each series (PDMA-5x, 10x and 20x) using Eq. 16 with χ_{12} = 0.498.

This correlation between thermodynamic and mechanical experiments supports quantitatively the idea of a partial cross-linking efficiency of MBA during synthesis. Taking into account that PDMA gels follow the same thermodynamic behavior at equilibrium in water ($\chi_{12} = 0.498$), it is possible to determine the conditions for swelling and deswelling as a function of the formulation parameters. This is shown in Figure 16, where the effective degree of cross-linking $(x:m)_e$ has been plotted *versus* the initial monomer composition $(m:w)_0$.

As previously discussed with the data of Figure 12, for each monomer concentration, one can find a critical amount of cross-linker allowing the preparation of gels in their equilibrium state ($Q_0 = Q_e$). These specific conditions are given by the curve of Figure 16. Below this curve,

when the degree of cross-linking is too low or the monomer concentration is too high, the gel will swell when placed in pure water while the opposite behavior (deswelling and syneresis) will be observed during synthesis.

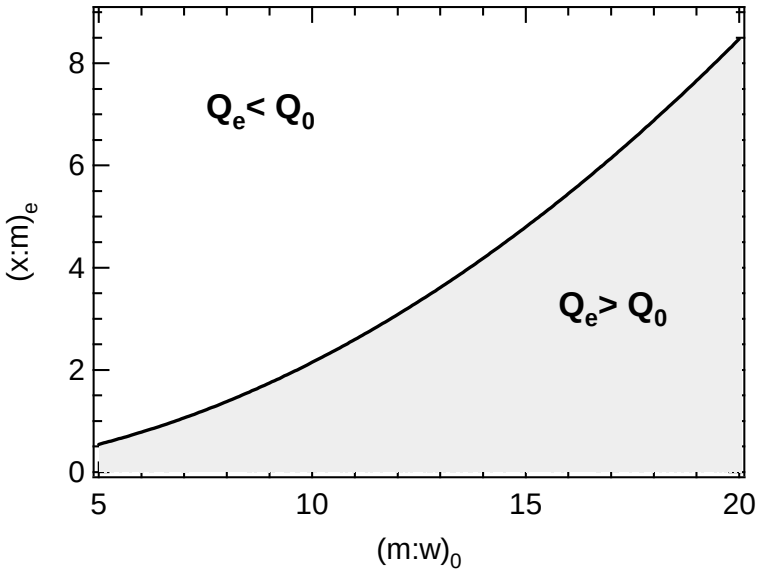

Figure 16 - Swelling/deswelling map of PDMA hydrogels in pure water as a function of their initial monomer composition $(m:w)_0$ and effective degree of cross-linking $(x:m)_e$.

This critical behavior can be described explicitly using Eq. 16 and assuming that the polymer volume fraction is rather small ($\phi_2 << 1$):

$$\left(0.5-\chi_{12}\right)\phi_2^2+\frac{\phi_2^3}{3}=\left(1-\frac{2}{f}\right)\frac{\phi_0^{2/3}\phi_2^{1/3}}{N}. \qquad \textbf{Eq. 21}$$

Moreover, taking into account that PDMA gels are close to their Θ-conditions ($\chi_{12}=0.498$) the first term of Eq. 21 can be ruled out and the effective degree of cross-linking can be written as a function of swelling values:

$$N=3\left(1-\frac{2}{f}\right)\phi_0^{2/3}\phi_2^{-8/3}=3\left(1-\frac{2}{f}\right)Q_0^{-2/3}Q_e^{8/3}. \qquad \textbf{Eq. 22}$$

Combining Eq. 17, Eq. 20, Eq. 22 and using our own parameters we finally get:

$$(x:m)_e=\frac{200v_{spe}^{pol}M_0}{3V_1\left(f-2\right)}Q_0^{2/3}Q_e^{-8/3}\sim Q_0^{2/3}Q_e^{-8/3}\sim\left(m:w\right)_0^{-2/3}Q_e^{-8/3}; \qquad \textbf{Eq. 23}$$

and for the specific conditions $Q_e=Q_0$:

$$(x:m)_e\sim Q_0^{-2}\sim(m:w)_0^2. \qquad \textbf{Eq. 24}$$

The scaling relations of Eq. 23 and Eq. 24, which appear in Figure 15 and in Figure 16, are very good tools to understand and predict how the architecture of the network impact the swelling behavior of the network. Nevertheless, we have to keep in mind that the efficiency of cross-linking during polymerization is not predictable *a priori* and also depends on the same parameters $\left[(x:m)_e = f\{(x:m),(m:w)\}\right]$ and that, consequently, experiments cannot be fully replaced by theory.

As previously explained, hydrogels will be covalently attached to glass plates for adhesion experiments and it is very important to limit swelling/deswelling behavior in aqueous environments in order to avoid any dramatic stress formation at the gel/glass interface. For that purpose we will work close to the iso-swelling conditions $Q_0 = Q_e$ ($\alpha = 1$), conditions which are experimentally and theoretically specified in Figure 12 and in Figure 16.

2-3- Mechanics: rheology

All along this study, the gel samples, either PDMA or PAM, were prepared between two identical glass plates treated hydrophobic with octadecyltrichlorosilane. After synthesis, the gel plates were dialyzed for at least one week to reach their swelling equilibrium. The samples were tested in the linear regime, at a deformation equal to 0.1%, and with a normal force around 10% (of the total normal force scale of the rheometer).

As shown in Figure 17, all PDMA samples have a frequency-independent G'. As reported with compression tests, the modulus increases with increasing cross-linker amount or initial monomer concentration. For a monomer concentration (m:w) = 10 wt% (diamonds in Figure 17) , the elastic plateau increases from 3.2, to 10.9 kPa for cross-linker ratios (x:m) varying from 0.8 to 10 mol%. Similarly, for a fixed cross-linker ratio (x:m) = 2 mol% (blue data in Figure 17), the elastic modulus increases from 1.7 to 11.8 kPa with initial monomer concentration increasing from (m:w) = 5 to 20 wt%, respectively. These relative variations are clearly shown on Figure 18, where the shear modulus has been plotted *versus* the initial monomer concentration (m:w).

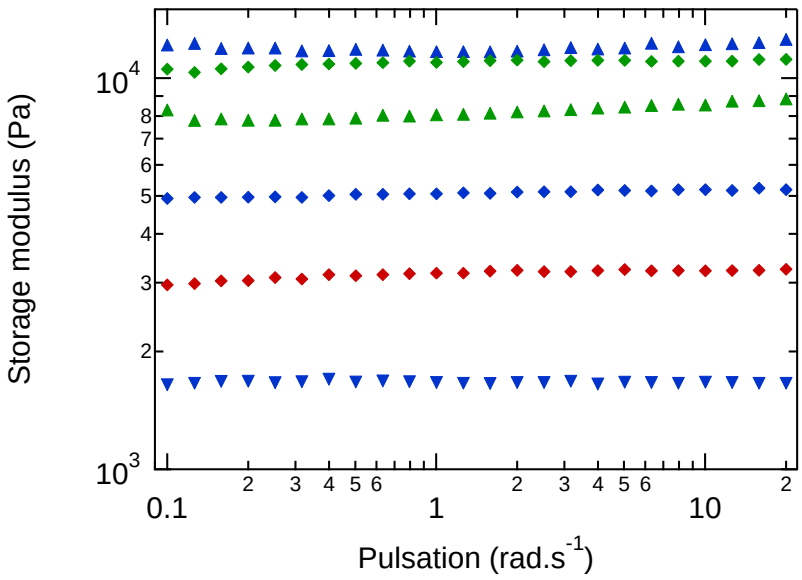

Figure 17 - Storage modulus as a function of pulsation in a frequency sweep measurement of different PDMA hydrogels – Characteristics at the synthesis are as follow: ♦ (m:w)=10; ▲ (m:w)=20; ▼ (m:w)=5; red: (x:m)=0.8; blue: (x:m)=2; green: (x:m)=10.

On Figure 18-top, the elastic and viscous moduli measured in rheology are given for different cross-linker ratios as a function of the monomer mass concentration at the synthesis. We observe that the loss modulus remains at least one order of magnitude below the storage modulus, which is the signature that the gels samples are all very elastic.
Nevertheless, regardless the representation, the main difference with previous compression tests (results are reminded in Figure 18-bottom) is that rheology gives elastic moduli which are much lower than those determined under compression.

For (x:m) = 2 mol%, the elastic modulus increases with the monomer mass concentration, and at a given monomer mass concentration, the elastic modulus increases with the cross-linker ratio; this is consistent with the variations observed in compression tests. But for highly cross-linked gels with (x:m) = 10 mol%, the trend is reversed. This is unexpected and can only be explained by a problem during the measurement: immersed in water, highly cross-linked gels have proven to be sliding at the interface between the gel and the rheometer. To avoid this issue, the immersion was performed in paraffin oil instead of water. Here, since the elastic plateau is rather regular, the contact between the gel and the geometry is probably only partial.

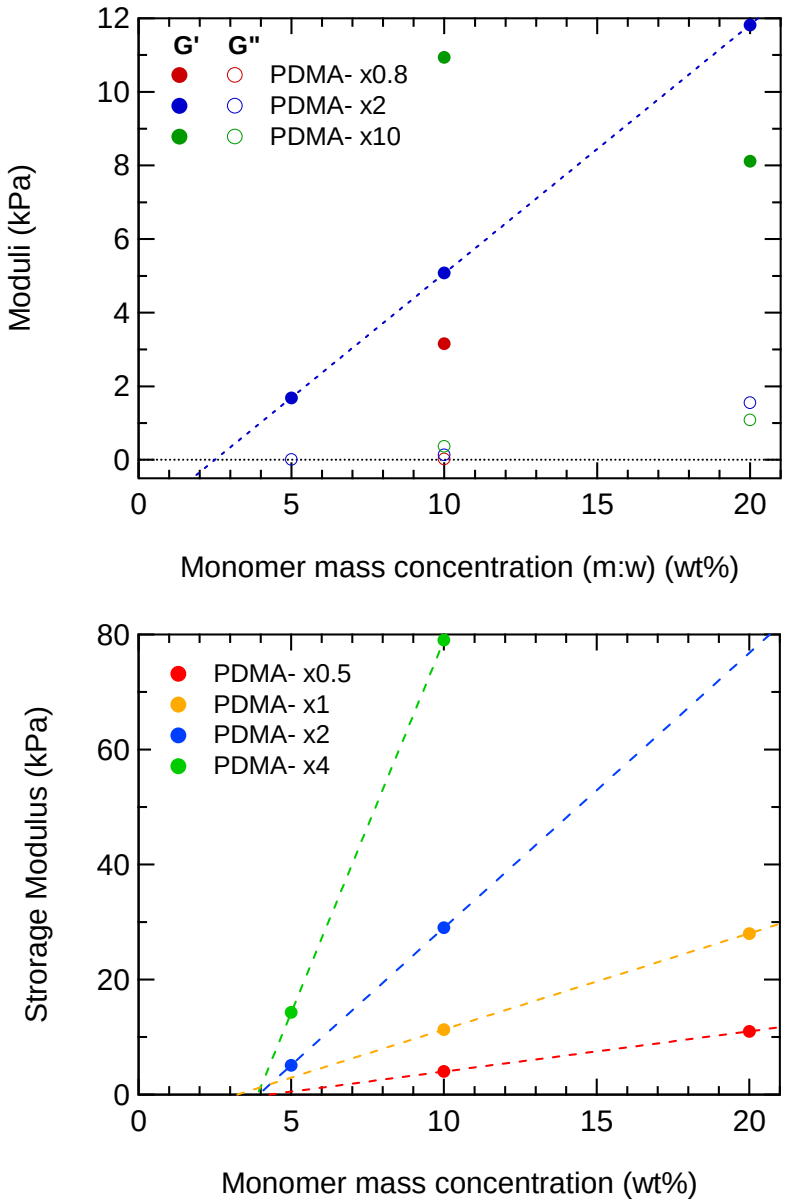

Figure 18 - Storage (●) and loss (○) moduli for PDMA hydrogels, as a function of the monomer mass concentration at the preparation conditions (m:w), for different cross-linker ratios. These values have been determined by dynamic rheology (top) and compression tests (bottom).

With PAM gel samples, the same qualitative behaviors have been observed, as shown on Figure 19 and on Figure 20. We highlight that the behavior of these gels is very elastic, with storage modulus at least one order of magnitude higher than loss modulus.

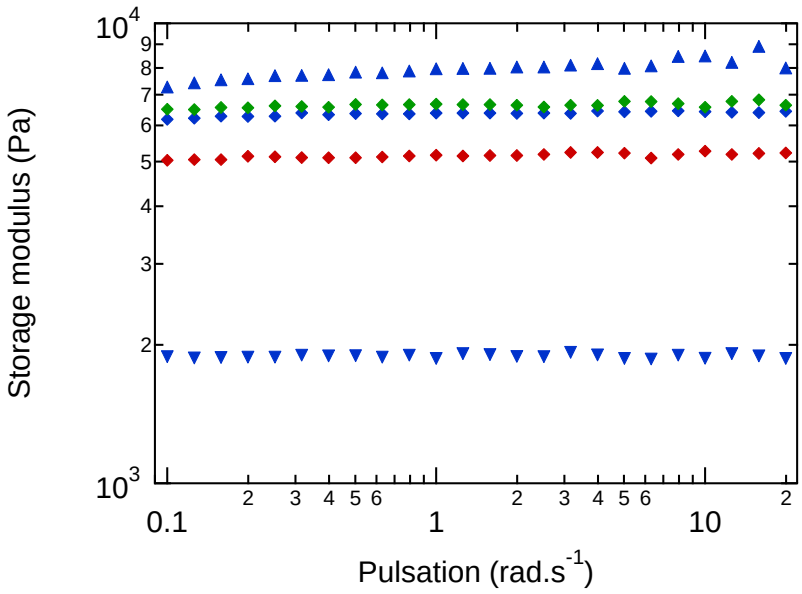

Figure 19 - Storage modulus as a function of pulsation in a frequency sweep measurement of different PAM hydrogels – Characteristics at the synthesis are as follow: ♦ (m:w)=10; ▲ (m:w)=20; ▼ (m:w)=5; red: (x:m)=0.8; blue: (x:m)=2; green: (x:m)=10.

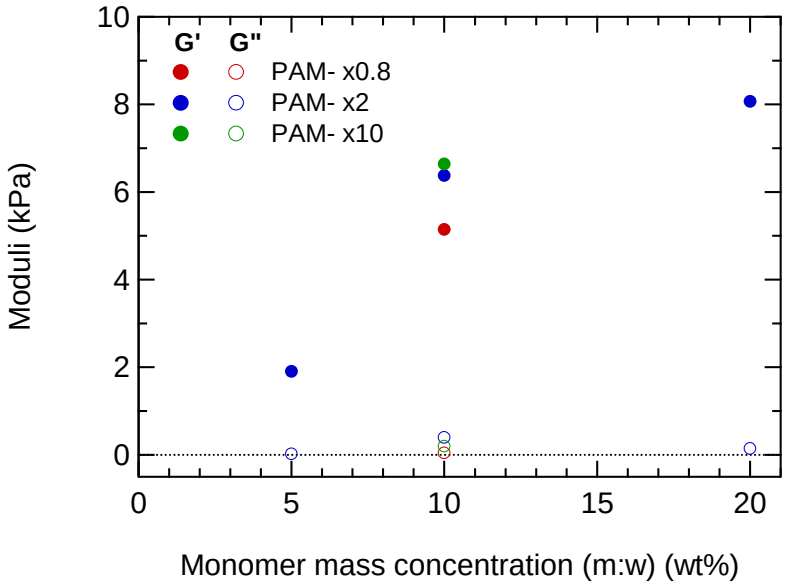

Figure 20 - Storage (●) and loss (○) moduli for PAM hydrogels, as a function of the monomer mass concentration (m:w) at the preparation conditions. Red: (x:m)=0.8; blue: (x:m)=2; green: (x:m)=10.

As a conclusion, the results obtained from rheology prove that both PDMA and PAM gels are highly elastic with a low dissipative behavior. The comparison between mechanical tests carried out by shearing and compression also emphasized a large difference between "surface" and bulk properties. The weak elastic moduli obtained by shearing are likely to be

explained by surface inhomogeneities (lower degree of cross-linking, smaller kinetic chains,…) that take place during the polymerization/gelation process.

2-4- Structure

Another way to investigate the structure of the gels is to use small angle neutron scattering on protonated gels swollen in deuterium oxide. Extrapolated from the approach of De Gennes for semi-dilute solutions [21], SANS gives access to the thermal correlation length ξ. He constructs a scaling form for the variation of ξ by considering two limiting conditions. For a volume fraction ϕ equal to the overlap volume fraction ϕ^*, the coils are in contact and the thermal correlation length is in the order of magnitude of the size of the coils R_F. For $\phi > \phi^*$, the network structure depends on the concentration and not on the degree of polymerization N since the chains are much longer than ξ. Then, $\xi \propto R_F(\phi/\phi^*)^m$, with m such that $\xi \propto N^0$. In a good solvent, $R_F \propto N^{3/5}$ and $\phi^* \propto N^{-4/5}$, and thus $m = -3/4$. In a Θ-solvent, $R_F \propto N^{1/2}$ and $\phi^* \propto N^{-1/2}$, and thus $m = -1$. As a consequence, the variation of ξ depends on the quality of the solvent and for a good solvent:

$$\xi \propto \phi^{-3/4}, \qquad \textbf{Eq. 25}$$

While for a bad solvent,

$$\xi \propto \phi^{-1}. \qquad \textbf{Eq. 26}$$

As a consequence, we have plotted ξ as a function of the volume fraction at equilibrium ϕ_2 on Figure 21 for PDMA-(m:w)x2 gels. The results have been fitted with a power law, and the size of the thermal blob ξ varies with $\phi_2^{-0.68}$, which is in good agreement with the expected variation for a polymer solution in good solvent. It is however to be noted that the limited data available for ξ make it difficult to draw a clear conclusion. The investigation of the variation of ξ at higher temperature will give a deeper insight on the solvent quality.

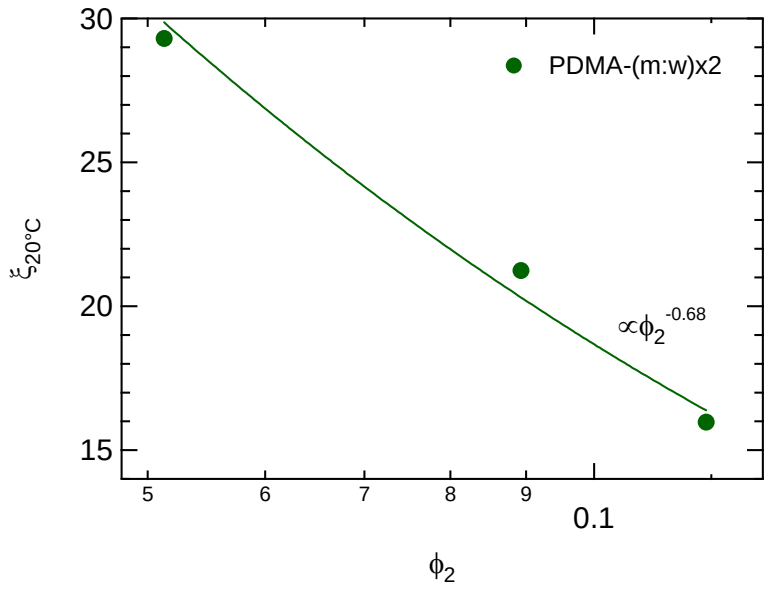

Figure 21 - Size of the thermal blob ξ at 20°C as a function of the monomer mass concentration at equilibrium ϕ_2. The curve is a power law corresponding to an exponent equal to 0.68.

All the sizes of the thermal blobs determined for PDMA hydrogels range from 16 to 32 Å. These values can be compared with the theoretical predictions: in a recent approach, Norisuye *et al.* [7] and Shibayama [12] described the variation of the thermal correlation length more quantitatively and they expressed it as:

$$\xi = b\left[12\left(1-2\chi_{12}+\phi\right)\phi\right]^{-1/2}, \qquad \textbf{Eq. 27}$$

with b^3 and χ_{12} being the volume occupied by a segment and the Flory interaction parameter, respectively. The size of the thermal blob is then expected to be independent of N, the average number of monomers between cross-links. Taking for instance the gel PDMA-10x2, the volume fraction is equal to $\phi_2 \approx 8.9\,10^{-2}$, the Flory interaction parameter is kept equal to $\chi_{12} = 0.498$ (as previously found for the PDMA hydrogels with the analysis of the compression tests) and the monomer size b can be evaluated approximately at 8 Å (similar to the value found for PNIPAM by Norisuye *et al.* [7]). Then, the size of the thermal blob is found equal to $\xi = 25\,\text{Å}$, which is comparable to the result obtained in our experiments (21 Å).

Control samples of PAM gels have been probed at 20°C and 60°C. For them, no difference appear in the absolute intensity of the SANS signal, as shown on Figure 22 where the data measured for PAM gels at 20 and 60°C merge on the whole range of wave vectors. On the contrary, for PDMA gels, the intensity scattered is higher and the thermal blob is bigger at

60°C than at 20°C. The increase of the size of the thermal blob and the increase of the absolute intensity both demonstrate that the quality of D_2O as a solvent is visibly deteriorated for PDMA hydrogels and not for PAM hydrogels. This result is consistent with the results from swelling measurement and compression tests. It is also supported by the results from Gundogan *et al.* [11] who expressed the Flory interaction parameter χ_{12} between PDMA and water as a function of the polymer volume fraction ϕ_2 as $\chi_{12} = 0.47 + 0.036\phi_2$. It suggests that the quality of water as a PDMA solvent is not only dependent on the temperature, but is probably changing slightly with the gel concentration, making the simple analysis of Figure 21 particularly difficult.

On Figure 22, the data obtained for PDMA gels show a change of slope while the data for PAM gels only have one slope. The Panyukov-Rabin fits on the PAM-(m:w)x1 and PAM-(m:w)x2 data gave ξ between 10 and 13 Å, that is to say in a range twice lower than that obtained with PDMA gels.

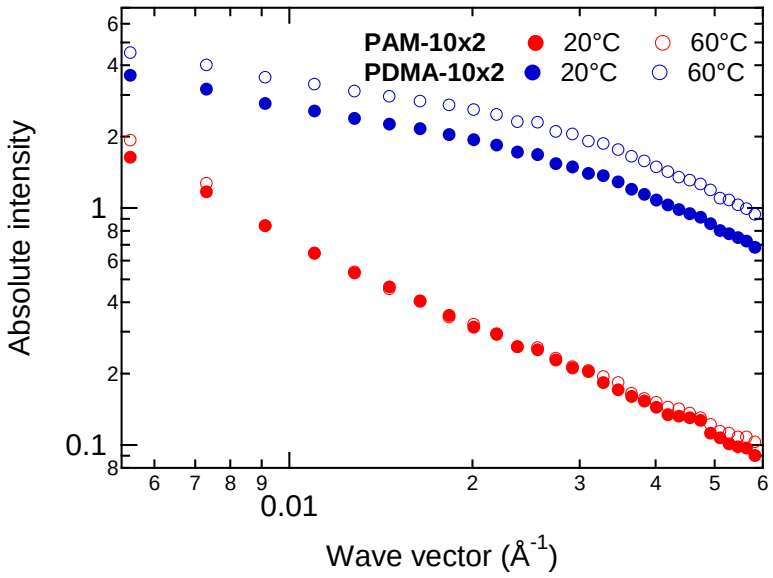

Figure 22 - Scattering spectrum *I(q)* of the gels PAM-10x2 and PDMA-10x2 obtained at 20°C and 60°C.

Finally, Figure 23 enhances the fact that the thermal correlation length changes with temperature for PDMA gels and is insensitive to it for PAM gels, confirming that water is a rather good solvent for PAM but is not really a good solvent for PDMA, especially at high temperature. The influence of temperature on ξ is weaker with both the monomer concentration (m:w) and the cross-linker ratio (x:m).

The second correlation length that can be found with the Panyukov Rabin fits of the data is the inhomogeneity correlation length Ξ. Norisuye *et al.* [7] have studied its variation depending on the conditions at synthesis and have found that Ξ increases rather quickly with the cross-linker concentration, evaluating it in the range of the blob size ξ at very low cross-linker concentration up to 200 Å for a cross-linker molar ratio of 5 mol% in PNIPAM gels with (m:w) ≅ 8 wt%. Our results do not show any clear variation but the typical length Ξ was always found rather insensitive to temperature and between 57 and 69 Å, that is to say about three times higher than ξ. Our results are in agreement with results obtained by Horkay *et al.* [22] on PDMS gels swollen in octane or poly(vinyl acetate) gels swollen in isopropyl alcohol, and it is comparable to their results for poly(vinyl alcohol) hydrogels [23].

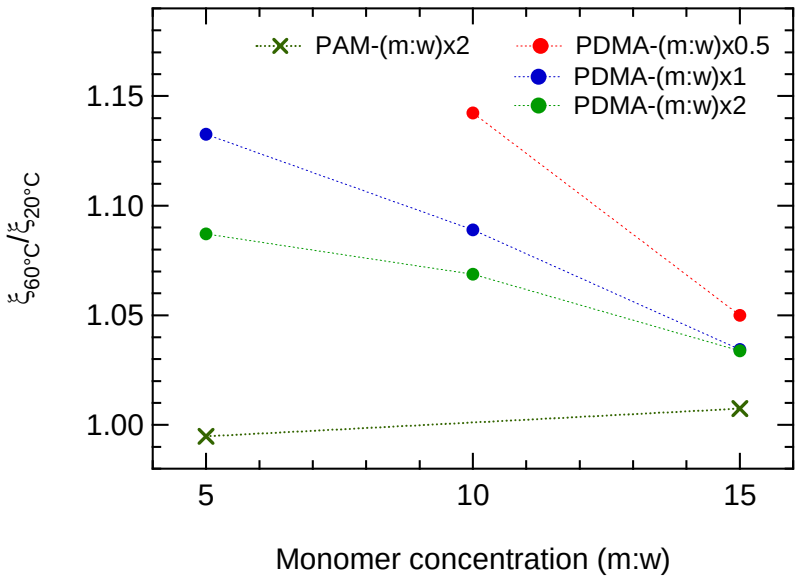

Figure 23 - Direct comparison of the thermal correlation length ξ at 60°C and 20°C as a function of the monomer mass concentration (m:w) at synthesis and for different cross-linker ratios for PDMA gels. Results obtained with control samples of PAM are shown as a reference.

As a conclusion, we have measured the thermal correlation length ξ at 20°C for PAM and PDMA gels and found it in the range of 10-13 Å and 16-32 Å respectively. The inhomogeneity correlation length Ξ was deduced from the Panyukov Rabin fits for the data obtained with PDMA gels and was found around 65 Å (± 5 Å).

The same experiments were carried out at 60°C and no difference in scattering was observed for PAM gels. However, the PDMA gels showed an increase in the scattered intensity, consistent with a higher concentration than at 20°C, that is to say a deswelling of the gel when

heating. Furthermore, the values obtained for the thermal blob were slightly increased, meaning that deuterium oxide becomes a worst thermodynamic solvent for PDMA at higher temperature, whereas PAM scattering was found insensitive to the temperature in the range 20-60°C.

3- Conclusion

Neutral PDMA and PAM hydrogels have been synthesized, using methylene-bis-acrylamide as cross-linker and potassium persulfate/TEMED as redox initiator. The synthesized gels are reproducible, transparent and very elastic, as suggested by compression tests and rheology. However, as polymerization and cross-linking happen concurrently, structural defects are expected. They usually lead to softer materials. This was confirmed here by the swelling measurements (higher than the theoretical prediction) and the compression tests (which gave softer moduli than expected), which both characterize the elasticity of the network and as a consequence its mean cross-link density. A deeper investigation of the structure was carried out thanks to small angle neutron scattering. It led to the conclusion that the thermal blob of the PAM is about two times smaller than the one of the PDMA and that the gels are bearing heterogeneities comparable in size. The results obtained from rheology were however the most unexpected, since the storage moduli found *via* this method are not in agreement with the ones obtained from compression tests, and they are very far from the theoretically expected results. This very significant gap between the results obtained with two different mechanical techniques can only arise from an experimental issue which will be further investigated in Chapter 4.

4- References

[1] Flory, P. J. *Faraday Discussions of the Chemical Society* **1974**, *57*, 7-18.
[2] Rubinstein, M.; Dobrynin, A. V. *Curr Opin Colloid In* **1999**, *4*, 83-87.
[3] Drury, J. L.; Mooney, D. J. *Biomaterials* **2003**, *24*, 4337-4351.
[4] Shoichet, M. S. *Macromolecules* **2010**, *43*, 581-591.
[5] Caldorera-Moore, M.; Peppas, N. A. *Adv. Drug Deliv. Rev.* **2009**, *61*, 1391-1401.
[6] Qiu, Y.; Park, K. *Adv. Drug Deliv. Rev.* **2001**, *53*, 321-339.
[7] Norisuye, T.; Masui, N.; Kida, Y.; Ikuta, D.; Kokufuta, E.; Ito, S.; Panyukov, S.; Shibayama, M. *Polymer* **2002**, *43*, 5289-5297.
[8] Obukhov, S. P.; Rubinstein, M.; Colby, R. H. *Macromolecules* **1994**, *27*, 3191-3198.
[9] Nakajima, T.; Furukawa, H.; Tanaka, Y.; Kurokawa, T.; Osada, Y.; Gong, J. P. *Macromolecules* **2009**, *42*, 2184-2189.
[10] Orakdogen, N.; Okay, O. *J Appl Polym Sci* **2007**, *103*, 3228-3237.
[11] Gundogan, N.; Okay, O.; Oppermann, W. *Macromol Chem Physic* **2004**, *205*, 814-823.
[12] Shibayama, M. *Small Angle Neutron Scattering on Gels*; Springer-Verlag: Berlin Heidelberg, **2008**; Vol. 14.
[13] Candau, S.; Bastide, J.; Delsanti, M. *Advances in Polymer Science* **1982**, *44*, 27-71.
[14] Horkay, F.; Hecht, A. M.; Mallam, S.; Geissler, E.; Rennie, A. R. *Macromolecules* **1991**, *24*, 2896-2902.
[15] Mallam, S.; Horkay, F.; Hecht, A. M.; Rennie, A. R.; Geissler, E. *Macromolecules* **1991**, *24*, 543-548.
[16] Panyukov, S.; Rabin, Y. *Phys Rep* **1996**, *269*, 1-131.
[17] Miquelard-Garnier, G.; Demoures, S.; Creton, C.; Hourdet, D. *Macromolecules* **2006**, *39*, 8128-8139.
[18] Miquelard-Garnier, G. In *Thèse de Doctorat*: Paris VI, **2007**.
[19] Mark, J. E.; Erman, B. *Rubberlike Elasticity - A Molecular Primer*; John Wiley & Sons: New York, **1988**.
[20] Gong, J. P.; Katsuyama, Y.; Kurokawa, T.; Osada, Y. *Adv Mater* **2003**, *15*, 1155-+.
[21] De Gennes, P. G. *Scaling Concepts in Polymer Physics*, 1st ed.; Cornell University Press: New York, **1979**.
[22] Horkay, F.; Hecht, A. M.; Zrinyi, M.; Geissler, E. *Polym Gels Netw* **1996**, *4*, 451-465.
[23] Horkay, F.; Hecht, A. M.; Geissler, E. *Macromolecules* **1994**, *27*, 1795-1798.

CHAPTER 4 – INTERPOLYMER COMPLEXES IN AQUEOUS SOLUTION: VOLUME AND SURFACE STUDY

After having synthesized and characterized the objects that are to be used to measure the adhesion of hydrogels on "smart" brushes, the objective of this second chapter is to determine the type of interactions occurring between these objects.
The first step consists in removing the polymer from the surface and in releasing the constraints imposed by the cross-linking points of the gel to study the interpolymer complexes that form in solution between a proton-donor poly(acrylic acid) and a proton-acceptor poly(acrylamide) or poly(*N,N*-dimethylacrylamide). The objective is to determine the environmental parameters that influence the complexation between these polymer pairs. We have established the pH-temperature phase diagrams for these polymers at a given polymer concentration. How is the domain where the interactions are formed shifted by changing a few parameters such as the polymer concentration, the ionic strength or the ratio of a monomer residue in statistical copolymers of acrylamide and *N,N*-dimethylacrylamide?

Before studying the extent of the interactions of these polymer pairs at interfaces, we characterize the surfaces of the gels that will be used during the adhesion tests. We first investigate the best way to covalently stick a gel on a transparent hard substrate. Then, we try to explain the unexpected results from Chapter 3, where the measurement of the gel modulus gave very different results between compression tests and rheology. We attributed this gap to a surface issue and as a consequence, we characterize the free surfaces of gels depending on the nature of the surface of the mold used for its synthesis. The objective is to determine what mold surface is the most adapted to minimize the difference between rheology and compression tests, that is to say: in which conditions does the surface characteristics of the gel are the closest to those in bulk?

The last step of this study is to determine the extent of the interactions characterized in solution in the first part of this Chapter once they occur at interfaces, between a brush, and a gel, the surface composition of which has been determined. We use a characterization technique that allows to determining the density profile of the brush in the direction normal to the surface at the polymer scale: neutron reflectivity. We investigate the influence of the gel characteristics (chemistry, concentration) and of the brush (length of the chains, grafting densities) on the conformation of the chains.

The main objective of this thesis is to control and tune adhesion on surfaces, using polymers able to form complexes at the interface. Many types of interactions can lead to the formation of interpolymer complexes (IPC), such as hydrogen bonding, electrostatic and ionic interactions, hydrophobic interactions, Van der Waals forces, charge-transfer interactions and associations of these interactions often found in specific biological systems [1]. The interest of these interactions is that they are sensitive to their environment, for instance temperature, pH or ionic strength, solvent, electric or magnetic field… Limiting our study to the formation of IPC through hydrogen bonding, the previous works have been summarized in many reviews and a lot of corresponding articles [2]. In general, the formation of H-bonded IPC is observed between a poly(carboxylic acid) and a non-ionized polymeric proton-acceptor.

The prime choice poly(carboxylic acid) which has attracted many efforts is poly(acrylic acid) (PAA). It has been mixed in water with non-ionic polybase (in the sense of Lewis), such as poly(ethylene oxide) (PEO), poly(acrylamide) (PAM) and its derivatives, poly(*N*-vinyl-2-pyrrolidone) (PVP), etc. The study of the formation of the IPC was followed with different classical methods [3] such as gravimetry [4], potentiometry [4,5], turbidimetry [6-9], viscosimetry [5,9-12], fluorescence study after the labeling of one of the polymers [12,13], light scattering [8], etc. The structure of the IPC and the most favorable H-bonds have been determined thanks to small angle neutron scattering [14] and infrared [8] or NMR spectroscopy [15].

It has been shown that in water solution, the formation of the IPC between the non-ionic polymer and the PAA could only happen below a critical pH [6], for which the PAA is protonated enough. Then, it was suggested that the value of the critical pH is an indicator of the complexing ability of the polymer: as the critical pH increases, the PAA becomes less protonated; if the IPC forms with a lower protonation ratio in the PAA (*i.e.* at higher pH), then the proton-acceptor polymer has a better complexing ability. The absence of complexation between corresponding monomers and the relatively low values of critical pH led to the idea that the complexation involves cooperative effects, such as “non-interrupted linear sequences of bonds”, described by a ladder structure [4,5,7,13] and at the origin of the so-called “zipper effect” [16].

However, it was rare enough to find any proof of temperature effect on these systems to assume that their phase behavior was not sensitive to it [5]. We can cite Aoki *et al.* [7] or Shibunama *et al.* [8] who investigated temperature effects in polymer mixtures composed of PAA and PDMA. Aoki *et al.* [7] have built thermo-sensitive interpenetrated networks

composed of PAA and PDMA and Shibunama *et al.* [8] have evidenced their temperature-dependant interactions with the specific synthesis of PAA-*graft*-PDMA.

Transferred from solution onto interfaces or surfaces, the complexation of polymers has been widely studied, for instance in all the layer-by-layer systems [17]. In biophysics science, polymeric layers have been used to adsorb diverse objects such as proteins or cells. Polymeric brushes in particular have been used to adsorb proteins [18], antibody fragments [19], cells and bacteria [20,21]. Poly(acrylic acid) brushes have tuned the adsorption of various proteins [18,22-24] or enzymes [25].
The thermodynamics of the adsorption of nano-particles on a brush has been described by Currie *et al.* [26]. They distinguish three types of adsorption: they depend on the type of interactions in the system and on the parameter of the brush and of the particles. In the primary adorption, the nanoparticles ignore the brush and adsorb directly with the substrate; the secondary adsorption consists in an interaction occurring at the brush-solvent interface; finally, in the ternary adsorption, the adsorbed particles are distributed within the brush. In most cases, the adsorption of objects on polymeric brushes is not reversible. However, the thermodynamics of the adsorption of polymers onto brushes differs from this description. But it is also different from the thermodynamics of the formation of interpolymer complexes in solution since the grafted polymers have no translational entropy.
Is it possible then to use specific and tunable interactions between polymers involving a grafted polymer layer to tune adsorption? Can we create a macroscopic switchable adhesion by using specific interactions between a brush and a swollen elastic solid made of interacting polymeric chains? Can we vary the energy needed to pull off a grafted polymeric layer from the surface of a chemically cross-linked hydrogels when modifying their environment and thus, their interactions?

The novelty of this work is to focus first on the combined effects of pH and temperature for complexes of very simple systems made of poly(*N,N*-dimethylacrylamide-*co*-acrylamide) and PAA of relatively short molar masses. Then, the interpolymer complexation is studied on a surface, with the PAA being grafted on silicon samples.

In the first part of this chapter, we focus on the interpolymer complexes in solution for the PAA-PAM and PAA-PDMA polymeric pairs. We show that the behavior of these complexes towards temperature is antagonistic, due to the complexity of the specific interactions

between PDMA and PAA. We further investigate the formation of IPC between PAA and copolymers of acrylamide and *N,N*-dimethylacrylamide, who show an intermediate behavior.
In the second part of the chapter, the interactions in solution are transferred at a solid interface: grafted PAA brushes are in contact with PDMA or PAM hydrogels. Their interaction has been probed by neutron reflectivity studying the influence of the presence of the hydrogel on the structure of the brush.

1- Interactions in solution of homo- and co-polymers of acrylamide and *N,N*-dimethylacrylamide with poly(acrylic acid)

In the first part of this chapter, the study is focused on the conditions for which interactions occur in solution between the two polymeric pairs. The pairs are composed of a pH-sensitive proton-donor poly(acrylic acid) and the proton-acceptors made of homo- and co-polymers of acrylamide and *N,N*-dimethylacrylamide. This section starts with the synthesis of the polymers and copolymers and the methods used to probe the presence of interactions. It is prolonged by the study of the interactions in solution, mainly as a function of pH and temperature.

1-1- Homo- and co-polymers synthesis and characterization

1-1-1- Principle of the synthesis of the copolymers

Two different protocols were used for the synthesis of the polymers. For the poly(*N,N*-dimethylacrylamide) and the copolymers, we adapted a method previously used in the laboratory by Bokias *et al.* [27] for the controlled synthesis of poly(*N*-isopropylacrylamide) and poly(acrylic acid). Their synthesis allowed the control of the molar mass of the polymer changing the concentration of the redox initiator based on persulfates. With the objective to reach 30 $kg.mol^{-1}$ polymers, we chose to use a mixture of ammonium persulfate and sodium metabisulfate with equal concentration of 10^{-2} $mol.L^{-1}$. However, the synthesis of homo-poly(acrylamide) with persulfate initiators [28] had previously led to high molecular masses and polydispersities superior to 5, probably due to a high propagation constant in the order of

$6-18.10^3$ L.mol^{-1}.s^{-1}. Then, we used a chain transfer polymerization previously adapted in the lab, using thiols as chain transfer agents [29] for aqueous radical polymerization.

1-1-2- Protocol of radical polymerization

Materials

Poly(acrylic acid) (PAA, $M_w \sim 50\,000$ g.mol^{-1}) was obtained from Polysciences Inc., and poly(N-vinyl-2-pyrrolidone) (PVP, $M_w \sim 40\,000$ g.mol^{-1}) was a product from Fluka. Both were used as received and were solubilized in water at 10 wt%.

The acrylamide (AAm) and N,N-dimethylacrylamide (DMA) monomers were purchased respectively from Sigma and Aldrich and were used as received. Potassium persulfate (KPS, 99%) and sodium metabisulfite (≥ 97%) were from Acros Organics; ammonium persulfate (≥ 99.5%) and N,N,N',N'-tetramethylethylenediamine (TEMED, redistilled, ≥ 99.5%) from Sigma-Aldrich; 4,4'-azobis(4-cyanovaleric acid) (75%) and ammonium chloride (≥ 99.5%) from Aldrich and finally 3-mercaptopropionic acid (≥ 99%) from Fluka.

Synthesis of homo- and co-polymers

Poly(acrylamide). 3-Mercaptopropionic acid (19.2 mg) and acrylamide (13 g) were stirred in milli-Q water at 60°C while nitrogen bubbling through the solution. 4,4'-Azobis(4-cyanovaleric acid) (0,507 g) was diluted in Milli-Q water (18 mL) and dissolved adding drop by drop a 1-molar solution of sodium hydroxide. After being deoxygenated the initiator solution was added to the monomer solution. After 1 hour, the temperature was decreased to 50°C and the reaction was continued during 1.5 hour. After stopping the reaction, the solution was concentrated. The polymer was then precipitated in ethanol, filtrated, washed and dried.

Poly(*N,N*-dimethylacrylamide) and poly(acrylamide-*co*-*N,N*-dimethylacrylamide). Ammonium chloride (26.75 mg) and the proper quantities of monomers (0.5 M in total, see Table 1) were dissolved in water (50 mL) and the pH of the mixture was adjusted around 5-6 with a few droplets of a solution at 10^{-1} M of hydrogen chloride before being deoxygenated with nitrogen bubbling during 1 hour. A 1-mL solution of sodium metabisulfite (95 mg) and a 1-mL solution of ammonium persulfate (114 mg) were prepared, deoxygenated, and then added to the monomer solution under nitrogen atmosphere, which initiate the polymerization. The reaction was allowed to proceed at room temperature during 24 h. The final solution was

dialyzed through milli-Q water using a membrane with a MWCO equal to 6 to 8 $kg.mol^{-1}$. The polymer was finally recovered by freeze-drying.

Name	% AM	% DMA	AM mass	DMA mass	Yield (%)
PDMA	0	100		4.978 g	47.3
$P(AM_{10}$-*co*-$DMA_{90})$	10	90	0.360 g	4.462 g	42.6
$P(AM_{30}$-*co*-$DMA_{70})$	30	70	1.068 g	3.381 g	68.8
$P(AM_{50}$-*co*-$DMA_{50})$	50	50	1.774 g	2.491 g	49.2
$P(AM_{70}$-*co*-$DMA_{30})$	70	30	2.489 g	1.641 g	58.3
$P(AM_{90}$-*co*-$DMA_{10})$	90	10	3.218 g	0.502 g	45.6
PAM	100	0	13,02 g		53.8

Table 1 - Experimental conditions for the synthesis of copolymers of *N,N*-dimethylacrylamide and acrylamide.

1-1-3- Polymer chemical characterization

All the samples have been characterized by Nuclear Magnetic Resonance (NMR) and Size Exclusion Chromatography (SEC).

SEC gave access to the weight-average molar mass (M_w) of the polymer and to its polydispersity (PDI). An aqueous Viscotek SEC system equipped with three Shodex OH Pack columns thermostated at 25°C was used. The calibration was based on poly(ethylene oxide) standards. The eluent was either a 0.5 M solution of lithium nitrate or sodium nitrate.

For ^1H NMR, the polymers have been dissolved in deuterium oxide with a concentration about 20 mg/mL. Measurements have been carried out on a Bruker Spectrometer at 400 MHz. The chemical shift was recalibrated using the chemical shift of water (4.8 ppm). Results have been treated with the software Win-NMR. The relative concentration in AM and DMA in the polymer chain was calculated by comparing the relative integration of the peaks corresponding to the neutrons of the back-bone $\left(-C\mathbf{H}_2-C\underset{|}{\mathbf{H}}-, 1.2\text{-}2.8\,\text{ppm}, 3H\right)$ with those of the two methyl groups on the amide function of DMA $\left(N(C\mathbf{H}_3)_2, 2.8\text{-}3.2\,\text{ppm},\ 6H\right)$.

	% of AM	% of DMA	M_w (kg.mol^{-1})	PDI
PDMA	0	100	30.5	2.0
$CopAM_{24}$	23.9	76.1	25.3	2.0
$CopAM_{34}$	33.9	66.1	40.3	2.2
$CopAM_{52}$	52.1	47.9	29.0	2.0
$CopAM_{69}$	69.4	30.6	28.6	2.1
$CopAM_{95}$	94.8	5.2	26.3	2.0
PAM	100	0	126	1.7

Table 2 - Characteristics of the homo- and co-polymers of AM and DMA synthesized.

The synthesis by chain transfer using a mercaptan led to masses M_w in the order of 126 kg.mol^{-1} with a polydispersity lower than 2, which is rather low for this type of radical polymerization and these masses. The synthesis initiated by persulfates gave masses M_w for PDMA and its co-polymers lower masses, in the range of 25 to 40 kg.mol^{-1} with polydispersity around 2. Looking at the copolymerization process and the resulting copolymer structure, we can briefly remind the classical definition of the propagation constant k_{ij} corresponding to the reaction:

$$\sim M_i^{\bullet} + M_j \xrightarrow{k_{ij}} \sim M_i M_j^{\bullet},\ i,j = \begin{cases} 1 \\ 2 \end{cases}$$

with $\sim M_i^{\bullet}$ the polymer chain terminated with a radical derived from monomer M_i. In the case of the radical copolymerization of AM (monomer M_1) and DMA (monomer M_2), McCormick *et al.* [30] have determined the following reactivity ratios: $r_1 = \frac{k_{11}}{k_{12}} = 0.78 \pm 0.04$ and $r_2 = \frac{k_{22}}{k_{21}} = 1.11 \pm 0.06$, with $r_1 r_2 = 0.86$. These results mean that DMA tends to react a little bit faster than AM on a growing chain, but the reaction constants are all very close to one another. On the basis of these data, we can consider that the distribution of AM and DMA in the polymer chain is almost random with only a small drift of the monomer composition of polymer chains during the conversion. As we can see in Table 2, the composition of our copolymers remains very close to the monomer feed ratio, except for $CopAM_{95}$ and $CopAM_{24}$ that have been prepared with lower amounts of AM: 90 instead of 95 mol% and 10 instead of 24 mol%, respectively. As most of copolymerizations have been carried out until full

completion, this discrepancy could be attributed to a fractionation of copolymer chains during purification; longer chains being richer in AM comonomer.

1-1-4- Preparation of the samples

Solutions containing 10 wt% of polymer in water were initially prepared. The samples at 0.25 wt% for each polymer contained 1 mL of PAA solution, 1 mL of another polymer solution and 8 mL of Milli-Q water. Then, pH was adjusted using 1M and 0.1M solutions of NaOH or HCl. When investigating the ionic strength effect, solid NaCl was slowly added to reach the right concentration. If needed, pH was adjusted during this procedure to avoid the formation of macro-aggregates. Then, the solutions were heated or cooled to determine the temperature transition of the associations.

1-1-5- Determination of the cloud points: formation of IPC

By definition, the cloud point of a mixture of polymers in a solvent corresponds to the temperature at which some of the dissolved matter is not completely soluble. In the solution, it corresponds to the apparition of aggregates rich in polymer. This phase transition is accompanied by changes in some of the physical properties of the solution. Because of the diffusion of light by the aggregates, the solution becomes turbid. The apparition of aggregates replacing polymer chains in good solvents makes the variation of the viscosity of the solution changes at the cloud point. Finally, when the formation of the solid is associated with a high enthalpic phase transition, differential scanning calorimetry can be used to determine the cloud point [2].

In this study, the determination of the cloud points were mainly carried out using a UV-visible light spectrometer (with wavelengths ranging from 200 to 1 200 nm) containing a chamber allowing stirring and controlled temperature (through a Peltier device). The temperature range was typically from 7.5°C to 70°C with a heating rate about 0.7°C/min. Some of the cloud points were determined with the naked eye, after checking reproducibility with spectrometry. When turbid, the solution containing the PAA-PAM polymeric pair appears whitish or milky. The solution with PAA and PDMA is more opalescent, slightly bluish.

The bundle of spectra obtained after a temperature sweep were as shown on Figure 1. Here, the transmission increases with temperature (except in the near infrared region), which means that the sample becomes more limpid when increasing the temperature.

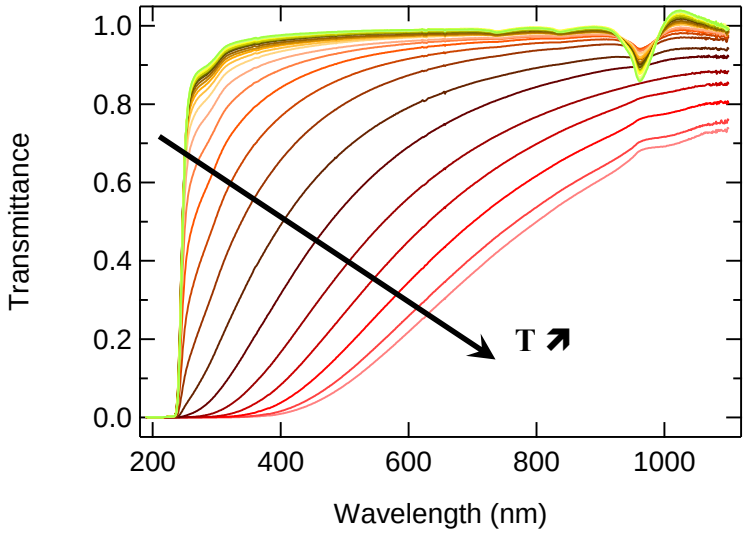

Figure 1 - UV-visible spectra for an aqueous solution containing 0.25 wt% in PAA and in $CopAM_{69}$ adjusted at pH 2.93. The spectra were measured every 2.5°C between 7.5°C and 70°C.

Using these data, we have plotted on Figure 2 the transmittance for a given wavelength as a function of temperature for the whole visible spectrum (usually considered between 380 nm and 780 nm). Figure 2 makes it explicit that the cloud point measurement using a spectrometer needs a better definition as it is not possible to find the same transition temperature when varying the wavelength (might its definition be a limit value of the transmittance, or the intersection between the slopes at high temperature and at intermediate temperature).

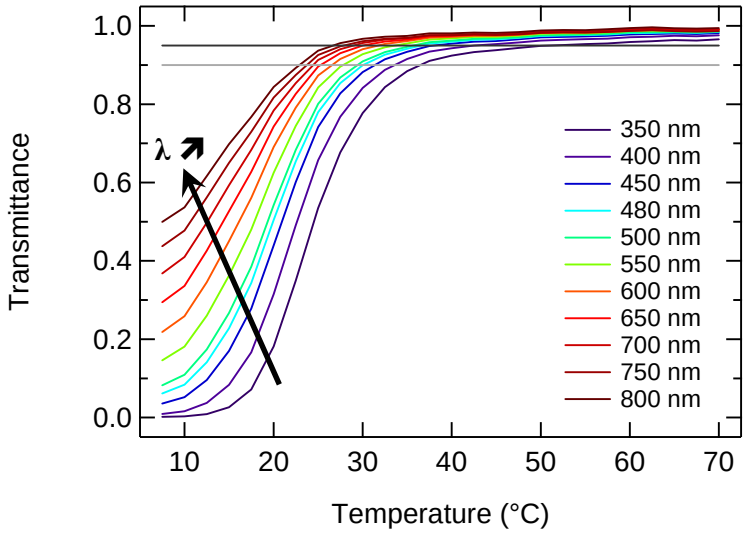

Figure 2 - Transmittance as a function of temperature for an aqueous solution containing 0.25 wt% in PAA and in $CopAM_{69}$ adjusted at pH 2.93, for various wavelengths in the visible light spectrum.

Then, we correlate the spectral measurement with the eye measurement and we observe that the cloud point observed with the naked eye corresponds – to within a degree Celsius – to a transmittance equal to 0.90 for a wavelength equal to 480 nm.

1-2- Interpolymer complexes of poly(*N,N*-dimethylacrylamide) or poly(acrylamide) with poly(acrylic acid)

1-2-1- Phase diagram pH-temperature of homo-polymer pairs

Poly(acrylic acid) and poly(acrylamide) have already proven to form interpolymer complexes in the literature but the effect of temperature on these complexes, which is not widely documented, is first presented here. Combined effects of pH and temperature on mixtures of PAA and PAM concentrated equally at 0.25 wt% in water are shown on Figure 3. At room temperature, complexes appear for pH lower than 3.05. Nevertheless, it is possible to form or dissolve the same complexes for pH between 1.8 and 3.2. In this pH range, the interpolymer complexes can be dissolved by increasing the temperature in a range between 0 and 65°C. The polymer mixture shows an upper critical solution temperature which depends on pH. The bonding/debonding interactions are due to hydrogen bonds, which are expected to weaken when the temperature is increased. Then, the UCST is the expected type of transition for this interpolymer complex.

The cloud point measurement was performed while increasing and decreasing the temperature of the solution. The transition temperature for the same solution is slightly shifted to lower temperature when the solution is cooled. This temperature hysteresis can be attributed to the slow dynamics for the debonding and the molecular redispertion of the two polymers compared to the heating rate.

The thermodynamics of the formation of these complexes has been investigated recently by Deng *et al.* [16] and they showed that the complexation of PAA with PAM is an enthalpy-driven process ($\Delta H^0 < 0$) with a loss of configurational entropy ($\Delta S^0 < 0$).

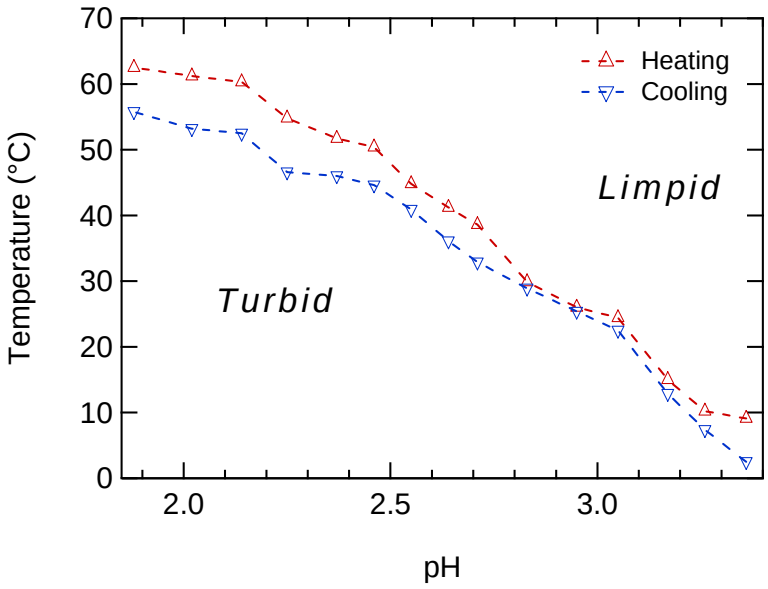

Figure 3 - Variation of the cloud point temperature as a function of pH: phase diagram of a system containing 0.25 wt% in PAA and in PAM in water. Cloud point measurements were performed while heating the solution (Δ) or cooling the solution (▽). The one-phase system is at high pH, in the limpid domain.

The same study was carried out on the couple of poly(acrylic acid) and poly(*N,N*-dimethylacrylamide) (see Figure 4). At room temperature, the formation of the interpolymer complexes occurs at pH below 3.47 for mixtures of PAA with PDMA equally concentrated at 0.25 wt% in water. This result is consistent with previous results [9]. But for this system, the association is reinforced and favored at high temperature. For pH ranging from 3.45 to 3.70, a clear solution at low temperature turns into turbid at high temperature. The association of these two polymers in water solution with increasing temperature has already been published previously [8]. This transition, with a lower critical solution temperature, can not be adequately described by a simple H-bonded interpolymer complex.

PDMA, which is water-soluble in the usual temperature range in water (0-100°C), shows a chemical structure of its monomer unit in-between those of PAM and poly(*N,N*-diethylacrylamide) (PDEA). If PAM is completely water-soluble, it is not the case of PDEA which is known for its LCST around 32°C. Then, a partial hydrophobic behavior of PDMA can be expected and theoretical extrapolations have predicted that PDMA could have a hypothetical LCST in water at a temperature higher than 200°C [31]. With a similar approach, the PAA is water-soluble in the whole pH range, but it is chemically close to poly(methacrylic acid) which undergoes a transition and becomes “supercoiled” at pH below 2 because of hydrophobic effects.

It might then appear as reasonable to partially attribute the formation of this interpolymer complex to a hydrophobic interaction. It seems that for a limited range of pH, corresponding to a given ionization of the PAA and as a consequence to a certain hydrophobicity of this polymer, the H-bond and hydrophobic interactions between PDMA and PAA are favored compared to a total solvation of PDMA.

Similar results were obtained by other authors [32,33], who found that the minimal critical length – which corresponds to the number of monomer units needed for the formation of complexes – increases with temperature for the PAA-PEO polymeric pair and decreases for the PMAA-PEO pair, due to the increased hydrophobicity of PMAA compared to that of PAA.

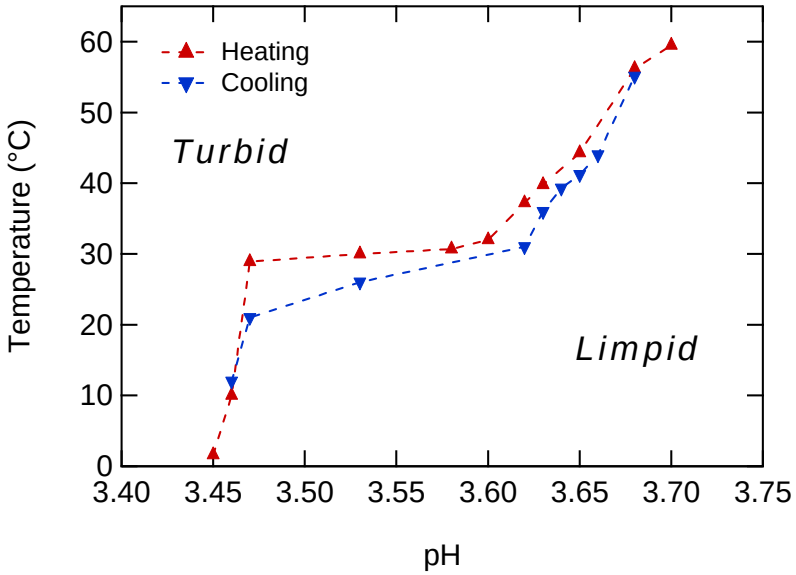

Figure 4 - Variation of the cloud point temperature as a function of pH: phase diagram of a system containing 0.25 wt% in PAA and in PDMA in water. Cloud point measurements were performed while heating the solution (▲) or cooling the solution (▼). The one-phase system is at high pH, in the limpid domain.

Thermodynamically, this association is expected to allow a gain in entropy as an increase in temperature favors its formation ($\Delta S^0 > 0$) and the associated enthalpy is expected to be positive ($\Delta H^0 > 0$).

Finally, we have shown that for two proton-acceptor polymers with similar chemical structure such as PAM and PDMA, their association in solution with a proton-donor such as PAA, the mechanisms of the formation of interpolymer complexes are so different that one of the two couples shows a LCST behavior while the other has a UCST behavior.

1-2-2- Effect of polymer concentration

The study of the interpolymer complexes has been preferentially carried out at low concentration, which prevents the formation of macro-aggregates and precipitates. Nevertheless, we have also investigated the effect of the concentration in polymer. The apparition of the interpolymer complexes is expected to be favored when increasing the concentration in polymer.

In fact, this is what is observed for the mixtures of PAM and PAA in water. Figure 5 gives the pH needed to see the apparition of complexes at room temperature when acidifying the system. The more concentrated the system is and the more the interactions between the two polymers are favored. This is consistent with what was found by Mun *et al.* [6]: when increasing the concentration by an order of magnitude, they found that the pH of transition increased by 0.3 unit, which is a bit higher than what we obtain (0.15). However, they worked with polymers of higher masses and they have shown that the influence of the molecular weight on aggregation: the complexation is favored with long chains.

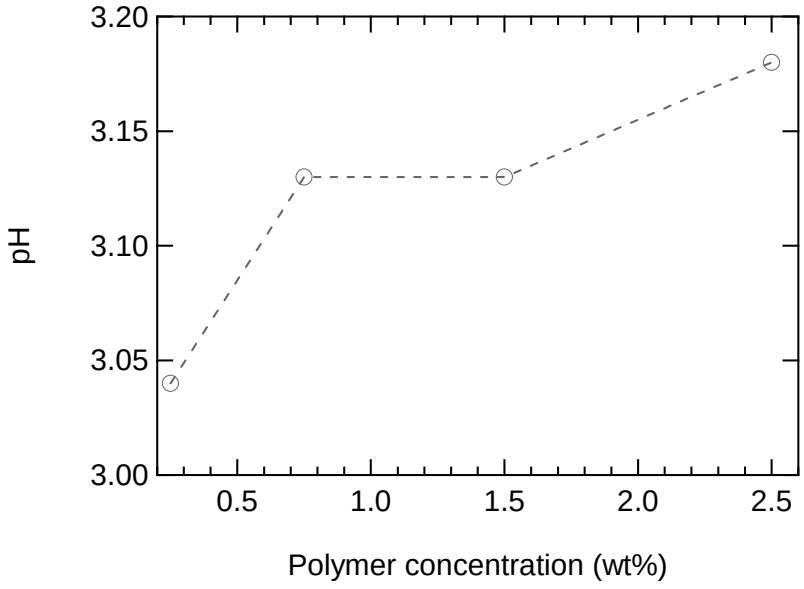

Figure 5 - pH corresponding to the formation of complexes in the solution at room temperature as a function of polymer concentration for a system containing PAA and PAM in water. The one-phase system is at high pH.

With PDMA on the contrary, the polymer concentration has been tripled and we observed a counterintuitive result. As shown on Figure 6, the phase diagram is shifted towards higher temperature or lower pH when the concentration is increased whereas the expectations suggest that the turbidity should have occurred at higher pH, when PAA was less adapted to

form the complexes. However, this shift is lower than 0.05 unit of pH, which is within the inaccuracy of the measure.

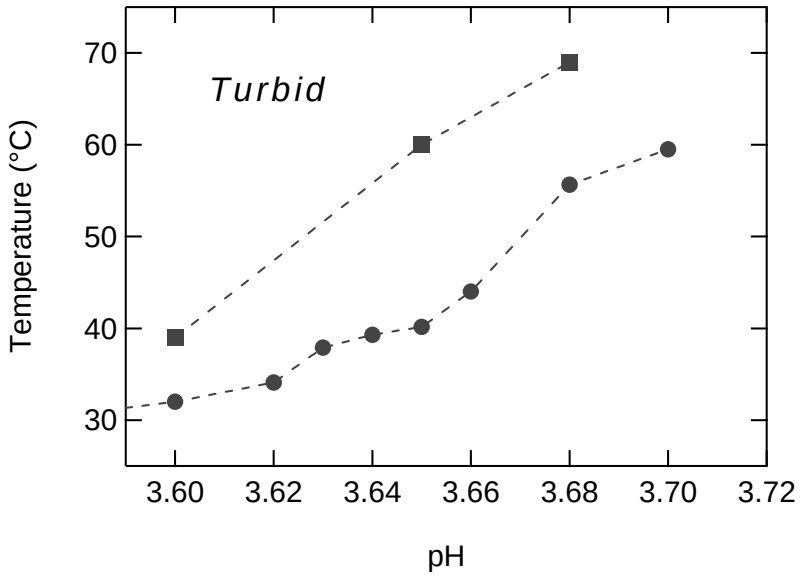

Figure 6 - Variation of the cloud point temperature as a function of pH: phase diagram of a system containing 0.25 wt% (●) or 0.75 wt% (■) in PAA and in PDMA in water. The one-phase system is at high pH.

1-2-3- Effect of ionic strength

The effect of ionic strength on complexation has been reported to be dependent on the polymeric pair studied. On Figure 7, we report the results obtained on the two polymeric pairs of PAA, and PDMA or PAM.

These results clearly show that the effect of ionic strength follows two tendencies. At low salt concentration, the critical pH of complexation varies slowly; above a specific NaCl concentration, the effect of ionic strength becomes particularly significant. Then, from the absence of added salt to the highest concentrations, the critical pH varies of about 1 unit. Furthermore, the specific concentration – which connects the two tendencies – strongly depends on the polymeric pair as it varies of about one order of magnitude from PDMA-PAA to PAM-PAA pairs.

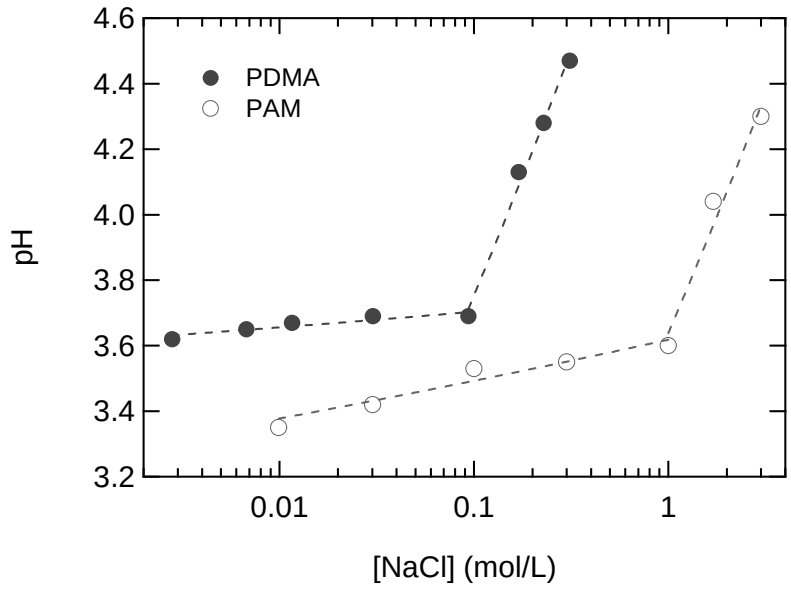

Figure 7 - pH corresponding to the formation of complexes in the solution at room temperature as a function of sodium chloride concentration for two systems: one containing PAA and PAM at 0.25 wt% in water (○), the other containing PAA and PDMA at 0.75 wt% in water (●). The one-phase system is at high pH.

Since the same weak polyelectrolyte is used for the two polymeric pairs, a similar influence of the ionic strength on the complexation could be expected for both pairs. However, the strong effect of ionic strength appears at lower concentration for PDMA than for PAM. This is probably due to the deterioration of the thermodynamic quality of the solvent by the addition of inorganic salt, which would have a major effect on PDMA whose hydrophobicity is higher than that of PAM. As a consequence, the hydrophobic effect of these interactions in water becomes very important, which facilitates the complexation. Furthermore, the conformational state of the PAA weak polyelectrolyte is highly sensitive to ionic strength: by adding salt, the ionized units along the chains are screened. It leads to a less stretched conformation which increases the complexation cooperativeness of the polymers whose conformational state is closer than in the absence of added salt. As a consequence, the variation below the specific concentration can be attributed to the increasing screening of the charges on the PAA whereas at higher salt concentration, the deterioration of the thermodynamic quality of the solvent can explain the higher sensitivity to the ionic strength.

These results are in agreement with those of Mun *et al.* [6] who also studied the effect of the monovalent cation and shown that the bigger – or the softer – the monovalent cation, the better the interactions. They also investigated the effect of the addition of copper(II) chloride $CuCl_2$ in the PAM-PAA polymeric pair system. In the absence of PAM, the addition of

copper(II) Cu^{2+} to PAA solution increases turbidity because of electrostatic and donor-acceptor interactions which induces complexation by bridging ionized monomer pairs. In the presence of PAM and for pH values below the critical pH, turbidity is slightly higher in the presence of copper(II), which seems to have no effect on the critical pH of transition but on the solution turbidity, probably because of the formation of triple complexes implying PAA, Cu^{2+} and PAM.

1-2-4- Interactions between pairs of P(AM-*co*-DMA) and PAA

As the type of interactions in water between PAM and PAA seems rather different than the one between PDMA and PAA because the first system shows a transition with a LCST when the second shows a UCST, we studied the interactions of PAA with P(AM-*co*-DMA). Wang *et al.* [13] have already performed a fluorescence study between these polymers but they were not interested in the effect of temperature. Here, we have two extreme behaviors regarding the temperature effects. For PAM, the H-bonds lead the interactions and they are broken when the mixture is heated. For PDMA, the hydrophobic interactions play a major role and the complexes are reinforced by heating the solution. For polymers made of both acrylamide and *N,N*-dimethylacrylamide, which of the hydrophobic interactions or H-bonding will predominate?

This question is partly answered in Figure 8. We can note that starting from PAM and increasing the DMA ratio in the copolymer makes the phase transition shift continuously from the one observed with PAM to the one observed with PDMA. Then, the critical pH at ambient temperature increases monotonously with the ratio of DMA in the copolymer. This is consequently an interesting way to change the critical pH without changing the chain length, the concentration or the ionic strength. It appears also clearly that the pH range for which the temperature dependence of the IPC is observed goes through a minimum when increasing the DMA ratio inside the copolymer.

This is approximately the case for the complexation between PAA and $CopAM_{34}$ that can be tuned with the temperature only in a very narrow pH range (around 0.1 unit over 60 °C). Moreover, when plotted as a function of temperature, the transmittance curves of this complex can decrease quickly at first, and then be almost constant but with a value lower than 90% at 480 nm. A solution adjusted at 0.15 pH unit below the critical pH, which was whitish or milky at low temperature, becomes opalescent when increasing the temperature.

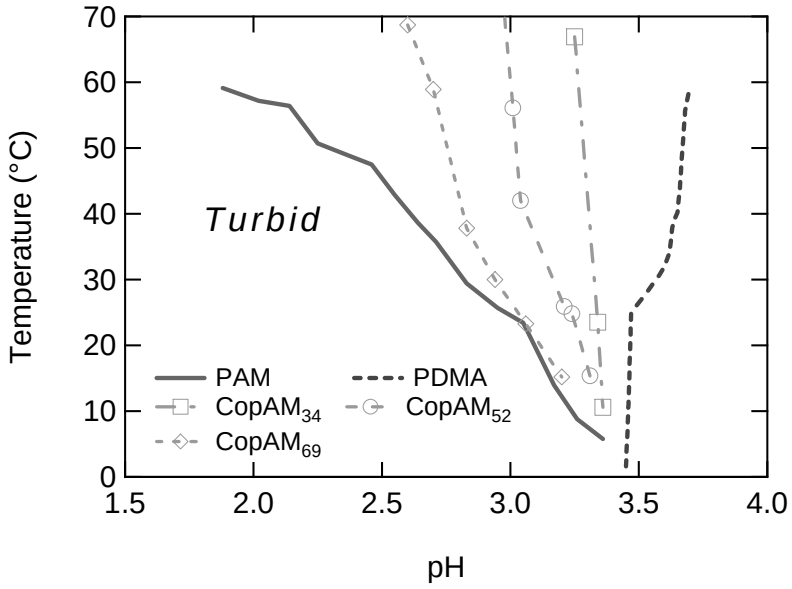

Figure 8 - Phase diagram of different polymeric pairs made of PAA and a copolymer of AM and DMA. The polymers are at 0.25 wt% in water. The one-phase system is at high pH.

Some similar behavior, when the transmittance decreases at first and then increases with temperature, was previously observed on the polymeric pairs PAA-PVP and PMAA-PEO in water [1]. This effect can be explained by the relative importance of the hydrogen bonding effect compared to the hydrophobic interactions. Then, on a thermodynamic point of view, the quasi independence toward temperature for the formation of complexes of this copolymer $CopAM_{34}$ with PAA suggests that its entropy of formation is close to zero $\Delta S^0 = 0$.

1-2-5- Comparative results with PAA-PVP complexes

Another polymeric pair has been investigated, consisting of PAA with poly(*N*-vinyl-2-pyrrolidone) (PVP). Working at a mass concentration of 0.25 wt% in water for both polymers, the critical pH at ambient temperature was found to be around 4.4. However, around this critical pH, the formation of the IPC could not be tuned by temperature, but the transmittance decreased slightly upon heating, suggesting that the enthalpic contribution to the formation of the complex is particularly strong. Concerning the effects of ionic strength, the effect was found to be a bit different than the one observed for the PDMA-PAA and PAM-PAA pairs. The two tendencies previously described were observed (see Figure 9), but at low ionic force, an increase in the salt concentration was unfavorable to the formation of the IPC, contrary to what was obtained with the other pairs, and in accordance with the results found by Nurkeeva *et al.* [34].

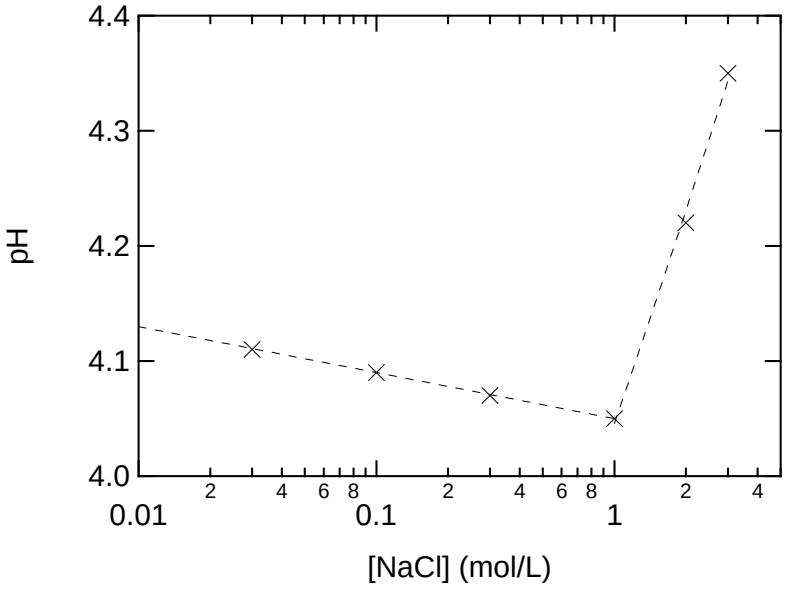

Figure 9 - pH dependence of the complex formation *versus* salt concentration at room temperature for a mixture containing PAA and PVP at 0.25 wt% in water. The one-phase system is at high pH.

Finally, we observed that the temperature has an effect on the formation of the IPC for polymeric pairs presenting a low critical pH at room temperature. Figure 10 sums up the pH range in which temperature can tune the formation of the IPC: the lower the critical pH and the wider the temperature range is. This relation was observed only with homo-polymers for which the type of interaction does not change inside the chain.

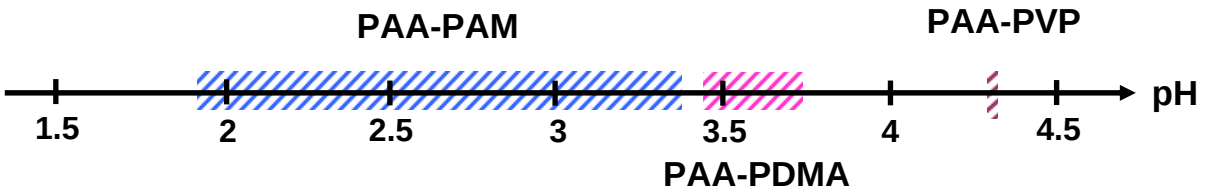

Figure 10 - Schematic representation of the pH range in which the temperature (from 5 to 70°C) can tune the formation of the interpolymer complexes for polymeric pairs made of the proton-donor PAA and a proton-acceptor being PAM, PDMA or PVP.

It seems that the critical pH at ambient temperature is a signature of the complexing ability of the proton-acceptor, as suggested by Mun *et al.* [6]. Then, the polymeric pair presenting the lowest complexing ability must be the most inclined to be sensitive to the temperature. Finally, the use of proton-acceptor copolymers made of one polymer presenting an LCST and the other a UCST with the proton-donor is probably the only way to decrease the influence of

temperature on the IPC formation by reducing the entropic effects. Besides, it allows to playing on the critical pH at ambient temperature.

1-2-6- Conclusion

The formation of complexes between polymeric pairs consisting of PAA as proton-donor and homopolymers and copolymers of AM and DMA has been investigated by turbidimetry.

The association in solution between PAA and PAM occurs for a pH between 1.8 and 3.3. The complexes of the latter polymers formed in this pH range are sensitive to temperature. We have shown that the complexation tends to be weaker as the temperature increases, and that the temperature transition for the solubility of the mixtures of these polymers is a UCST behavior.

The association between PAA and PDMA occurs at higher pH, in a range between 3.45 and 3.75, which suggests the higher complexation ability of PDMA compared to PAM. These complexes are also sensitive to temperature but the complexes are reinforced when the temperature increases. The solubility transition associated to this polymeric pair is an LCST behavior. It underlines the importance of the hydrophobic interactions added to the hydrogen bonding in the reinforcement of the complexes of this polymeric pair.

The effect of the ionic strength on these complexes has shown two tendencies: the first one slowly increased the critical pH at room temperature, probably due to the increasing the screening of the charges on PAA with the ionic strength; and the second one was influencing the critical pH on about 1 unit of pH, because of the deterioration of the thermodynamic quality of the solvent at high salt concentration.

The use of copolymers of AM and DMA for the complexation with PAA has shown to give results that are intermediate between those obtained with the PDMA and PAM homopolymers. The critical pH for a given temperature is between those obtained for the homopolymers, and the shape of the phase diagram stiffens when increasing the ratio of PDMA up to 66 mol% in the copolymer. In that case, the stability of the complex PAA/ $CopAM_{34}$ does not depend on the temperature.

Finally, this study raises a few questions: does the ability of a proton-acceptor monomer to interact with a proton-donor monomer depend on its environment? Or does the formation of complexes have to involve “long” bonded sequences of contiguous monomers interacting with the same sequence of the other polymer? Our results suggest that the presence of AM in the copolymers decreases the effect of hydrophobic reinforcement of the complexes as the

transition turns from an LCST to a UCST when increasing the amount of AM. But can we infer, as the "zipper effect" suggests, that some AM monomers interact directly with PAA for pH where the homo-polymer PAM does not show any interaction with PAA?

2- Surfaces and interfaces of gels

This thesis focusing on the adhesion properties of hydrogels, we have taken a particular interest in the study of the surfaces of these soft materials. To be able to perform a flat-flat contact test with a good reproducibility, it is necessary to obtain a layer of gel covalently attached on a flat surface and with a good reproducibility concerning the free surface composition.

We have first studied the best way to attach gel layers on transparent and rigid plates. Then, we investigated the influence of the plate removed from the gel on the quality of its free surface. It appears that the mold chemistry has a strong influence on the free surface of the gels.

2-1- Principle of the synthesis of hydrogels near surfaces

The objective is to obtain a flat gel layer with a low amplitude roughness, covalently attached to a rigid surface so that the strain and the response of the substrate to a stress of a few newtons can be considered negligible compared to those of the gel. We have studied various surface modifications to reach these goals. The basic principle is represented schematically on Figure 11, in which two grey transparent substrates have been differently modified. The blue one is tailored to covalently bind the gel, the red one to be easily removed from the gel surface after polymerization and cross-linking.

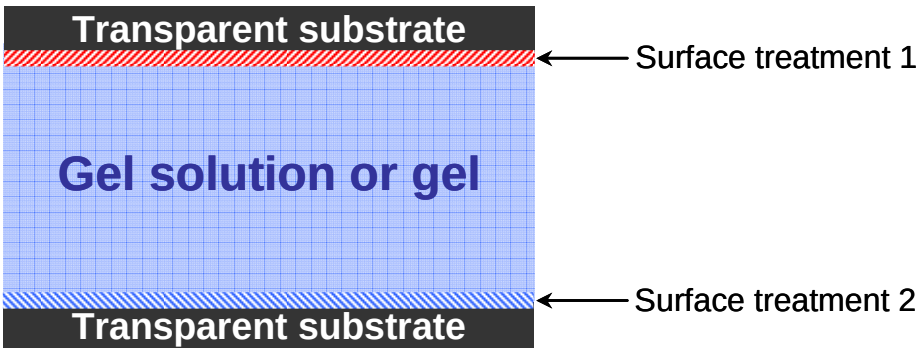

Figure 11 - Schematic representation of the mold used for the preparation of gel samples designed for adhesion experiments. The light blue polymer solution – before gelation – is poured between two transparent and rigid modified plates: one red modification allows the plate to be easily removed from the gel; the blue modification allows the gel to stick to the second plate.

As it has been previously shown in this chapter, silicon can be modified thanks to its native silica layer, with small molecules able to change its surface chemistry. In order to get transparent surfaces, we have decided to work on silica, with various degrees of purity, from simple glass to quartz.

To chemically bond the gel to the plate, we used a surface treatment of the silica with a silane terminated with a double bond able to co-polymerize with the other monomers during the gel formation. The polymerization reaction results in a gel covalently bonded to the substrate. Assuming that the gel is synthesized close to its swelling equilibrium, it will not be affected by a subsequent immersion in an excess of pure water.

On the other hand, the second plate was modified with different hydrophobic silanes in order to easily remove the plate from the gel surface.

2-2- Silanizations

Prior to any surface modification, the substrate was cleaned and rejuvenated by an immersion in an active "piranha" solution, extensively rinsed with Milli-Q water and dried with a nitrogen flow.

2-2-1- Surface modifications for the covalent attachment of the gels

Silicon wafers were used during the optimization of the formation of a self-assembled monolayer terminated by a double-bond able to copolymerize with the other monomers of the gel. We characterized these SAM with ellipsometry. Then, once the SAM was properly anchored on the silicon wafers, a highly elastic PDMA-10x2 gel (with a monomer concentration of 10 wt% and a cross-linker ratio of 2 mol%) was synthesized on the modified surface. Then, we tried to unstick the gel from the wafer with a simple peeling test. When the gel was found to fracture instead of unsticking, that is to say when the cohesion of the gel was weaker than the adhesion at the surface, we considered the test positive.

From different experiments performed with various silanes, we finally selected a mono-functional chloro-silane which gave, with short reaction times, a controlled SAM for synthesis carried out at low concentration. We obtained reproducible thicknesses of 8 Å with the 3-methacryloxypropyldimethylchlorosilane (92%) at 0.15 vol% in extra-dry toluene during 2 hours. Although the peeling tests were positive with silica wafers, the covalent binding of the gel applied on glass plates was not reproducible and some of them came off during

dialysis. We chose to keep the same synthesis and change the substrate to quartz plates, whose silica purity is higher than that of the glass. The new peeling tests on quartz modified substrates have proven reproducibly positive.

2-2-2- Surface modifications for the removal of the gels

The second plate, which has to be removed from the gel without damaging it, has been treated with hydrophobic silanes as the gels contain more than 90 wt% of water. We have used three different silanes to tune the hydrophobicity of the mold plate: hexamethyldisilazane (HMDZ, 98.5%) is a small molecule which passivates the surface with simple methyl groups; octadecyltrichlorosilane (OTS, 97%) corresponds to aliphatic saturated chains of 18 carbons and gives access to more hydrophobic surfaces than HMDZ; finally 1H,1H,2H,2H-perfluorodecyltrichlorosilane (FTS, 97%) is shorter than OTS but its chain is fluorinated and its grafting results in surface more hydrophobic.

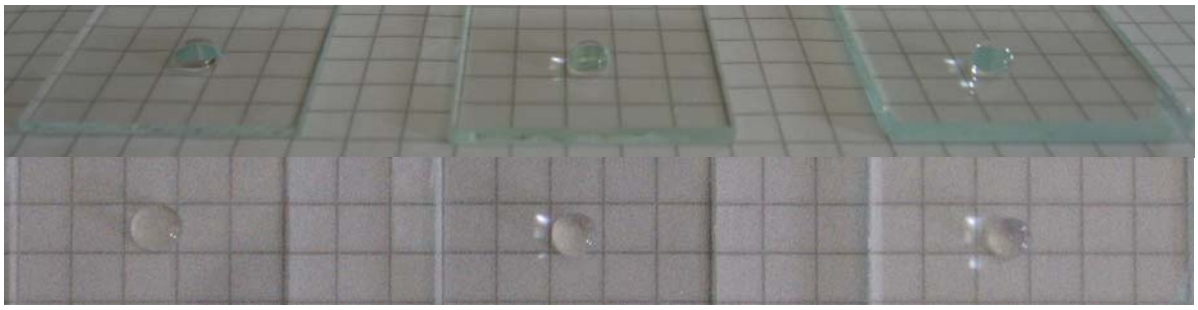

HMDZ, $\theta = 85° \pm 5°$ OTS, $\theta = 110° \pm 5°$ FTS, $\theta = 120° \pm 5°$

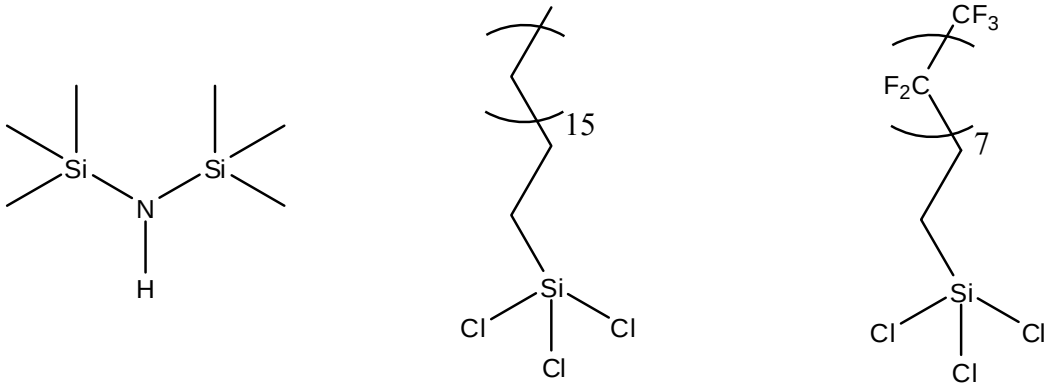

Figure 12 - Pictures of 25 µL water droplets on treated glass substrates, corresponding contact angles and semi-developed formula of the corresponding silanes.

For HMDZ, the surface modification was carried out with a vapor phase method: after rejuvenation, glass substrates were placed in a close environment with a few droplets of

HMDZ for 2 hours; the glass plates were then removed from the reactor and rinsed with water. The high contact angle on the glass observed during rinsing and the absence of remaining pinned droplets on the surface without any drying were the evidence of a successful modification. For OTS [35] and FTS, the silanization was performed in toluene with a concentration of 0.15 vol% during 2 hours at room temperature. The glass plates were then extensively rinsed with toluene and sonicated prior to drying with a gentle flow of nitrogen. The contact angle with water was finally evaluated to ensure the quality of the hydrophobic modification, as shown in Figure 12. The contact angle varied from 85° on HMDZ-treated to 120° on FTS-treated glass plates [36].

With all these hydrophobic treatments, the removal of the second glass plate of the gel mold happened without causing any visible damage to the surfaces of the gels.

2-2-3- Storage and use of gel-covered substrates

After being modified, the various substrates were kept in Petri dishes in the dark at ambient temperature. For the synthesis of gel samples, we generally used two modified plates to build a mold for the gel, as represented in Figure 13. For the synthesis of gel samples for rheology with parallel-plate geometry or for neutron scattering or reflectivity, the two glass slides were identically treated hydrophobic. For the synthesis of gel samples to be used in adhesion tests, one slide was treated hydrophobic, the other showed double-bonds at the surface.

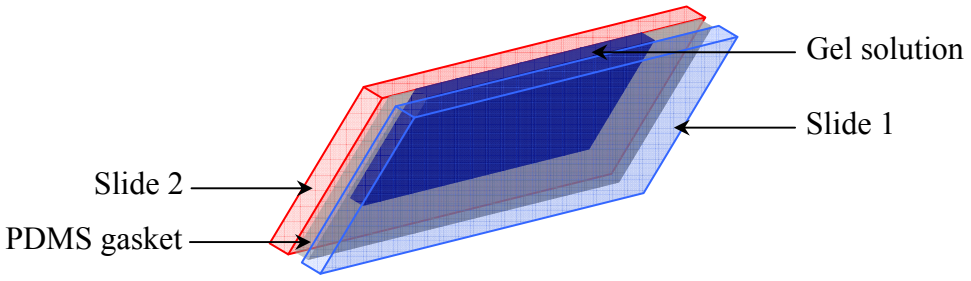

Figure 13 - Schematic representation of the typical mold for the synthesis of gel plates. Two silanized slides – either in glass or quartz – are separated by a leakproof homemade poly(dimethylsiloxane) joint. The solution for the gel synthesis is poured between the two glass plates prior to gelation.

2-3- Quality of the surface of the gel

A large discrepancy was found between the storage modulus obtained in rheology (small strains in shear) and the modulus obtained with compression tests (in large strain) or even tensile tests. This suggested strongly that the surface composition of the gel was different from that of the bulk and it lead us to investigate this point in more details.
We therefore used different surfaces to mold the gels and used rheology and neutron reflectivity to characterize the properties of the gel and their structure.

2-3-1- Rheology

For the rheology study, we synthesized identical PDMA-10x2 hydrogels, changing only the surface treatment of the glass plates of the mold. We used the three silanized glass substrates described before (OTS, FTS and HMDZ). A fourth synthesis was made by pouring the reaction medium into a polypropylene (PP) Petri dish and under nitrogen atmosphere so that the surfaces were in contact either with PP or Air. Rheology was performed using the very same protocol presented in the previous chapter, beginning with two deformation sweeps and then applying a frequency sweep. Although the same values were initially expected for the storage modulus, it is not the case as we can see in Figure 14. Indeed, the mean storage modulus obtained for the four different molds are in the same order of magnitude but varies from 3.0 kPa for the Air-PP mold to 8.3 kPa for the HMDZ-treated mold.

This apparent variation of the measured elastic modulus for the same gels can only be due to by a surface effect [37]: when changing the surface characteristics of the mold, the surface structure of the gel varies and a gradient, either in monomer concentration or in cross-linker concentration, is probably present at the gel surface. Here, the variation seems to scale with the hydrophilic character of the mold surface for the three silanized surfaces: the storage modulus increases when the mold becomes more hydrophilic.

For the Air-PP mold, this analysis is a bit twisted since the two surfaces of the mold are different: PP has a contact angle equal to $\theta = 100° \pm 5°$ but air is probably the most hydrophobic since its surface tension with water is very high: $\gamma_{air-water} = 72.8\,\mathrm{mJ.m^{-2}}$. A small deviation from the elastic plateau is observed (on Figure 14) with the latter sample. This might be due to its high thickness (around 2.4 mm) which is unavoidable taking into account

large surface tension effects: the thickness needed to obtain a regular spreading pancake of water on PP is high.

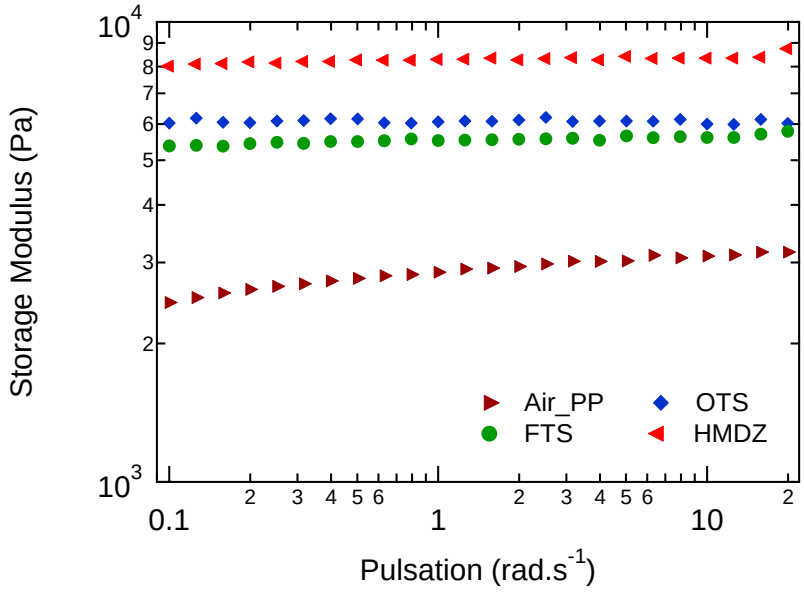

Figure 14 - Measured storage modulus as a function of pulsation in a frequency sweep measurement of the same PDMA-10x2 hydrogel, changing the surface characteristics of the mold: ♦ OTS; ► Air and PP; ◄ HMDZ; ● FTS.

2-3-2- Neutron reflectivity

To characterize in detail this concentration gradient and to determine if its origin is a lack of monomer or of cross-linker density, we have performed neutron reflectivity with the same PDMA gels synthesized in deuterium oxide. As mentioned earlier, neutron reflectivity is sensitive to the profile of the neutron scattering density between two semi-infinite media separated by a "flat" interface. When arriving from the semi-infinite media 1 (silicon here), the neutron beam is reflected off the semi-infinite media 2 (PDMA gel in our case) which has a higher neutron scattering density $\rho_2 > \rho_1$. The difference in neutron scattering density between the two semi-infinite media is specific of the position of the total reflection plateau. The latter is obtained for wave vectors below the critical wave vector q_c, which can be written as:

$$q_c = \frac{2\pi}{\lambda_c}\sin\theta_c = \sqrt{4\pi(\rho_2 - \rho_1)}\,. \qquad \textbf{Eq. 1}$$

As for silicon, the neutron scattering density is well known and equal to $\rho_1 = 2.0810^{-6}$ Å^{-2}. Determining the critical wave vector for silicon wafers in contact with identical gels being

synthesized in various molds gives directly access to the polymer concentration in the gel near the surface of the silicon substrate. PDMA-10x2 hydrogels have been synthesized as described previously and dialyzed in the same deuterium oxide buffer at pH 2. The silicon wafers were modified with identical PAA brushes as described earlier in this chapter. For each gel, two reflectivity experiments, represented on Figure 15 were carried out: (A) in the first one, the gel, immersed in deuterium oxide, was put on top of the silicon wafer and confined in an adapted chamber to avoid evaporation/exchange; (B) in the second one, a load was added on top of the gel so that it was compressed of about 10 to 20%.

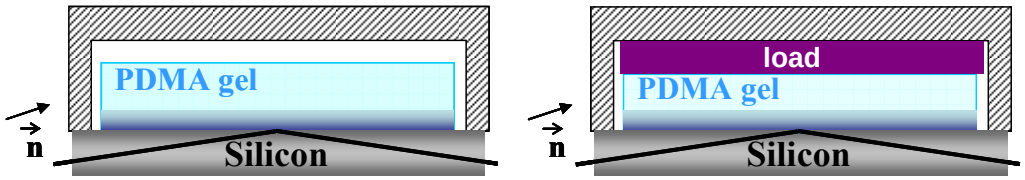

Figure 15 - Set up for neutron reflectivity experiments. (A): the gel sample is put on top of the silicon wafer in the presence of deuterium oxide in a closed chamber; (B): the gel sample is compressed of about 10% on the silicon wafer in the presence of deuterium oxide in a closed chamber.

The neutron reflectivity curves obtained are given in Figure 16. We have added the best fit to the experimental data, and we have plotted a simulation, assuming that the gel is ideally and uniformly swollen in bulk and at the surface[i].

In Figure 16-top, are shown the data from experiments A. The curves obtained from the gel synthesized in contact with air and OTS- and FTS- modified surfaces are very close to the reflectivity curve obtained in the presence of pure deuterated water. This means that for gels synthesized in those conditions (against surfaces such as FTS- or OTS-modified glass substrate, or with a free surface) and simply put in contact with the silicon surface, a polymer depleted layer forms near their surface. The average volume fractions of polymer have been estimated from the simulation and the results are summarized in Table 3. For gel synthesized against FTS- or OTS-modified glass substrate, or with a free surface, the average volume fractions at the surface range from 0.4% to 1.5% whereas the expected volume fraction is equal to 7.1% which corresponds to the swelling at equilibrium Q_e of the hydrogel

[i] The brush conformation is supposed to be identical to experiment B – OTS in this simulation where only the index of the second semi-infinite medium has been modified. The same procedure with any other experiment would have lead to a similar result.

PDMA-10x2 determined in Chapter 3: $Q_e = 14$. However the gel synthesized in an HMDZ-modified mold behaves differently and the data show that the surface polymer density is much higher at 3.8%.

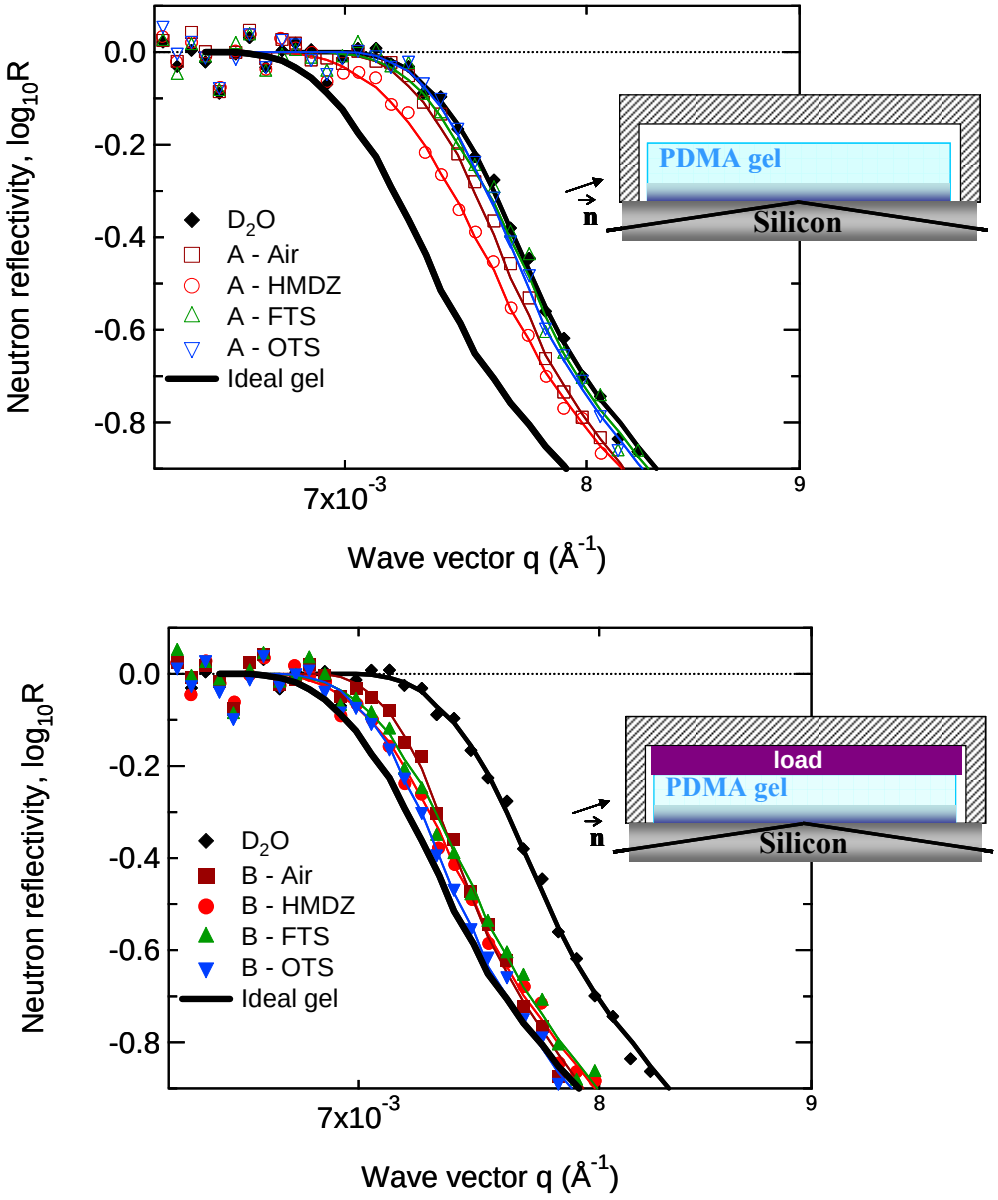

Figure 16 - Neutron reflectivity curves, near the total reflection plateau. Open symbols correspond to experiments A and filled symbols to experiments B. The experimental data (dots) are shown with their best fit (corresponding line). The second semi-infinite medium is either water (black), or equilibrated PDMA gels synthesized with a free surface or with the mold surfaces silanized with HMDZ, FTS or OTS. The bold black line corresponds to an ideal PDMA gel as second semi-infinite medium.

Data from experiments B are shown on Figure 16-bottom. In this case, the hydrogels are compressed on the silicon substrate. For all surfaces, the total reflection plateau is close to the

limit that should be observed for a uniformly swollen gel. The mean polymer density exceeds 5.1% and becomes close to – but remains below – the polymer density in the ideal gel, which is equal to 7.1%. By comparing the results from experiments B with those from experiments A, the local polymer concentration near the interface increases regardless of the preparation conditions when the gel is compressed in contact and it gets very close to the average bulk composition[ii].

Synthesis condition	$\rho_2 - \rho_1$ for experiment A	ϕ_{pol} and Q for experiment A	$\rho_2 - \rho_1$ for experiment B	ϕ_{pol} and Q for experiment B
D_2O, pH 2	4.38	$\phi_{pol} = 0\%$		
Air	4.30	$\phi_{pol} = 1.5\%;\ Q = 69$	4.10	$\phi_{pol} = 5.1\%;\ Q = 19$
HMDZ	4.17	$\phi_{pol} = 3.8\%;\ Q = 26$	4.02	$\phi_{pol} = 6.5\%;\ Q = 15$
FTS	4.34	$\phi_{pol} = 0.7\%;\ Q = 138$	4.05	$\phi_{pol} = 6.0\%;\ Q = 17$
OTS	4.36	$\phi_{pol} = 0.4\%;\ Q = 275$	4.00	$\phi_{pol} = 6.9\%;\ Q = 14$
Ideal gel	3.99	$\phi_{pol} = 7.1\%;\ Q_e = 14$		

Table 3 - Polymer concentration at interfaces ϕ_{pol} and corresponding local swelling Q as a function of the mold surface for PDMA-10x2 hydrogels.

2-3-3- Discussion

From rheology and neutron reflectivity experiments, we have shown that the mold used for the synthesis of the gel has a pronounced effect on its surface morphology. The first consequence is a gradient of concentration at the interface, which probably leads to a weak shear modulus in the parallel plates rheology experiment and to a misplaced total reflection plateau in the neutron reflectivity experiments. From these experiments though, we find that the mold surface that has the minimum impact on the surface of the gel compared to its bulk properties is the HMDZ-modified mold: its surface reaches a concentration equal to 3.8% which is far higher than what was obtained from the other synthesis and shows the highest shear modulus measured in rheology, around 8.3 kPa.

[ii] However, since the compression method did not allow a quantitative reproducibility, the small variations observed within the experiments B can not be discussed.

Such an effect of the mold surface on the macroscopic surface properties of the gel (namely friction) has been shown for double network gels before [38], but to the best of our knowledge it is the first time that a difference in polymer composition near the surface is directly measured by neutron reflectivity.

More specifically, Gong and her group [38,39] (and references therein) showed that the surface swelling of their gels was higher if the mold was hydrophobic than if it was hydrophilic. It suggests that the concentration in monomer or in cross-linker was locally weaker near the surface than in bulk. They first attributed this difference to the high interfacial energy between the polymer solution before synthesis and the hydrophobic substrate [40]. Then they suggested that molecules of oxygen adsorbed on the substrate would locally modify the polymerization process [41].

If this scenario is correct, working in a glove box with modified glass substrates stored under a nitrogen atmosphere for a few days could remove the effect of the substrate. In our case, we favor the use of a partially hydrophobic treatment with HMDZ. This easy vapor phase silanisation results in gels with surface characteristics close to the bulk ones, as determined with rheological measurement and with neutron reflectivity. However, the surface of the gel remains less concentrated in monomer and cross-linker than the bulk, but once under compression, no difference in concentration could be observed between the surface and the bulk.

2-4- Conclusion

We have developed a method to covalently stick a gel, composed of more than 90 wt% of water, onto a glass-like substrate. To this end, we have used quartz slides which have been silanized with a double-bond functionalized silane, the 3-methacryloxypropyl-dimethylchlorosilane. Then, the polymerization reaction was performed in contact with this modified quartz surface and the grafted silanes reacted as a co-monomer during the polymerization, attaching covalently the gel to the glass surface. To ensure a better adhesion and reproducible samples with flat surfaces, we synthesized gels close to their swelling equilibrium and with a low sensitivity to their environment, to avoid the development of a strong shear stress at the quartz-gel interface, or the appearance of wrinkles at the free surface.

The characteristics of the free surface of the gel are essential for adhesion phenomena but we showed that it strongly depends on the nature of the mold which influences the local polymerization process.

Nevertheless, we also demonstrated that when the gel is compressed, the concentration of the surface tends to be very close to the concentration in bulk. It means that for an adhesion measurement on hydrogels with a contact test, the polymer density probed during the experiment corresponds to the one in the bulk.

3- Gel-brush interfacial interactions

After having studied the interactions in solution between the polymeric pairs PAA-PDMA and PAA-PAM, the investigation of these interactions at interfaces has been considered. Besides the macroscopic mechanical approach consisting in an adhesion test (in the last two chapters), we have decided to probe the interactions between these systems at the polymer chain scale using neutron reflectivity.

Neutron reflectivity is a classical technique which gives access to the profile of neutron scattering density at a planar interface and we have already exploited it to determine the monomer volume fraction for PAA brushes at various pH and to evaluate the local polymer concentration at the surface of hydrogels. Here, we are using the technique at the interface between a protonated polymer brush and a protonated gel swollen in deuterium oxide. We show that in these conditions, the reflectivity data can be used immediately to determine the profile of the brush.

As a consequence, we investigated the effect of the presence of the gel on the brush conformation in different conditions, either when no interaction occurs between the brush and the gel at pH 9, or when interpolymer complexes are supposed to form at pH 2. This analysis was further investigated to point out the relative influence of both the hydrogel characteristics (namely its chemistry and its concentration) and the brush characteristics (namely its grafting density and the length of the grafted chains) on the conformation of the brush. Finally, the effect of the temperature on the structure of the brush was investigated with the PAM hydrogel, which has been shown to form thermoresponsive complexes with PAA on a wide range of pH.

3-1- Experimental section

Synthesis of PAM and PDMA gels. The synthesis of PAM and PDMA gels has been described in Chapter 2. The procedure is reminded here: *acrylamide (AM) or N,N-dimethylacrylamide (DMA), MBA and KPS are initially dissolved in deuterium oxide. The solution is deoxygenated with a bubbling of nitrogen during 20 to 30 min.*

For PDMA gels, the polymerization is initiated by the addition of TEMED as co-initiator in the solution which is homogenized and quickly poured in a mold placed in a nitrogen

atmosphere. For PAM gels, the solution is transferred in a mold placed in a nitrogen atmosphere, and then it is heated at 40°C.

The reaction is let to proceed during at least 4 hours. The mold characteristics are essential since they strongly influence the surface properties of the gel. As thoroughly discussed previously, we favored the use of two hexamethyldisilazane modified glass plates separated by a poly(dimethylsiloxane) home-made joint.

Then, the gel is demolded and immersed in deuterium oxide equilibrated at a given pH, which is renewed accordingly to the sample size in order to dialyze residual molecules out of the gel and to finally equilibrate the hydrogel at the right pH. The gel is finally stored in this solution until final use.

In Table 4 are presented the synthesis characteristics of the different samples used during this study.

$100\frac{[MBA]}{[DMA]}$	$\frac{100.m_{DMA}}{m_{DMA}+m_w}$	DMA (g)	MBA (mg)	KPS (mg)	TEMED (µL)	D_2O (g)
2	10	1	31.1	27.3	15	9

$100\frac{[MBA]}{[AM]}$	$\frac{100.m_{AM}}{m_{AM}+m_w}$	AM (g)	MBA (mg)	KPS (mg)	D_2O (g)
2	5	0.5	22.0	19.0	9.5
2	10	1	44.0	38.0	9
2	15	1.5	154.0	57.0	8.5

Table 4 - Formulations of PAM and PDMA hydrogels.

Synthesis of PAA brushes. The synthesis of PAA and PNIPAM brushes has been extensively described in Chapter 2. The steps of the synthesis are briefly recalled. *After being cleaned and rejuvenated in a piranha solution (70 vol% of sulfuric acid (97%) and 30 vol% of hydrogen peroxide (35%) heated at 150°C for 20 min), the silicon mono-crystals are extensively rinsed with Milli-Q water and dried under a nitrogen flux. They are immediately placed in a reactor under nitrogen atmosphere and immersed in a 2 vol% solution of 3-glycidoxypropyl-trimethoxysilane in extra-dry toluene for 5 hours at room temperature. The silicon substrate are then rinsed with toluene and dried under a nitrogen flux.*

PNIPAM. A PNIPAM brush has been used as a control sample. A 1 wt% solution of carboxy-terminated PNIPAM in THF is deposited on the substrate and the solvent is evaporated to

form a reservoir of PNIPAM chains on top of the expoxy-functionalized surface, which is then heated at 150°C under vacuum during 24 hours. The mono-crystals are finally removed from the oven and placed in a bath of Milli-Q water to remove ungrafted PNIPAM chains.
PAA. A 1 wt% solution of carboxy-terminated PtBuA long chains in THF is deposited on the epoxy-modified silicon crystal and a polymeric film is formed by solvent evaporation. The substrate topped with the PtBuA reservoir is heated at 120°C under vacuum during 24 hours. The substrate is thoroughly rinsed in THF. A second 1 wt% solution of PtBuA short chains in THF is then deposited on the substrate to form another reservoir of polymer. After being heated during 48 hours at 120°C under vacuum, the silicon crystal is rinsed again, dried, and the sample is pyrolyzed at 200°C under vacuum during 2 hours. Finally, it is immersed overnight in Milli-Q water equilibrated at pH 2.
The characteristics of PAA brushes are given in Table 5.

Brush type	Mn (g/mol)	γ (Å)	σ (nm^{-2})	σ^{tot} (nm^{-2})	D (Å)	γ^{tot} (Å)
Short brushes	3 650	21	0.43		15	
Medium Long brushes	2 360 23 610	8 25	0.25 0.074	0.33	18	33
Dense long brushes	2 360 23 610	4 42	0.13 0.013	0.26	20	46

Table 5 - Mean characteristics of the poly(acrylic acid) brushes: molar mass M_n of the grafted chains, dry thickness γ and grafting density σ for each sample. The total grafting density σ^{tot}, the mean distance between grafting points D and the total thickness γ^{tot} are also listed.

Neutron reflectivity experiments. The procedure for neutron reflectivity experiments and their analysis is presented in Annex. *Neutron reflectivity measurements were performed at silicon-liquid interface on the reflectometer EROS at the Laboratoire Léon Brillouin, CEA-Saclay (France). We used protonated polymer brushes and deuterated water or gel in order to enhance the contrast between the polymer and the immersing medium, and to optimize the reflectivity signal*[iii]*. The reflectivity data curves were fitted to determine the coherent*

[iii] It could have been possible to use deuterated PAA backbones and normal water, which would have increased the contrast between the brush and the solvent and keep the hydrogen bonds un-modified. However, other problems would have been raised. First, the propagating medium (silica) would have had a lower neutron scattering length than the reflecting medium (water), leading to the absence of a total reflection plateau which is

scattering length density profile in the direction normal to the interface $\rho(z)$. *We used a reliable model-independent method describing the brush as a set of layers (each characterized by a fixed thickness* h_i *and a scattering length density* ρ_i *for the layer* i *starting at the distance* z_i *from the surface) connected using error functions of fixed width* σ_i *to get a continuous profile. The procedure consisted of choosing a scattering length density profile and finding the corresponding parameters for which the calculated reflectivity curve fits the best the experimental reflectivity data. The polymer density profile* $\phi(z)$ *was then deduced from* $\rho(z)$, *knowing the coherent scattering densities of the polymer* ρ_{Pol} *and of deuterium oxide (or* D_2O*-swollen gel)* ρ_{D_2O}*:*

$$\phi(z) = \frac{\rho(z) - \rho_{D_2O}}{\rho_{Pol} - \rho_{D_2O}}. \qquad \textbf{Eq. 2}$$

Finally, we compared the density profile of the PAA brushes when they are simply immersed in water and when they are in contact with a gel in the same environmental conditions (temperature and pH), as represented in the two schemes of the Figure 17.

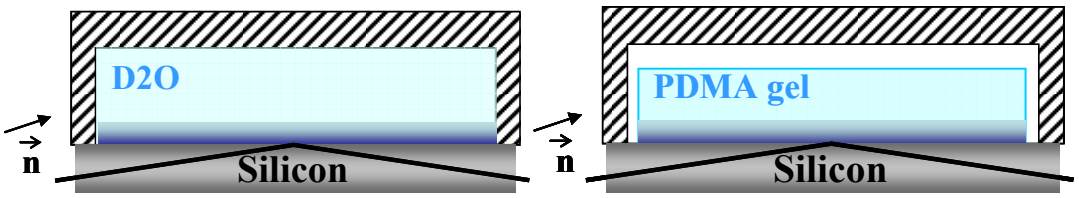

Figure 17 - Schematic representation of the experimental conditions for neutron reflectivity experiments for brushes immersed in water or in contact with a gel.

Neutron reflectivity experiments with a gel as a reflecting semi-infinite medium have already been reported by La Spina *et al.* [42]. However the depleted form of the polymer profile obtained in water and with the gel seemed rather inconsistent with theoretical expectations [43,44]. To check the influence of the gel on the determination of the structure of the brush, we have used a control sample. The effect of temperature on a PNIPAM brush was investigated. We used a PNIPAM brush of molar mass M_n = 121 000 g.mol^{-1} with a dry

essential for fitting the data. Then, water has a high content of hydrogen which has a very high incoherent neutron scattering, leading to a strong increase of the signal-to-noise ratio. Finally, these experiments would have been very expensive.

thickness of about 110 nm. It was immersed in deuterium oxide or in contact with a PAM-10x2 hydrogel equilibrated at pH 9. The temperature was set either to 20°C or 60°C, using a setup as shown in Figure 18.

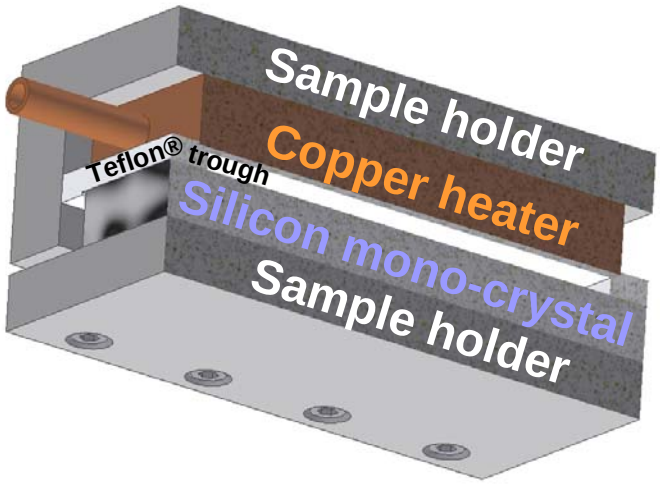

Figure 18 - Schematic cut of the samples used for the measurement of neutron reflectivity. The sample holder maintain together the silicon mono-crystal in contact with a Teflon® trough in which is placed the immersing medium (water or gel). This trough can be heated with a copper heater through which thermostated fluid is circulated.

PAM (from the gel) and PNIPAM (from the brush) are known not to form complexes in water at any pH or temperature conditions, but PNIPAM is a well studied thermo-sensitive polymer for its LCST in water at 32°C. Thus, a significant difference in the conformation of the brush is expected for the PNIPAM brush immersed in water when changing the temperature from 20°C to 60°C.

The reflectivity curves obtained in water at 20°C and at 60°C are shown on Figure 19. Comparing these curves, one can first notice the difference in the Kiessig fringes, which are more pronounced at 60°C and which are the signature of a steeper density profile. At 20°C, the brush is stretched away from the surface with a maximum extension of 1 400 Å. On the contrary at 60°C, the brush is collapsed on the surface (maximum extension below 400 Å) with a small depleted layer and a high polymer fraction (~ 0.6) close to the surface. The LCST has caused the apparition of two phases: polymer-poor and a polymer-rich. Nevertheless, the PNIPAM chains are not completely collapsed on the surface since the polymer profile is not the one of a dry brush.

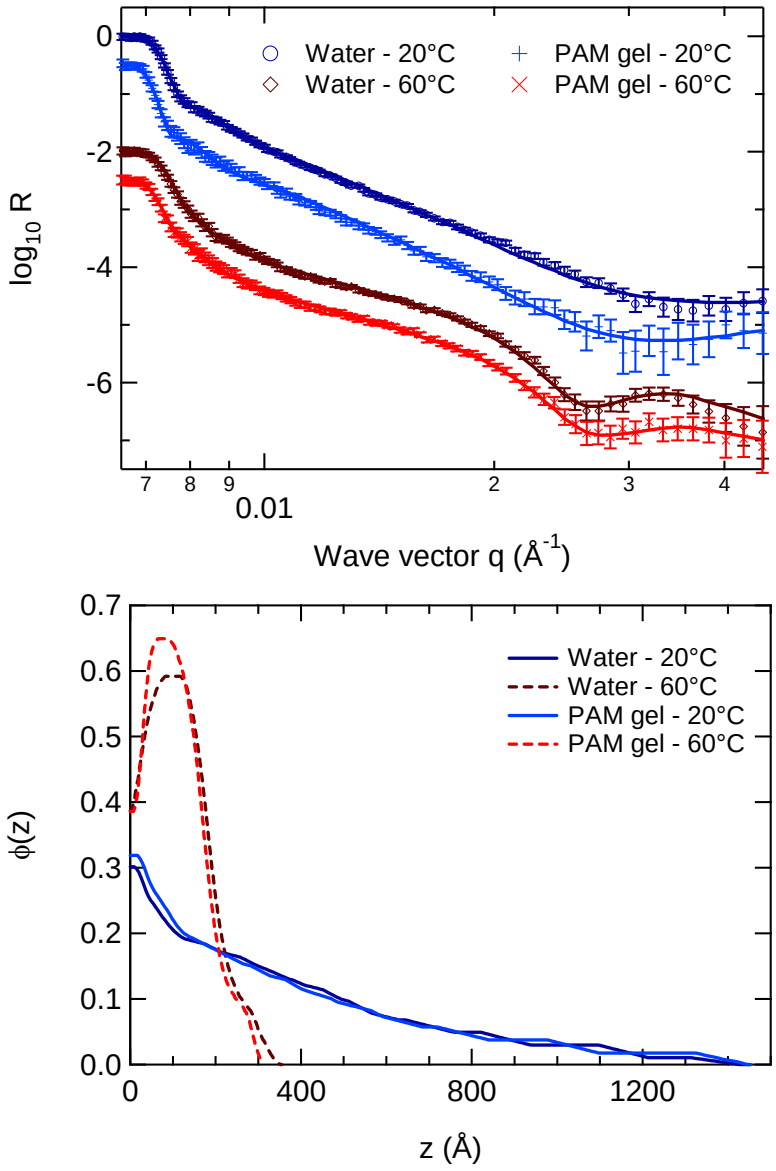

Figure 19 - Neutron reflectivity curves (top) and polymer volume fraction corresponding (bottom) to the best fit of the reflectivity data for temperature-responsive PNIPAM brushes.

In the presence of the PAM gel, the profiles are nearly identical. As it could be expected, no effect of the gel is to be seen and the reflectivity allowed to verifying this result. The Small Angle Neutron Scattering does not usually disturb the experiments of reflectivity. However, it was necessary to verify it and in our case, the absence of disturbances can be explained by the very small volume of gel probed in an equivalent SANS experiment. Neutron reflectivity is sensitive to the first few thousands of Angstrom of the surface which means that the volume of gel probed during the experiment is in the order of 0.5 mm^3, that is to say two orders of magnitude smaller than the volume probed in a SANS experiment. As a consequence, the SANS signal is very weak and does not influence the one of the reflectivity, which is obtained

from planar waves delocalized on the whole surface. It has been verified thanks to the experiment with PNIPAM and thanks to the measurement of the non-specular signal, equivalent to the one measured when the second semi-infinite medium is water.

The conclusion of this test performed with a PNIPAM brush is that, in the absence of polymer/polymer interactions, the presence of the gel does not influence the brush volume fraction, whether it is swollen or collapsed.

3-2- Effect of pH on the structure of the brush in contact with a gel

The objective of this part is to determine whether the presence of the gel affects the structure of the brush, at pH 9 and at pH 2. In water at pH 9, the PAA brush is completely ionized and it is expected to be stretched away from the surface with a Gaussian profile. At pH 2 in water, the brush has a parabolic profile and is less stretched than at pH 9. The results obtained in water for the PAA brushes are extensively discussed in Chapter 2.

As it has been shown in the first part of this chapter, no interaction is expected to occur in basic conditions between the PAA chains of the brush and the PDMA or PAM of the gel (see Figure 20-left). Then, no modification is expected on the structure of the brush. On the contrary in acidic conditions, PAA and PDMA or PAM form interpolymer complexes (see Figure 20-right) and the question is: does the presence of interactions modify the structure of the brush?

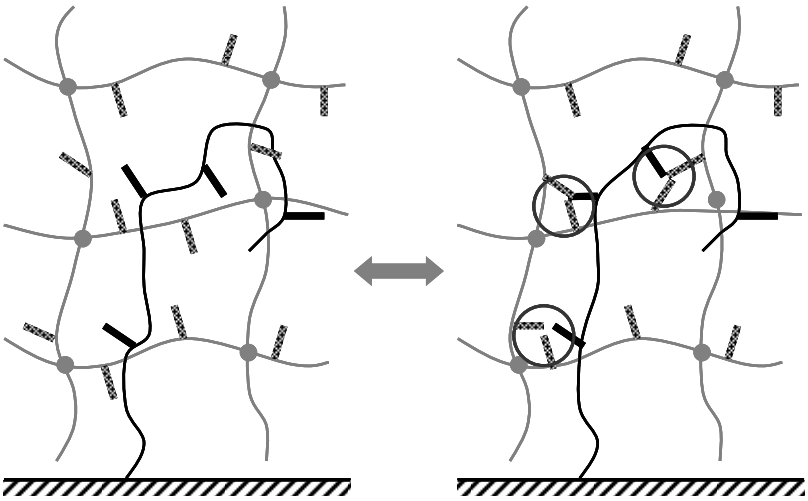

Figure 20 - Schematic representation of the two pH conditions when the brush is in contact with a gel. At pH 9, the brush is ionized and unable to interact with the gel (left) whereas at pH 2, the PAA of the brush form interpolymer complexes with the polymer of the gel (right).

We report in Figure 21 the results obtained at pH 9 for a system composed of dense and long brushes as described in Table 5. For one the samples, we show the neutron reflectivity data and the polymer density profile fitting best the experimental data, when the brushes are immersed in deuterium oxide or in contact with a hydrogel. The neutron reflectivity curves do not change much for the same sample, whether the gel is immersed in water or in contact with the gel. Then, the polymer density profiles obtained at pH 9 are very close. In the presence of the gel, the profiles obtained are almost the same.

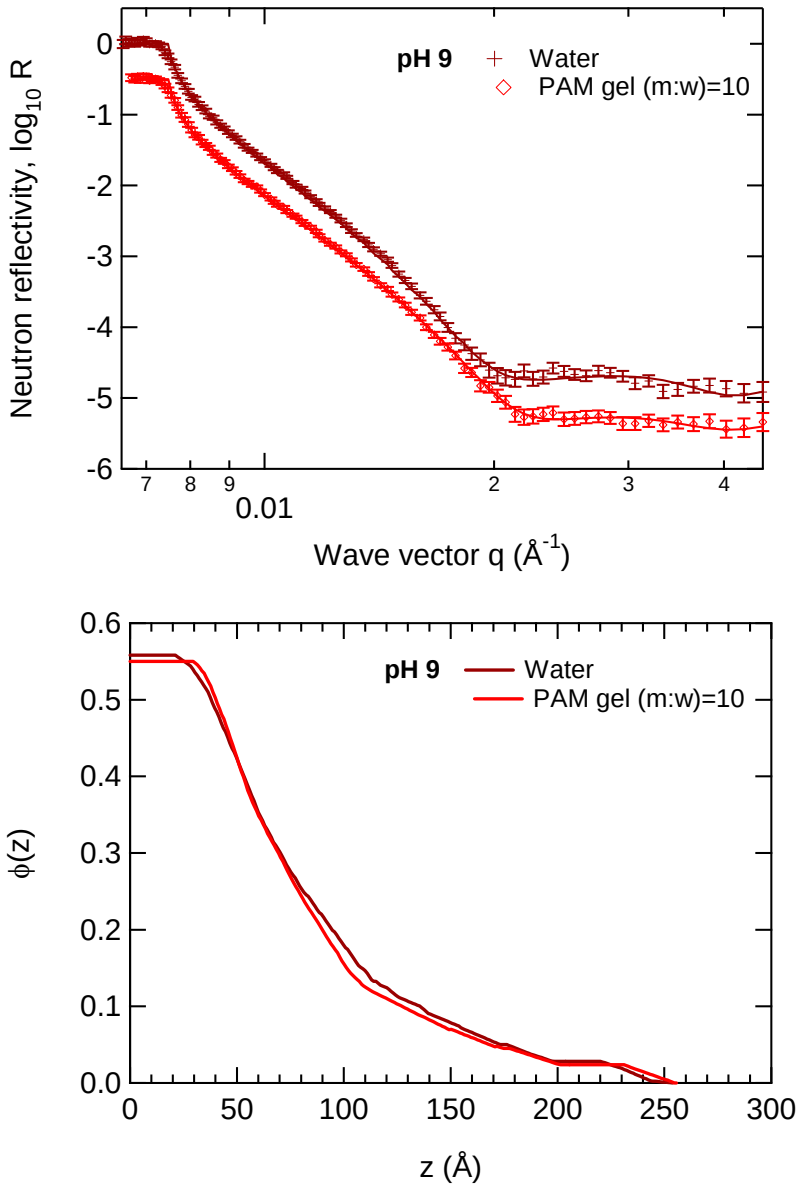

Figure 21 - Neutron reflectivity curves (top) and polymer volume fraction (bottom) corresponding to the best fit of the reflectivity data for the samples of dense and long brushes described in Table 5. Experiments are carried out at pH 9, in water or in contact with a gel.

In all cases, the polymer fraction profiles are the same: the same result was found with changing the gel or varying the characteristics of the brush at pH 9. It means that the presence of the gel does not affect the structure of the brush when no interaction takes place between them.

Figure 22 shows the results obtained at pH 2 for the same system of dense and long brushes, when the brush is in water and in contact with a PAM gel.

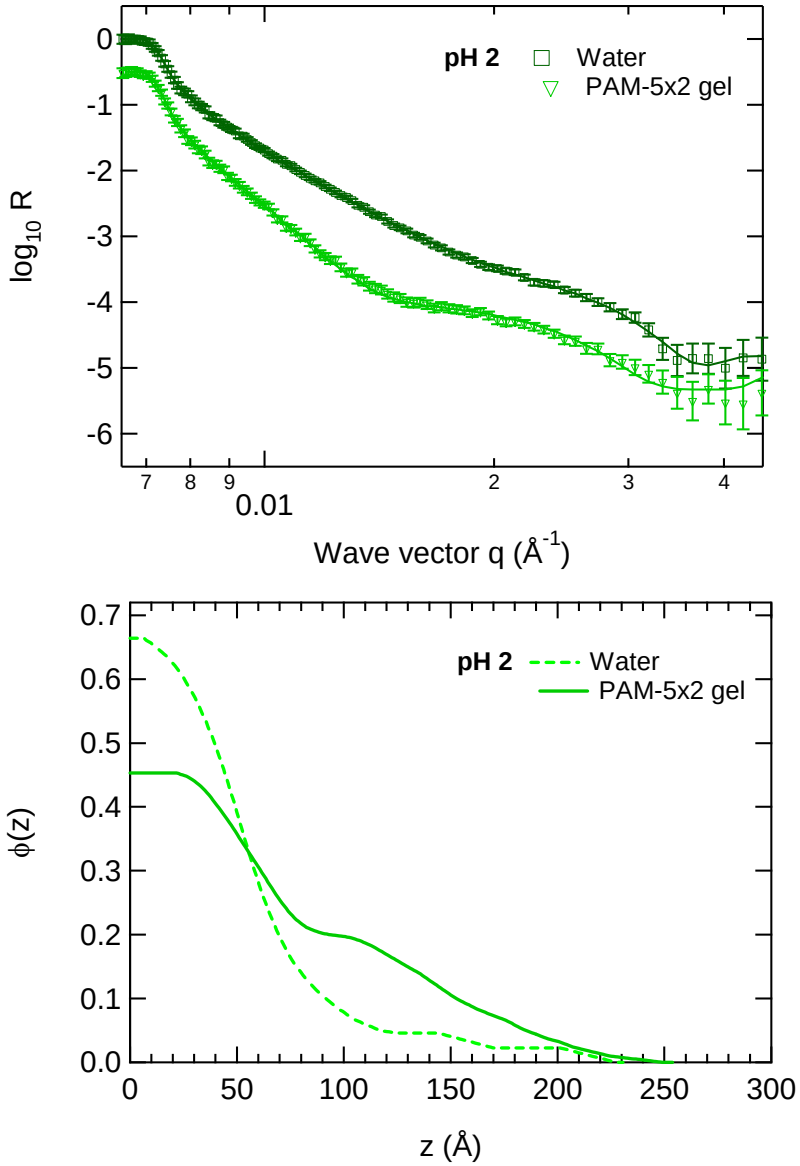

Figure 22 - Polymer volume fraction corresponding to the best fit of the reflectivity data for the samples of dense and long brushes described in Table 5. Experiments are carried out at pH 2, in water or in contact with a gel.

Clearly, the conformation of the brush is additionally stretched away when it is in contact with the gel. The mean characteristics of the brushes obtained from the profiles are summarized in Table 6. For this sample, the stretching at pH 2 in the presence of the gel is even higher than the one of the brush at pH 9.

For many different experiments carried out at pH 2, we found that in each case, the mean height of the brush is extended of at least 15% when it is in contact with the gel. The additional extension due to the presence of the gel can only be explained by some interpenetration of the brush inside the gel. This effect differs from what was observed for a gel and a brush interacting through Coulombic interactions by La Spina *et al.* [42]. They described no interpenetration of the brush inside the gel when the gel, in contact with the brush, is not compressed enough [45,46]. Here, our neutral gels are not compressed, but we favored the use of HMDZ-treated mold for their synthesis which limits the local swelling at the surface of the gel, as mentioned above in the part 2 of this chapter.

These first experiments lead to two conclusions:

- At pH 9, in the absence of interactions between the polymers constituting the brush and the gel, the conformation of the brush is not affected by the presence of the gel and it remains identical to the one in water.
- At pH 2 on the contrary, the swelling ratio of the brush in the presence of a gel can be noticeably increased so that it is in the range of (or higher than) the swelling ratio obtained at pH 9. This fact tends to indicate that the H-bonds are the source of a stretching in the order of magnitude of the electrostatic repulsion inside the ionized PAA brush.

Immersing medium	Specification	γ (Å)	h (Å)	$\bar{\phi}$	h/γ
Water/gel, pH 9	Sample 1	43	116	0.36	2.77
	Sample 2	50	120	0.42	2.40
Water, pH 2		43	89	0.48	2.07
PAM gel, pH 2	(m:w) = 5	46	132	0.34	2.87

Table 6 - Mean characteristics of swollen poly(acrylic acid) brushes when varying the immersing medium. The dry thickness γ, the mean height h, the mean volume fraction of polymer inside the brush $\bar{\phi}$ and the swelling ratio h/γ are listed.

3-3- Effect of the characteristics of the gel

3-3-1- Chemistry of the gel

Based on the conclusion that the surface interactions have a tendency to additionally stretch the brush from the surface, the first question that we raise is the following: knowing that the polymeric pairs PAA-PDMA and PAA-PAM are able to form interpolymer complexes at low pH, is there a variation in the strength of their interactions at a given pH and are we able to characterize this variation with neutron reflectivity?

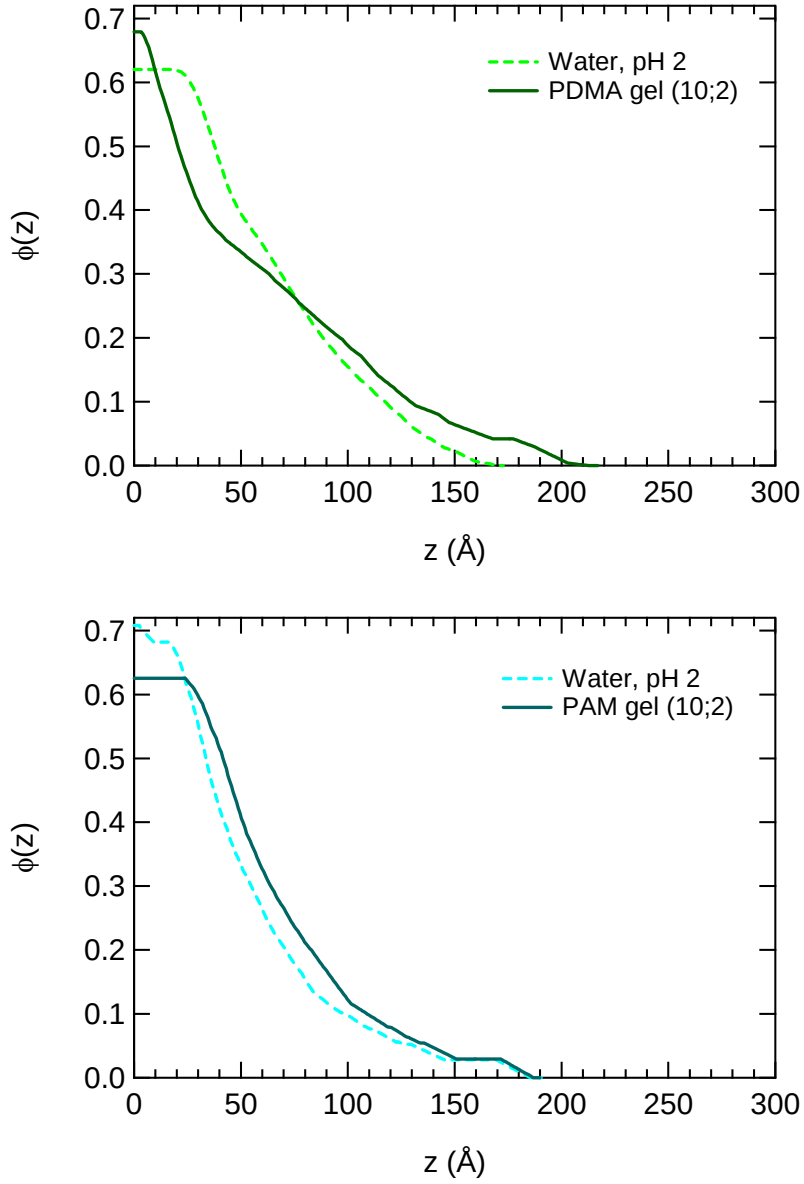

Figure 23 - Polymer volume fraction corresponding to the best fit of the reflectivity data for the samples of dense and long brushes described in Table 5. Experiments are carried out at pH 2, in water or in contact with a PDMA gel (top) and in water or in contact with a PAM gel (bottom).

To answer this question, we have carried out neutron reflectivity measurements on similar brushes. We have compared the profile[iv] of the brush at pH 2 when the immersing medium is water or when it is a gel, either PDMA or PAM. The polymer density profiles are plotted on Figure 23 and the average characteristics of the brushes deduced from the concentration profile are given in Table 7.

Test	Immersing medium	γ (Å)	h (Å)	$\bar{\phi}$	h/γ
PAM/water	Water	40	81	0.49	2.02
	PAM gel (10;2)		95	0.42	2.38
PDMA/water	Water	45	92	0.49	2.04
	PDMA gel (10;2)		111	0.40	2.50

Table 7 - Mean characteristics of swollen poly(acrylic acid) brushes when varying the immersing medium. The dry thickness γ, the mean height h, the mean volume fraction of polymer inside the brush $\bar{\phi}$ and the swelling ratio h/γ are listed.

The profiles obtained at pH 2 in water are very similar and the swelling ratio of the brush is about 2. In contact with the PDMA gel, the limit extension of the brush is further from the surface than in water and consecutively, the mean height of the brush and its swelling ratio are increased by 25%. In contact with the PAM gel, the limit extension of the brush remains identical to that in water but the surface polymer fraction is decreased and the profile is additionally stretched, leading to an increase of 20% of the swelling ratio of the brush.

Even if the brush seems more stretched away from the surface in contact with a PDMA gel by comparison with a PAM gel of similar characteristics, it is difficult and it would be tendentious to draw general conclusions on the basis of these small differences.

We will simply keep in mind that the presence of the gel – either PAM or PDMA – stretches almost equivalently the concentration profile of the brush of about 20 to 25%.

[iv]Figure 19, Figure 21 and Figure 22 clearly enlighten the high quality of the fits of the neutron reflectivity data. In all cases presented in this manuscript, the data were fitted to the best. However, since it is impossible to directly analyze the raw data, only the polymer density profiles corresponding to the best fits are presented in the following sections.

3-3-2- Effect of the gel concentration

To investigate the effect of the gel concentration on the conformation of the brush, we have focused the study on PAM-(m:w)x2 gels, synthesized with (m:w) equal to either 5, 10 or 15 wt% of monomer at the synthesis (Table 4). The measurements on these gels were carried out with different silicon mono-crystals. As a reference, we have produced the results obtained in water for two mono-crystals. As shown in the previous paragraph, the profiles obtained for two repeats of dense long PAA brushes (Table 5) at pH 2 are represented on Figure 24 and their average characteristics are given in Table 8. It can be noticed that they are very close; the swelling ratio is around 2 for both of them.

For each brush profile obtained in the presence of the gel (Figure 24), the brush is more stretched away from the surface than when immersed in water. Even if the shape of the profile does not vary much when changing the immersion conditions and if the maximal extension of the chains does not change much, the mean height calculated for each sample differs from one another (Table 8 and Figure 25). The swelling ratio values deduced from the data clearly demonstrates that the presence of the gel tends to stretch the brush conformation: the brush in water at pH 2 has a swelling ratio around 2, which differs from the swelling ratio of the brush when in contact with the gel, the latter exceeding 2.38.

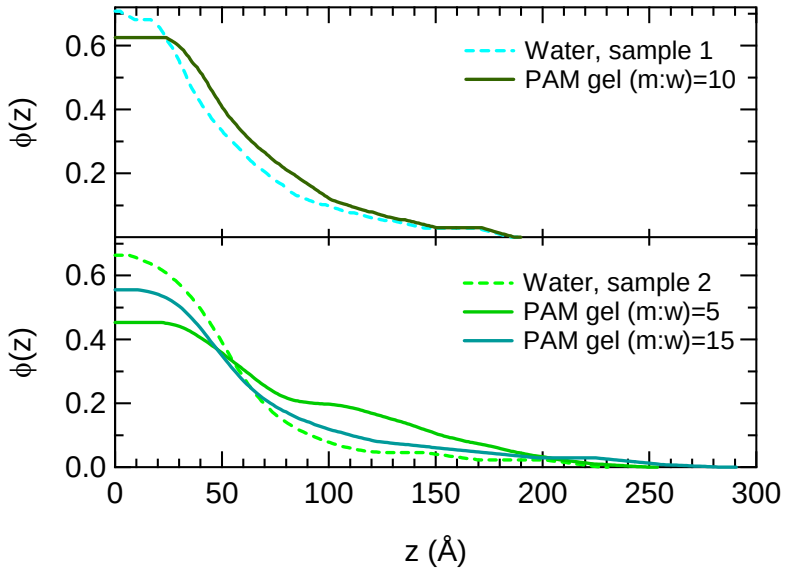

Figure 24 - Polymer volume fraction corresponding to the best fit of the reflectivity data for the samples of dense and long brushes described in Table 5. Experiments are carried out at pH 2, in water or in contact with a gel.

These swelling ratios are very close, if not higher, than the values obtained for brushes immersed in water at pH 9 (around 2.5). Finally, with the variation of the polymer concentration inside the gel, we were not able to determine a trend (Figure 25), but the average swelling ratio in the presence of the gel is around 2.62 ± 0.25.

Immersing medium	Specification	γ (Å)	h (Å)	$\bar{\phi}$	h/γ
Water pH 9	pH 9-Sample 2	50	120	0.42	2.40
Water pH 2	pH 2-Sample 1	40	81	0.49	2.02
	pH 2-Sample 2	43	89	0.48	2.07
PAM gel pH 2	(m:w) = 5	46	132	0.34	2.87
	(m:w) = 10	40	95	0.42	2.38
	(m:w) =15	43	116	0.37	2.70

Table 8 - Mean characteristics of swollen poly(acrylic acid) brushes when varying the immersing medium. The dry thickness γ, the mean height h, the mean volume fraction of polymer inside the brush $\bar{\phi}$ and the swelling ratio h/γ are listed.

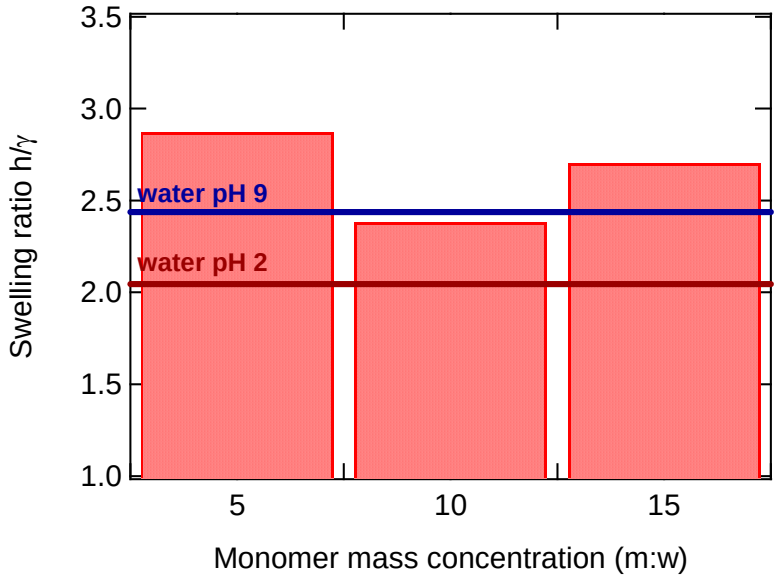

Figure 25 - Swelling ratio of the PAA brush at pH 2 in contact with PAM of varying monomer mass concentration (m:w). For comparison, the mean swelling ratio of the same PAA brushes at pH 2 and 9 are drawn.

When changing the characteristics of a gel (either its chemistry at a given concentration or its concentration for PAM gels), the brush is additionally stretched at pH 2 in the presence of interactions. This stretching can be noticeably important and reach values higher than those

obtained for the ionized PAA brush. The stretching seems almost equivalent at pH 2 for PAM gel and PDMA gel with a 10 wt% monomer concentration. When the concentration is varied between 5 wt% and 15 wt%, no trend could be observed.

3-4- Effect of the characteristics of the brush

3-4-1- Grafting density

Another way to change the number of grafted chains relative to the concentration of the gel is to vary the grafting density of the brush. To investigate this effect, we kept constant the characteristics of the PDMA gel used here (seeTable 4 - Table 4 and Table 5). The profile fitting best the reflectivity curves are presented in Figure 26.

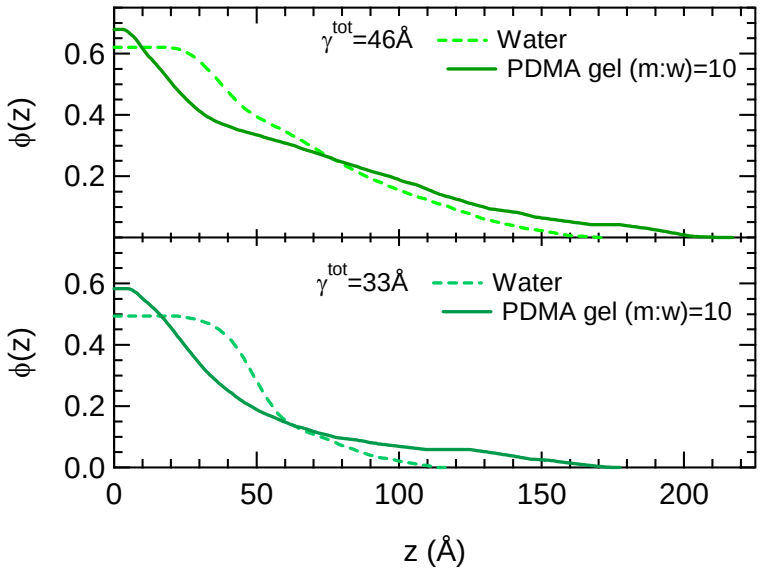

Figure 26 - Polymer volume fraction corresponding to the best fit of the reflectivity data for the samples of dense and long brushes described in Table 5. Experiments are carried out at pH 2, in water or in contact with a gel.

The increased extension of the brushes induced by the presence of the gel appears clearly from the profiles of the brushes: first, the maximal extension of the brushes is clearly higher when the gel is interacting with them and their mean height is extended by at least 20%. This is obviously stated in Table 9 which gives the mean height of the brushes and their swelling ratio. The swelling ratio is increased of 27% at low grafting density and of 23% at higher grafting density when in contact with a PDMA gel. Once more, it is hard to conclude from

these differences, beside the facts that both the maximum extension and the swelling are stronger in the presence of the PDMA gel.

γ (Å)	Immersing medium	h (Å)	$\bar{\phi}$	h/γ
28	Water	63	0.45	2.25
	PDMA gel	80	0.30	2.86
45	Water	92	0.49	2.04
	PDMA gel	111	0.40	2.50

Table 9 - Mean characteristics of swollen poly(acrylic acid) brushes when varying the immersing medium. The dry thickness γ, the mean height h, the mean volume fraction of polymer inside the brush $\bar{\phi}$ and the swelling ratio h/γ are listed.

As it was previously found for PAA brushes in contact with PAM gels, the presence of PDMA gels equilibrated at pH 2 influences the polymer density profile beyond the experimental sensitivity/inaccuracy. The shape of the profile of the brush was recurrently determined as elongated when in contact with a PDMA or PAM gel. As a consequence, the formation of polymer complexes at interfaces modifies the brush conformation and the strength of the interactions could be extrapolated from this complementary stretching. The fact that in the presence of gel, the swelling ratio can be extended to values obtained for similar brushes at pH 9 tends to indicate that the H-bond are the source of a stretching in the order of magnitude of the electrostatic repulsion inside the PAA brush.

3-4-2- Chain length

The results obtained for PAA brushes with short chains ($M_n = 2360$ g.mol^{-1}, DPI = 1.1 and $\sigma = 4.3\ 10^{-1}$ chains.nm^{-2}) are represented on Figure 27. The mean characteristics of the structure of the brushes obtained at pH 2 and at pH 9 are given in Table 10. First of all, one should note that, despite the fact that the PAA chains are charged at pH 9 and protonated at pH 2, the extension of the chains in pure water is not very different (Figure 27, swelling ratios of 2.87 at pH 2 and 3.04 at pH 9). As explained in Chapter 2, this apparently surprising result is due to the high grafting density of the chains for which there is no difference of the mean height for the polyelectrolyte brush and the neutral brush and the technique is not sensitive enough to make a strong distinction between them.

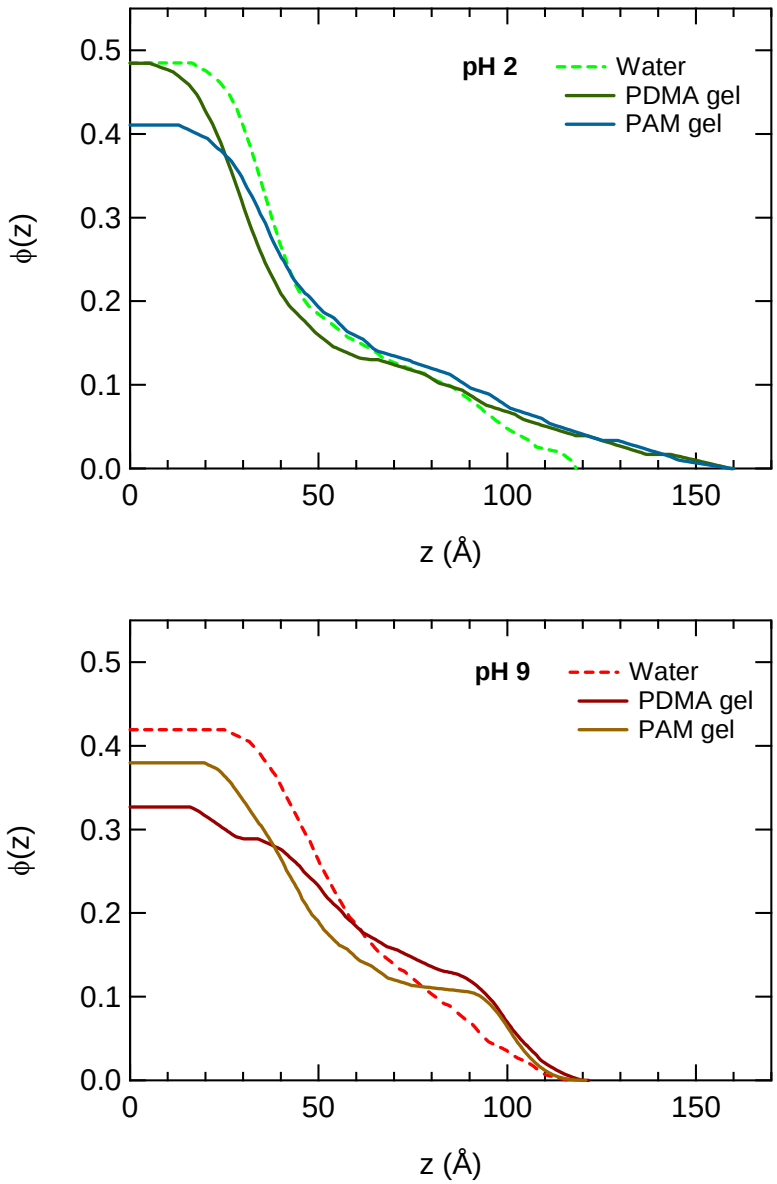

Figure 27 - Polymer volume fraction corresponding to the best fit of the reflectivity data for the samples of dense and long brushes described in Table 5. Experiments are carried out at pH 2, in water or in contact with a gel.

At pH 9, the profiles obtained in the presence of the PDMA or PAM gels do not extend further from the surface than those obtained for the brushes immersed in water. The mean heights obtained from the profiles in the presence of the gels are equal to the one obtained in water within a 2 Å accuracy. The corresponding mean volume fraction of the brush and its swelling ratio are given in Table 10 depending on its environmental conditions.

At pH 2, the polymer density profiles seem to be a bit more stretched in the presence of the gels than in water, the mean height of the brush being increased of about 10 Å. The brush reaches swelling ratio values which are higher than those obtained at pH 9.

pH	Immersing medium	h (Å)	$\bar{\phi}$	h/γ
pH 2	Water	66	0.35	2.87
	PDMA gel	74	0.31	3.18
	PAM gel	76	0.31	3.23
pH 9	Water	70	0.33	3.04
	PDMA gel	72	0.32	3.13
	PAM gel	72	0.32	3.13

Table 10 - Mean characteristics of swollen poly(acrylic acid) brushes when varying the immersing medium. The dry thickness γ, the mean height h, the mean volume fraction of polymer inside the brush $\bar{\phi}$ and the swelling ratio h/γ are listed.

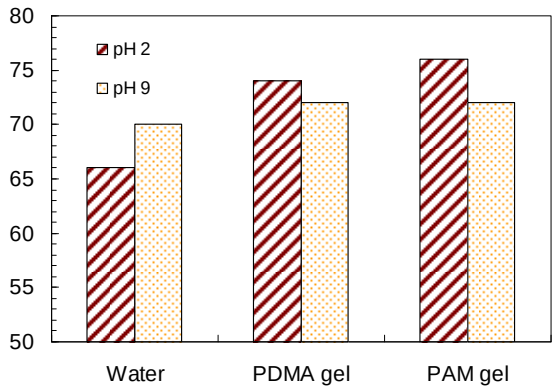

Figure 28 - Mean height (Å) of short PAA brushes (described in Table 5) when changing the environment: water, PDMA gel or PAM gel at pH 2 and pH 9. In contact with a gel, the brush is more stretched at pH 2 than at pH 9.

As a conclusion, we have shown that for short and dense PAA brushes – whose conformation is not much different between pH 2 and pH 9 – the presence of a PDMA or PAA gel in acidic conditions tends to stretch the brush away from the surface (see Figure 28) while at pH 9, no clear effect could be observed.

3-5- Can interpolymer complexes be tuned by temperature at interfaces?

As it was shown in the first part of this chapter, PAA and PAM interactions are tunable by temperature on a wide range of pH, from 1.8 to 3.2. It is then tempting to wonder whether these interactions were sensitive to temperature when reproduced at interfaces. To this end, we have chosen to work at a pH for which the transition temperature was in the temperature range reasonably accessible for a reflectivity measurement. At pH 2.6, the transition temperature in solution was found close to 40°C, so the gel was equilibrated at this pH and reflectivity measurement were carried out at 20°C and at 60°C.

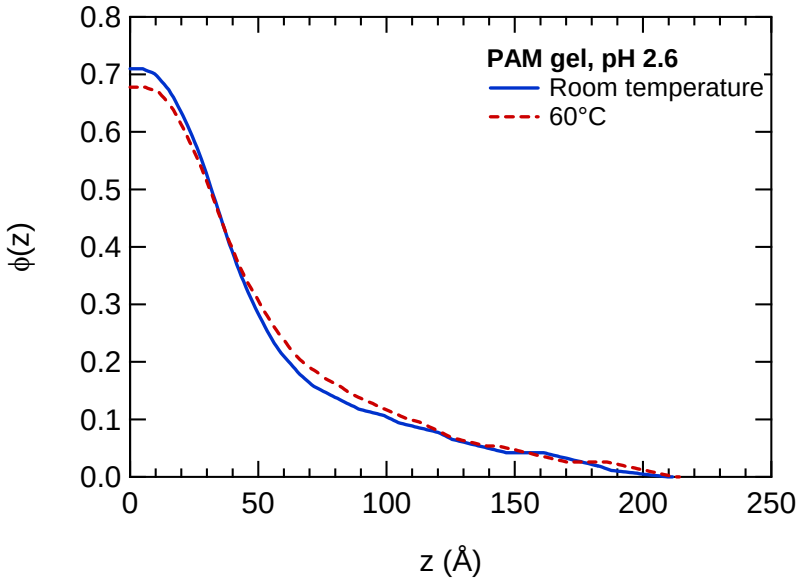

Figure 29 - Polymer volume fraction corresponding to the best fit of the neutron reflectivity curves for the dense long brushes described in Table 5. Experiments are carried out in contact with a PAM-10x2 gel equilibrated at pH 2.6 at 20°C and at 60°C.

We used a dense and long PAA brush and a PAM gel with a monomer mass concentration of 10% and a cross-linker molar ratio equal to 2%. The polymer fraction profiles are plotted on Figure 29 and the mean characteristics deduced from these results are given in Table 11. The profiles obtained for the two different temperatures are very close and no effect of the temperature on the conformation of this brush was really evidenced.

This ineffectiveness of temperature can be explained by three facts at least. First, the concentrations inside the brush and inside the gel exceed by far the concentration that were used to build the phase diagram, and the polymer concentration has a major effect on the

complexation of polymers as it was shown in the first part of the chapter and by other authors [6]. Second, when transferred to interfaces and in presence of gels, the thermodynamics of the interactions are modified since the entropy of translation of the polymer chains is highly affected. And third, widely evoked but rarely extensively explained, the change of hydrogen isotope could impact the H-bonds.

pH	Temperature	h (Å)	$\bar{\phi}$	h/γ
pH 2.6	20°C	87	0.48	2.07
	60°C	92	0.46	2.19

Table 11 - Mean characteristics of the swollen poly(acrylic acid) brushes in contact with a PAM gel when changing the temperature. The dry thickness γ of the brush is equal to 42 Å, and the mean height *h*, the mean volume fraction of polymer $\bar{\phi}$ and the swelling ratio h/γ are given.

3-6- Conclusion

We have shown that the presence of a gel as a reflecting semi-infinite medium did not alter the reflectivity study of the conformation of polymer brushes. As a consequence, we were able to determine the effect of the adsorption of a gel on the conformation of PAA brushes.

At high pH (pH 9), when there is no interactions between the polymer brush and the hydrogel, the structure of the brush remained unmodified.

However at pH 2, in the conditions where PAA brushes strongly interact with PDMA or PAM, we have found that these interactions modify the conformation of the PAA brush in contact with a PDMA or PAM gel. In all cases, the brush was more stretched in the presence of the gel than when immersed in water equilibrated at pH 2. In some cases, the complementary stretching due to the interactions was strong enough to extend the brush beyond the stretching obtained at pH 9. The most important effects were observed with long brushes and when the gel was at low concentration or when the brush had a lower grafting density. For short brushes of very high grafting density, no conclusive stretching was observed. Furthermore, no effect of the temperature on the structure of the brush was found for a brush in contact with a PAM gel when working at an intermediate pH 2.6.

4- Conclusion

In this chapter, we have demonstrated that the polymers chosen to switch the adhesion are able to interact on a different way as a function of pH. PAM is able to create links with PAA mainly through hydrogen bonding. The resulting complexes are highly sensitive to temperature and are broken when heating the solution. A phase transition with a UCST comprised between 5°C and 60°C is observed for this polymeric pair for the pH range between 1.8 and 3.2. When decreasing the pH, the strength of the complex increases. The interactions formed between PDMA and PAA involve both hydrogen bonds and hydrophobic interactions and consequently the polymeric pair undergoes a phase transition with an LCST, in a very narrow range of pH: between 3.45 and 3.75. The use of copolymers of AM and DMA with PAA made it possible to change the critical pH at room temperature continuously from 3 to 3.5 when increasing the DMA content in the copolymer. It also reduced the sensibility of the complexes towards temperature and made it almost insensitive when the AM content reached 70 mol%.

Before quantifying the effect of these interactions at interfaces, we have given a protocol to covalently attach a hydrogel on a transparent quartz surface. We have also proven that the quality of the free surfaces of a gel was strongly dependant on the nature of the surface of the mold used for its synthesis. Using three different surface treatments of various hydrophobicities, we have demonstrated, by rheology and neutron reflectivity, that the gradient in polymer concentration at the surface of the gel was stronger when the mold surface was more hydrophobic. A glass mold simply silanized with HMDZ by vapor phase showed the smallest difference in concentration between the surface of the gel and the bulk and this process has been selected for the synthesis of our hydrogels. Furthermore, we have shown that under a reasonable compression, the concentration at the gel surface was almost the same than in the bulk, proving that the measurements of the adhesion by contact test performed in the following chapters probe a hydrogel at a monomer concentration equivalent to that in the bulk.

Finally, when transferred to interfaces, the interactions between PAA and PDMA or PAM have proven to modify the structure of the grafted brush by extending its profile from the surface. This is the first systematic study of the effect of the gel in contact with a polymer brush. It has been clearly shown that specific interactions between the brush and the gel occur

and lead to an increased swelling of the brush which is comparable to the one of the ionized PAA brush. Therefore, the interactions through H-bonds between the neutral PAA brush and the gel are responsible of a stretching similar to the stretching due to electrostatic repulsion inside the ionized PAA brush. This elongation can be explained by the interpenetration of the brush inside the gel network when both are in contact. This is consistent with contact test results that are presented in Chapter 6.

5- References

[1] Tsuchida, E.; Abe, K. *Advances in Polymer Science* **1982**, *45*, 1-119.
[2] Khutoryanskiy, V. V.; Dubolazov, A. V.; Mun, G. A. In *Hydrogen-bonded interpolymer complexes. Formation, structure and applications.*; Khutoryanskiy, V. V.; Staikos, G., Eds.; World Scientific, **2009**; p 376.
[3] Bekturov, E. A.; Bimendina, L. A. *Advances in Polymer Science* **1981**, *41*, 99-147.
[4] Eustace, D. J.; Siano, D. B.; Drake, E. N. *J Appl Polym Sci* **1988**, *35*, 707-716.
[5] Bian, F. L.; Liu, M. Z. *Eur Polym J* **2003**, *39*, 1867-1874.
[6] Mun, G. A.; Nurkeeva, Z. S.; Khutoryanskiy, V. V.; Sarybayeva, G. S.; Dubolazov, A. V. *Eur Polym J* **2003**, *39*, 1687-1691.
[7] Aoki, T.; Kawashima, M.; Katono, H.; Sanui, K.; Ogata, N.; Okano, T.; Sakurai, Y. *Macromolecules* **1994**, *27*, 947-952.
[8] Shibanuma, T.; Aoki, T.; Sanui, K.; Ogata, N.; Kikuchi, A.; Sakurai, Y.; Okano, T. *Macromolecules* **2000**, *33*, 444-450.
[9] Sotiropoulou, M.; Bokias, G.; Staikos, G. *Macromolecules* **2003**, *36*, 1349-1354.
[10] Sotiropoulou, M.; Bossard, F.; Balnois, E.; Oberdisse, J.; Staikos, G. *Langmuir* **2007**, *23*, 11252-11258.
[11] Staikos, G.; Bokias, G.; Karayanni, K. *Polym Int* **1996**, *41*, 345-350.
[12] Sivadasan, K.; Somasundaran, P.; Turro, N. J. *Colloid Polym Sci* **1991**, *269*, 131-137.
[13] Wang, Y. C.; Morawetz, H. *Macromolecules* **1989**, *22*, 164-167.
[14] Sotiropoulou, M.; Oberdisse, J.; Staikos, G. *Macromolecules* **2006**, *39*, 3065-3070.
[15] Li, B.; Xu, L.; Wu, Q.; Chen, T.; Sun, P.; Jin, Q.; Ding, D.; Wang, X.; Xue, G.; Shi, A. C. *Macromolecules* **2007**, *40*, 5776-5786.
[16] Deng, L.; Wang, C. H.; Li, Z. C.; Liang, D. H. *Macromolecules* **2010**, *43*, 3004-3010.
[17] Decher, G. *Science* **1997**, *277*, 1232-1237.
[18] Hollmann, O.; Gutberlet, T.; Czeslik, C. *Langmuir* **2007**, *23*, 1347-1353.
[19] Iwata, R.; Satoh, R.; Iwasaki, Y.; Akiyoshi, K. *Colloid Surface B* **2008**, *62*, 288-298.
[20] Collett, J.; Crawford, A.; Hatton, P. V.; Geoghegan, M.; Rimmer, S. *J R Soc Interface* **2007**, *4*, 117-126.
[21] Zdyrko, B.; Klep, V.; Li, X. W.; Kang, Q.; Minko, S.; Wen, X. J.; Luzinov, I. *Mat Sci Eng C-Bio S* **2009**, *29*, 680-684.
[22] Hollmann, O.; Steitz, R.; Czeslik, C. *Phys Chem Chem Phys* **2008**, *10*, 1448-1456.
[23] Hollmann, O.; Czeslik, C. *Langmuir* **2006**, *22*, 3300-3305.
[24] Reichhart, C.; Czeslik, C. *Langmuir* **2009**, *25*, 1047-1053.
[25] Cullen, S. P.; Liu, X.; Mandel, I. C.; Himpsel, F. J.; Gopalan, P. *Langmuir* **2008**, *24*, 913-920.
[26] Currie, E. P. K.; Norde, W.; Stuart, M. A. C. *Adv Colloid Interfac* **2003**, *100*, 205-265.
[27] Bokias, G.; Durand, A.; Hourdet, D. *Macromol Chem Physic* **1998**, *199*, 1387-1392.
[28] Rodriguez, F.; Givey, R. D. *J Polym Sci* **1961**, *55*, 713-&.
[29] Henriquez, C.; Bueno, C.; Lissi, E. A.; Encinas, M. V. *Polymer* **2003**, *44*, 5559-5561.
[30] McCormick, C. L.; Chen, G. S. *J Polym Sci Pol Chem* **1984**, *22*, 3633-3647.
[31] Liu, H. Y.; Zhu, X. X. *Polymer* **1999**, *40*, 6985-6990.
[32] Ikawa, T.; Abe, K.; Honda, K.; Tsuchida, E. *J Polym Sci Pol Chem* **1975**, *13*, 1505-1514.
[33] Kabanov, V. A.; Papisov, I. M. *Vysokomolekulyarnye Soedineniya Seriya A* **1979**, *21*, 243-281.

[34] Nurkeeva, Z. S.; Mun, G. A.; Khutoryanskiy, V. V.; Bitekenova, A. B.; Dubolazov, A. V.; Esirkegenova, S. Z. *Eur Phys J E* **2003**, *10*, 65-68.
[35] Kulkarni, S. A.; Mirji, S. A.; Mandale, A. B.; Gupta, R. P.; Vijayamohanan, K. P. *Mater Lett* **2005**, *59*, 3890-3895.
[36] Ward, L. J.; Badyal, J. P. S.; Goodwin, A. J.; Merlin, P. J. *Polymer* **2005**, *46*, 3986-3991.
[37] Kurokawa, T.; Gong, J. P.; Osada, Y. *Macromolecules* **2002**, *35*, 8161-8166.
[38] Gong, J. P.; Osada, Y. *Prog Polym Sci* **2002**, *27*, 3-38.
[39] Gong, J. P. *Soft Matter* **2006**, *2*, 544-552.
[40] Gong, J. P.; Kii, A.; Xu, J.; Hattori, Y.; Osada, Y. *J. Phys. Chem. B* **2001**, *105*, 4572-4576.
[41] Peng, M.; Gong, J. P.; Osada, Y. *The Chemical Record* **2003**, *3*, 40-50.
[42] La Spina, R.; Tomlinson, M. R.; Ruiz-Perez, L.; Chiche, A.; Langridge, S.; Geoghegan, M. *Angew Chem Int Edit* **2007**, *46*, 6460-6463.
[43] Milner, S. T.; Witten, T. A.; Cates, M. E. *Europhys Lett* **1988**, *5*, 413-418.
[44] Milner, S. T.; Witten, T. A.; Cates, M. E. *Macromolecules* **1989**, *22*, 853-861.
[45] Sokoloff, J. B. *Soft Matter* **2010**, *6*, 3856-3862.
[46] Sokoloff, J. B. *J Chem Phys* **2008**, *129*, -.

CHAPTER 5 – HOW TO MEASURE ADHESIVE PROPERTIES IN AQUEOUS MEDIA? A SYSTEM BASED ON "PROBE-TACK"

Measuring the strength of molecular interactions or the macroscopic adhesion of bodies under water is a challenging problem that concerns both biologists and physicists. The former seek to understand the phenomena involved in the adhesion of marine animals or in the muco-adhesion for example while the latter are generally more interested in the quantification of specific interactions, their range and their dynamics. The diversities of materials – stiff or soft – and of geometries justify why different experimental tests have been developed to probe specific underwater interactions.

For a deeper insight of the objectives of this chapter, the previously proposed tests for underwater adhesion or for swollen media will be shortly reviewed, with an emphasis on their adaptability to macroscopically measuring the energy of adhesion between a hard surface and a swollen material. Leaving apart the microscopic tests that require a statistical treatment of the data, all the macroscopic tests are more or less close to the real-life problems. However, they all present limitations, mainly arising from the presence of water. Answering a few of the issues encountered in the other tests, a new experimental setup for performing underwater adhesion tests is proposed. It consists in a flat-flat contact test that gives a macroscopic value of the energy of adhesion in a simple and reproducible way, and that is adaptable to many different systems, synthetic or not.

We define the specificity of the test and of the samples to be used for such a test. The resulting specifications for the needed samples are then detailed and from a first run of experiments, we show and explain what results are to be expected from such a setup and what are its limitations.

1- An experimental setup for a measurement of underwater adhesion

Despite the great need for quantitative underwater adhesion tests, the literature remains particularly poor in this area. A few devices and methods have been proposed to measure the interaction forces between surfaces and molecules. Some of them are particularly adapted for the measurement of the adhesion between hydrophobic and non-swollen materials. They must be distinguished from the ones that allow the measurement of interactions between soft and swollen materials. In both cases, specific difficulties are inherent to any underwater force measurements and for swollen materials. What are these difficulties? And what adhesion tests, generally corresponding to force measurements [1-3] have been developed or adapted to be performed underwater? Is it possible to propose a new experimental test that compensates for some the inconveniences of the already existing ones?

1-1- Working underwater or on swollen materials: difficulties

Methods to measure forces between surfaces in an aqueous environment have mainly been developed in the areas of cellular and marine biology but the same issues have been encountered in the physics of interfaces. The presence of a solvent in a classical adhesion measurement disturbs the usual results, mainly because of the physico-chemical properties of the solvent. Its properties including the permittivity, viscosity or density are indeed very different from the characteristics of air. We can distinguish the effect of the solvent on the usual interactions and sources of adhesion between surfaces from its disturbances of the measurements on classical experiments.

In terms of interactions first, the usual electrostatic forces (and their derivatives) are modified by the change in dielectric permittivity. In the presence of water, the electrostatic forces that develop between solids are expected to be weakened since its permittivity is about 80 times higher than the permittivity of air. Most of the specific interactions are then expected to be screened, except for hydrophobic interactions which can only exist when the solvent used is water [4].
Leaving apart the specific interactions and considering the thermodynamics of surfaces, using water as the environmental medium changes also the surface tensions. Even if interfacial

phenomena are not the only phenomena occurring in macroscopic adhesion, their effect is major on the interactions between solid surfaces. Pocius even demonstrates that its presence tends to thermodynamically destabilize classical adhesive joints [5].

Then, the measurement of the adhesive properties can be modified by artefacts on the force measurement and on the distances.

The direct optical measurement of the distance or of the contact area between the two materials is made difficult by the very close refractive index of a swollen material with its immersing environment. Some authors have compensated for this inconvenience by using experimental subtleties that will be discussed in the next section.

The principal difference between the measured force and the "real" force between the surfaces is attributable to the viscosity of the solvent: when getting two surfaces close to each other in a solvent, the solvent has to be expelled from the interstitial space between the surfaces: if the experiment is performed in a much more viscous environment than air, the drainage of the liquid film [6] can control the interaction force. The latter can be positive due to viscosity effects when the two surfaces are close even if they are not in contact. The reverse problem – of a negative force due to re-entrant liquid – occurs when pulling apart the two surfaces as the created interstitial space has to be filled.

Additionally, due to its chemical structure (dipolar moment, specific interactions with one of the surfaces) the solvent can form more or less organized layers at the surface in which its physical properties have been reported to change and modify the measured force [7]. This specific effect depends on the nature of the solvent, and in water, it is added to the effect of hydration forces due to polar interactions between the surfaces through water.

Finally, water is a medium that tends to be polluted with time, from the solvation of carbon dioxide from air that modifies the acidic conditions of the water to the development of bacteria in the worst cases.

In conclusion, characterizing the adhesion under water or in the presence of water, on swollen materials or on adsorbed layers involves many mechanisms, some of them specific of water which is highly polar and very dissociating, and others due to the hydrodynamic specificities of a liquid.

1-2- What are the quantitative tests to measure underwater adhesion?

The scale at which the adhesion or the interactions can be measured or evaluated ranges from single molecule measurements to macroscopic measurements through intermediate methods. Some of the techniques and studies that have been previously used for this purpose are presented in the following paragraphs. Here, we will distinguish the tests performed on single molecules from the macroscopic tests dealing with surfaces. Within the class of macroscopic tests, the tests developed for hard surfaces are distinguished to the ones adapted to deformable materials. The possibility to adapt them to swollen materials is discussed.

Atomic Force Microscopy derived techniques

Single-molecule force spectroscopy (SMFS) [8] is usually based on the use of an atomic force microscope (AFM). The principle of the technique consists in measuring the force exerted on the AFM tip when approaching it and subsequently removing it from a surface. Classically, the AFM tip and/or the probed surface are modified with a coating of small molecules and/or polymers, as shown on Figure 1-left. The first studies were carried out on bio-molecules, such as DNA and proteins in the early 1990's, and a bit later on synthetic polymers such as PMAA [9,10], PAA [11] or PDMA [12].

Working with a single molecule (which is attached or adsorbed between two solid surfaces) gives access to the entropic elasticity of the molecule, and when reaching higher forces, to the desorption force from the surface where the interaction is the weakest. It is also possible to work with two different interacting molecules, one grafted on the AFM tip and the other one on the surface; then, one can in principle measure the force needed to break the specific interactions between the two molecules.

A great advantage of this method is that it allows to measure or to observe events that cannot be observed on many molecules, such a conformational reorganization or failure of single bonds. However, the exact structure of the AFM tip can only be characterized with difficulty which is the source of experimental inaccuracy; and a great number of tests have to be performed as the results originates from events with statistically variable occurrences.

Also inspired from the AFM instrument, the colloidal force spectroscopy was first proposed in 1991 by Ducker *et al.* [13-15]. In this particular technique, a hard colloidal particle is

attached on the AFM tip (see Figure 1-right). The colloidal particle and the probed surface are modified with the desired surface treatment. This technique has recently been used to probe cell adhesion [16] and to study the effect of roughness on the interactions between surfaces under water [17]. Even more recently, Erath *et al.* [18] have stuck a soft colloidal ball on the tip of the AFM and have then built a micro-JKR tester.

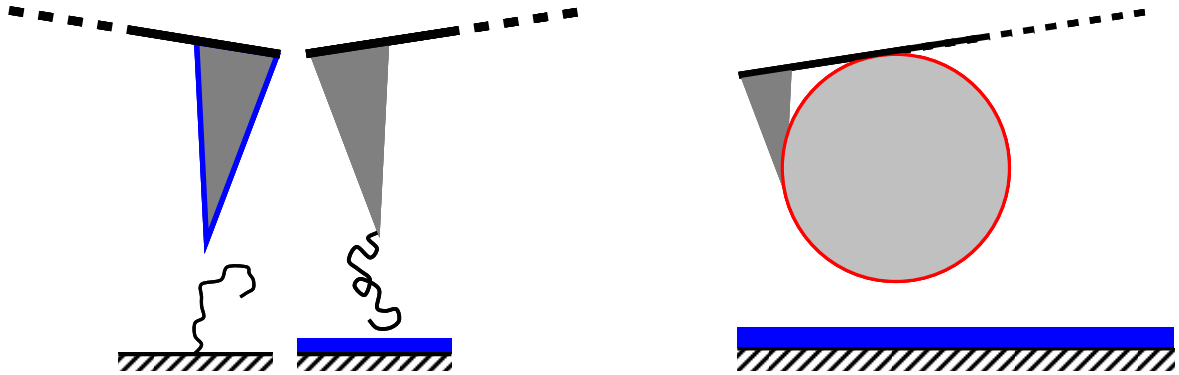

Figure 1 - Left: schematic of the single molecule force spectroscopy. In one case, the AFM tip is specially coated to adsorb specific macromolecules at its surface and probes a planar substrate coated with such macromolecules. In the second case, a polymer is grafted on the AFM tip with is approached to a surface which is specially coated, either with small molecules or with other polymers.

Right: Schematic of the colloidal force spectroscopy: a colloidal particle, usually hard and that can be coated, is probing a modified substrate.

Colloidal force spectroscopy presents the same advantages and disadvantages as the previous technique, and is obviously not suitable to measure a macroscopic adhesion. Apart from the AFM method, optical tweezers and micropipette suction have been used in parallel to measure the interactions between surfaces at the single molecule scale and the characteristics of bonds in an aqueous environment on soft or swollen materials [19].

Surface Force Apparatus

Complementary to the techniques presented previously, the interactions between surfaces have been investigated using the surface force apparatus (SFA) or surface force balance, which has been proposed by Israelachvili *et al.* in 1976 [20,21] where an underwater measurement of forces between hard mica surfaces has been proposed (see Figure 2). The seminal article about the technique was published a bit later and the method has attracted a lot of work, either to improve and develop the technique [22] or simply to use the apparatus and characterize new systems.

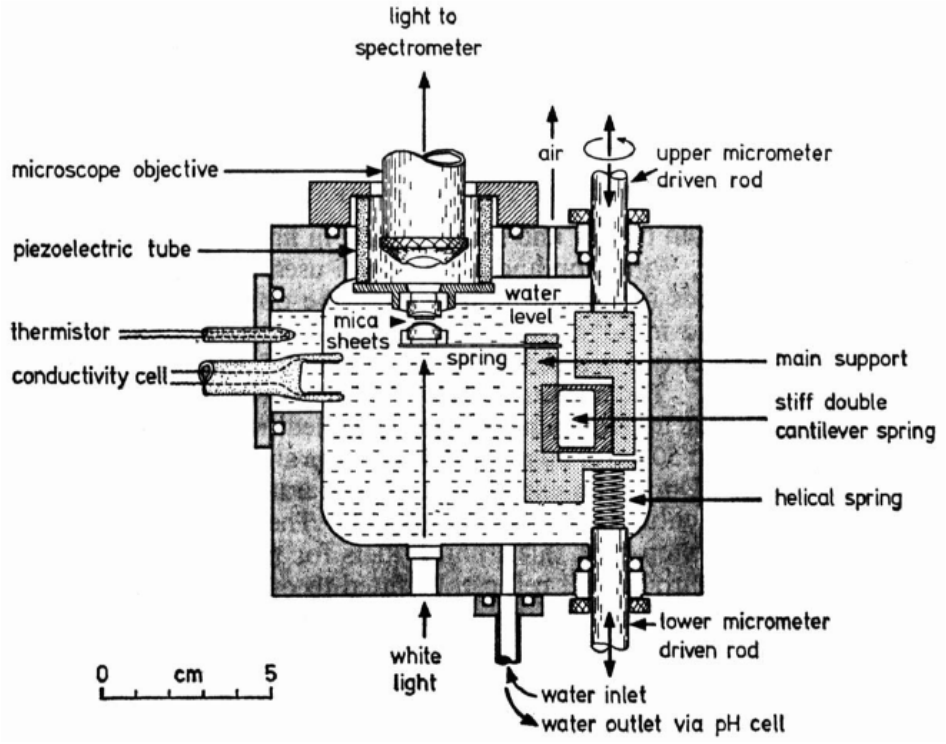

Figure 2 - Surface force apparatus according to [21].

This technique developed from its beginning to be adapted to a liquid environment (as suggested by Figure 2) has been extensively used to measure the interaction forces between solid substrates [23,24] and coated substrates, changing the quality of the solvent for polymers [25,26] or the ionic strength for charged surfaces, for the use in biological systems [19].

The main limitation of this technique is the distance measurement: it is accessible by light interferences between the two hard substrates. As a consequence, the difference of refractive index for a swollen material with the immersing medium is not strong enough to allow the measurement of the distance (see Figure 3). However, for small molecule layers or polymer brushes, the method can be fruitful. Recently, Tareste *et al.* [27] used the technique to measure the forces between retinoid-coated surfaces to distinguish the part of the interactions due to hydrogen bonding and to hydrophobic interactions. Malham *et al.* [28] have characterized the surface behavior of PNIPAM brushes, such as adhesion and friction, as a function of their grafting density.

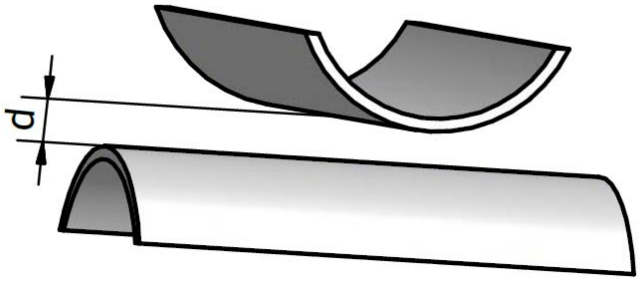

Figure 3 - Schematic representation of the two crossed cylinders of the SFA, and representation of the distance d between them.

JKR test

Another, now classic, macroscopic method has been inspired by the analysis of Johnson, Kendall and Roberts to measure the adhesion between two surfaces, with at least one material being a rubbery (soft) material. In a standard configuration, a deformable lens made of the material to be probed is tested in contact with a hard transparent surface. In their original publication, Johnson *et al.* reported experiments that were conducted under water [29].

Twenty years later, Chaudhury and Whitesides [30] carried out experiments in mixtures of water and methanol and between two identical surfaces. Other examples of the use of the JKR test under water have been reported [31-33] making it a method of choice for measuring adhesion under water between hydrophobic materials.

We can however only cite two examples of using a JKR-inspired technique to measure the adhesion between hydrogels.

Sakasegawa *et al.* [34], using crossed cylinders, used the technique to measure the adhesion between hydrogels. However, their measurements were performed in air and they had to use an ink, placed on one of the cylinders to measure the contact area on the other cylinder after the experiment.

When using the JKR-type test to measure the contact between a hydrogel and a brush, La Spina *et al.* [35] have carried out underwater measurements: a half-spherical lens made of hydrogel was put into contact with a planar brush. However in these conditions, measuring the contact area between the gel and the substrate cannot be carried out through the gel because of the very close refractive index of the gel and of water, but the contact area has to be extrapolated from a side-view of the system.

Membrane test

Inspired from the sphere-flat contact test from JKR-type experiments, an adhesive test based on the contact between a rigid substrate and a membrane was first proposed by Flory *et al.* [36]. The first method, that involves a flat hard substrate, gives access to weak energies of adhesion between soft materials by a highly sensitive inflation of the membrane. The system was adapted for underwater systems by using hydrophobic membranes [37], as shown on Figure 4.

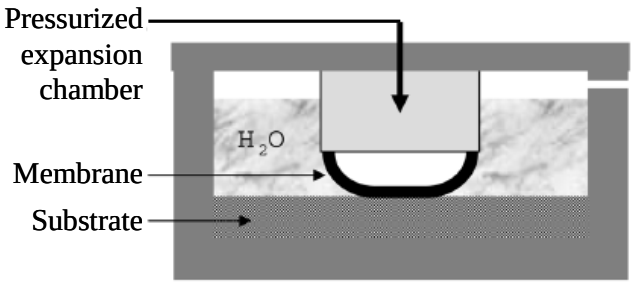

Figure 4 - Schematic drawing of the membrane inflation apparatus from [37].

In particular, this technique has recently been used by Guvendiren et *al.* [37] to investigate the adhesion of membranes functionalized with block copolymers containing a block with DOPA (3,4-dihydroxy-L-phenylalanine which is a mussel adhesive protein, see Chapter 1 and [38]) on TiO_2 substrates or tissues, such as hairless pig skin. They showed that adhesiveness was increased for both substrates by adding the DOPA-functionalization to the membranes. However, with this technique, they used the negative release pressure as an indication of adhesiveness but did not get any quantitative values for the adhesion energies.

Peel test

The peel test is probably one of the most used tests in industry to evaluate the mechanical performance of a soft adhesive. Two strips of materials are stuck together, one of which is flexible and sometimes plastically deformed during the test [5]. A crack is initiated and propagated by pulling apart the two materials as shown on Figure 5 [39]. Remaining on topic, this test has for instance been used to measure the adhesion between a membrane and a substrate [40]. It has been used as an underwater test to characterize the adhesion between retinal implants coated with a thermo-sensitive polymer and enucleated pig's eyes *ex vivo*

(see [41], reader discretion is advised) by measuring the pull-off force as a function of temperature.

Kurokawa *et al.* [39] have performed in-air tests on double-network hydrogels mechanically attached on porous model substrates when performing the synthesis. The tensile force was applied at an angle of 90° with the substrate. This method implies that the sample of gel tested is highly elastic and strong enough not to fracture when submitted to traction and bending, or in other words, that the adhesion energy is weaker than the fracture energy of the material; it is the case for double-network hydrogels.

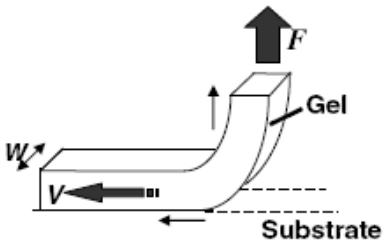

Figure 5 - Peel test at 90°, taken from [39].

1-3- Probe-tack inspired test: advantages

Many tests have been proposed and developed to perform underwater adhesion tests but very few are adapted to the measurement of the macroscopic adhesion of a swollen material immersed in its solvent.

Already used for the adhesion of gels, the test derived from the SFA [34] technique is not really suitable since the measurement of the contact area can only be obtained by using a dye, which modifies the interface and the measurement; the peeling test performed by pulling at 90° requires the use of specifically reinforced gels such as double-network or interpenetrated network gels, but the simplest materials can not be used.

Then, only the test proposed by La Spina *et al.* [35] and derived from the JKR-type test seems adapted to the measurement of adhesion under water even if the visualization of the contact area is indirect. One of the advantages of the flat-flat test is to give access to quantitative measurements of the macroscopic adhesion in conditions which are very close to reality.

The probe-tack inspired test is shown schematically on Figure 6, and the force measured as a function of time is schematized on Figure 7. From this experiment and these measurements, it is possible to measure the adhesion energy between a rigid punch and the soft material: it is

the work necessary to give to un-stick the punch from the probed material, that is to say the area filled under the curve of Figure 7, when the force F is plotted as a function of the displacement x. It is usually normalized by the area of contact A:

$$W_{adh} = \frac{1}{A}\int_{x \geq x_0} F(x).dx\,, \qquad \textbf{Eq. 1}$$

where $x \geq x_0$ corresponds to the region of the detachment for which $F(x) \geq 0$.

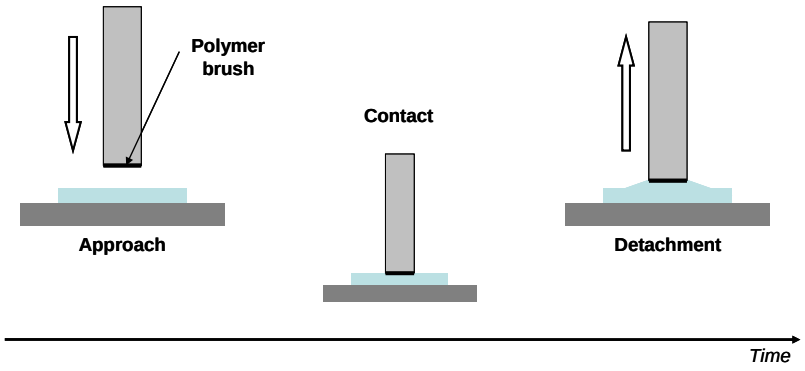

Figure 6 - Schematic representation of the flat-flat contact test as a function of the time. First, the punch is approached at constant velocity to the tested film until it is in contact with the soft material and a certain stress is applied. Then, the displacement is stopped and the punch and the materials are maintained immobile for a determined duration. Finally, the punch is pulled off at constant velocity. Force and displacement are measured during the experiment.

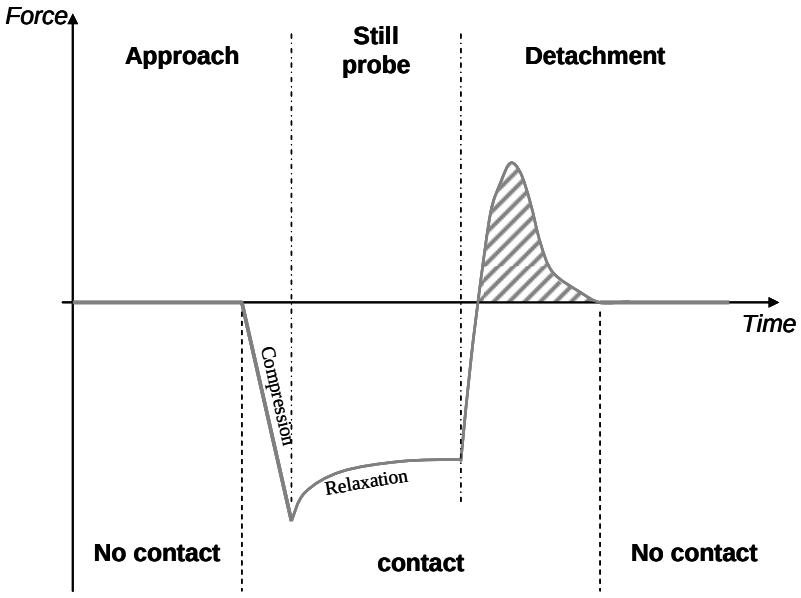

Figure 7 - Schematic representation of the typical force measured in flat-flat contact test (or in a probe-tack test) as a function of time.

1-4- New experimental setup

We have developed a new experimental setup based on the flat-flat contact test and specifically adapted to the characterization of the adhesion of soft materials under water. The working principle is represented on Figure 8: a layer of the soft or swollen sample is attached on the bottom substrate and immersed in water; the modified hard substrate is stuck on a mobile punch, which is moved down to come in contact with the soft material. If properly aligned, the two materials come in contact, with a contact area equal to the area of the hard material. After the preset experimental conditions have been achieved (e.g. contact stress and contact time), the probe can be pulled off at a constant velocity. During the experiment, the displacement of the punch and the force applied on it are measured as a function of time.

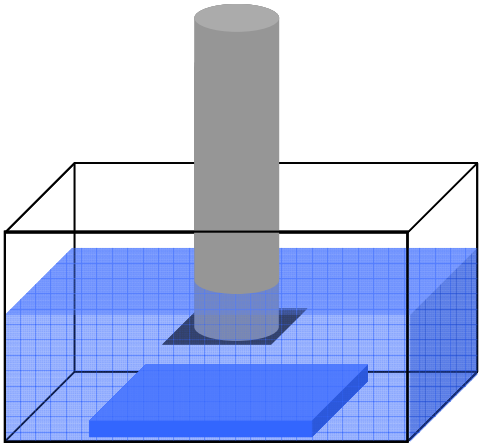

Figure 8 - Schematic representation of the immersed flat-flat contact test: the soft material is stuck at the bottom of a trough and immersed. The punch is immersed before probing the soft material.

Although the general principle is the same than that of a regular probe test, some important differences need to be addressed in the design of the apparatus. The setup must be able to work in air and immersed and the temperature and pH of the water needs to be easily adjustable. Then the thickness of the gel layer should not be too small to avoid major alignment problems and ensure a full contact removing therefore the need of a direct optical measurement of the contact area. Finally the load cell should be sensitive enough to measure very small forces reproducibly.

A commercial Instron machine (model 5565 for tensile and compression tests) fitted with a load cell of 10 N was used for all the adhesion tests. The noise of the load cell is of the order of 0.1 mN and its nominal resolution is of 0.5%, from 1% to 100% of the full scale.

The sample-holder of the soft and immersed gel sample has a rather complex design. It is mostly made in anodized aluminium alloys and is illustrated on Figure 9.

It consists of a simple sample-holder adapted for glass slides of width 2.5 cm or glass discs of diameter 3 cm (Figure 9-a and c). It is inserted in a trough (the sample trough) which has a lateral window and a bottom circular window. The trough can be thermostated by a liquid circulating around it in jacket (the thermostating jacket) as can be seen on Figure 9-d. The sample trough and its jacket are clamped together with screws and a Teflon® gasket sandwiched between two cross-linked poly(dimethylsiloxane) PDMS gaskets. The whole device is then fixed to the Instron machine through an alignment device and a fixation composed of a split pin and a locknut. The alignment is insured thanks to micrometric screws placed in three points.

(a)

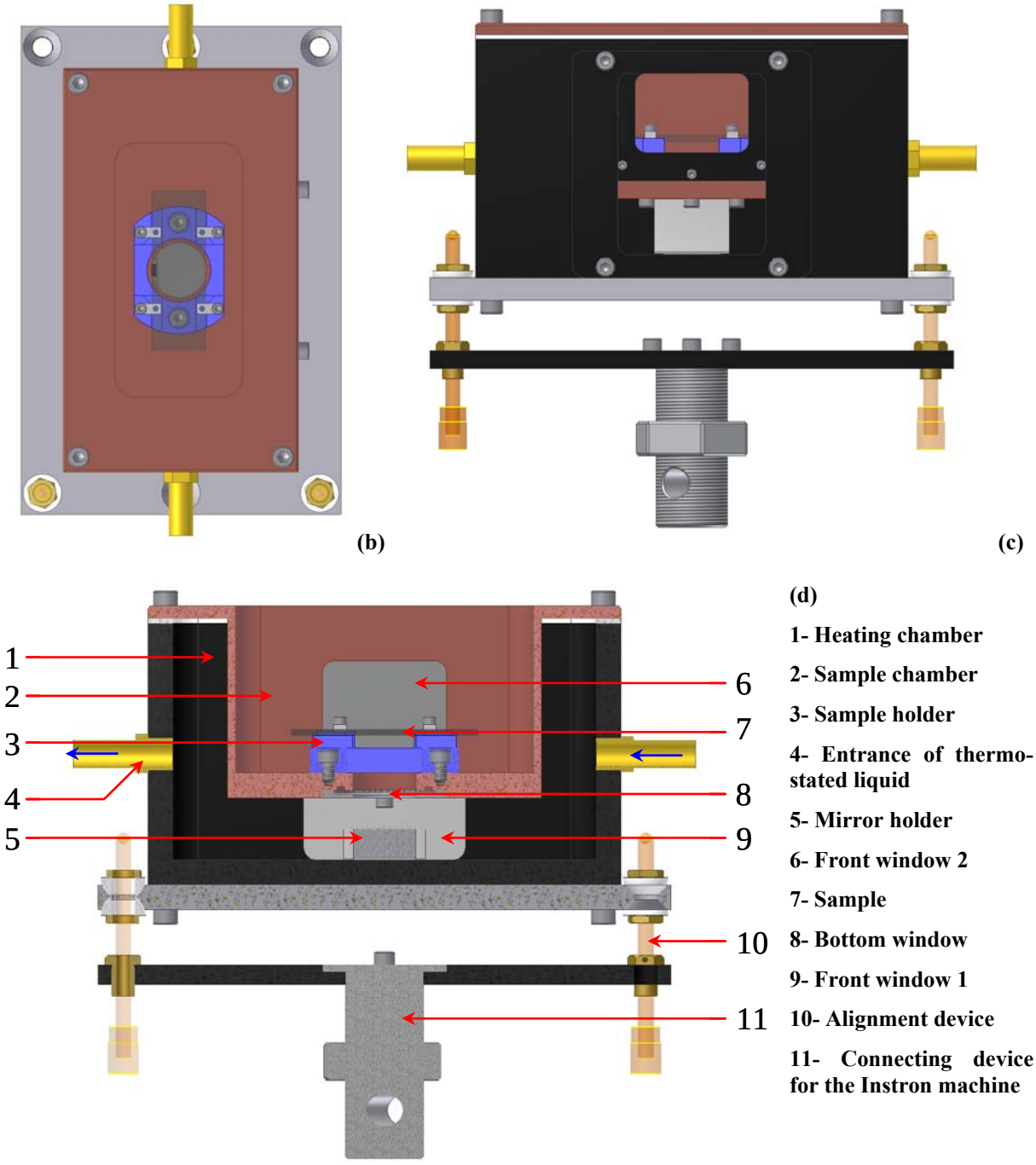

Figure 9 - Different views of the experimental setup for the measurement of adhesion on soft swollen immersed substrate. (a) is a 3D-views. (b) is a front view, (c) is a top view and (d) a longitudinal cut back-view.

Visualization (see Figure 9-b) is made from the side – since both the trough have aligned polycarbonate windows giving a visual on the sample – and from the bottom thanks to the lateral window of the thermostating trough, the bottom window of the sample trough and a mirror at 45°. The sealing of the windows is provided from flat PDMS gaskets.

The hard surface, which consists of a silicon wafer, was stuck (with a cyanoacrylate glue) on a stainless steel cylindrical punch of an appropriate diameter and the punch was fixed to the load cell (see Figure 10) with a mandrel (or arbor of a drilling machine). The connection to the load cell is insured thanks to a split pin and a locknut whose function is to prevent loosening between the punch and the load cell.

Figure 10 - Picture of the sample-holder of the punch. Based on a commercial mandrel of a drilling machine, it allows a tight junction between the load cell and the punch.

A picture of the whole experimental setup with the Instron machine is shown in Figure 11.

Figure 11 - Picture of the setup for underwater adhesion measurement adapted on the Instron 5565 machine.

Thanks to the width of the sample trough, the temperature and the pH can be measured *in situ* without disturbing the measurement. Since the sample trough is supposed to resist many different solvents, including water at high or low pH, it has been completely coated with a poly(vinylidene fluoride) (PVDF)-derived polymer layer; the inside screws are in stainless steel and free mechanical pieces to maintain the samples are in poly(methyl methacrylate) (PMMA).

With a standard circulating cryothermostat, it is possible to change the temperature inside the sample chamber from 23 to 45°C in a few minutes. The change in ionic strength and pH can then be performed *in situ*; however, it should be noted that the diffusion of the new experimental conditions inside the tested material is often slow.

2- Description of the materials tested: sample specifications

The choice of the flat-flat contact test and the design of the experimental setup have incidences on the specifications and requirements of the studied systems. The setup proposed is of course adaptable to JKR-type tests, and to various types of samples. Here, we focus our discussion on the case of a punch consisting of a hard flat surface facing a soft swollen material, for instance a chemically cross-linked gel. We discuss how and in which limits the experimental setup restricts the type of samples and materials which can be tested, how the size of the samples influences the measurements. We finally present the way the adhesion tests are analyzed after alignment.

2-1- Tested materials

To carry out the proposed immersed flat-flat test, the soft and hard materials probed must fulfill different conditions.

One of the first prerequisite to perform a flat-flat adhesion test on a soft material is to have a flat layer of this soft material firmly stuck on a hard substrate. As this material is immersed in a possibly changing environment, it is necessary to control the swelling behaviour of the material as a function of its environment. The environment and the gel must be adapted in order not to strongly modify the gel dimensions when changing the experimental conditions.

If the swelling of the gel changes significantly after it is covalently bound to the glass substrate, some issues may arise. First, strong shear stresses may develop at the glass/gel interface, leading to a spontaneous detachment of the soft material from the substrate. Even if it does not detach, wrinkles can appear at the free surface of the gel, preventing a complete contact with the probe surface during the adhesion test.

Therefore, we chose carefully the chemically cross-linked hydrogel samples used in the adhesion tests. A preliminary study was carried out to make sure that the swelling at the

preparation conditions remained very close to the swelling at equilibrium in pure water (cf. Chapter 3). The choice of a neutral hydrogel guaranteed the relatively low sensitivity of the material when changing the ionic strength or the pH of the water.
Considering the hard surface, no essential specification is necessary except from its size. We have used a planar silicon wafer modified with polymer brushes stuck on a stainless steel punch of adapted diameter. However, it would be possible to work with a spherical lens to perform sphere on flat tests since the setup is clearly adaptable, or one might think about attaching another soft material on a silicon wafer. The functionalized silicon wafers used are described extensively in Chapter 2.

2-2- Accuracy of the measurement

The size and the shape of the probed samples are important. First, the shape of the hard surface has proven to modify the residual stress when measuring the adhesion on membranes by pull-off test [42]. Second, the confinement ratio (equal to the mean radius of the hard surface divided by the thickness of the gel) plays an important role in the distribution of the normal stress and on the apparition of instabilities when pulling a punch from a soft solid [43]; third, the larger the contact area, the better the signal-to-noise ratio.
In our case with the low adhesion forces and the high deformability of the gels, the shape of the hard surface is expected to have a minor influence on the adhesion measurement and on the propagation of the interfacial crack. Then, mainly for convenience reasons, we have chosen to work with square punches since no wafers (smaller than 1” in diameter) could be bought with round shapes at a reasonable cost and their hand-polished fabrication led to a lot of waste with a particular difficulty to obtain nice round shapes.
Then, to decrease the problem of alignment, we have chosen to work with a rather low level of confinement: the gel sample was synthesized with a thickness of about 1 mm and the punch size was 1×1 cm^2.

2-3- Observations and alignment

Due to the very close refractive indexes of the gel and of the water, no observations could be made in immersed conditions from below through the mirror at 45°. As a result, it is not possible to properly align probe and gel in the immersed state.

The alignment step was performed in the “in-air” state prior to any underwater measurement. The punch was approached to the gel surface and the contact was observed for contact stresses lower than the one used for the adhesion test. If the contact was not total, the gel sample was aligned until the contact was total for a stress lower than 20% of the contact stress applied during the adhesion test. The soft sample and the hard surface were kept a little tilted to avoid:

- the imprisonment of an air bubble during the approach;
- the cavitations that are often observed in probe tack experiments when the confinement is important.

One possibility to make the contact visible could have been to use a beam splitter cube with faces cross-polarized; the polymers being birefringent when a stress is applied, the contact might be visible thanks to this setup schematized on Figure 12. However, due to the high dilution of the gel samples and their low thickness, the possibility of an underwater visualization of the contact from the bottom view was not ensured and this suggested setup has not been tested.

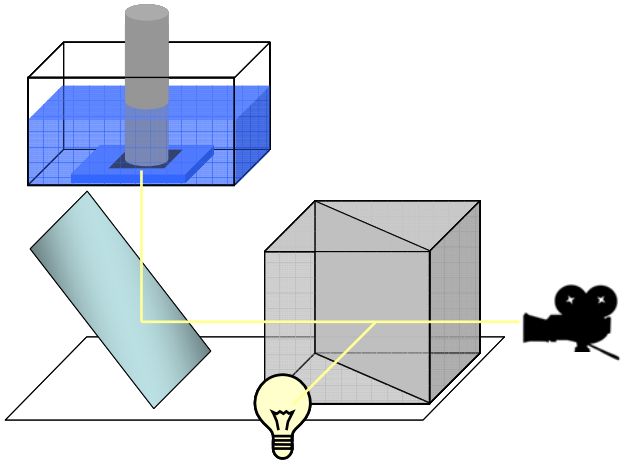

Figure 12 - Schematic representation of a setup allowing to potentially visualize the contact on a transparent gel immersed in water.

3- First results and data analysis

We proposed a setup which allows the measure of the macroscopic adhesion between an immersed flat gel and a polymer planar brush, with a control of the environment (pH, temperature…) and of the alignment. The flat-flat contact test fixes the initial contact area, even if the propagation of the crack cannot be observed during the pull-off.

One of the reasons to work under water is of course to overcome the effects of surface tension which play a major role in dry experiments on swollen gels. We will now discuss data analysis and differences between dry and immersed measurements. The weak hydrodynamic effects from immersion will also be slightly discussed since they naturally appear as an expected side-effect of working in a solvent. Finally, we explore the possibilities to change the experimental conditions during the test.

3-1- Dry and wet measurements

The Instron machine 5565 measures force and crosshead position as a function of time. These raw data are plotted on Figure 13, where the displacement has been shifted so that its minimum value is equal to zero. Three main differences can be observed between in-air and underwater measurement for experimental conditions otherwise identical (they are indicated by arrows).

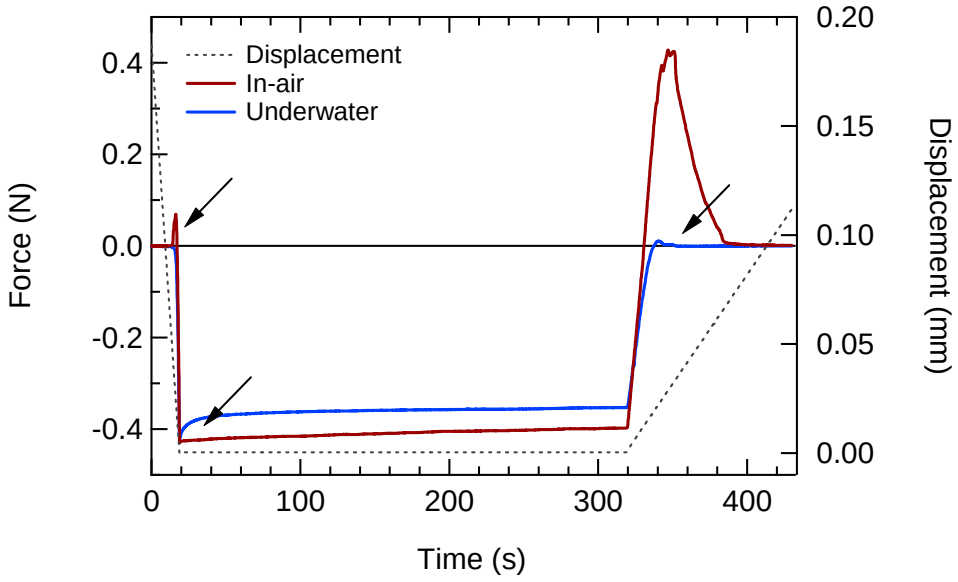

Figure 13 - Raw data obtained from an adhesion test. The force applied on the punch and its displacement are recorded as a function of time. Here are represented two results obtained between a PAA planar brush and a PDMA gel when the experiment is performed in-air or underwater.

The first difference is the “jump to contact” that can be observed for the in-air experiment and which is absent in the underwater experiment. This is due to surface tension: the punch, coated with a PAA brush, is highly hydrophilic and the gel contains about 90% of water. When the punch touches the gel in one point, the triple line moves quickly so that the contact

spreads rapidly and the water in the gel minimizes its contact area with air. The result is an extension of the gel which leads to tensile forces. When immersed underwater, this effect due to the surface tension of water is eliminated since the differences in surface tension are strongly reduced.

The second difference is the relaxation of the gel once the contact force has been reached. This strong difference in the relaxation of the same gel enlightens the differences of the mechanical behavior of a gel when fully immersed or when exposed to air. In the case of in-air measurement, the relaxation is lower than 8% of the initial contact force after 300 seconds and it is twice higher in the case of an underwater measurement (about 15%). The first seconds after the imposed force is reached are of great importance. This difference can be explained as follows: when compressed in-air, the gel has to create and increase its surface with air since its volume remains constant. The creation of additional interface is unfavorable. Furthermore, the excessive swelling of the non-compressed zone can only be canceled by the removal of excess water by its evaporation but this process is too slow compared to the duration of the experiment to be observed. When compressed underwater, the syneresis is easier so the gel can expel the excess water in the immersing medium [44,45] since the creation of an increased immersed surface is energetically negligible.

Finally, the third difference is the size of the adhesion peak, which is much higher in the case of the in-air measurement. This third difference is also due to the surface tensions. To discuss it, we will make the hypothesis that the adhesion results from interfacial interactions and that no bulk dissipation occurs during the experiment. If so, the surface adhesion energy can be written as a resultant of:

- The specific interactions between the gel and the brush γ_{spe};
- The surface tensions created by the detachment (between the gel and the "immersing medium" γ_{gel-IM} and between the brush and the "immersing medium" $\gamma_{brush-IM}$);
- The surface tension removed (between the brush and the gel $\gamma_{brush-gel}$) which must be subtracted:

$$W_{adh} = \gamma_{spe} + \gamma_{brush-IM} + \gamma_{gel-IM} - \gamma_{brush-gel}, \quad \textbf{Eq. 2}$$

where "IM" stands for "immersing medium" and can either be water or air.

The surface tension between water and the gel is low since the gel is made of a hydrophilic polymer swollen with a water content of about 90% and does not present a dry top layer [46,47]. The surface tension between the PAA brush and water is rather low since PAA is

hydrophilic [48]. Hence, when making an underwater experiment, one removes almost all the effects of surface tensions and measures the effects of the specific interactions between the gel and the brush since $\gamma_{brush-water} \approx \gamma_{gel-water} \approx \gamma_{brush-gel} \approx 0$. On the contrary, in-air measurements are at the origin of non-specific results since $\gamma_{brush-air} + \gamma_{gel-air} \approx 120\ \text{mJ.m}^{-2}$ are added. This difference of approximately 120 mJ.m^{-2} corresponds to the one measured between the two curves of Figure 13 where it is clearly visible that the specific interactions can be much lower than the effects due to surface tension.

As a conclusion, it is essential to work underwater to overcome non-specific effects due to surface tension and then be able to measure the specific interactions between a brush and a gel on a macroscopic surface.

3-2- Data processing

The adhesion energy is obtained from the raw data as follows: as shown in Figure 13 and Figure 14-top, the raw data obtained corresponds to the force and the displacement recorded as a function of time. Usually, the goal of the data processing is to obtain the adhesion energy W_{adh}. The easiest way to obtain the value of W_{adh} from the data is to plot the force as a function of the displacement and calculate the area hatched in the inset and normalize it by the contact area A, which corresponds to the calculation of W_{adh} in Eq. 1.

To compare the different tests, we have chosen to adopt a representation which is widely used for classical probe-tack tests and plot the nominal stress σ as a function of the nominal strain ε. The stress is obtained by dividing the force by the punch area A:

$$\sigma = \frac{F}{A}. \qquad \textbf{Eq. 3}$$

The displacement was shifted so that the zero is obtained when the force becomes positive during the detachment. It does not correspond to the first contact or to the total contact but it is a way to overcome the alignment defects. Depending on the definition of the zero, less than 5% of error can be brought to the value of the strain. The strain is then obtained by normalizing the displacement by the initial thickness of the gel layer l_0 (which is around 1 mm in general).

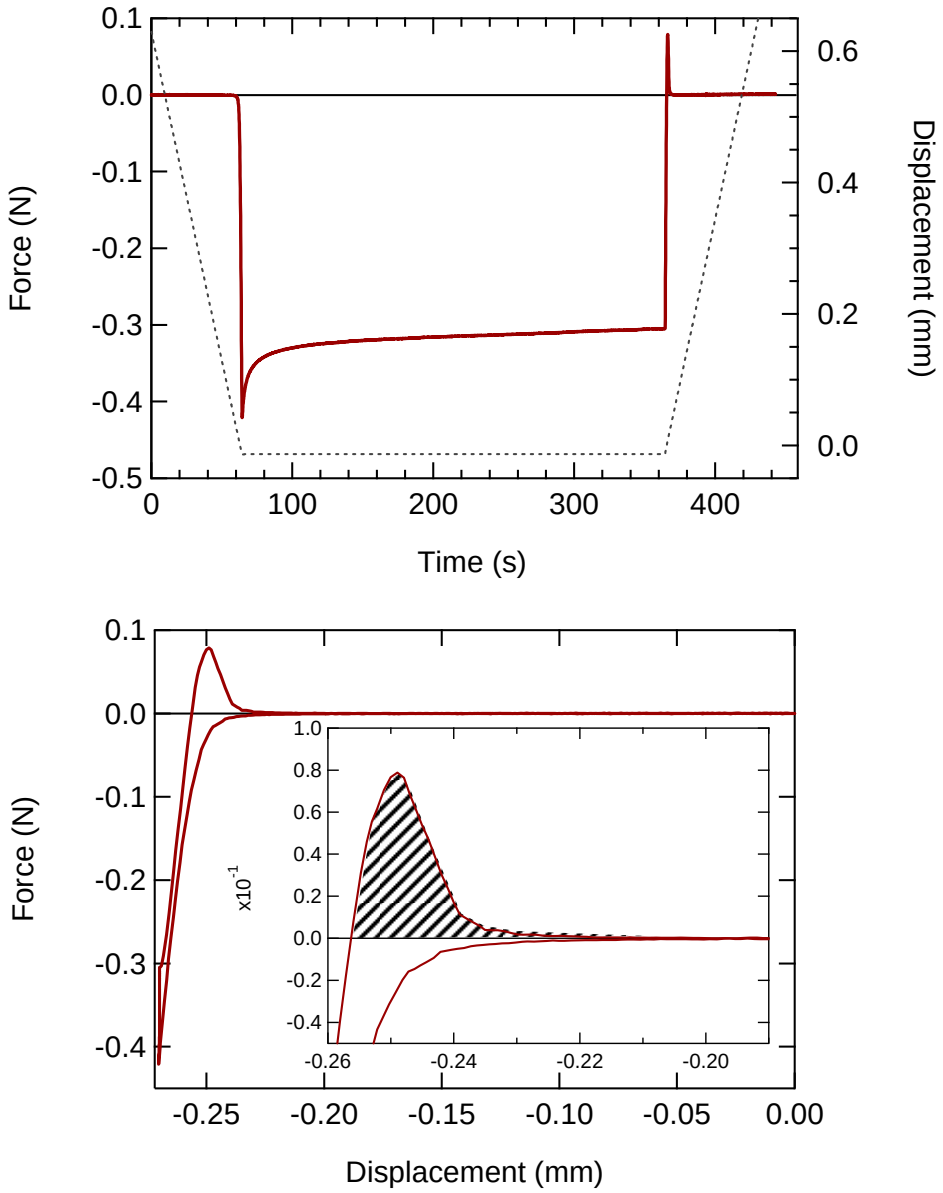

Figure 14 - Raw data obtained from an adhesion test. The force applied on the punch and its displacement are recorded as a function of time (top graph). On the bottom graph, the force is plotted as a function of the displacement. The filled area in the inset corresponds to adhesion energy for the total surface of the punch.

After having made these definitions, it is possible to re-write Eq. 1 as follows:

$$W_{adh} = l_0 \int_0^{+\infty} \sigma . d\varepsilon \, . \qquad \textbf{Eq. 4}$$

The typical stress-strain curve is shown on Figure 15. Its axes are proportional to the axes of the force-displacement curve of Figure 14.

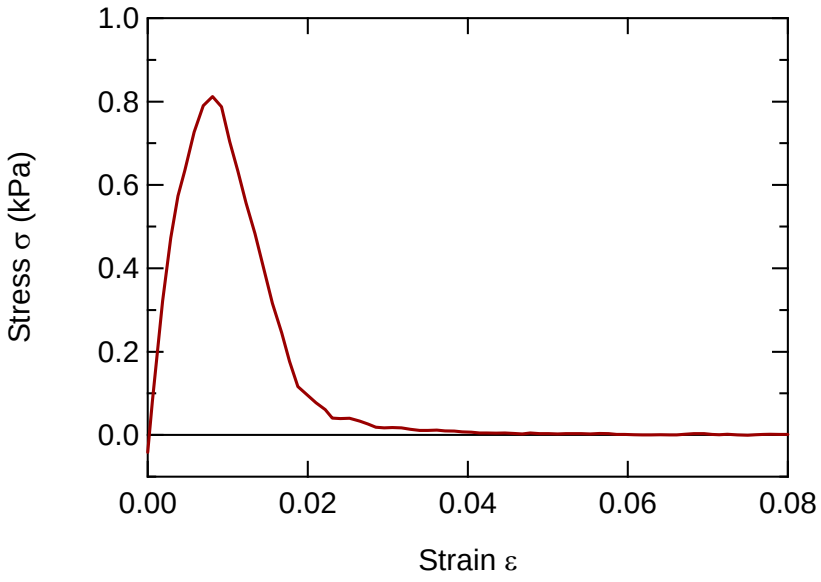

Figure 15 - Typical stress *vs.* strain plot of the raw data presented in Figure 14.

3-3- Hydrodynamic effects

The main possible disadvantages of working in a solvent are presented in general at the beginning of the chapter in 1-1- page 184. In our case for a macroscopic flat-flat contact test, three related hydrodynamic effects, schematically shown on Figure 16 have to be considered:

- the expulsion of the solvent during the approach and the expulsion of a possible hydration layer, which can be slow, particularly for thin solvent layers. This hydration layer is predicted to remain even for relatively high stresses when the brush or the gel are charged [49,50];
- the applied negative hydrostatic pressure when pulling apart the gel and the brush, comparable to the effect at the origin of cavitation occurring in probe-tack tests on pressure sensitive adhesives [51];
- the hydrodynamic effect of reentrant liquid between two solids pulled apart during the detachment process.

A first argument against these issues is that the gel is neutral and permeable to water. Then, experimental examples that demonstrate the absence of hydrodynamic effects are reported and explained.

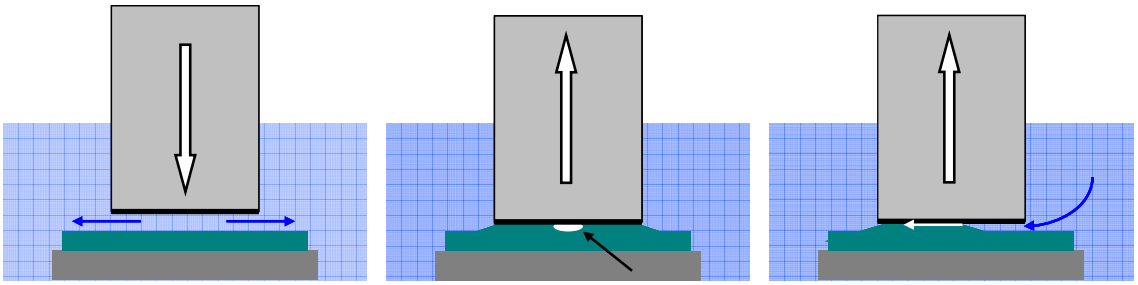

Figure 16 - Schematic of the hydrodynamic and hydrostatic effects that can modify the underwater measurement of adhesion. On the left, hydration layer or layers of solvent are slow to expulse from between the gel and the punch because of its confinement and the viscosity of the solvent. In the middle, cavitation appears while detaching the gel from the brush. On the right, the propagation of the triple line to the left leads to a flow of solvent which is confined between the punch and the gel and which can be dissipative.

Expulsion of the solvent during approach

In the absence of charge on the polymers, the hydration layer does not resist to low stresses: Sokoloff [49,50] has mainly attributed its presence to the osmotic pressure due to counter-ions in ionized polymer gels and brushes. Furthermore, we have shown with the same flat-flat immersed test in a related study [52] that a strong polycationic hydrogel with a ionization ratio of 10% could interact with a neutral brush by hydrogen bonding and with a polyanionic brush by electrostatic interactions. This was the proof that the hydration layer for polyelectrolyte gels can be overcome under reasonable stresses (4 kPa) to create H-bonds with a neutral brush or Coulombic interactions with an oppositely charged brush. We observe the same type of interactions with our neutral gels, which is the proof that no hydration layer remains between the gel and the brush.

Furthermore, in the case of in-air measurements, when the punch and the gel were perfectly aligned, a bubble of air was invariably pinned in the middle of the contact area between the gel and the brush. Then under water, to avoid the formation of undetectable water bubbles and to facilitate the evacuation of the solvent between the gel and the brush, a slight misalignment was always applied.

Cavitation during detachment?

It is possible to draw a parallel between the flat-flat immersed test performed here and the classical probe-tack test carried out in-air on soft viscoelastic adhesives, where detachment occurs by cavitation for weakly cross-linked adhesives [51]. Could we observe cavitation in our experiments? The gel is very elastic (G' ~ 1 000 G") and the adhesion forces are very low

compared to the atmospheric pressure. As a consequence, no air or vacuum bubble was ever observed. However one may wonder about the existence of a water bubble where the gel is no longer in contact with the brush. Because this water bubble would not neat much depression to nucleate (there is no surface tension involved), it is very possible that debonding starts in the center. However the precise dynamics of the debonding would be hard to visualize and the debonding always occurs following a process of interfacial failure by the propagation of a triple line at the gel-brush interface.

Hydrodynamic effect during detachment

The third possible artifact that could occur during the immersed adhesion test is the viscous dissipation due to the entrant flow of solvent between the gel and the punch when the triple line recedes. This flow can be dissipative because of its confinement, and the dissipated energy is expected to depend on the velocity and viscosity of the fluid, that is to say on the debonding velocity and on the alignment. A simple calculation with drastic assumptions (the gel and the punch are solid surfaces forming an angle θ and the punch is removed at a constant vertical velocity U; the velocity of the fluid is equal to zero at the surface of the punch and of the gel…) gives a dissipated viscous energy that is of the order of:

$$E_{vis} = -\frac{3}{2}\eta U \frac{A}{\theta^2}, \qquad \textbf{Eq. 5}$$

where η is the viscosity of water. It is to be noted that a perfect alignment would lead to infinite dissipated energy since water would have to flow at an infinite velocity to fill the space created between the gel and the punch by pulling the two surfaces (assumed to be hard) apart.

Since the gel is viscoelastic and deformable, the velocity of the triple line will be limited by the dissipation inside the gel close to the triple line, as suggested on Figure 17. The experimental dissipated energy in the liquid is then far below the theoretical values, which are in the order of[1] a few $mJ.m^{-2}$.

[1] For example, for the sample presented in 3-2-, the first contact and the total contact are observed for a variation of displacement of around 20 µm for a square punch of 1 cm^2. Then, $\theta \approx 2.10^{-3}$ and with $U \approx 10^{-5}$ $m.s^{-1}$, $\eta = 10^{-3}$ Pa.s, the energy loss per unit area is about $E_{vis} = -2.5 10^{-3}$ $J.m^{-2}$. It is in the order of magnitude of some measurements of specific adhesion energies measured between the brush and the gel.

Additionally, as it was mentioned for the pressure effect during detachment, it should be observed for all experiments carried out with the same alignment conditions and debonding velocity. As it is shown on Figure 18, in the absence of specific interactions, the measured force goes back to nil even for debonding velocities as high as 100 µm.s^{-1}.

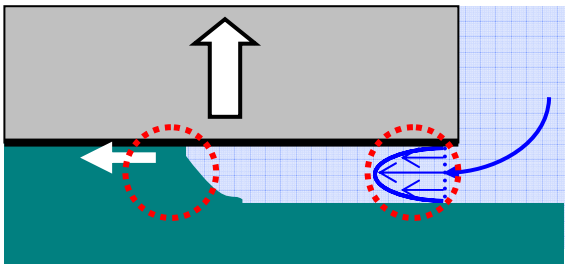

Figure 17 - Schematic representation of the detachment of the aligned punch and gel. In this case, the viscoelasticity of the gel limits the velocity of the triple line, so that the dissipation due to the confined Poiseuille flow in the liquid remains negligible.

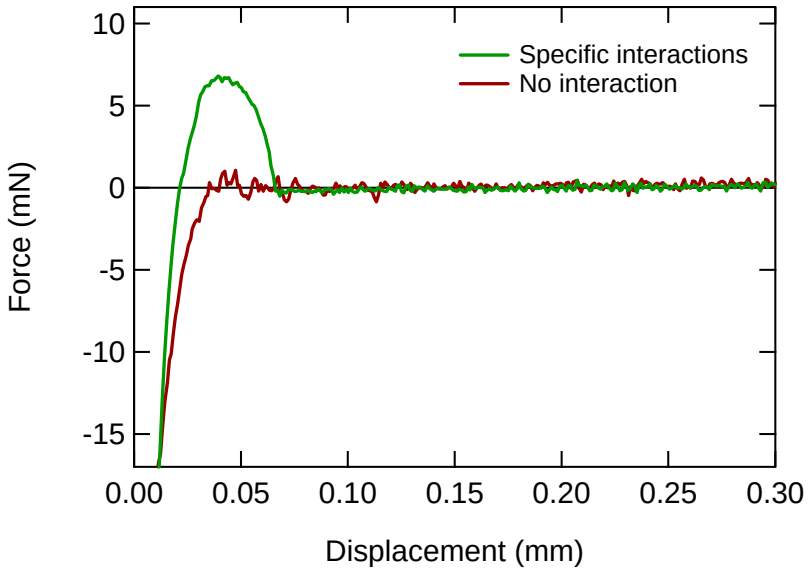

Figure 18 - Two force-displacement curves (during detachment) obtained for the same samples in the same alignment conditions; the acidity of the immersing medium is changed. In one case, H-bonding is expected between the gel and the brush and an adhesion peak is observed while in the other case, no interaction is expected between the two materials.

3-4- Setting the experimental conditions

For an appropriate measurement of the adhesion energy, one must choose the range of experimental parameters leading to meaningful results. Apart from the immersing medium,

three main parameters should be set: these parameters are the contact stress, the contact time and the debonding velocity.

Contact time

The duration of the contact must be long enough to expel the solvent from between the gel and the brush. A minimum of 10 seconds is recommended since it is the time necessary for the main part of the total mechanical relaxation of the gel to have occurred when it is underwater, as can be seen on Figure 13 and Figure 14-top.
In addition to being adapted to the solvent expulsion and the main mechanical relaxation of the materials, the duration of the contact must be adapted to the type of interactions – and their dynamics – that are formed at the interface between the brush and the gel. In our case, we use polymers that form intermolecular complexes. The dynamics of the formation of these complexes has then to be taken into account when performing the measurement. For coulombic interactions, we observed that the interactions were low but effective enough to probe the adhesion after a short contact time of about 10 s [52]. For H-bonding interactions, a minimum of 30 s is necessary to obtain a clear adhesion peak, as it will be shown in Chapter 6. Results obtained when varying the contact time will be further presented and investigated, but for our systems, we have usually worked with a contact time of 300 s, which is a good compromise between the waiting time and the accuracy of the measurement.

Contact stress

The contact stress between the brush on the punch and the gel has to be adapted since at least two conditions must be verified:

- The contact stress must be high enough so that the contact between the gel and the punch is total. It has to be chosen in parallel with the precision of alignment required to obtain a total contact. However, it must be lower than the maximum stress before damage of the gel or the brush occurs.
- More restrictive, it is mandatory to avoid a strong shear strain at the contact between the gel and the brush, which damages the brush and breaks the specific interactions when the gel is still under compression, leading to the absence of adhesion peak as shown on Figure 19.

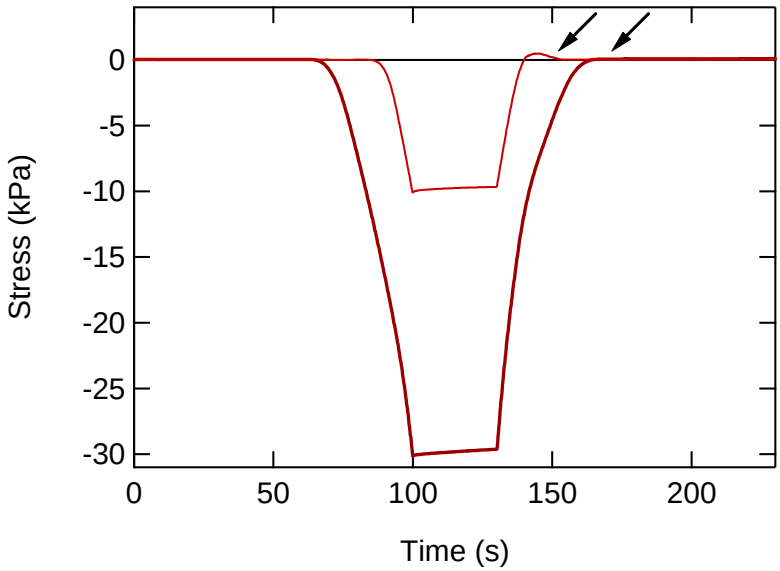

Figure 19 - Stress as a function of time with the same samples at pH 2 (PAA-l,d brush with PDMA-10x2 gel). The two experiments are carried out with varying the contact stress; at high contact stress, no adhesion can be measured whereas at low contact stress, the adhesion peak gives the energy of adhesion.

For layers of gels of thickness about 1 mm and with a storage modulus equal to 25 kPa, we have chosen to work at 4 kPa. At higher compressions (10 kPa), a strong decrease of the adhesion energy was observed. This effect can be explained by the existence of shear stresses due to incompressibility that cause a relative motion of the gel and the brush at the interface and destroy the interactions in the first steps of the debonding process; since they are long to form, they can not recreate before the detachment. At lower compressions, a total contact between the punch and the gel requires a very good alignment.

Debonding velocity

Finally, the last important parameter that has to be taken into account is the debonding velocity. It is important for many reasons.

- The unwanted hydrodynamic effect occurring during detachment varies linearly with the velocity U (see Eq. 5).
- In an adhesion test, it is difficult to decorrelate the interfacial effects from the bulk effects. The mechanical tests performed on the gels (rheology and compression tests) have shown that the gels used for the adhesion tests are highly elastic and minimally dissipative. However, the deformation of the gel at the triple line can reach the non-linear domain of deformation, leading to higher levels of dissipation as often observed

for adhesion tests. The probability to obtain an enhanced bulk dissipation increases with the debonding velocity U .

- At very low debonding velocity, the interactions between the gel and the brush are probed on a time scale longer than the average lifetime of a bond or sticker [53]. The stickers can then recombine to form the same bond, move to another site to form a new bond, or in our case, get solvated by the surrounding water. If the chains are slowly pulled away, then the recombination occurs quickly enough to prevent the stretching of the chains, which macroscopically leads to a total absence of adhesion peak in the measured force.

On Figure 20, we show the variation of the surface adhesion energy as a function of the debonding velocity. It appears clearly that for velocities lower than 1 µm.s^{-1}, no adhesion could be measured. Then, the adhesion increases slightly until it reached 10 µm.s^{-1}. For higher velocities, the adhesion energy increases almost linearly with the debonding velocity; this is either the signature that the interactions are all pulled together, leading to an increased adhesion energy, or that bulk dissipation or hydrodynamic effects are measured. For a typical measurement, we have chosen to work with a debonding velocity of 10 µm.s^{-1}.

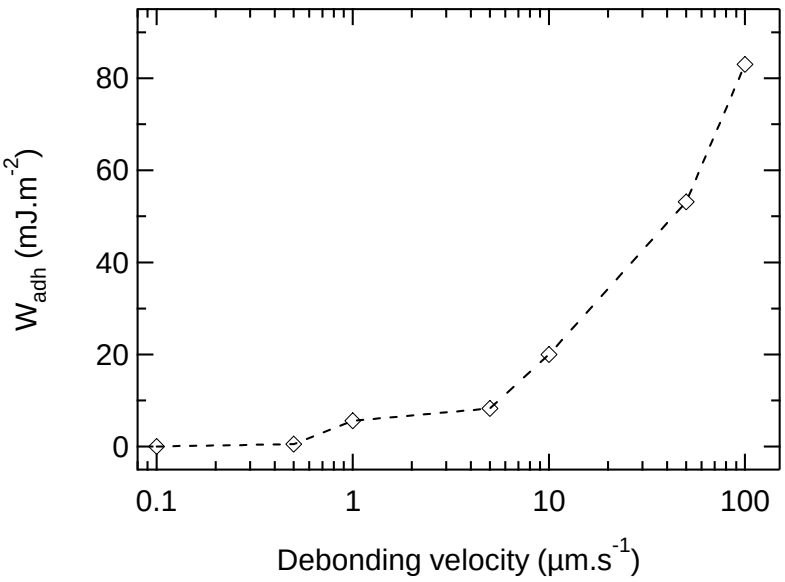

Figure 20 - Surface adhesion energy W_{adh} as a function of the debonding velocity U from [52]. The brush consists of a PAA-l,m brush (with σ_{long} = 1.0 10^{-1} chains.nm^{-2}). The hydrogel is synthesized in water with DMA (10 wt% of water) and [2-(methacryloyloxy) ethyl] trimethyl-ammonium chloride (MAETAC) and N,N'-methylene-bis-acrylamide (MBA) with a molar ratio DMA:MAETAC:MBA equal to 90:10:8; with the notations of Chapter 3 this hydrogel P(DMA$_{90}$-*co*-MAETAC$_{10}$)-10x8 is equilibrated in an aqueous solution at pH 9 with [NaCl] = 10^{-2} M.

Experimental conditions are very important for this type of delicate experiments to obtain meaningful data. It is absolutely mandatory to:

- Perform a pre-alignment of the sample which insures a total contact rapidly after the first contact but which is not perfect to avoid the pinning of bubbles between the punch and the gel, and to reduce potential hydrodynamic effects and bulk dissipation in the gel.
- Impose a contact force adapted to the size of the punch and to the storage modulus of the gel.
- Maintain a contact time long enough for the gel to partially relax and for the interactions to form at the interface.
- Detach the gel and the brush with a debonding velocity in a medium range allowing to probe the interactions and to limit the unwanted effects.

4- Conclusion

In the absence of available standard methods to probe the adhesion between a soft swollen material such as a gel, and a rigid surface, we have developed a new experimental setup designed to measure the adhesion in a flat-flat contact test. The advantage of this proposed setup is to be close to the phenomena that can be met in the marine environment or in the muco-adhesion. It is made to obtain quantitative macroscopic adhesion energies in a repeatable way.

The materials that can be probed are often easily synthesized since they are flat. The samples we put in contact consist of:

- a planar brush grafted on a 1 cm^2 silicon wafer, the latter being stuck on a punch;
- a 1 mm-thick gel covalently attached on a quartz slide.

The sizes of the samples are adapted for a reasonable confinement of the gel layer so that the alignment between the two surfaces remains easy; furthermore, the contact area is wide enough to perform quantitative measurement of forces. During the test, the planar brush is put in contact with the flat gel and the energy of adhesion is measured while pulling them apart.

Another asset of the proposed experimental setup is the possibility to change the environmental conditions *in situ*, mainly the temperature and the nature of the solvent. Many different solvents, including water, can be used with the setup. In the case of our systems, the interactions between the gel and the brush are expected to be tunable as a function of pH, temperature and ionic strength. The space inside the sample trough allows the measure of the characteristics of the solution by inserting measurement electrodes for temperature, pH or ionic strength or to change its characteristic, for instance by imposing a potential with a working electrode.

Being able to perform wet measurements is the best way to get rid of the surface tension effects that play a major role in dry measurements on swollen materials. However, some hydrodynamic artefacts may disturb the force measurement or the establishment of the contact between the two samples. The best way to make them negligible is to work with a slight misalignment between the two surfaces, maintain the contact at a weak stress during more than 30 seconds, and use a reasonable debonding velocity. When these precautions are taken,

the hydrodynamic effects and the possible shear stress between the surfaces do not perturb the measurements.

Thanks to the development of this setup and to the determination of the most suitable range of experimental conditions, many other systems could potentially be tested with the setup. For example, biological tissues that can be stuck on a glass plate, or a population of cells that can be grown on gels [54] are in the range of materials adapted to the test.

Now that the setup is presented, the next chapter will focus on the specific interfacial interactions between a hydrogel of PDMA or PAM and a tunable brush of PAA. We will see that it gives access to rearrangement dynamics of the polymeric complexes and the interactions measured on adhesion have already been characterized at the polymeric chain scale by neutron reflectivity in Chapter 4.

5- References

[1] Awaja, F.; Gilbert, M.; Kelly, G.; Fox, B.; Pigram, P. J. *Prog Polym Sci* **2009**, *34*, 948-968.
[2] Christenson, H. K.; Claesson, P. M. *Adv Colloid Interfac* **2001**, *91*, 391-436.
[3] Claesson, P. M.; Ederth, T.; Bergeron, V.; Rutland, M. W. *Adv Colloid Interfac* **1996**, *67*, 119-183.
[4] Israelachvili, J. N. *Intermolecular and Surface Forces*, 2nd Edition ed.; Academic Press: New York, **1992**.
[5] Pocius, A. V. *Adhesion and Adhesives Technology: an Introduction*, 2nd Edition ed.; Carl Hanser Verlag: Munich, **2002**.
[6] Chan, D. Y. C.; Horn, R. G. *J Chem Phys* **1985**, *83*, 5311-5324.
[7] Israelachvili, J. N.; Pashley, R. M. *Nature* **1983**, *306*, 249-250.
[8] Neuman, K. C.; Nagy, A. *Nat Methods* **2008**, *5*, 491-505.
[9] Ortiz, C.; Hadziioannou, G. *Macromolecules* **1999**, *32*, 780-787.
[10] Zhang, D.; Ortiz, C. *Macromolecules* **2004**, *37*, 4271-4282.
[11] Sonnenberg, L.; Parvole, J.; Borisov, O.; Billon, L.; Gaub, H. E.; Seitz, M. *Macromolecules* **2006**, *39*, 281-288.
[12] Zhang, Z.; Tomlinson, M. R.; Golestanian, R.; Geoghegan, M. *Nanotechnology* **2008**, *19*, 035505.
[13] Ducker, W. A.; Senden, T. J.; Pashley, R. M. *Nature* **1991**, *353*, 239-241.
[14] Butt, H. J.; Jaschke, M.; Ducker, W. *Bioelectroch Bioener* **1995**, *38*, 191-201.
[15] Luckham, P. F. *Adv Colloid Interfac* **2004**, *111*, 29-47.
[16] Thompson, M. T.; Berg, M. C.; Tobias, I. S.; Rubner, M. F.; Van Vliet, K. J. *Biomaterials* **2005**, *26*, 6836-6845.
[17] Wallqvist, V.; Claesson, P. M.; Swerin, A.; Ostlund, C.; Schoelkopf, J.; Gane, P. A. C. *Langmuir* **2009**, *25*, 9197-9207.
[18] Erath, J.; Schmidt, S.; Fery, A. *Soft Matter* **2010**, *6*, 1432-1437.
[19] Leckband, D. *Cell Mol Bioeng* **2008**, *1*, 312-326.
[20] Israelachvili, J. N.; Adams, G. E. *Nature* **1976**, *262*, 773-776.
[21] Israelachvili, J. N.; Adams, G. E. *J Chem Soc Farad T 1* **1978**, *74*, 975-&.
[22] Parker, J. L.; Christenson, H. K.; Ninham, B. W. *Rev Sci Instrum* **1989**, *60*, 3135-3138.
[23] Perkin, S.; Chai, L.; Kampf, N.; Raviv, U.; Briscoe, W.; Dunlop, I.; Titmuss, S.; Seo, M.; Kumacheva, E.; Klein, J. *Langmuir* **2006**, *22*, 6142-6152.
[24] Chai, L.; Klein, J. *Langmuir* **2009**, *25*, 11533-11540.
[25] Taunton, H. J.; Toprakcioglu, C.; Fetters, L. J.; Klein, J. *Macromolecules* **1990**, *23*, 571-580.
[26] Taunton, H. J.; Toprakcioglu, C.; Fetters, L. J.; Klein, J. *Nature* **1988**, *332*, 712-714.
[27] Tareste, D.; Pincet, F.; Lebeau, L.; Perez, E. *Langmuir* **2007**, *23*, 3225-3229.
[28] Malham, I. B.; Bureau, L. *Langmuir* **2010**, *26*, 4762-4768.
[29] Johnson, K. L.; Kendall, K.; Roberts, A. D. *Proc R Soc Lon Ser-A* **1971**, *324*, 301-&.
[30] Chaudhury, M. K.; Whitesides, G. M. *Langmuir* **1991**, *7*, 1013-1025.
[31] Haidara, H.; Chaudhury, M. K.; Owen, M. J. *J Phys Chem-Us* **1995**, *99*, 8681-8683.
[32] Nolte, A. J.; Chung, J. Y.; Walker, M. L.; Stafford, C. M. *Acs Appl Mater Inter* **2009**, *1*, 373-380.
[33] Loskofsky, C.; Song, F.; Newby, B. M. Z. *J Adhesion* **2006**, *82*, 713-730.

[34] Sakasegawa, D.; Suzuki, A. *J Polym Sci Pol Phys* **2009**, *47*, 1778-1788.
[35] La Spina, R.; Tomlinson, M. R.; Ruiz-Perez, L.; Chiche, A.; Langridge, S.; Geoghegan, M. *Angew Chem Int Edit* **2007**, *46*, 6460-6463.
[36] Flory, A. L.; Brass, D. A.; Shull, K. R. *J Polym Sci Pol Phys* **2007**, *45*, 3361-3374.
[37] Guvendiren, M.; Brass, D. A.; Messersmith, P. B.; Shull, K. R. *J Adhesion* **2009**, *85*, 631-645.
[38] Kamino, K. *J Adhesion* **2010**, *86*, 96-110.
[39] Kurokawa, T.; Furukawa, H.; Wang, W.; Tanaka, Y.; Gong, J. P. *Acta Biomater* **2010**, *6*, 1353-1359.
[40] Lin, Y. A.; Yao, S. H.; Xu, Q. A. *Cell Mol Bioeng* **2010**, *3*, 247-255.
[41] Tunc, M.; Cheng, X. H.; Ratner, B. D.; Meng, E.; Humayun, M. *Retina-J Ret Vit Dis* **2007**, *27*, 938-942.
[42] Wang, S. J.; Li, X. *Thin Solid Films* **2010**, *518*, 6036-6039.
[43] Webber, R. E.; Shull, K. R.; Roos, A.; Creton, C. *Phys Rev E* **2003**, *68*, -.
[44] Takigawa, T.; Morino, Y.; Urayama, K.; Masuda, T. *Polym Gels Netw* **1996**, *4*, 1-5.
[45] Lin, W. C.; Shull, K. R.; Hui, C. Y.; Lin, Y. Y. *J Chem Phys* **2007**, *127*.
[46] Haraguchi, K.; Li, H. J.; Okumura, N. *Macromolecules* **2007**, *40*, 2299-2302.
[47] Monteux, C.; Tay, A.; Narita, T.; De Wilde, Y.; Lequeux, F. *Soft Matter* **2009**, *5*, 3713-3717.
[48] Muller, P.; Sudre, G.; Theodoly, O. *Langmuir* **2008**, *24*, 9541-9550.
[49] Sokoloff, J. B. *J Chem Phys* **2008**, *129*, -.
[50] Sokoloff, J. B. *Soft Matter* **2010**, *6*, 3856-3862.
[51] Shull, K. R.; Creton, C. *J Polym Sci Pol Phys* **2004**, *42*, 4023-4043.
[52] Ducrot, E. In *Rapport de Stage - Master de Chimie de Paris Centre*: Paris VI, **2010**.
[53] Leibler, L.; Rubinstein, M.; Colby, R. H. *Macromolecules* **1991**, *24*, 4701-4707.
[54] Chen, Y. M.; Yang, J. J.; Gong, J. P. *J Adhesion* **2009**, *85*, 839-868.

CHAPTER 6 – TUNABLE ADHESION BETWEEN A BRUSH AND A GEL

At this point of the thesis, the synthesis and the characterization of the objects that are to be used to measure the adhesion of hydrogels on "smart" brushes have been carefully carried out (Chapters 2 and 3). The study of the associative properties of the polymers in solution and at interfaces (Chapter 4) is applied to the macroscopic adhesion of gels on brushes. To this end, we use the experimental setup and conditions presented in the Chapter 5.

The first and most important part of this Chapter aims at determining the variation of the energy of adhesion as a function of the environmental conditions and thus, at answering the main question of this PhD project: is it possible to tune the adhesive properties of a gel on a surface, from the absence of adhesion to a strong and positive adhesion? The proton-donor brush of poly(acrylic acid) is put in contact with the proton-acceptor hydrogels of poly(*N*,*N*-dimethylacrylamide) and of poly(acrylamide). We determine the domain of pH where the interactions at the interface between the gel and the brush lead to a macroscopic adhesion. Then, to what extent can the variation of the adhesion with pH be compared with the results obtained for the formation of molecular complexes in solution?

For a better understanding of the formation of these interactions, we use three experimental parameters to probe the kinetics involved in the creation of the interactions and their breakage? The equilibration time of the gel at a given pH is systematically changed and gives access to the diffusion of the acidity in the gel. As the tests are performed in a good solvent of the polymers, one can expect that the reorganization of the interactions is fast, and varying the contact time is a way to determine this reorganization kinetics of the complexes at the interface. From another point of view, the debonding velocity can be used as a tool to probe the half-life of the interactions.

Then, thanks to the work of Etienne Ducrot in his Master's thesis which I supervised, a comparison is made between H-bonded complexes and Coulombic complexes. The differences in the resulting adhesion are highlighted, in terms of energies and kinetics. Finally, we investigate how the neutron reflectivity study of the structure of the brushes at the interface with the gel from Chapter 4 gives additional information to the adhesion tests.

Polymers are well-known for adsorbing on surfaces. The reason is often that the interaction between the polymer and the surface is more favorable than that of the solvent with the surface [1]. Two main types of adsorption can be distinguished: the first one consists of the adsorption of a homopolymer, the monomers of which have the same interaction with the substrate. In the second case, the polymer is end-functionalized with a tail that preferentially adsorb on the surface. Many theoretical studies have been performed on the adsorption of polymers at surfaces to predict the conformation of the chains, the concentration of monomer at the surface which differs from that in solution, or the amount of grafted chains at the surface [2-6]. In biology, the specific interactions of polymers on surfaces are commonly used for DNA microarrays. Experimentally, the adsorption of synthetic polymers has been used for instance for the formation of layer-by-layer systems [7], and the functionalization of surfaces for robotic micro-handling [8] could be extended to polymeric systems. The most used interaction for the layer-by-layer systems is the Coulombic force since it is one of the strongest interactions. However, neutral polymers can also adsorb on surfaces. In the case of poly(*N*,*N*-dimethylacrylamide), its relatively strong interaction with glass or silica allowed the formation of tremendously reinforced hydrogels in which silica nanoparticles are inserted [9]. On the contrary, the same addition of silica in poly(acrylamide) hydrogels did not affect the behavior of the material to such an extent [10]. Zhang *et al.* [11] studied the underwater adsorption of PDMA on silicon wafer as a function of pH. They used force spectroscopy for a characterization at the molecular level and the quartz crystal microbalance to measure the mesoscopic adsorbed quantity. They showed that the interaction is reinforced at low pH, when the native silica layer bears mostly hydroxyl groups –O–H at the surface, and it is twice lower at high pH when the oxide surface is anionic.

Here, we investigate the reversible adhesion of polymer networks swollen to equilibrium on surfaces. To make the adhesion reversible, the choice of functionalized surfaces is made. With these systems, it is possible to vary the interaction potential between the surface and the polymer network so that the interaction is reversible and the macroscopic adhesion too. This idea has already been used during the PhD of Elodie Siband [12], whose project was to create pH- and thermo-sensitive macromolecular associations in solution and on surfaces. She used two systems. The pH-sensitive one was based on poly(acrylic acid) brushes (negatively charged for $pH > pKa \approx 4.5$) and neutral polymer side-grafted with cationic grafts (for $pH < 9.8$). She demonstrated that the cationic polymer could adsorb on the surface at pH 7 but not at pH 3 and that this adsorption was reversible. The thermo-sensitive system was composed of poly(N-isopropylacrylamide) brushes and the same polymer in solution. At high temperature

superior to the LCST of PNIPAM, the polymer in solution tends to adsorb on the surface whereas it is not the case at low temperature.

Using neutral hydrogels for their dimensional stability, the objective is to create a reversible adsorption that could lead to a macroscopic adhesion which could essentially be tuned by changing the environmental conditions. To reach this, we have chosen to work with short-ranged interactions, mainly based on hydrogen bonds between the hydrogel and a pH-sensitive brush of poly(acrylic acid). The systems have been synthesized, characterized and their interactions in solution and at interfaces at the molecular level are investigated in the previous chapters 2, 3 and 4. The setup and the methodology for measuring an underwater adhesion of swollen materials are described in chapter 5. With such a system, we aim at gaining insight on many parameters of the surface interactions such as the kinetics of formation of the interactions, or how they can be linked to the strength of the complexes and to the macroscopic adhesion being measured. Finally, we will briefly discuss our results in comparison to those obtained with Coulombic interactions.

1- Effects of environmental changes on the adhesion

1-1- Effect of pH at equilibrium

In this first part, we measure the effect of pH on the adhesion of a gel on a PAA brush in water. The objects alone were studied in Chapters 3 and 2 respectively and their macroscopic interaction is discussed here. Unless otherwise specified, the time of contact is equal to 300 s, the average contact compressive stress applied is 4 kPa (*i.e.* roughly 15% of the modulus for those gels) and the debonding velocity is equal to 10 µm.s^{-1} for all the adhesion tests of this chapter.

The typical stress strain curves when the PDMA or PAM gel and the PAA brush adhere to one another are presented on Figure 1. They result from the data treatment detailed in Chapter 5. In the case of a PDMA gel, as for a PAM gel, the adhesion peak corresponds to an interfacial failure mode of debonding.

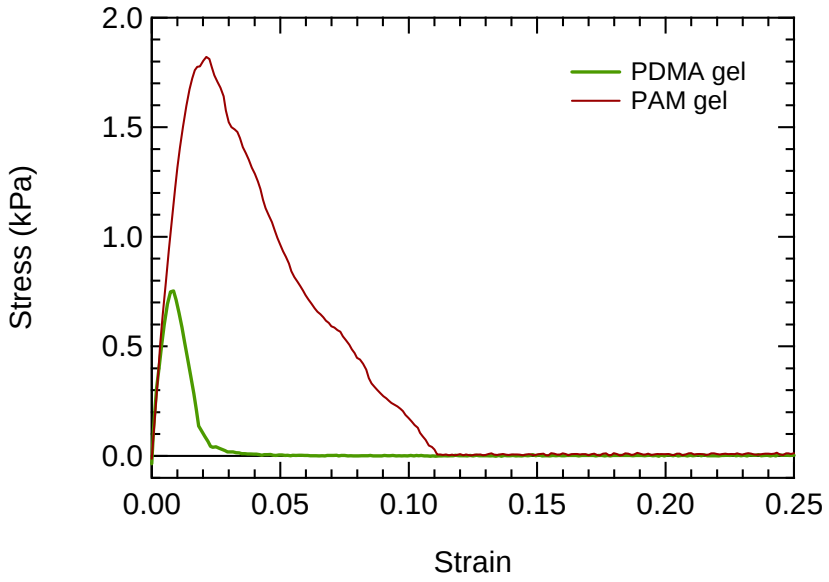

Figure 1 - Stress strain curves in the case of adhesive forces for a PAA-l,m brush facing a PDMA-10x2 hydrogel equilibrated at pH 2 or a PAM-10x2 hydrogel equilibrated at pH 3.

When the hydrogel is made of PDMA, the maximum stress when debonding is found below 1 kPA and the deformation in tensile forces is below 3% in strain. The energies of adhesion obtained are in the range of 10 mJ.m^{-2}.

For a similarly cross-linked and swollen PAM gel, the maximum stress can reach values twice higher than for the PDMA hydrogel, around 1.8 kPa, and the resulting maximum deformation

of the gel is three to four times higher, in the order of 10% in strain. The resulting energy of adhesion is one order of magnitude higher than that obtained with PDMA gels, that is to say around 100 $mJ.m^{-2}$.

PAA brush against a PDMA hydrogel

The pH-sensitive behavior of the adhesion of a PAA brush against a PDMA gel is demonstrated on Figure 2. In this case, PDMA-10x2 hydrogels equilibrated at various pH are probed in immersed condition against a PAA-l,m brush ($\sigma = 4.3\ 10^{-2}$ chains.nm^{-2}). The adhesion peak clearly depends on the pH of the solution in which the gel and the brush are equilibrated. At lower pH, when the brush is more protonated, the adhesion peak is higher, which means that the energy of adhesion is higher. At pH 4, the adhesion is strongly reduced, almost inexistent compared to what is observed at pH 2. This figure demonstrates the existence of a pH-sensitive and tunable adhesion, which is one of the main objectives of the PhD.

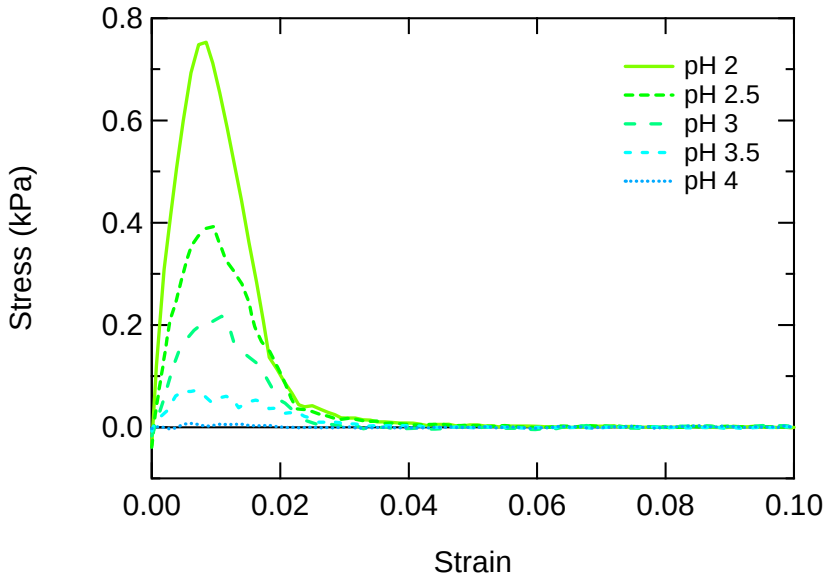

Figure 2 - Stress strain curves in the case of adhesive forces for PDMA-10x2 hydrogels equilibrated at various pH facing a PAA-l,m brush.

PAA brush against a PAM hydrogel

The same experiment (identical duration and stress of contact) was carried out on PAM-10x2 hydrogels with a similar PAA-l,m ($\sigma = 8.0\ 10^{-2}$ chains.nm^{-2}) brush immersed and equilibrated at various pH, as shown on Figure 3. Qualitatively similar results to those obtained with

PDMA-10x2 hydrogels are observed, except that adhesion is now not measurable for pH > 5. In this case too, the adhesion is strongly dependent on pH.

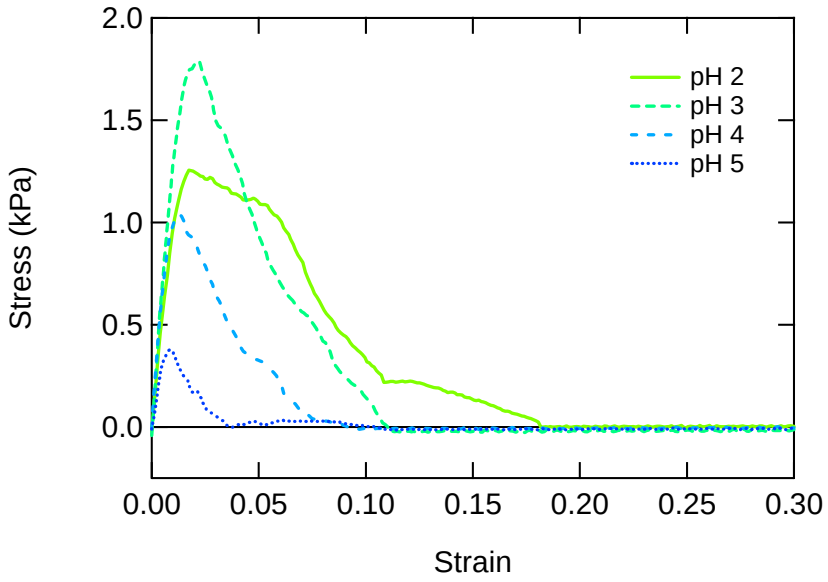

Figure 3 - Stress strain curves in the case of adhesive forces for PAM-10x2 hydrogels equilibrated at various pH facing a PAA-l,m brush.

Comparison between the two systems

For further comparison, the energies of adhesion of the two systems have been calculated, with the methodology described in Chapter 5, and plotted together as a function of pH on Figure 4. With this representation, one easily notices the differences between the two systems. The adhesion on PAM hydrogels is one order of magnitude higher than the one measured on PDMA hydrogels, and the transition between adhesive interactions and the absence of interaction occurs at a higher pH.

The analysis of these results is far from being obvious: is the interaction monomer-monomer stronger or the areal density of connections higher with PAM? Is the areal density of connections higher because the kinetics of the formation of the PAM-PAA interfacial complexes is faster than for PDMA-PAA?

To make the discussion easier, the energy of interaction can be obtained in terms of thermal energy per chain of the brush by using its grafting density as follows:

$$W_{adh}(kT/chain) = \frac{W_{adh}(mJ/m^2)}{4.1 \times \sigma(chain.nm^{-2})}. \qquad \textbf{Eq. 1}$$

Using Eq. 1, the energy of adhesion for the PDMA gel on the brush is estimated at 51 *kT* per chain which is lower than what is found for PAM gel, that is to say 280 *kT* per chain. Even if the interaction between the brush and the gel, and particularly the PDMA gel, does not only correspond to H-bonding, these energies can be compared in terms of number of H-bonds per chain. In the case of the PDMA hydrogel, the energy of adhesion would correspond to a few H-bonds per chains (~ 10 *kT* per H-bonds [13]). For the PAM hydrogel, the interaction seems strong enough so that cooperative effects can not be excluded.

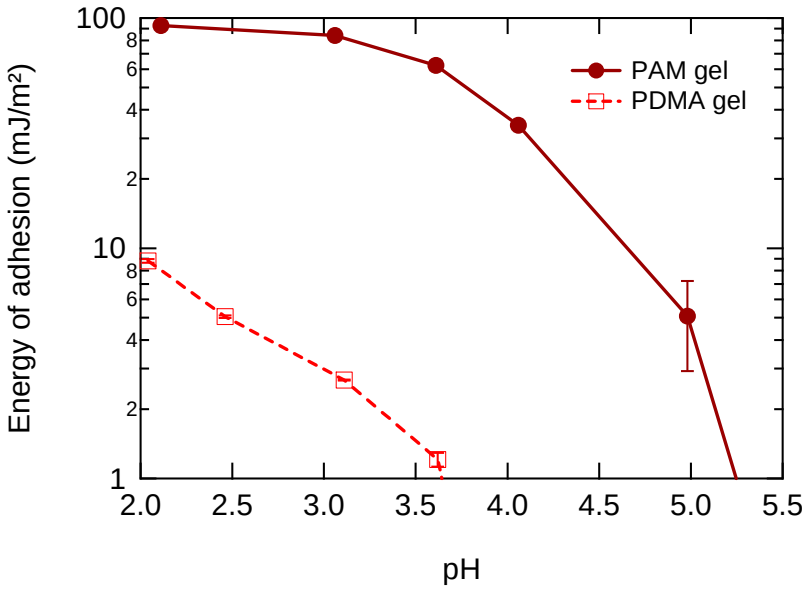

Figure 4 - Energy of adhesion between a PAA-l,m brush and a PDMA-10x2 or a PAM-10x2 hydrogel as a function of pH.

On Figure 5, the same energy of adhesion expressed per chain of the brush is represented together with the ranges of pH where the complexation of PAM or PDMA with PAA occurs in solution (see Chapter 4). For the PDMA-PAA polymer pair, the onset of adhesion at the surface corresponds quantitatively to the complexation transition in solution, as observed with our visual cloud point method. For pH below 3.5, the PDMA and PAA are complexed in solution. The same complexation occurs at the surface between the PAA brush and the PDMA gel resulting in a macroscopic adhesion of the order of one H-bond per chain at pH 3.5.

On the contrary, the onset of adhesion for the PAA brush with the PAM hydrogel is shifted to higher pH compared to the transition observed for the complexation of the same polymeric pair. It means that the complexation at the interface is favored in comparison with the one in solution. Different reasons can be invoked to explain this phenomenon, such as an increased

concentration for the adhesion measurement compared to the experiments carried out in solution. Another reason might be the difference of entropy between the associated state and the dissociated state: in solution, the translational entropic loss of the polymer chains due to complexation is higher than at surfaces where the chains are already immobilized; thus, the association can be favored.

Alternatively, the strong difference between the adhesion of PDMA hydrogel and of PAM hydrogel on the PAA brushes can also be explained by the kinetics of the formation and optimization of the interpolymer complexes at the surface. If the PAM-PAA polymeric pair tends to rearrange its complexes faster than the PDMA-PAA pair, it follows that the connection between the brush and the gel is better optimized and the adhesion energy is stronger.

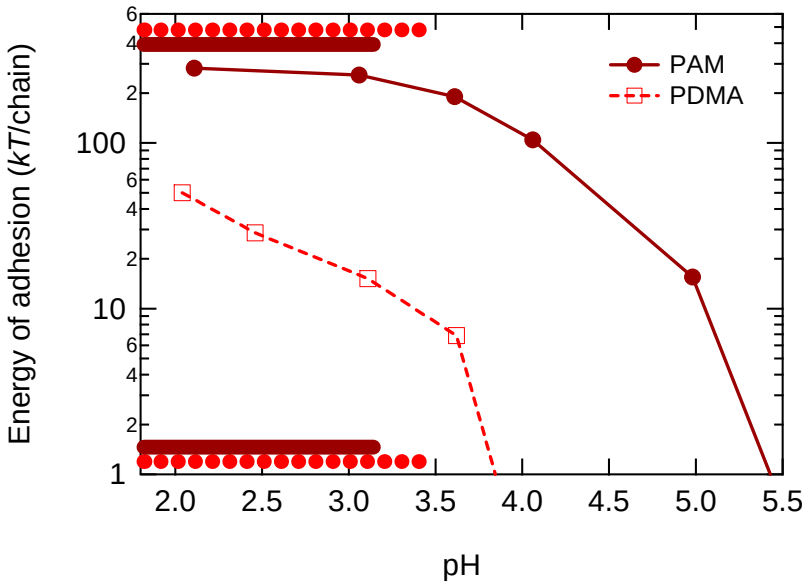

Figure 5 - Energy of adhesion between a PAA-l,m brush and a PDMA-10x2 or a PAM-10x2 hydrogel as a function of pH. The range of pH for which the complexation occurs in solution are below pH 3.5 and 3.1 for the PAA-PDMA and PAA-PAM the pairs respectively, the zones are schematized by the thick lines, phase diagrams are in Chapter 4.

Finally, the experiment performed at a given pH could be reproduced many times without any modification of the result obtained, proving that neither the gel nor the brush are being damaged during the experiment.

In conclusion, a change in pH of the environment causes a reversible transition from non-interacting materials to macroscopically adhering materials. Consistent with the measurements of the interactions in solution, the adhesion is stronger at low pH and decreases

when the pH increases. For PDMA, the pH range where macroscopic adhesion is observed corresponds well to the pH range for which the polymers form interpolymer complexes in solution whereas for PAM, the pH range where adhesion is observed is clearly wider than for the in-solution interactions. The strength of the adhesion between a PAM hydrogel and a PAA brush shows the cooperative effects of multiple H-bonds along the polymeric chains.

1-2- Changing the pH *in situ*: diffusion effects

Our original idea was that it should be possible to change the adhesive properties between the brush and the gel when they are in contact, by changing the pH *in situ*. As a consequence, we have performed adhesion tests on a PDMA-10x2 hydrogel equilibrated at pH 2 at the beginning of the experiment. Then, a first adhesion test was carried out with the time of contact equal to 300 s, the average contact compressive stress applied of 4 kPa and the debonding velocity equal to 10 $\mu m.s^{-1}$. The solution was then adjusted to a higher pH and when no variation of pH could be observed for 1 min, another test was performed and so on. The PAA brush was a PAA-l,m brush ($\sigma = 5.2\ 10^{-2}$ chains.nm^{-2}) and the results are shown on Figure 6-top. The adhesion energies obtained are compared with those obtained from the PDMA-10x2 hydrogels equilibrated at a given pH and presented in the previous paragraph. Since the brush is slightly different, the adhesion energies have been normalized against the maximum values, obtained at pH 2.

The first result is that for an immersing solution at pH 9, we still obtain adhesion. This is explained by the fact that the gel is not completely equilibrated, meaning that the pH inside the gel is lower than the pH in the solution due to a slower diffusion inside the gel than in the solution. It means that if the pH of the solution is equal to 9, inside the gel, the pH is probably closer to 4. As a consequence, by varying the pH of the solution, mastering the equilibration time to wait, and selecting the contact duration adequately, it is possible to determine the diffusion inside the gel since the adhesion between the gel and the brush is a probe of the acidity inside the gel.

Another point here is to demonstrate that changing the acidity of the solution while the gel and the brush are in contact would lead to no change in adhesion if the time of contact is not long enough for the acidity to diffuse at the interface from the surrounding solution.

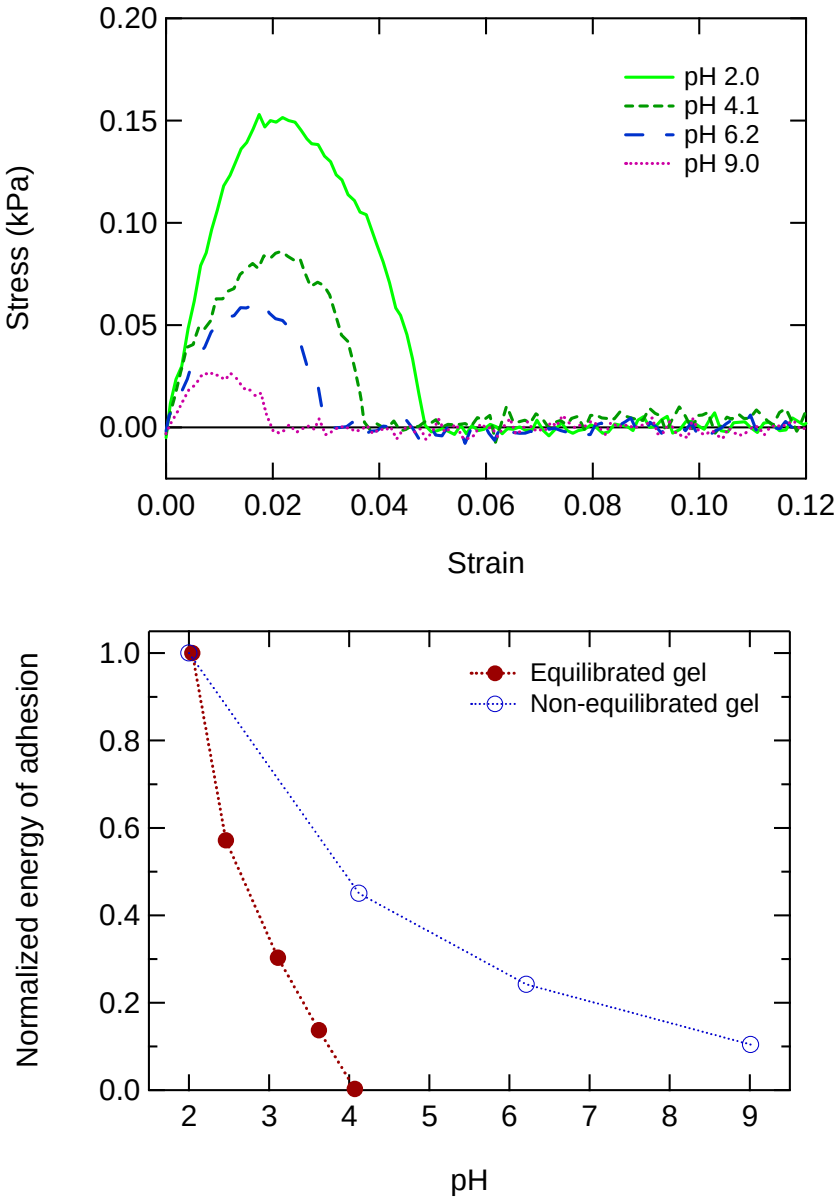

Figure 6 - Stress strain curves (top) at different pH for PDMA-10x2 gels when changing the pH *in situ*, starting from pH 2; we wait 5 min between equilibration of the solution and the beginning of the adhesion test (top). Corresponding normalized energy of adhesion (bottom) as a function of pH, for equilibrated gels (from Figure 2).

La Spina *et al.* [14] have performed similar experiments with PAA brushes against a hydrogel of poly[2-(dimethyl amino)ethyl methacrylate] (a polybase). At low pH, they interact through H-bonds whereas at high pH, the interactions are Coulombic. They found that a free standing gel tends to detach from the substrate when changing the immersing medium from water at pH 5.8 to water at pH 1.1. If the contact stress is low during attachment, the time needed for the gel to detach is about 7 h, and for high contact stresses, they had to wait for a few days. These results are in accordance with ours, demonstrating that the diffusion of the acidity in the gel is slow.

1-3- Changing the temperature in contact

Now that we have demonstrated that working with various gels equilibrated at various pH gave access to a tunable adhesion, and that changing the conditions *in situ* would lead to particularly long equilibration time, we wondered what would be the effect of a change in the temperature. Since the experimental setup has been built so that the temperature can be modified, we have performed tests with a temperature varying during the contact.

All these tests were performed with PDMA-10x2 hydrogels at pH 3.5. However, we were not able to measure any macroscopic adhesion. Figure 7 shows the variation of the force and of the temperature as a function of the time for these experiments.

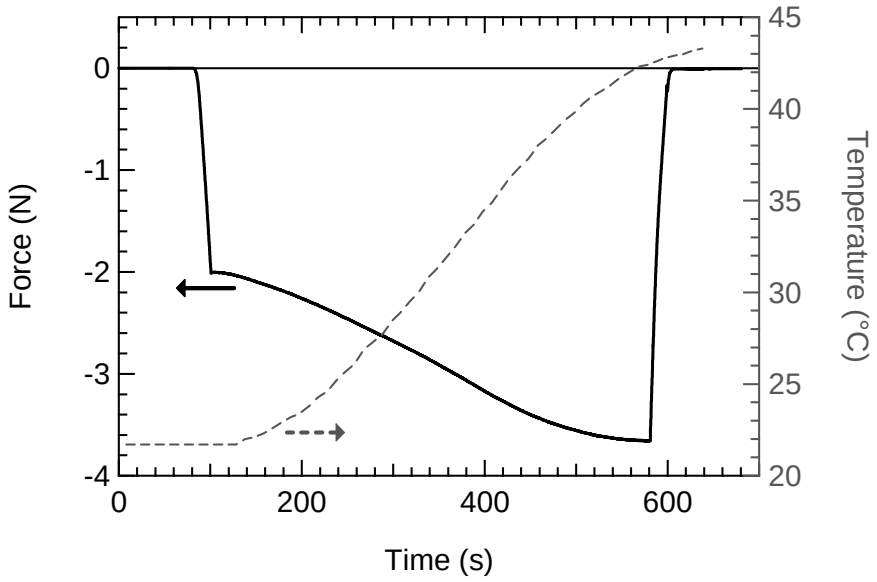

Figure 7 - Force and temperature as a function of time.

At the moment when contact is made, the temperature increases from 22°C to 43°C in 8 min. The gel shows a strong reaction towards temperature variations since it does not relax as usual but on the contrary, it gets stiffer. By increasing the temperature about 20°C, the force applied on the punch is almost doubled.

A direct consequence of the experimental conditions is the absence of macroscopic adhesion: first, the adhesion was predicted to be weak since at low temperature, the adhesion is expected to be around a few $mJ.m^{-2}$; second, the strong increase in the contact force probably causes a slippage of the gel at the interface with the brush due to shear forces, and then, the

interactions can not reform by lack of time. As a comparison, La Spina *et al.* [14] applied a load around 50 mN during 15 min, suggesting that the time needed for the interactions to settle is long. This kinetics effect will be discussed in the next part of the chapter.
Finally, no other measurement was performed with varying the temperature during the experiment.

1-4- Conclusion

The adhesion between the PDMA or PAM hydrogel and the PAA brush can be tuned by changing the pH at which the gel is equilibrated. For both hydrogels, the energy of adhesion is the highest at pH 2 and decreases monotonically when increasing the pH. Limited to a 300 s contact on a PAA brush, PDMA hydrogels exhibited a maximum interaction about 10 $mJ.m^{-2}$ whereas energies of adhesion one order of magnitude stronger were measured with PAM hydrogels. These values around 100 $mJ.m^{-2}$ are in the range of the thermodynamic work of adhesion and they remain weak compared to energies of adhesion of measured in air [15,16].
A strong temperature dependence of the gel mechanics has been demonstrated, which prevented us to further investigate the effect of temperature while the brush and the gel are in contact. However, the modification of the pH *in situ* has shown that the diffusion of the solution characteristics inside the gel was rather slow. We could observe a residual adhesion in a solution equilibrated at pH 9 on a gel previously equilibrated at pH 2. For such measurements, the contact time and the equilibration time are key parameters and in the next paragraph, we investigate the role of contact duration on the energy of adhesion.

2- Determination of specific complexation kinetics

As discussed in the previous chapter (and in the previous paragraph), kinetic effects are important and directly affect the measurement of the energy of adhesion. In Chapter 5, we discussed extensively the necessity to fix the parameters of the measurement in reasonable ranges so that it is not disturbed by artifacts. However, playing on the contact duration or on the debonding velocity gave rise to variations of the energy of adhesion that can not be explained by artifacts. In fact, it gives information about specific kinetics occurring at the interface between the gel and the brush, which is the focus of this part.

2-1- Rearrangement kinetics of the complexes by varying the time of contact

The measurement of the energy of adhesion between a PDMA-10x2 hydrogel and a PAA-l,m brush is the strongest at pH around 2. However, the strength of the interactions depends on the contact time. With the same materials that have been used in paragraph 1-2- page 227, we have measured the adhesion while varying the time of contact. The contact stress is fixed at 4 kPa and the debonding velocity is 10 µm.s^{-1}.

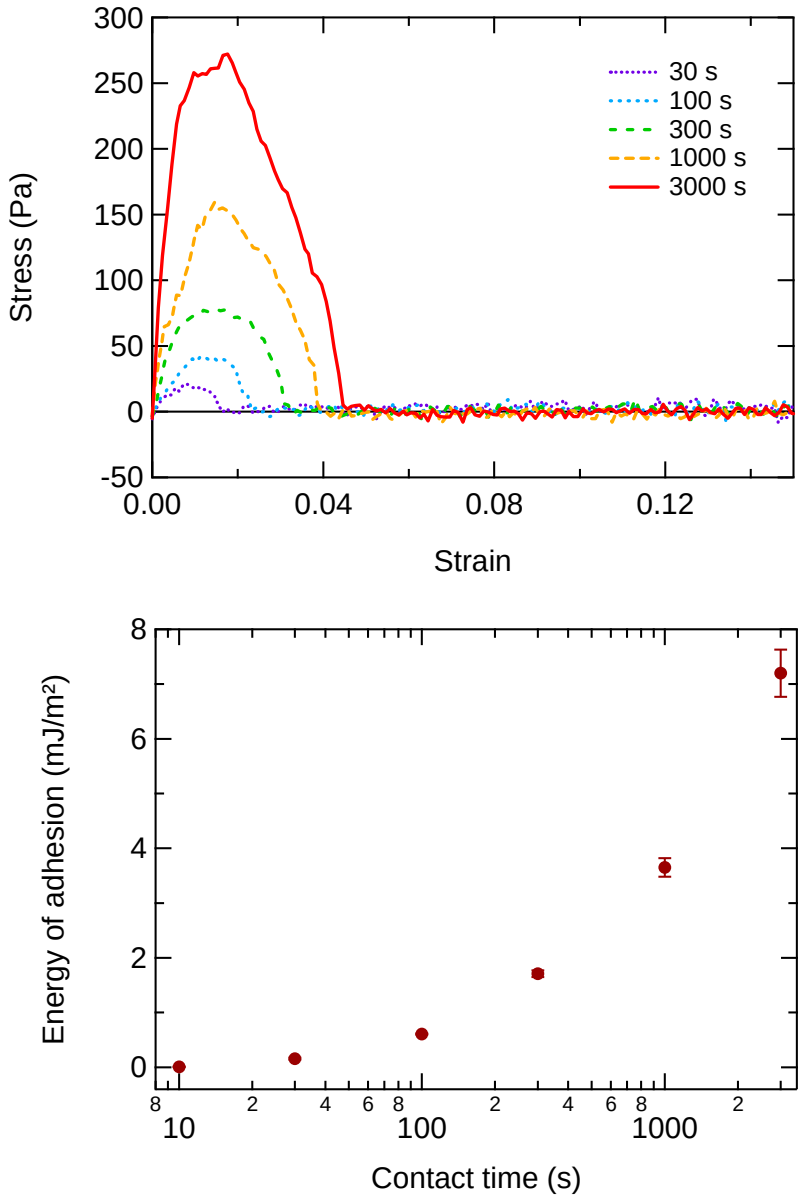

Figure 8 - Stress-strain curves (top) and energies of adhesion (bottom) between a PAA-l,m brush and a PDMA-10x2 hydrogel equilibrated and immersed at pH 2, as a function of contact duration. The measurement at 10 s did not show any adhesion peak.

Figure 8-top represents the stress-strain curves obtained when varying the contact time from 30 s to 3 000 s and the measured energies of adhesion are represented on Figure 8-bottom.
After a 10 s contact, no adhesion peak was visible. As a consequence, the interactions between the gel and the brush were too weak to allow the measurement of a macroscopic adhesion. The two reasons can be: (i) that the number of H-bonds between the gel and the brush is too low or (ii) that a thin film of water is present between the gel and the brush, preventing them to interact. For contact times higher than 30 s, a peak of adhesion is measured, suggesting that the film of water is removed. Furthermore, the energy of adhesion increases monotonically with contact time. It shows that the reorganization of the interactions at the interface – for optimizing the number of H-bonds and the adhesion – is a slow process. At first, this slow kinetics appears counterintuitive: since both polymers are in a good solvent with a low viscosity, one might expect their rearrangement kinetics to be fast.

However two facts have to be considered: first, when the polymers interact, they form a phase rich in polymer, containing very little solvent, which can explain why the kinetics is slowed down. Second, to obtain a rearrangement of a part of the chain, the chains have to follow a dynamic similar to the one involved in reptation: the chains of the brush have to break a few bonds at a time to induce a new path through the gel and increase the quality or the number of interactions.
La Spina *et al.* do not show the effect of the contact duration on their results but they have used a contact time in the order of 15 min (900 s) which is in the order of magnitude of the contact duration chosen for our usual experiments (300 s). Further comparisons concerning the contact time will be made in paragraph 4- below.

2-2- Debonding velocity

Complementary to the contact time, the debonding velocity plays a role on the energy of adhesion. In classical adhesive systems, the influence of the velocity is linked to the bulk dissipative effects that are essential in the usual in-air adhesives, while at infinitesimal velocities the thermodynamic work of adhesion only is measured. For our systems however, the hydrogels are highly elastic materials, as demonstrated in Chapter 3, and as a consequence, the bulk dissipative effects are expected to be small if not negligible. Additionally in Chapter 4, we discussed the possible effects due to viscous dissipation in the immersing medium on the adhesion, but the absence of adhesion peak at high pH even at high

debonding velocities (100 µm.s^{-1}) invalidates this hypothesis. A study of the variation in adhesion with debonding velocity remains essential.

The stress-strain curves for a system identical to that of the previous paragraph are shown on Figure 9-top for various debonding velocities. The contact is maintained during 300 s at 4 kPa. The energies of adhesion calculated from these curves are represented as a function of the debonding velocity on Figure 9-bottom.

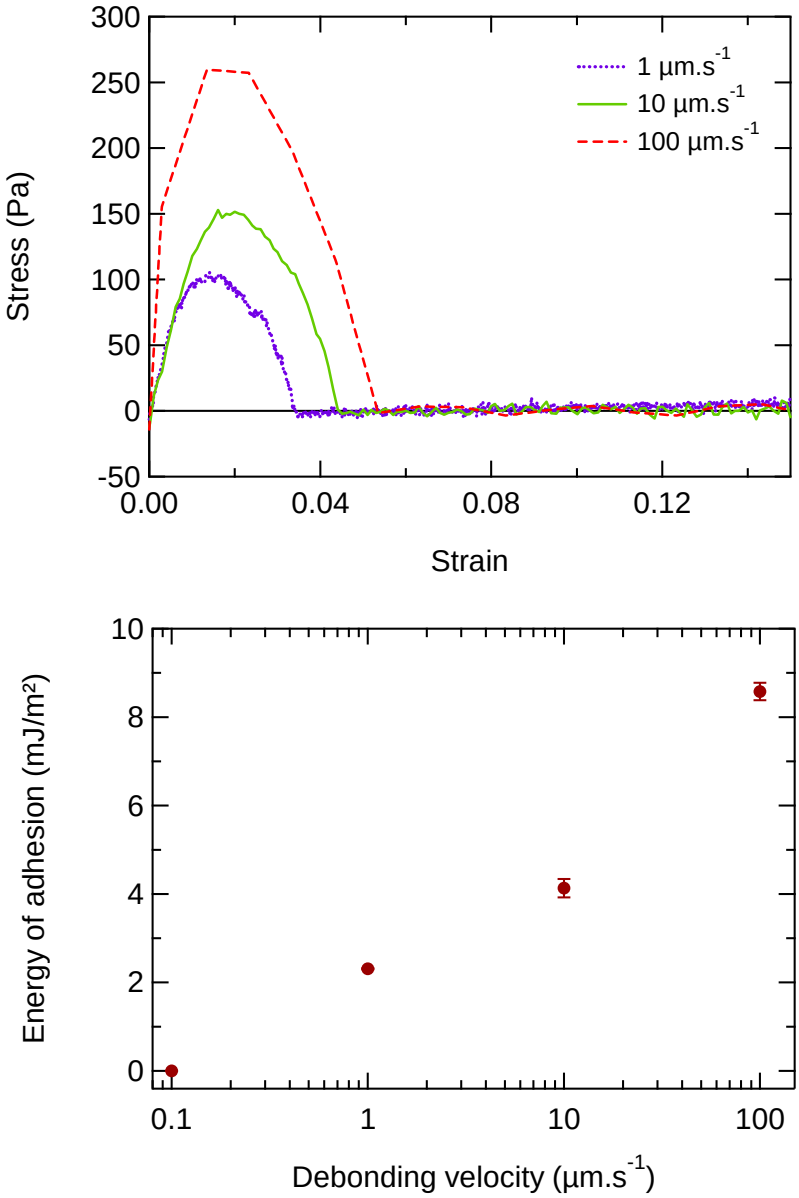

Figure 9 - Stress-strain curves (top) and energies of adhesion (bottom) between a PAA-l,m brush and a PDMA-10x2 hydrogel equilibrated and immersed at pH 2, as a function of debonding velocity. The measurement at 0.1 µm.s^{-1} did not show any adhesion peak.

For a debonding velocity as low as 0.1 µm.s^{-1}, no adhesion peak was measured. Then, for increasing debonding velocities, the energy of adhesion increases. These results suggest that at low debonding velocities, the H-bonds between the brush and the gel – which are not frozen but dynamic – are rearranged, gradually over the entire surface with surrounding water as an H-bonding competitor. In this case, the rearrangement occurs without putting the gel under traction and then, no macroscopic effect can be measured. On the contrary, as the brush is pulled off faster, the interactions between the chains of the brush and those of the gel do not have enough time to reorganize and they are probed on the whole surface at the same time, which leads to a macroscopic and measurable tensile force as the probe is pulled away from the gel. Finally, varying the debonding velocity is a way to change the time given to the complexes to rearrange.

3- Relationship between structure and macroscopic adhesion

It is interesting now to try to link the adhesive properties studied in this chapter with the structural study of the brush at the interface with the gel, which was carried out in Chapter 4. In fact, is it at all possible to link the adhesive properties to the extent of the modification of the brush structure?

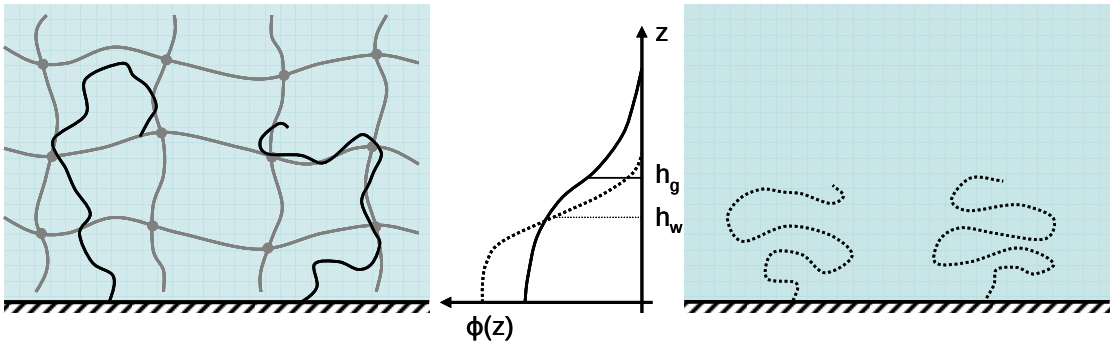

Figure 10 - Schematic representation of the brush structure against the gel and against water at pH 2. The brush is more extended in the presence of the gel, which has been shown by neutron reflectivity in Chapter 4. h_g and h_w are the mean heights of the brush in the presence of the gel, and in water respectively.

In this part, we discuss the energies involved in the stretching of the brush and those measured with the adhesion tests. If the system is at thermodynamic equilibrium, the loss in

free energy due to the additional stretching of the brushes induced by the presence of the gel, as schematized on Figure 10, might be a way to measure or characterize the energy of the interactions. This elastic energy can be statistically calculated using a Flory-type self-consistent approach:

$$F_{el}(kT/chain) = \frac{h_g^2 - h_w^2}{R_0^2}. \qquad \textbf{Eq. 2}$$

By using this expression with the value of $R_0 \approx 41$ Å and with the results of Chapter 4, we obtain an additional elastic energy in the range of 1.5-6 *kT*/chain. This is much smaller than the in-air thermodynamic work of adhesion and it is also far below the energy of adhesion measured under water with the PDMA-10x2 hydrogel, which is the weakest and of the order of 50 *kT*/chain. The accuracy of neutron reflectivity does not allow to draw direct and simple conclusions, even if the brush is on average more stretched in the case of the PAM gels, which means that its elastic energy restituted when pulling off the gel is slightly higher.

However, other effects are present in the energy of adhesion measured, such as the breakage of the bonds in itself, probably at the origin of a cooperative effect, the possible disentanglement, etc. Also one can invoke a Lake-Thomas type of energy dissipation where the chain in the brush is being stretched before the bonds break.

4- Electrostatic interactions and H-bonding: a comparison

For comparison, hydrogels bearing permanent electrostatic charges were synthesized to compare the effect of the electrostatic interactions with the one involving H-bonds interactions. Etienne Ducrot [17] during his Master's thesis optimized the synthesis of these hydrogels so that their swelling does not vary much with slight variations of ionic strength around 10^{-2} M. The gels were synthesized with *N,N*-dimethylacrylamide (DMA) as main monomer, [2-(methacryloyloxy) ethyl] trimethyl-ammonium chloride (MAETAC) as cationic monomer and *N,N'*-methylene-bis-acrylamide as crosslinker with a ratio 90:10:8. They were dissolved in a 10^{-2} M aqueous solution of NaCl so that the mass ratio water-DMA was equal to 9. The initiation was carried out with the redox initiators KPS and TEMED as described in Chapter 3 ([KPS] = [TEMED] = [DMA]/100). The high degree of cross-linking ensured a high dimensional stability of these hydrogels, named P(DMA_{90}-*co*-$MAETAC_{10}$)-10x8.

Against a PAA brush, the interactions as a function of pH are depicted on Figure 11: at low pH, the PAA brush is neutral and protonated. It is able to form H-bonds with all the

monomers of the hydrogel. At high pH, the brush is anionic and can only form Coulombic interactions with the cationic monomers. As a consequence, at low pH, a great number of H-bonds can be expected, whereas at high pH, a smaller number electrostatic interactions are present.

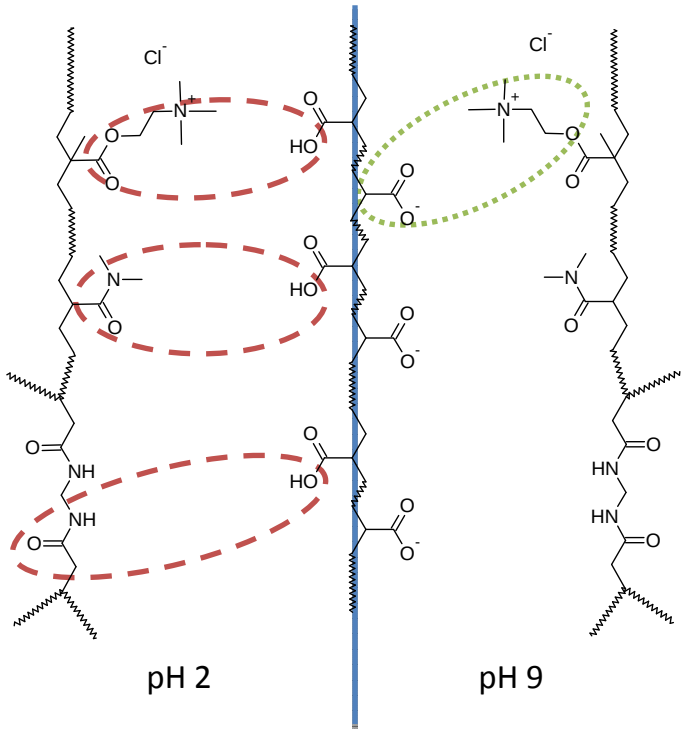

Figure 11 - Schematic representation of the specific interactions occurring at low and high pH between a P(DMA$_{90}$-*co*-MAETAC$_{10}$)-10x8 hydrogel and a PAA brush.

Figure 12 shows the energy of adhesion between the P(DMA$_{90}$-*co*-MAETAC$_{10}$)-10x8 hydrogels and the PAA-l,m brush ($\sigma = 1.0\ 10^{-1}$ chain.nm^{-2}) as a function of contact time at pH 2 and 9. For comparison, the results obtained with an identically cross-linked PDMA-10x8 hydrogel (with no ionized monomer) are presented at pH 2.

The energy of adhesion is clearly increased at pH 9, compared to that at pH 2. The reinforcement of the adhesion is the signature of the reinforcement of the interactions by the apparition of electrostatic bonds, which are definitely stronger than H-bonds, resulting in a macroscopic adhesive effect far stronger. The energy of adhesion at 10^3 s, around 100 mJ.m^{-2} is of the order of magnitude of what was found by La Spina *et al.* [14] for a completely ionizable hydrogel against a permanently charged brush. After 20 min of contact, the energy of adhesion does not vary, meaning that the interactions between the gel and the brush appear

to be at equilibrium. At pH 2, the adhesion is much smaller and much longer to stabilize. Its value remains the same with and without ionized monomers, clearly demonstrating that they do not play a part in the interactions at low pH.

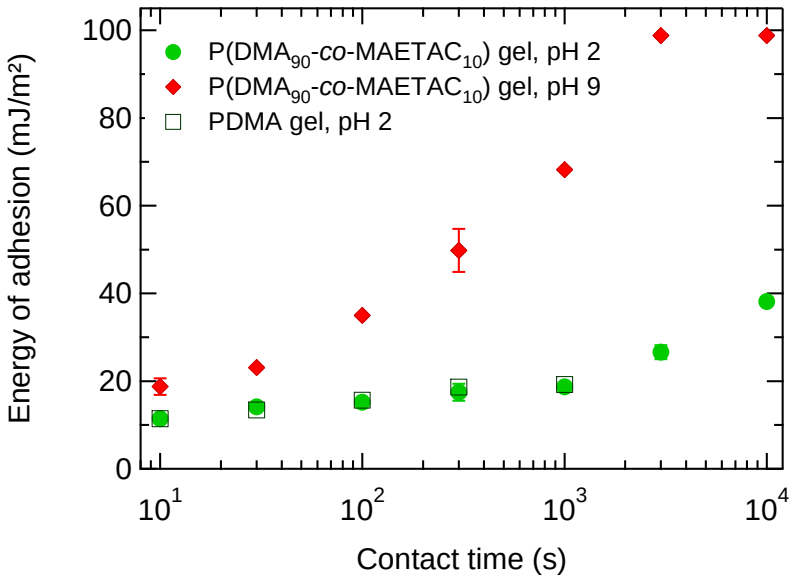

Figure 12 - Energy of adhesion for P(DMA_{90}-*co*-$MAETAC_{10}$)-10x8 hydrogels.

As a conclusion, the Coulombic interactions are an interesting way to obtain strong complexes at interface between the gel and the brush, particularly compared to the H-bonded ones. Here, the macroscopic adhesion was increased up to 5 times between low and high pH. However, the presence of ions in the network tends to make the gel more sensitive towards its environment, and particularly pH and ionic strength. As a consequence, it is mandatory to control its swelling, which is the *sine qua non* condition to keep identical mechanical and structural properties of the gel and hence meaningful comparisons between adhesion forces and energies.

This preliminary work with electrostatic interactions provides some interesting outlooks. First, it is possible to work with a higher ionization rate of the gel, so that the number of interactions and the adhesion are enhanced. Second, the charge distribution can be modified, for instance with the insertion of small polycationic grafts or macromonomers in the bulk of a neutral hydrogel or at its surface. The cooperativity effect observed with H-bonding might be observed, resulting in the reinforcement of the adhesion between the brush and the gel at high pH.

5- Conclusion

The possibility to tune the adhesive properties of a gel by using a polymer brush sensitive towards its environment has been demonstrated. By using a PAA brush, the energy of adhesion was nil at high pH and up to 10 $mJ.m^{-2}$ for PDMA-10x2 hydrogels while it reached 100 $mJ.m^{-2}$ with PAM-10x2 hydrogels at low pH.

Qualitatively, the variation of the adhesion with the pH occurred as expected: adhesion is weaker at a higher pH. In other words, the adhesion decreases when the pH gets closer to the range of pH for which the interpolymer complexes can not form in solution.

We demonstrated that the time of contact and the debonding velocity are key parameters controlling the measured energies of adhesion. Varying systematically equilibration time, contact time and debonding velocity gives access to the kinetics (i) of formation of the complexes at the interface, (ii) to their half-lives and (iii) to the diffusion properties of the pH inside the gels. We show that the establishment of equilibrated H-bonded complexes is particularly long since the energy of adhesion continues to increase as a function of contact time in the range of an hour. We also show that the diffusion of the pH inside the gel is a slow process since with a short equilibration time for the gel, adhesion energies were found positive at pH for which no complexes ought to have been formed.

Between the macroscopic adhesion obtained from H-bonded interfacial complexes and electrostatic or Coulombic complexes, it is demonstrated that the electrostatic complexes lead to a reinforced energy of adhesion, and that the kinetics of reorganization of these complexes seem to be faster.

However, quantitatively, the effect of the change in the monomer structure of the gel, from the PDMA to the PAM, on the magnitude of the measured adhesion changes remains unexplained. Furthermore, the structural analysis of the brush at the interface gives some qualitative information about the adhesive strength but the energy of adhesion which depends on many parameters can not be easily deduced from the neutron reflectivity experiments.

6- References

[1] Netz, R. R.; Andelman, D. *Physics Reports-Review Section of Physics Letters* **2003**, *380*, 1-95.
[2] De Gennes, P. G. *Journal De Physique* **1976**, *37*, 1445-1452.
[3] Alexander, S. *Journal De Physique* **1977**, *38*, 977-981.
[4] Alexander, S. *Journal De Physique* **1977**, *38*, 983-987.
[5] Skvortsov, A. M.; Gorbunov, A. A. *Vysokomolekulyarnye Soedineniya Seriya A* **1986**, *28*, 73-79.
[6] Shull, K. R. *Journal of Chemical Physics* **1991**, *94*, 5723-5738.
[7] Nolte, A. J.; Chung, J. Y.; Walker, M. L.; Stafford, C. M. *Acs Applied Materials & Interfaces* **2009**, *1*, 373-380.
[8] Dejeu, J.; Gauthier, M.; Rougeot, P.; Boireau, W. *Acs Applied Materials & Interfaces* **2009**, *1*, 1966-1973.
[9] Carlsson, L.; Rose, S.; Hourdet, D.; Marcellan, A. *Soft Matter* **2010**, *6*, 3619-3631.
[10] Lin, W. C.; Fan, W.; Marcellan, A.; Hourdet, D.; Creton, C. *Macromolecules* **2010**, *43*, 2554-2563.
[11] Zhang, Z.; Tomlinson, M. R.; Golestanian, R.; Geoghegan, M. *Nanotechnology* **2008**, *19*, 035505.
[12] Siband, E. In *Thèse de Doctorat*: Paris VI, **2009**.
[13] Douglas, B. D.; McDaniel, D. H.; Alexander, J. J. *Concepts and Models of Inorganic Chemistry*, 3rd Edition ed.; John Wiley & Sons: New York, **1994**.
[14] La Spina, R.; Tomlinson, M. R.; Ruiz-Perez, L.; Chiche, A.; Langridge, S.; Geoghegan, M. *Angewandte Chemie-International Edition* **2007**, *46*, 6460-6463.
[15] Brown, H. R. *Macromolecules* **1993**, *26*, 1666-1670.
[16] Brochard-Wyart, F.; De Gennes, P. G.; Leger, L.; Marciano, Y.; Raphael, E. *Journal of Physical Chemistry* **1994**, *98*, 9405-9410.
[17] Ducrot, E. In *Rapport de Stage - Master de Chimie de Paris Centre*: Paris VI, **2010**.

GENERAL CONCLUSION

We investigated the switchable adhesion between pH-sensitive brushes of poly(acrylic acid) (PAA) and neutral hydrogels of poly(acrylamide) (PAM) and poly (*N*,*N*-dimethylacrylamide) (PDMA). These polymers can interact in aqueous solution when the quality as a H-bond donor of the polyacid is strong enough to form complexes with poly(acrylamides) that are H-bond acceptors. Using this fully reversible association that depends on the acidity of the medium, the specific interactions were used at the interface between gels of (poly(acrylamides)) and the brush (PAA) to obtain an immersed adhesion.

In order to determine the type of interactions involved in the complexes of PAA-PAM and of PAA-PDMA and to characterize the experimental parameters that influence the complexation, the association of PAA with homopolymers and copolymers of acrylamide and *N*,*N*-dimethylacrylamide (DMA) was studied in solution. Complexes between PAA and PAM were observed for pH values below 3.3 and they are responsive to temperature over a pH range from 1.8 to 3.3. In this pH range, the transition of solubility is a UCST-type behavior; in other words, the complexation weakens as the temperature increases. With PDMA, PAA forms complexes at pH below 3.75, and for the pH range between 3.45 and 3.75, an LCST-type transition of solubility was observed over a temperature range between 0 and 70°C. The results obtained with the copolymers are intermediate to those of the homopolymers: at a given temperature, the transition of solubility can be adjusted between the two homopolymers by varying the copolymer composition. When the copolymer contains 66 mol% of DMA, the

stability of the formed complex no longer depends on temperature: the LCST component of the association of PDMA with PAA counterbalances exactly the UCST component of PAM.

To transfer the study of these associations at the interfaces, we synthesized the materials needed to obtain a macroscopic reversible adhesion.
The synthesis of PAA brushes was performed by a "grafting onto" strategy. It consists in a simple and reproducible synthesis which leads to well characterized brushes with varying grafting densities. The formation of these brushes takes place in two main steps after silanization of the substrate: grafting and deprotection. Indeed, the acid of the PAA should be protected by a tert-butyl group during the grafting step and the surface must be passivated by grafting oligomers before deprotection. The latter occurs in two stages: the first is a pyrolysis step, which has the advantages of being fast and maintaining a constant grafting density while converting all the chains. It is followed by a soft hydrolysis at pH 2, which leads to (bimodal) brushes of PAA.
The structure of these brushes has been characterized by neutron reflectivity. Thanks to the neutron contrast between the hydrogenated brush and the deuterated water (good solvent of the brush), neutron reflectivity gives access to the profile of the monomer concentration in the direction normal to the substrate. The stretching of the PAA brushes depends on the pH and our results are consistent with the scaling laws and the predicted shapes of the profiles for neutral systems at low pH and charged systems at high pH. We have shown that for very high grafting densities, the swelling of neutral and ionized brushes in good solvent was equivalent. Moreover, for the weakest grafting density of long chains, the bimodal form of the profile was clearly emphasized and the profiles have been successfully deconvoluted to extrapolate the swelling associated with each chain length.

Meanwhile, neutral hydrogels of PDMA and PAM have been synthesized by free radical polymerization. The objective is to optimize the synthesis of these neutral hydrogels in order to perform adhesion tests. Our gels must show a swelling behavior which is insensitive to the changes of environmental conditions (pH, ionic strength, temperature) and a mechanical behavior which is not dissipative. During the synthesis, the cross-linking was performed by adding a co-monomer with a functionality equal to 4, methylene-bis-acrylamide (MBA) during polymerization. This "one-pot" synthesis method has lead to very elastic gels in a simple and reproducible way. The concomitant polymerization and cross-linking is generally the source of gels with high structural defects. The presence of heterogeneities was confirmed

by various characterization methods. The swelling studies, added to the mechanical properties measured by compression tests at equilibrium swelling, were used to measure the elasticity of the network and hence its average density of cross-linker. Finally, it was shown that, whatever the proportion of monomer during the synthesis, a relative concentration of cross-linker could be adjusted so that the gel is formed at equilibrium swelling. This is essential for the synthesis of gels bonded to flat substrates, necessary for the adhesion tests; the gels were covalently attached during the polymerization by adding a co-monomer grafted at the surface of the mold.

The analysis of the structure of the PDMA and PAM hydrogels has been further investigated by a small angle neutron scattering study. We found that the size of the thermal blob for the PAM gels is about twice smaller than that of the PDMA gels. Furthermore, the gels showed the presence of heterogeneities of about 100 Å. A rheology study clearly confirmed the high elasticity of the synthesized hydrogels. However, the moduli obtained with rheology were found different to those from compression tests, which can be explained by a concentration heterogeneity between the bulk and the surface of the gel. A detailed analysis of the surface of the hydrogels performed by neutron reflectivity has shown the effect of the nature of the gel mold. The more hydrophobic the mold is, the stronger the concentration difference between the bulk of the PDMA gel and its surface; the smallest difference was obtained with molds silanized hexamethyldisilazane. Nevertheless, under compression, the surface concentration becomes identical to that in bulk, which corresponds to the case of the adhesion tests.

The observation of the interactions at the interface between the brush of PAA and the gels of PDMA and PAM was performed in two completely distinct ways.

With the first method, at the scale of the brush, we measured the density profile of the brush by neutron reflectivity. After demonstrating that a hydrogenated gel swollen in heavy water did not alter the profile of the PAA brush, we were able to determine the effect of the adsorption of a hydrogel on the conformation of the surface-attached chains. At high pH, in the absence of specific interactions between the brush and the gel, the structure of the brush is the same whether it is swollen in water or in the gel. On the contrary, at low pH and in the presence of interactions, the brush is more swollen in the presence of the gel than in water. Due to specific interactions with the gel, this additional stretching of the brush may exceed the swelling observed with the same brush at pH 9, showing that the specific interactions stretch the chains similarly to the electrostatic repulsion in the weak polyelectrolyte. This effect can be explained by the interpenetration of the brush within the gel.

The second method, which is macroscopic, consists of an adhesion test developed in the laboratory for this thesis. In the absence of standardized test to measure the immersed adhesion involving a soft material, we have developed a flat-flat contact test under water. The advantage of this test is to be close to "real-life" conditions that may be encountered in the marine environment or in some applications of mucoadhesives, such as patches or other healing gels. Our test allows to measure quantitatively and reproductively the energy of adhesion between 1 millimeter-thick gels stuck on quartz plates and brushes attached on 1 centimeter square silicon wafers. The dimensions of the samples give access to quantitative measurements of forces while remaining at the origin of a reasonable confinement that facilitates the alignment between the gel and the brush. The major advantages of this system are to overcome the effects of surface tension – that are always present for swollen materials – while giving the possibility of changing the experimental conditions *in situ* and observing the contact from the side and from below.

The development of this experimental setup and of the protocols suitable for measuring the adhesion between immersed gels and brushes has demonstrated the reversibility of the adhesion with pH. At high pH, the adhesion between the PAA brush and the gels is zero, whereas at low pH, it reaches values around 10 $mJ.m^{-2}$ for PDMA hydrogels and 100 $mJ.m^{-2}$ for PAM hydrogels. Qualitatively, the adhesion decreases with the measured pH; but quantitatively, even if the adhesion remains in the range of thermodynamic energies of surfaces, the differences observed between PDMA and PAM gels remain tricky. The effects of the experimental parameters, such as the contact time, the debonding velocity or the time of equilibration of the gel at a given pH, have been investigated. These parameters are a way to access the kinetics of association and reorganization of the interfacial complexation in their lifetime and the diffusion characteristics of the pH inside the gel. The characteristic times of diffusion in the gel and reorganization of the complexes are rather long, in the range of ten minutes to an hour, while the lifetime of the bonds are rather short. Finally, a comparison with electrostatic interactions was carried out and showed that their presence enhances significantly the adhesion compared to hydrogen bonds alone.

Our project could be continued following diverse ideas.

First, keeping the same monomers and the same interactions, performing more systematic measures of the adhesion between the gel and the brush would provide access to more subtile effects. Varying the chain length or the grafting density of the brush would determine their

impact on the adhesion and on the dynamics associated with them. Changing the gel characteristics (modulus, swelling, random copolymers) would also bring new results. Moreover, the responsiveness of the adhesion to pH has been clearly demonstrated, but new experiments that implicate other stimuli such as temperature or ionic strength would be interesting. Finally, as the PAA forms complexes with many other polymers, the use of new gels would probably give some clues about the differences observed between the adhesion of the PDMA or PAM gels. With new monomers, it is also possible to consider associative phenomena controlled by light or electric field.

CONCLUSION GÉNÉRALE

Nous avons étudié l'adhésion stimulable entre des brosses de poly(acide acrylique) (PAA) stimulables et des hydrogels neutres de poly(acrylamide) (PAM) et poly(*N*,*N*-diméthylacrylamide) (PDMA). Ces polymères peuvent s'associer en solution aqueuse lorsque les qualités de donneur de proton du polyacide sont suffisantes pour une complexation avec les accepteurs de proton que sont les poly(acrylamides). En utilisant cette spécificité d'association totalement réversible qui dépend de l'acidité du milieu, les associations spécifiques ont été utilisées à l'interface entre les gels (poly(acrylamides)) et la brosse (PAA) pour obtenir une adhésion immergée stimulable.

Afin de déterminer le type d'interactions impliquées dans les complexes PAA-PAM et PAA-PDMA et pour caractériser les paramètres expérimentaux qui influencent la complexation, l'association du PAA avec les homopolymères et les copolymères statistiques de l'acrylamide et du *N*,*N*-diméthylacrylamide (DMA) a été étudiée en solution. Des complexes entre le PAA et le PAM ont été observés pour des pH inférieurs à 3.3 et ils se sont révélés sensibles à la température sur une gamme de pH de 1.8 à 3.3. Dans cette gamme de pH, leur transition de solubilité suit un comportement de type UCST, c'est-à-dire que la complexation faiblit à mesure que la température augmente. Avec le PDMA, le PAA forme des complexes pour des pH inférieurs à 3.75, et pour la gamme de pH comprise entre 3.45 et 3.75, une transition de solubilité de type LCST a été observée sur une gamme de température comprise entre 0 et 70°C. Les résultats obtenus avec les copolymères statistiques sont intermédiaires à ceux des

homopolymères : à une température donnée, la transition de solubilité peut être ajustée entre celle des deux homopolymères en jouant sur la composition du copolymère. Lorsque le copolymère statistique contient 66 mol% de DMA, la stabilité du complexe formé ne dépend plus de la température, la composante LCST de l'association du PDMA compensant exactement la composante UCST du PAM.

Afin de pouvoir transférer l'étude de ces associations aux interfaces, nous avons synthétisé les matériaux nécessaires à l'obtention d'une adhésion macroscopique réversible.
La synthèse de brosses de PAA a été réalisée par une stratégie de « grafting onto ». Elle correspond à une synthèse simple pour obtenir de façon reproductible des brosses bien caractérisées de densités de greffage variables. La formation de ces brosses a lieu en deux étapes principales après silanisation du substrat : greffage puis déprotection. En effet, les fonctions acides du PAA doivent être protégées par un groupement *tert*-butyle pendant l'étape de greffage et la surface doit être passivée par un greffage d'oligomères avant la déprotection. Cette dernière s'effectue en deux temps : la première est une étape de pyrolyse, qui présente l'avantage d'être rapide et de conserver un taux de greffage constant tout en convertissant la totalité des chaînes. Elle est suivie d'une hydrolyse douce à pH 2 qui aboutit à l'obtention de brosses (bimodales) de PAA.
La structure de ces systèmes bimodaux a été caractérisée par réflectivité de neutrons. Cette dernière donne accès, grâce au contraste neutronique entre l'hydrogène de la brosse et le deutérium de l'eau (lourde) environnante, au profil de concentration en monomère dans la direction normale au substrat. L'étirement des brosses de PAA dépend du pH et nos résultats sont conformes aux lois d'échelles et aux formes de profil prédictives du comportement des systèmes neutres à pH faible et des systèmes chargés à pH élevé. Nous avons montré qu'à très forte densité de greffage, le gonflement des brosses neutres et chargées en bon solvant était équivalent. Par ailleurs, pour les densités de greffage de chaînes longues les plus faibles, la forme bimodale du profil a été clairement mise en évidence et les profils ont été déconvolués avec succès pour extrapoler le gonflement associé à chaque longueur de chaîne.

Parallèlement, des hydrogels neutres de PDMA et PAM ont été synthétisés par polymérisation radicalaire conventionnelle. L'objectif est d'optimiser la synthèse de ces hydrogels neutres afin de pouvoir effectuer des tests d'adhésion. Il nous faut obtenir des gels dont le gonflement est peu sensible aux variations des conditions environnementales (pH, force ionique, température) et dont le comportement mécanique est peu dissipatif. Lors de la synthèse, la

réticulation a été réalisée par l'ajout d'un co-monomère de fonctionnalité 4, le méthylène-bis-acrylamide (MBA), pendant la polymérisation. Cette méthode de synthèse « one-pot » a permis d'obtenir des gels très élastiques de façon très simple et reproductible. Cette simultanéité de la polymérisation et de la réticulation conduit généralement à des gels présentant de forts défauts de structure. La présence d'hétérogénéités a été confirmée par les différentes méthodes de caractérisation employées. Les études du gonflement jointes aux propriétés mécaniques mesurées par tests de compression à l'équilibre de gonflement, ont permis de mesurer l'élasticité du réseau et par là même sa densité moyenne de réticulation. Finalement, il a été montré que, quelle que soit la proportion de monomère au moment de la synthèse, une concentration relative en réticulant pouvait être ajustée afin que le gel soit formé à l'équilibre de gonflement. Ceci est essentiel pour la synthèse de gels collés sur substrats plans, nécessaires aux tests d'adhésion ; les gels ont été attachés de façon covalente au moment de la polymérisation en ajoutant un co-monomère greffé par silanisation sur le moule de synthèse.

L'analyse de la structure des hydrogels de PDMA et PAM a été approfondie par une étude de diffusion de neutrons aux petits angles qui a révélé que la taille du blob thermique du PAM est environ deux fois plus petite que celle du PDMA et que les gels présentaient des hétérogénéités d'une taille de l'ordre de 100 Å. Une étude de rhéologie a clairement confirmé le caractère très élastique des hydrogels synthétisés. Cependant, des différences de modules ont été observées par rapport aux tests de compression, ce qui s'explique par une hétérogénéité de concentration du gel entre sa masse et sa surface. Une analyse fine de la surface des hydrogels réalisée par réflectivité de neutrons a mis en évidence l'effet de la nature du moule de synthèse du gel. Plus le moule est hydrophobe et plus la différence de concentration en PDMA entre la masse du gel et sa surface est importante : la plus petite différence a été obtenue en utilisant des moules silanisés par phase vapeur avec l'hexaméthyldisilazane. Néanmoins, sous compression, la concentration de surface devient identique à celle en masse, ce qui correspond au cas des tests d'adhésion.

L'observation des interactions à l'interface entre la brosse de PAA et les gels de PDMA et de PAM a été effectuée de deux façons totalement distinctes.

Avec la première méthode, à l'échelle de la brosse, nous avons mesuré le profil de densité de concentration du polymère dans la brosse par réflectivité de neutrons. Après avoir démontré qu'un gel hydrogéné gonflé dans l'eau lourde n'altérait pas la mesure du profil de la brosse de PAA, nous avons pu déterminer l'effet sur la conformation des chaînes de la brosse de

l'adsorption d'un hydrogel. A pH élevé, en l'absence d'interactions spécifiques entre la brosse et le gel, la structure de la brosse est identique qu'elle soit gonflée dans l'eau ou dans le gel. Au contraire, à pH faible et en présence d'interactions, la brosse est plus gonflée en présence du gel que dans l'eau. Cet étirement additionnel de la brosse, dû aux interactions spécifiques avec le gel, peut excéder le gonflement observé pour la même brosse à pH 9, démontrant ainsi que les interactions spécifiques étirent la chaîne similairement à la répulsion électrostatique au sein du polyélectrolyte faible. Cet effet peut s'expliquer par l'interpénétration de la brosse au sein du gel.

La seconde méthode, macroscopique, consiste en un test d'adhésion développé au laboratoire pendant la thèse. En l'absence de test normalisé pour mesurer l'adhésion immergée impliquant un matériau mou, nous avons mis au point un test de contact plan-plan immergé. L'avantage de ce test est d'être proche des conditions qui peuvent être rencontrées en environnement marin ou dans le cadre de la mucoadhesion, pour des patches ou autres gels cicatrisants. Ce test permet de mesurer quantitativement et de façon reproductive l'énergie d'adhésion entre des gels d'un millimètre d'épaisseur collés sur plaque de quartz et des brosses fonctionnalisant des wafers de silicium d'un centimètre carré. Les dimensions des échantillons permettent des mesures quantitatives des forces tout en restant à l'origine d'un confinement raisonnable qui permette un alignement facile entre le gel et la brosse. Les atouts majeurs de ce système sont de s'affranchir des effets de tension de surface toujours présents pour des matériaux gonflés, tout en donnant la possibilité de modifier les conditions expérimentales *in situ* et en menant des observations du contact latérale et par en-dessous.
La mise au point de ce montage expérimental et des protocoles adaptés à la mesure de l'adhésion immergée entre les gels et les brosses a permis de démontrer sa réversibilité en fonction du pH. A pH élevé, l'adhésion entre la brosse de PAA et les gels est nulle, alors qu'à pH faible, elle atteint des valeurs de l'ordre de 10 $mJ.m^{-2}$ pour les hydrogels de PDMA et 100 $mJ.m^{-2}$ pour ceux de PAM. Qualitativement, l'adhésion mesurée diminue avec le pH mais quantitativement, même si l'on reste sur des ordres de grandeur d'adhésion thermodynamique, la différence de magnitude observée entre des gels de PDMA et de PAM reste difficile à expliquer. Les effets cruciaux des paramètres de l'expérience, que sont le temps de contact, la vitesse de détachement ou le temps d'équilibration du gel à un pH donné, ont été étudiés. Il a été montré qu'ils donnent accès aux cinétiques d'association et de réorganisation des complexes interfaciaux, à leur temps de vie ainsi qu'aux propriétés de diffusion du pH dans le gel. Les temps caractéristiques de diffusion dans le gel et de

réorganisation des complexes sont plutôt longs, de l'ordre de la dizaine de minutes à l'heure alors que les temps de vie des liaisons sont plutôt courts. Enfin, une comparaison avec les interactions électrostatiques a été menée et a permis de montrer qu'elles renforcent de façon considérable l'adhésion par rapport aux liaisons hydrogènes.

Ce travail de thèse peut être approfondi en suivant plusieurs pistes.
Tout d'abord, en gardant sur les mêmes monomères et les mêmes interactions, des mesures plus systématiques de l'adhésion entre les gels et la brosse donneraient accès à des effets plus fins. Des variations de la longueur des chaînes ou la densité de greffage de la brosse permettraient de déterminer leur impact sur l'adhésion et sur les dynamiques qui y sont associées. Des modifications des caractéristiques du gel (module, gonflement, copolymères statistiques) apporteraient aussi des résultats nouveaux. Par ailleurs, la stimulation de l'adhésion par le pH a clairement été mise en évidence, mais des tests faisant varier d'autres stimuli, comme la température ou la force ionique seraient intéressants. Enfin, comme le PAA forme des complexes avec de nombreux autres polymères, des tests avec de nouveaux gels permettraient peut-être d'expliquer les différences d'adhésion observées entre ceux de PDMA et de PAM. Avec de nouveaux monomères, il est aussi possible d'envisager des phénomènes associatifs contrôlés par la lumière ou encore le champ électrique.

ANNEX: NEUTRON REFLECTIVITY EXPERIMENTS

As mentioned previously, neutron or X-ray reflectivity are the only available methods with a sufficient resolution to investigate the conformation of solvated polymeric chains grafted on planar solid surfaces. Because we do not have heavy atoms in our polymers, neutron reflectivity using partially deuterated media is the technique of choice. The strength of the neutron reflectivity or neutron scattering techniques comes from the strong difference between the neutron scattering lengths of hydrogen and deuterium. It is possible then to create an enhanced contrast by the selective deuteration of one of the components of the system while keeping a nearly equivalent chemical structure. In our case, hydrogenated polymer brushes are swollen in a deuterated solvent.

Principle

The specular neutron reflectivity is sensitive to the coherent scattering length density profile in the direction normal to the interface, noted $\rho(z)$. The scattering length density can be related to the local atomic composition of the material and its density by:

$$\rho = \sum_i n_i b_i \,, \qquad \textbf{Eq. 1}$$

where n_i is the volume density of atoms i and b_i is the coherent scattering length of the atom i. The neutron scattering length density is about 10^{-6} Å^{-2}. As the volume concentration in polymer varies with respect to the distance from the surface z, so does ρ. In the kinematical

approximation, the reflectivity – which is the ratio of the reflected beam intensity to the incident beam intensity – can be expressed as a function of Fresnel reflectivity $R_F(q)$ and the wave vector q:

$$R(q) = R_F(q)\left|\int_0^{+\infty} \frac{d\rho}{dz}\exp(2iq.z).dz\right|^2, \quad \textbf{Eq. 2}$$

with k the wave vector equal to:

$$q = \frac{4\pi}{\lambda}\sin\theta, \quad \textbf{Eq. 3}$$

where λ is the neutron wavelength and $(\pi/2-\theta)$ the angle of incidence.

Fresnel reflectivity corresponds to the reflectivity of the abrupt interface between two homogeneous media with two different coherent scattering length densities ρ_1 and ρ_2. Fresnel reflectivity $R_F(q)$ is related to the critical wave vector q_c, which can be expressed as:

$$q_c = \sqrt{4\pi(\rho_2 - \rho_1)}, \quad \textbf{Eq. 4}$$

by the following relationship:

$$R_F(q) = \left|\frac{1-\sqrt{1-\frac{q_c^2}{q^2}}}{1+\sqrt{1-\frac{q_c^2}{q^2}}}\right|^2. \quad \textbf{Eq. 5}$$

For wave vectors inferior to the critical wave vector, the reflection is total ($R(q \le q_c) = 1$).

Experimental section

Neutron reflectivity measurements were performed at silicon-liquid interface on the reflectometer EROS at the Laboratoire Léon Brillouin, CEA-Saclay (France), under Fabrice Cousin's watchful and kind eye. We used protonated polymer brushes and deuterated water in order to enhance the contrast between the polymer and the solvent and to optimize the reflectivity signal.

Out of the wave guide, the multi-wavelength neutron beam first goes through a chopper which selects wave packets with the fastest propagating wavelength equal to 3 Å and the slowest one at 25 Å, as the velocity v of the neutron (of mass m_n) depends on its wavelength λ through De Broglie's relation:

$$v = \frac{h_P}{m_n\lambda}, \quad \textbf{Eq. 6}$$

with h_P the Planck constant. The beam is then collimated, sent through the silicon on the interface of the sample (see Figure 1) and detected. The "time of flight" method is used to determine the wavelength of the neutron detected according to Eq. 6.

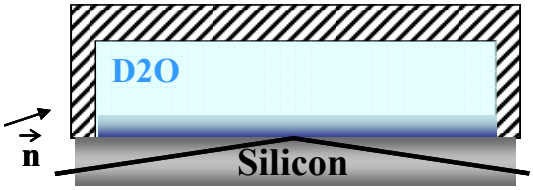

Figure 1 - Schematic drawing of the neutron reflectivity experimental set-up: a Teflon trough is filled with deuterium oxide and the silicon grafted surface is tightly clamped against it. An adapted copper heater could be adjusted on top of the Teflon trough to regulate the temperature.

A more accurate representation of the sample holder is given in Figure 2.

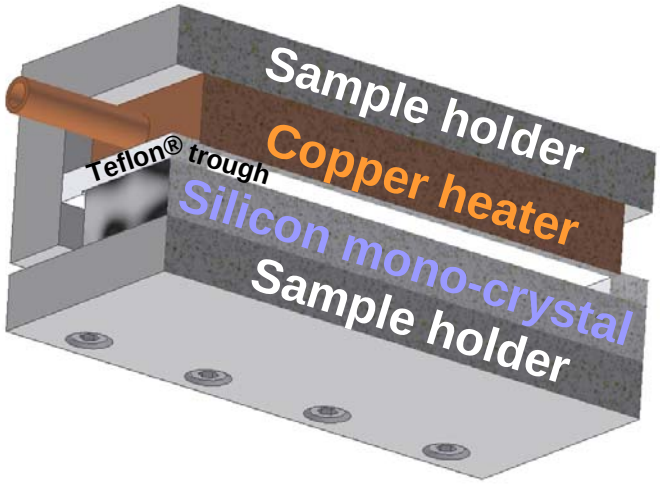

Figure 2 - Schematic cut of the samples used for the measurement of neutron reflectivity. The sample holder maintain together the silicon mono-crystal in contact with a Teflon® trough in which is placed the immersing medium (deuterated chloroform $CDCl_3$, deuterium oxide D_2O, or deuterium oxide swollen gel). This trough can be heated with a copper heater through which thermostated fluid is circulated.

The sample was tilted to optimize the signal measured and the detector was placed accordingly to the second semi-infinite media, so that the angle θ was set to 1.34° for deuterium oxide or deuterium oxide swollen gel and 0.67° for deuterated chloroform.

Determination of the polymer density profile

The reflectivity curves were normalized with respect to the total reflection plateau (for $q \leq q_c$). As the relation Eq. 2 cannot be invertible, the reflectivity curves need to be fitted to a simulated scattering density profile which best fits the experimental data. A reliable model-

independent method was chosen to determine $\rho(z)$. The brush was modeled as a set of layers, each characterized by a fixed thickness h_i and a scattering length density ρ_i for the layer i starting at the distance z_i from the surface. Two adjacent layers were connected using error functions of fixed width σ_i to get a continuous profile. The procedure consisted of choosing a scattering length density profile and finding the corresponding parameters for which the calculated reflectivity curve fits the best the experimental reflectivity data. The best fits are found in the least-squares sense, the residuals being the difference of the logarithms of the reflectivity data and of the calculated reflectivity, weighted by the signal-to-noise ratio.

This reliable method allowed the determination of a continuous scattering length density profile without making any assumption about its analytical form. The polymer density profile $\phi(z)$ was then deduced from $\rho(z)$, knowing the coherent scattering densities of the polymer ρ_{pol} and of deuterium oxide ρ_{D_2O}:

$$\phi(z) = \frac{\rho(z) - \rho_{D_2O}}{\rho_{pol} - \rho_{D_2O}}. \qquad \textbf{Eq. 7}$$

Calculated from the polymer density profile using:

$$\gamma = \int_0^{+\infty} \phi(z).dz, \qquad \textbf{Eq. 8}$$

the length γ is an important parameter because it is independent of the shape of $\phi(z)$. It corresponds to the thickness of the dry layer and has to be compared with the values measured by another technique such as ellipsometry. Profiles fitting well the experimental data but suggesting an unsuitable amount of grafted polymer are discarded.

The Table 1 lists the scattering length densities used along the fitting process.

Material	$\rho.10^6$ $\left(Å^{-2}\right)$, for the interface Si-Air	$\left(\rho - \rho_{Si}\right).10^6$ $\left(Å^{-2}\right)$, for the interface Si-D_2O
Silicon	2.07	0.00
Silica	3.47	1.40
Silane (GPS)	0.28	-1.79
Deuterium oxide	6.38	4.31
PAA	1.70	-0.37

Table 1 - Neutron coherent scattering length densities of various materials.

LIST OF REFERENCES - LISTES DES REFERENCES

Books, Book Chapters and Thesis

[1] Advincula, R. C.; Brittain, W. J.; Caster, K. C.; Rühe, J. *Polymer Brushes*; Wiley-VCH: Weinheim (Allemagne), **2004**.

[2] De Gennes, P. G. *Scaling Concepts in Polymer Physics*, 1st ed.; Cornell University Press: New York, **1979**.

[3] Douglas, B. D.; McDaniel, D. H.; Alexander, J. J. *Concepts and Models of Inorganic Chemistry*, 3rd Edition ed.; John Wiley & Sons: New York, **1994**.

[4] Flory, P. J. *Principles of Polymer Chemistry*; Cornell University Press, **1971**.

[5] Israelachvili, J. N. *Intermolecular and Surface Forces*, 2nd Edition ed.; Academic Press: New York, **1992**.

[6] Kendall, K. *Molecular Adhesion and its Applications: the Sticky Universe*; Kluwer: New York, **2001**.

[7] Mark, J. E.; Erman, B. *Rubberlike Elasticity - A Molecular Primer*; John Wiley & Sons: New York, **1988**.

[8] Pocius, A. V. *Adhesion and Adhesives Technology: an Introduction*, 2nd Edition ed.; Carl Hanser Verlag: Munich, **2002**.

[9] Brandrup, J.; Immergut, E. H.; Grulke, E. A.; Kurata, M.; Tsunashima, Y. *Polymer Handbook*, 4th ed.; Wiley Interscience: New York, **1999**; Vol. Viscosity - Molecular Weight Relationships and Unperturbed Dimensions of Linear Chain Molecules.

[10] Khutoryanskiy, V. V.; Dubolazov, A. V.; Mun, G. A. In *Hydrogen-bonded interpolymer complexes. Formation, structure and applications.*; Khutoryanskiy, V. V.; Staikos, G., Eds.; World Scientific, **2009**; p 376.

[11] Shibayama, M. *Small Angle Neutron Scattering on Gels*; Springer-Verlag: Berlin Heidelberg, **2008**; Vol. 14.

[12] Hägerström, H. In *Comprehensive Summaries of Uppsala Dissertations from the Faculty of Pharmacy*: Uppsala, **2003**.

[13] Miquelard-Garnier, G. In *Thèse de Doctorat*: Paris VI, **2008**.

[14] Sanjuan, S. In *Thèse de Doctorat*: Paris VI, **2007**.

[15] Siband, E. In *Thèse de Doctorat*: Paris VI, **2009**.

[16] Ducrot, E. In *Rapport de Stage - Master de Chimie de Paris Centre*: Paris VI, **2010**.

Articles

Alexander, S. *J Phys-Paris* **1977**, *38*, 983-987.

Alexander, S. *J Phys-Paris* **1977**, *38*, 977-981.

Anamelechi, C. C.; Truskey, G. A.; Reichert, W. M. *Biomaterials* **2005**, *26*, 6887-6896.

Aoki, T.; Kawashima, M.; Katono, H.; Sanui, K.; Ogata, N.; Okano, T.; Sakurai, Y. *Macromolecules* **1994**, *27*, 947-952.

Arleth, L.; Xia, X. H.; Hjelm, R. P.; Wu, J. Z.; Hu, Z. B. *J Polym Sci Pol Phys* **2005**, *43*, 849-860.

Awaja, F.; Gilbert, M.; Kelly, G.; Fox, B.; Pigram, P. J. *Prog Polym Sci* **2009**, *34*, 948-968.

Ayres, N.; Boyes, S. G.; Brittain, W. J. *Langmuir* **2007**, *23*, 182-189.

Ayres, N.; Cyrus, C. D.; Brittain, W. J. *Langmuir* **2007**, *23*, 3744-3749.
Bekturov, E. A.; Bimendina, L. A. *Advances in Polymer Science* **1981**, *41*, 99-147.
Bian, F. L.; Liu, M. Z. *Eur Polym J* **2003**, *39*, 1867-1874.
Biesalski, M.; Johannsmann, D.; Ruhe, J. *J. Chem. Phys.* **2002**, *117*, 4988-4994.
Biesalski, M.; Ruhe, J. *Macromolecules* **2002**, *35*, 499-507.
Biesalski, M.; Ruhe, J. *Macromolecules* **2004**, *37*, 1166-1166.
Bokias, G.; Durand, A.; Hourdet, D. *Macromol Chem Physic* **1998**, *199*, 1387-1392.
Borisov, O. V.; Birshtein, T. M.; Zhulina, E. B. *J Phys Ii* **1991**, *1*, 521-526.
Brochard-Wyart, F.; De Gennes, P. G.; Leger, L.; Marciano, Y.; Raphael, E. *J Phys Chem-Us* **1994**, *98*, 9405-9410.
Brochard-Wyart, F.; De Gennes, P. G. *J Adhesion* **1996**, *57*, 21-30.
Brown, H. R. *Macromolecules* **1993**, *26*, 1666-1670.
Burkett, J. R.; Wojtas, J. L.; Cloud, J. L.; Wilker, J. J. *J Adhesion* **2009**, *85*, 601-615.
Butt, H. J.; Jaschke, M.; Ducker, W. *Bioelectroch Bioener* **1995**, *38*, 191-201.
Caldorera-Moore, M.; Peppas, N. A. *Adv Drug Deliver Rev* **2009**, *61*, 1391-1401.
Candau, S.; Bastide, J.; Delsanti, M. *Advances in Polymer Science* **1982**, *44*, 27-71.
Carlsson, L.; Rose, S.; Hourdet, D.; Marcellan, A. *Soft Matter* **2010**, *6*, 3619-3631.
Chai, L.; Klein, J. *Langmuir* **2009**, *25*, 11533-11540.
Chan, D. Y. C.; Horn, R. G. *J. Chem. Phys.* **1985**, *83*, 5311-5324.
Chaudhury, M. K.; Whitesides, G. M. *Langmuir* **1991**, *7*, 1013-1025.
Chen, H.; Zajac, R.; Chakrabarti, A. *J. Chem. Phys.* **1996**, *104*, 1579-1588.
Chen, Y. M.; Yang, J. J.; Gong, J. P. *J Adhesion* **2009**, *85*, 839-868.
Chen, T.; Ferris, R.; Zhang, J. M.; Ducker, R.; Zauscher, S. *Prog Polym Sci* **2010**, *35*, 94-112.
Christenson, H. K.; Claesson, P. M. *Adv Colloid Interfac* **2001**, *91*, 391-436.
Claesson, P. M.; Ederth, T.; Bergeron, V.; Rutland, M. W. *Adv Colloid Interfac* **1996**, *67*, 119-183.
Collett, J.; Crawford, A.; Hatton, P. V.; Geoghegan, M.; Rimmer, S. *J R Soc Interface* **2007**, *4*, 117-126.
Cooperstein, M. A.; Canavan, H. E. *Langmuir* **2010**, *26*, 7695-7707.
Creton, C.; Kramer, E. J.; Hui, C. Y.; Brown, H. R. *Macromolecules* **1992**, *25*, 3075-3088.
Cullen, S. P.; Liu, X.; Mandel, I. C.; Himpsel, F. J.; Gopalan, P. *Langmuir* **2008**, *24*, 913-920.
Currie, E. P. K.; Wagemaker, M.; Stuart, M. A. C.; van Well, A. A. *Macromolecules* **1999**, *32*, 9041-9050.
Currie, E. P. K.; Sieval, A. B.; Fleer, G. J.; Stuart, M. A. C. *Langmuir* **2000**, *16*, 8324-8333.
Currie, E. P. K.; Norde, W.; Stuart, M. A. C. *Adv Colloid Interfac* **2003**, *100*, 205-265.
Czeslik, C.; Jackler, G.; Hazlett, T.; Gratton, E.; Steitz, R.; Wittemann, A.; Ballauff, M. *Phys Chem Chem Phys* **2004**, *6*, 5557-5563.
Dan, N.; Tirrell, M. *Macromolecules* **1993**, *26*, 6467-6473.
De Buyl, F.; Kretschmer, A. *J Adhesion* **2008**, *84*, 125-142.
De Gennes, P. G. *J Phys-Paris* **1976**, *37*, 1445-1452.
De Gennes, P. G. *Macromolecules* **1980**, *13*, 1069-1075.
DeAscentiis, A.; Degrazia, J. L.; Bowman, C. N.; Colombo, P.; Peppas, N. A. *J Control Release* **1995**, *33*, 197-201.
DeAscentiis, A.; Colombo, P.; Peppas, N. A. *Eur J Pharm Biopharm* **1995**, *41*, 229-234.
Decher, G. *Science* **1997**, *277*, 1232-1237.
Dejeu, J.; Gauthier, M.; Rougeot, P.; Boireau, W. *Acs Appl Mater Inter* **2009**, *1*, 1966-1973.
Deng, L.; Wang, C. H.; Li, Z. C.; Liang, D. H. *Macromolecules* **2010**, *43*, 3004-3010.
Dominguez-Espinosa, G.; Synytska, A.; Drechsler, A.; Gutsche, C.; Kegler, K.; Uhlmann, P.; Stamm, M.; Kremer, F. *Polymer* **2008**, *49*, 4802-4807.
Dong, R.; Lindau, M.; Ober, C. K. *Langmuir* **2009**, *25*, 4774-4779.

Dormidontova, E.; ten Brinke, G. *Macromolecules* **1998**, *31*, 2649-2660.
Dormidontova, E. E. *Macromolecules* **2002**, *35*, 987-1001.
Drury, J. L.; Mooney, D. J. *Biomaterials* **2003**, *24*, 4337-4351.
Ducker, W. A.; Senden, T. J.; Pashley, R. M. *Nature* **1991**, *353*, 239-241.
Erath, J.; Schmidt, S.; Fery, A. *Soft Matter* **2010**, *6*, 1432-1437.
Eustace, D. J.; Siano, D. B.; Drake, E. N. *J Appl Polym Sci* **1988**, *35*, 707-716.
Field, J. B.; Toprakcioglu, C.; Dai, L.; Hadziioannou, G.; Smith, G.; Hamilton, W. *J Phys Ii* **1992**, *2*, 2221-2235.
Figueruelo, J. E.; Monzo, I. S.; Gomez, C. M.; Soria, V.; Abad, C.; Campos, A. *Macromol Theor Simul* **2007**, *16*, 62-76.
Figueruelo, J. E.; Garcia-Lopera, R.; Monzo, I. S.; Abad, C.; Campos, A. *Express Polym Lett* **2008**, *2*, 313-329.
Flammang, P.; Ribesse, J.; Jangoux, M. *Integr Comp Biol* **2002**, *42*, 1107-1115.
Flammang, P.; Lambert, A.; Bailly, P.; Hennebert, E. *J Adhesion* **2009**, *85*, 447-464.
Flory, P. J. *Faraday Discussions of the Chemical Society* **1974**, *57*, 7-18.
Flory, A. L.; Brass, D. A.; Shull, K. R. *J Polym Sci Pol Phys* **2007**, *45*, 3361-3374.
Gong, J. P.; Kagata, G.; Osada, Y. *J Phys Chem B* **1999**, *103*, 6007-6014.
Gong, J. P.; Osada, Y. *Prog Polym Sci* **2002**, *27*, 3-38.
Gong, J. P.; Katsuyama, Y.; Kurokawa, T.; Osada, Y. *Adv Mater* **2003**, *15*, 1155-+.
Gong, J. P.; Kii, A.; Xu, J.; Hattori, Y.; Osada, Y. *J Phys Chem B* **2001**, *105*, 4572-4576.
Gong, J. P. *Soft Matter* **2006**, *2*, 544-552.
Granfeldt, M. K.; Miklavic, S. J.; Marcelja, S.; Woodward, C. E. *Macromolecules* **1990**, *23*, 4760-4768.
Gundogan, N.; Okay, O.; Oppermann, W. *Macromol Chem Physic* **2004**, *205*, 814-823.
Guvendiren, M.; Brass, D. A.; Messersmith, P. B.; Shull, K. R. *J Adhesion* **2009**, *85*, 631-645.
Haidara, H.; Chaudhury, M. K.; Owen, M. J. *J Phys Chem-Us* **1995**, *99*, 8681-8683.
Hammer, D. A.; Tirrell, M. *Annu Rev Mater Sci* **1996**, *26*, 651-691.
Haraguchi, K.; Li, H. J.; Okumura, N. *Macromolecules* **2007**, *40*, 2299-2302.
Hägerström, H.; Edsman, K. *J Pharm Pharmacol* **2001**, *53*, 1589-1599.
Hägerström, H.; Bergström, C. A. S.; Edsman, K. *J Pharm Pharmacol* **2004**, *56*, 161-168.
Henriquez, C.; Bueno, C.; Lissi, E. A.; Encinas, M. V. *Polymer* **2003**, *44*, 5559-5561.
Hollmann, O.; Czeslik, C. *Langmuir* **2006**, *22*, 3300-3305.
Hollmann, O.; Gutberlet, T.; Czeslik, C. *Langmuir* **2007**, *23*, 1347-1353.
Hollmann, O.; Steitz, R.; Czeslik, C. *Phys Chem Chem Phys* **2008**, *10*, 1448-1456.
Horkay, F.; Hecht, A. M.; Mallam, S.; Geissler, E.; Rennie, A. R. *Macromolecules* **1991**, *24*, 2896-2902.
Horkay, F.; Hecht, A. M.; Geissler, E. *Macromolecules* **1994**, *27*, 1795-1798.
Horkay, F.; Hecht, A. M.; Zrinyi, M.; Geissler, E. *Polym Gels Netw* **1996**, *4*, 451-465.
Howarter, J. A.; Youngblood, J. P. *Adv Mater* **2007**, *19*, 3838-+.
Huang, Y.; Leobandung, W.; Foss, A.; Peppas, N. A. *J Control Release* **2000**, *65*, 63-71.
Huang, Y. B.; Szleifer, I.; Peppas, N. A. *J. Chem. Phys.* **2001**, *114*, 3809-3816.
Ikawa, T.; Abe, K.; Honda, K.; Tsuchida, E. *J Polym Sci Pol Chem* **1975**, *13*, 1505-1514.
Ishida, M.; Nambu, N.; Nagai, T. *Chem Pharm Bull* **1983**, *31*, 1010-1014.
Israelachvili, J. N.; Adams, G. E. *Nature* **1976**, *262*, 773-776.
Israelachvili, J. N.; Adams, G. E. *J Chem Soc Farad T 1* **1978**, *74*, 975-&.
Israelachvili, J. N.; Pashley, R. M. *Nature* **1983**, *306*, 249-250.
Iwata, R.; Satoh, R.; Iwasaki, Y.; Akiyoshi, K. *Colloid Surface B* **2008**, *62*, 288-298.
Joanny, J. F.; Johner, A.; Vilgis, T. A. *Eur Phys J E* **2001**, *6*, 201-209.
Joanny, J. F. *Interface Sci* **2003**, *11*, 157-158.
Johnson, K. L.; Kendall, K.; Roberts, A. D. *Proc R Soc Lon Ser-A* **1971**, *324*, 301-&.

Kabanov, V. A.; Papisov, I. M. *Vysokomolekulyarnye Soedineniya Seriya A* **1979**, *21*, 243-281.
Kamino, K. *J Adhesion* **2010**, *86*, 96-110.
Kent, M. S.; Factor, B. J.; Satija, S.; Gallagher, P.; Smith, G. S. *Macromolecules* **1996**, *29*, 2843-2849.
Khandeparker, L.; Anil, A. C. *Int J Adhes Adhes* **2007**, *27*, 165-172.
Klein, J. *Annu Rev Mater Sci* **1996**, *26*, 581-612.
Ku, S. H.; Lee, J. S.; Park, C. B. *Langmuir* **2010**, *26*, 15104-15108.
Kulkarni, S. A.; Mirji, S. A.; Mandale, A. B.; Gupta, R. P.; Vijayamohanan, K. P. *Mater Lett* **2005**, *59*, 3890-3895.
Kurokawa, T.; Gong, J. P.; Osada, Y. *Macromolecules* **2002**, *35*, 8161-8166.
Kurokawa, T.; Furukawa, H.; Wang, W.; Tanaka, Y.; Gong, J. P. *Acta Biomater* **2010**, *6*, 1353-1359.
La Spina, R.; Tomlinson, M. R.; Ruiz-Perez, L.; Chiche, A.; Langridge, S.; Geoghegan, M. *Angew Chem Int Edit* **2007**, *46*, 6460-6463.
Lai, P. Y.; Binder, K. *J. Chem. Phys.* **1992**, *97*, 586-595.
Lai, P. Y.; Zhulina, E. B. *Macromolecules* **1992**, *25*, 5201-5207.
Laloyaux, X.; Mathy, B.; Nysten, B.; Jonas, A. M. *Langmuir* **2010**, *26*, 838-847.
Leckband, D. *Cell Mol Bioeng* **2008**, *1*, 312-326.
Lee, H. I.; Pietrasik, J.; Sheiko, S. S.; Matyjaszewski, K. *Prog Polym Sci* **2010**, *35*, 24-44.
Leger, L.; Raphael, E.; Hervet, H. *Adv Polym Sci* **1999**, *138*, 185-225.
Leger, L.; Creton, C. *Philos T R Soc A* **2008**, *366*, 1425-1442.
Lego, B.; Skene, W. G.; Giasson, S. *Macromolecules* **2010**, *43*, 4384-4393.
Leibler, L.; Rubinstein, M.; Colby, R. H. *Macromolecules* **1991**, *24*, 4701-4707.
Leung, S. H. S.; Robinson, J. R. *J Control Release* **1990**, *12*, 187-194.
Leung, S. H. S.; Robinson, J. R. *Acs Sym Ser* **1991**, *467*, 350-366.
Levicky, R.; Koneripalli, N.; Tirrell, M.; Satija, S. K. *Macromolecules* **1998**, *31*, 2616-2621.
Li, B.; Xu, L.; Wu, Q.; Chen, T.; Sun, P.; Jin, Q.; Ding, D.; Wang, X.; Xue, G.; Shi, A. C. *Macromolecules* **2007**, *40*, 5776-5786.
Lin, W. C.; Shull, K. R.; Hui, C. Y.; Lin, Y. Y. *J. Chem. Phys.* **2007**, *127*.
Lin, A. Y. M.; Brunner, R.; Chen, P. Y.; Talke, F. E.; Meyers, M. A. *Acta Mater* **2009**, *57*, 4178-4185.
Lin, W. C.; Fan, W.; Marcellan, A.; Hourdet, D.; Creton, C. *Macromolecules* **2010**, *43*, 2554-2563.
Liu, H. Y.; Zhu, X. X. *Polymer* **1999**, *40*, 6985-6990.
Liu, G. M.; Zhang, G. Z. *J Phys Chem B* **2008**, *112*, 10137-10141.
Loskofsky, C.; Song, F.; Newby, B. M. Z. *J Adhesion* **2006**, *82*, 713-730.
Luckham, P. F. *Adv Colloid Interfac* **2004**, *111*, 29-47.
Luzinov, I.; Julthongpiput, D.; Liebmann-Vinson, A.; Cregger, T.; Foster, M. D.; Tsukruk, V. V. *Langmuir* **2000**, *16*, 504-516.
Luzinov, I.; Julthongpiput, D.; Malz, H.; Pionteck, J.; Tsukruk, V. V. *Macromolecules* **2000**, *33*, 1043-1048.
Maeda, N.; Chen, N. H.; Tirrell, M.; Israelachvili, J. N. *Science* **2002**, *297*, 379-382.
Malham, I. B.; Bureau, L. *Langmuir* **2010**, *26*, 4762-4768.
Mallam, S.; Horkay, F.; Hecht, A. M.; Rennie, A. R.; Geissler, E. *Macromolecules* **1991**, *24*, 543-548.
McCormick, C. L.; Chen, G. S. *J Polym Sci Pol Chem* **1984**, *22*, 3633-3647.
Milner, S. T.; Witten, T. A.; Cates, M. E. *Europhys Lett* **1988**, *5*, 413-418.
Milner, S. T.; Witten, T. A.; Cates, M. E. *Macromolecules* **1988**, *21*, 2610-2619.
Milner, S. T.; Witten, T. A.; Cates, M. E. *Macromolecules* **1989**, *22*, 853-861.

Milner, S. T. *Science* **1991**, *251*, 905-914.
Minko, S.; Patil, S.; Datsyuk, V.; Simon, F.; Eichhorn, K. J.; Motornov, M.; Usov, D.; Tokarev, I.; Stamm, M. *Langmuir* **2002**, *18*, 289-296.
Miquelard-Garnier, G.; Demoures, S.; Creton, C.; Hourdet, D. *Macromolecules* **2006**, *39*, 8128-8139.
Monteux, C.; Tay, A.; Narita, T.; De Wilde, Y.; Lequeux, F. *Soft Matter* **2009**, *5*, 3713-3717.
Motornov, M.; Sheparovych, R.; Katz, E.; Minko, S. *Acs Nano* **2008**, *2*, 41-52.
Muller, P.; Sudre, G.; Theodoly, O. *Langmuir* **2008**, *24*, 9541-9550.
Mun, G. A.; Nurkeeva, Z. S.; Khutoryanskiy, V. V.; Sarybayeva, G. S.; Dubolazov, A. V. *Eur Polym J* **2003**, *39*, 1687-1691.
Murat, M.; Grest, G. S. *Phys Rev Lett* **1989**, *63*, 1074-1077.
Naji, A.; Seidel, C.; Netz, R. R. *Surface- Initiated Polymerization Ii* **2006**, *198*, 149-183.
Nakajima, T.; Furukawa, H.; Tanaka, Y.; Kurokawa, T.; Osada, Y.; Gong, J. P. *Macromolecules* **2009**, *42*, 2184-2189.
Netz, R. R.; Schick, M. *Europhys Lett* **1997**, *38*, 37-42.
Netz, R. R.; Schick, M. *Macromolecules* **1998**, *31*, 5105-5122.
Netz, R. R.; Andelman, D. *Phys Rep* **2003**, *380*, 1-95.
Neuman, K. C.; Nagy, A. *Nat Methods* **2008**, *5*, 491-505.
Nolte, A. J.; Chung, J. Y.; Walker, M. L.; Stafford, C. M. *Acs Appl Mater Inter* **2009**, *1*, 373-380.
Norisuye, T.; Masui, N.; Kida, Y.; Ikuta, D.; Kokufuta, E.; Ito, S.; Panyukov, S.; Shibayama, M. *Polymer* **2002**, *43*, 5289-5297.
Nurkeeva, Z. S.; Mun, G. A.; Khutoryanskiy, V. V.; Bitekenova, A. B.; Dubolazov, A. V.; Esirkegenova, S. Z. *Eur Phys J E* **2003**, *10*, 65-68.
Obukhov, S. P.; Rubinstein, M.; Colby, R. H. *Macromolecules* **1994**, *27*, 3191-3198.
Olivieri, M. P.; Wollman, R. M.; Hurley, M. I.; Swartz, M. F. *J Adhesion* **2010**, *86*, 111-130.
Orakdogen, N.; Okay, O. *J Appl Polym Sci* **2007**, *103*, 3228-3237.
Ortiz, C.; Hadziioannou, G. *Macromolecules* **1999**, *32*, 780-787.
Panyukov, S.; Rabin, Y. *Phys Rep* **1996**, *269*, 1-131.
Papaefthimiou, V.; Steitz, R.; Findenegg, G. H. *Chem Unserer Zeit* **2008**, *42*, 102-115.
Parker, J. L.; Christenson, H. K.; Ninham, B. W. *Rev Sci Instrum* **1989**, *60*, 3135-3138.
Peng, M.; Gong, J. P.; Osada, Y. *The Chemical Record* **2003**, *3*, 40-50.
Peppas, N. A.; Sahlin, J. J. *Biomaterials* **1996**, *17*, 1553-1561.
Peppas, N. A.; Keys, K. B.; Torres-Lugo, M.; Lowman, A. M. *J Control Release* **1999**, *62*, 81-87.
Perkin, S.; Chai, L.; Kampf, N.; Raviv, U.; Briscoe, W.; Dunlop, I.; Titmuss, S.; Seo, M.; Kumacheva, E.; Klein, J. *Langmuir* **2006**, *22*, 6142-6152.
Pincus, P. *Macromolecules* **1991**, *24*, 2912-2919.
Qiu, Y.; Park, K. *Adv Drug Deliver Rev* **2001**, *53*, 321-339.
Raphael, E.; Degennes, P. G. *J Phys Chem-Us* **1992**, *96*, 4002-4007.
Raviv, U.; Laurat, P.; Klein, J. *Nature* **2001**, *413*, 51-54.
Raviv, U.; Giasson, S.; Kampf, N.; Gohy, J. F.; Jerome, R.; Klein, J. *Langmuir* **2008**, *24*, 8678-8687.
Reichhart, C.; Czeslik, C. *Langmuir* **2009**, *25*, 1047-1053.
Retsch, M.; Walther, A.; Loos, K.; Muller, A. H. E. *Langmuir* **2008**, *24*, 9421-9429.
Rodriguez, F.; Givey, R. D. *J Polym Sci* **1961**, *55*, 713-&.
Roodenko, K.; Mikhaylova, Y.; Ionov, L.; Gensch, M.; Stamm, M.; Minko, S.; Schade, U.; Eichhorn, K. J.; Esser, N.; Hinrichs, K. *Appl Phys Lett* **2008**, *92*, -.
Rowe, M. A.; Hammer, B. A. G.; Boyes, S. G. *Macromolecules* **2008**, *41*, 4147-4157.
Rubinstein, M.; Dobrynin, A. V. *Curr Opin Colloid In* **1999**, *4*, 83-87.

Ruhe, J.; Ballauff, M.; Biesalski, M.; Dziezok, P.; Grohn, F.; Johannsmann, D.; Houbenov, N.; Hugenberg, N.; Konradi, R.; Minko, S.; Motornov, M.; Netz, R. R.; Schmidt, M.; Seidel, C.; Stamm, M.; Stephan, T.; Usov, D.; Zhang, H. N. *Polyelectrolytes with Defined Molecular Architecture I* **2004**, *165*, 79-150.
Sakasegawa, D.; Suzuki, A. *J Polym Sci Pol Phys* **2009**, *47*, 1778-1788.
Sanjuan, S.; Perrin, P.; Pantoustier, N.; Tran, Y. *Langmuir* **2007**, *23*, 5769-5778.
Sanjuan, S.; Tran, Y. *J Polym Sci Pol Chem* **2008**, *46*, 4305-4319.
Sanjuan, S.; Tran, Y. *Macromolecules* **2008**, *41*, 8721-8728.
Santos, R.; da Costa, G.; Franco, C.; Gomes-Alves, P.; Flammang, P.; Coelho, A. V. *Mar Biotechnol* **2009**, *11*, 686-698.
Seidel, C. *Macromolecules* **2003**, *36*, 2536-2543.
Sekine, T.; Nakamura, T.; Shimizu, Y.; Ueda, H.; Matsumoto, K.; Takimoto, Y.; Kiyotani, T. *J Biomed Mater Res* **2001**, *54*, 305-310.
Shibanuma, T.; Aoki, T.; Sanui, K.; Ogata, N.; Kikuchi, A.; Sakurai, Y.; Okano, T. *Macromolecules* **2000**, *33*, 444-450.
Shoichet, M. S. *Macromolecules* **2010**, *43*, 581-591.
Shull, K. R. *J. Chem. Phys.* **1991**, *94*, 5723-5738.
Shull, K. R.; Creton, C. *J Polym Sci Pol Phys* **2004**, *42*, 4023-4043.
Silberzan, P.; Leger, L.; Ausserre, D.; Benattar, J. J. *Langmuir* **1991**, *7*, 1647-1651.
Sivadasan, K.; Somasundaran, P.; Turro, N. J. *Colloid Polym Sci* **1991**, *269*, 131-137.
Skvortsov, A. M.; Gorbunov, A. A. *Vysokomolekulyarnye Soedineniya Seriya A* **1986**, *28*, 73-79.
Skvortsov, A. M.; Pavlushkov, I. V.; Gorbunov, A. A.; Zhulina, Y. B.; Borisov, O. V.; Pryamitsyn, V. A. *Vysokomolekulyarnye Soedineniya Seriya A* **1988**, *30*, 1615-1622.
Skvortsov, A. M.; Pavlushkov, I. V.; Gorbunov, A. A. *Vysokomolekulyarnye Soedineniya Seriya A* **1988**, *30*, 503-508.
Sokoloff, J. B. *J. Chem. Phys.* **2008**, *129*, -.
Sokoloff, J. B. *Soft Matter* **2010**, *6*, 3856-3862.
Sonnenberg, L.; Parvole, J.; Borisov, O.; Billon, L.; Gaub, H. E.; Seitz, M. *Macromolecules* **2006**, *39*, 281-288.
Soria, V.; Figueruelo, J. E.; Gomez, C. M.; Abad, C.; Campos, A. *Macromol Theor Simul* **2007**, *16*, 53-61.
Sotiropoulou, M.; Bokias, G.; Staikos, G. *Macromolecules* **2003**, *36*, 1349-1354.
Sotiropoulou, M.; Oberdisse, J.; Staikos, G. *Macromolecules* **2006**, *39*, 3065-3070.
Sotiropoulou, M.; Bossard, F.; Balnois, E.; Oberdisse, J.; Staikos, G. *Langmuir* **2007**, *23*, 11252-11258.
Staikos, G.; Bokias, G.; Karayanni, K. *Polym Int* **1996**, *41*, 345-350.
Takigawa, T.; Morino, Y.; Urayama, K.; Masuda, T. *Polym Gels Netw* **1996**, *4*, 1-5.
Tanaka, F.; Edwards, S. F. *Macromolecules* **1992**, *25*, 1516-1523.
Tareste, D.; Pincet, F.; Lebeau, L.; Perez, E. *Langmuir* **2007**, *23*, 3225-3229.
Taunton, H. J.; Toprakcioglu, C.; Fetters, L. J.; Klein, J. *Nature* **1988**, *332*, 712-714.
Taunton, H. J.; Toprakcioglu, C.; Fetters, L. J.; Klein, J. *Macromolecules* **1990**, *23*, 571-580.
Thomas, J. B.; Tingsanchali, J. H.; Rosales, A. M.; Creecy, C. M.; McGinity, J. W.; Peppas, N. A. *Polymer* **2007**, *48*, 5042-5048.
Thompson, M. T.; Berg, M. C.; Tobias, I. S.; Rubner, M. F.; Van Vliet, K. J. *Biomaterials* **2005**, *26*, 6836-6845.
Tokarev, I.; Motornov, M.; Minko, S. *J Mater Chem* **2009**, *19*, 6932-6948.
Tokarev, I.; Minko, S. *Soft Matter* **2009**, *5*, 511-524.
Toomey, R.; Tirrell, M. *Annu Rev Phys Chem* **2008**, *59*, 493-517.
Tran, Y.; Auroy, P. *J Am Chem Soc* **2001**, *123*, 3644-3654.

Treat, N. D.; Ayres, N.; Boyes, S. G.; Brittain, W. J. *Macromolecules* **2006**, *39*, 26-29.
Tsuchida, E.; Abe, K. *Advances in Polymer Science* **1982**, *45*, 1-119.
Tunc, M.; Cheng, X. H.; Ratner, B. D.; Meng, E.; Humayun, M. *Retina-J Ret Vit Dis* **2007**, *27*, 938-942.
Vajpayee, S.; Jagota, A.; Hui, C. Y. *J Adhesion* **2010**, *86*, 39-61.
Varenberg, M.; Gorb, S. *J R Soc Interface* **2008**, *5*, 383-385.
Vreeland, V.; Waite, J. H.; Epstein, L. *J Phycol* **1998**, *34*, 1-8.
Wallqvist, V.; Claesson, P. M.; Swerin, A.; Ostlund, C.; Schoelkopf, J.; Gane, P. A. C. *Langmuir* **2009**, *25*, 9197-9207.
Wang, Y. C.; Morawetz, H. *Macromolecules* **1989**, *22*, 164-167.
Wang, S. Q.; Zhu, Y. X. *Langmuir* **2009**, *25*, 13448-13455.
Wang, S. J.; Li, X. *Thin Solid Films* **2010**, *518*, 6036-6039.
Ward, L. J.; Badyal, J. P. S.; Goodwin, A. J.; Merlin, P. J. *Polymer* **2005**, *46*, 3986-3991.
Webber, R. E.; Shull, K. R.; Roos, A.; Creton, C. *Phys Rev E* **2003**, *68*, -.
Wittmer, J.; Joanny, J. F. *Macromolecules* **1993**, *26*, 2691-2697.
Wu, T.; Gong, P.; Szleifer, I.; Vlcek, P.; Subr, V.; Genzer, J. *Macromolecules* **2007**, *40*, 8756-8764.
Yim, H.; Kent, M. S.; Huber, D. L.; Satija, S.; Majewski, J.; Smith, G. S. *Macromolecules* **2003**, *36*, 5244-5251.
Zdyrko, B.; Klep, V.; Li, X. W.; Kang, Q.; Minko, S.; Wen, X. J.; Luzinov, I. *Mat Sci Eng C-Bio S* **2009**, *29*, 680-684.
Zhang, D.; Ortiz, C. *Macromolecules* **2004**, *37*, 4271-4282.
Zhang, Z.; Tomlinson, M. R.; Golestanian, R.; Geoghegan, M. *Nanotechnology* **2008**, *19*, 035505.
Zhang, J. L.; Han, Y. C. *Chem Soc Rev* **2010**, *39*, 676-693.
Zhu, X.; Yan, C.; Winnik, F. M.; Leckband, D. *Langmuir* **2007**, *23*, 162-169.
Zhulina, E. B.; Borisov, O. V.; Priamitsyn, V. A. *J Colloid Interf Sci* **1990**, *137*, 495-511.
Zhulina, E. B.; Borisov, O. V.; Brombacher, L. *Macromolecules* **1991**, *24*, 4679-4690.
Zhulina, E. B.; Borisov, O. V.; Birshtein, T. M. *J Phys Ii* **1992**, *2*, 63-74.
Zhulina, E. B.; Birshtein, T. M.; Borisov, O. V. *Macromolecules* **1995**, *28*, 1491-1499.
Zobell, C. E. *J Bacteriol* **1943**, *46*, 39-56.

EXTENDED ABSTRACT IN FRENCH – RÉSUMÉ SUBSTANTIEL EN FRANÇAIS

Les hydrogels réticulés chimiquement sont des réseaux de polymère hydrophile gonflés dans l'eau. Leur propriété de réservoir d'eau, leur élasticité et leur fragilité en font des matériaux qui ne sont pas naturellement collants. Cependant, en environnement marin, la patelle sécrète un adhésif non-permanent constitué d'un hydrogel naturel de polysaccharides et de protéines. En prenant la nature comme modèle, les hydrogels sont des matériaux de choix pour les applications pharmaceutiques et biotechnologiques. *In vivo*, ils sont utilisés en tant que mucoadhésifs pour leur capacité à relarguer graduellement un principe actif et leur propriété de barrière physique. Ils participent à la vectorisation de substance active ou à l'accélération des processus de soins de brûlures ou de plaies. Ils servent aussi dans la construction de tissus artificiels ou en tant qu'implants rétiniens…

Alors que les propriétés de gonflement ou les propriétés mécaniques des gels ont été largement étudiées, il apparaît que les phénomènes d'adhésion à l'interface entre un hydrogel et une surface sont bien moins compris. Le plus souvent, ce problème est résolu de façon empirique. Le développement d'une méthode macroscopique fiable qui donnerait des résultats quantitatifs de l'adhésion immergée est indispensable à la compréhension des interactions spécifiques de surface dans le cadre de problèmes de bioadhésion.

L'objectif de l'étude est la création d'une adhésion réversible et stimulable qui ouvrirait le champ à de nombreuses applications, tout en déterminant les paramètres des interactions à la surface d'hydrogels. Notre approche est basée sur l'utilisation d'un système modèle dans lequel l'association par liaisons hydrogènes est stimulable. Ces interactions peuvent se produire entre le gel et un substrat couvert par une brosse de polymère sensible au pH, comme suggéré Figure 3.

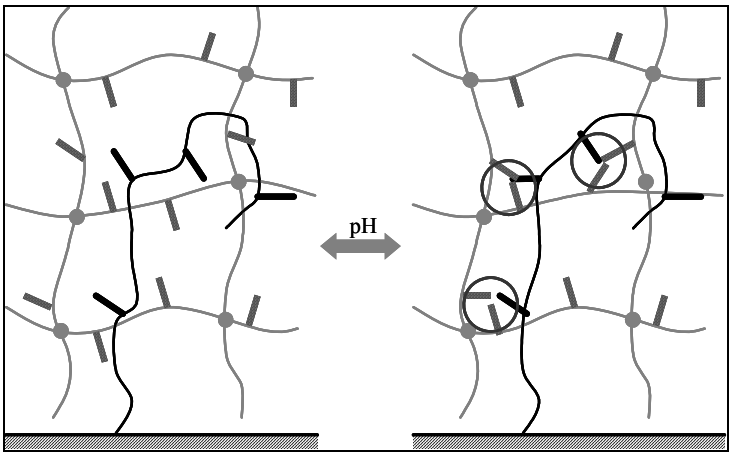

Figure 3 - Schéma de la formation de liaisons spécifiques entre un hydrogel et une brose de polymère.

Des hydrogels neutres de poly(*N,N*-diméthylacrylamide) (PDMA) et de poly(acrylamide) (PAM) ont été élaborés et leurs propriétés viscoélastiques et de gonflement ont été étudiées. En parallèle, des brosses de polyélectrolyte faible stimulables *via* le pH, le poly(acide acrylique) (PAA), ont été synthétisées en adoptant la méthode de « grafting to ». Les interactions entre le PAA, donneur de proton, et les poly(acrylamides) ont été étudiées en solution par une méthode de turbidimétrie, permettant de déterminer les paramètres qui jouent un rôle sur la complexation. Finalement, les propriétés d'adhésion entre la brosse de polymère et l'hydrogel sont caractérisées par une nouvelle méthode de contact plan-plan immergée qui permet de modifier *in situ* les caractéristiques de la solution aqueuse (pH, force ionique, température).

1- Matériaux

1-1- Brosses de poly(acide acrylique)

Synthèse

Des monocouches auto-assemblées (SAM) ont été synthétisées pour diverses applications, comme la synthèse des échantillons de gel pour les tests d'adhésion. Des SAM ont aussi été synthétisées comme précurseur pour les brosses de polymères.

Des brosses de PAA ont été synthétisées par la méthode de « grafting to » comme présenté Figure 4. La première étape consiste à greffer une SAM de γ-glycidoxypropyl-trimethoxysilane. Ensuite, un film de poly(*tert*-butylacrylate) (PtBuA) terminé acide carboxylique est déposé sur la surface fonctionnalisée époxyde. Le greffage est assuré par chauffage à 120°C sous vide (au-dessus de la température de transition vitreuse du PtBuA, au-dessus de la température d'activation de la réaction de l'acide carboxylique sur l'époxyde, mais en dessous de la température de dégradation du PtBuA). Afin de passiver la surface, un deuxième greffage d'oligomères, ou chaînes courtes de PtBuA est greffé par la même méthode. Pour finir, la brosse (bimodale) de PtBuA est le plus souvent convertie en brosse de PAA *in situ* par pyrolyse à 200°C sous vide suivie d'une hydrolyse douce dans l'eau à pH 2. Chaque étape de la synthèse de la brosse a été caractérisée par ellipsométrie, spectroscopie infrarouge par réflexion totale atténuée, et par réflectivité de neutrons.

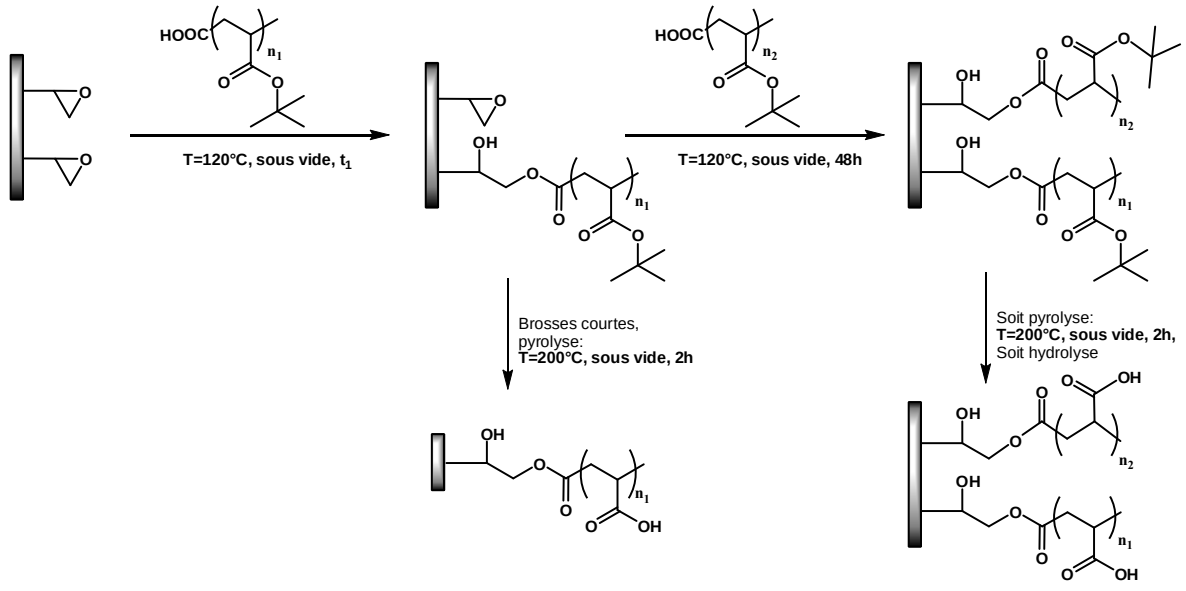

Figure 4 - Formation de brosses de poly(acide acrylique) par la méthode de "grafting to".

Structure

La structure de ces systèmes bimodaux a été caractérisée par réflectivité de neutrons. Cette dernière donne accès, grâce au contraste neutronique entre l'hydrogène de la brosse et le deutérium de l'eau (lourde) environnante, au profil de concentration en monomère dans la direction normale au substrat. L'étirement des brosses de PAA a été caractérisé par la mesure du taux de gonflement, c'est-à-dire le rapport de l'épaisseur moyenne de la brosse gonflée L sur l'épaisseur moyenne à sec γ. Comme le PAA est un polyacide faible, son taux de gonflement L/γ, qui dépend toujours de la densité de greffage σ, dépend aussi du pH ; en effet, en milieu acide, la brosse est hydrogénée et neutre alors qu'à pH basique, la brosse est ionisée et additionnellement étirée par des effets électrostatiques. Des mesures ont été effectuées à deux pH différents, à pH 2 et à pH 9. Les résultats expérimentaux donnent des taux de gonflement toujours supérieurs à 2 qui sont en bon accord avec les lois d'échelles.

A pH 9 quand la brosse est chargée, elle adopte la conformation d'une brosse de polyélectrolyte fort et son profil est Gaussien. A pH 2 lorsque le PAA est non-ionisé, la brosse est en bon solvant, moins étirée et elle adopte un profil de type « tangente hyperbolique » (voir Figure 5-gauche).

A très forte densité de greffage, le gonflement des brosses neutres et chargées en bon solvant est équivalent, conformément aux prédictions théoriques (voir Figure 5-droite). Par ailleurs, pour les densités de greffage de chaînes longues les plus faibles, la forme bimodale du profil a été clairement mise en évidence et les profils ont été déconvolués avec succès pour extrapoler le gonflement associé à chaque longueur de chaîne.

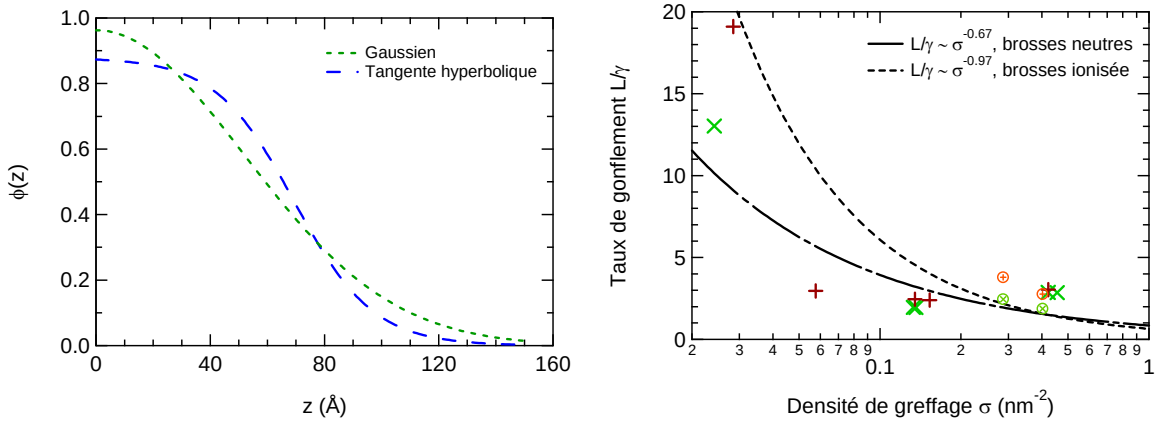

Figure 5 - Gauche : profiles types pour des brosses de polymères ionisés (Gaussien) et neutres (Tangente hyperbolique) en bon solvent.

Droite : taux de gonflement de brosses de PAA (×) neutres à pH 2, et (+) ionisées à pH 9. Aux fortes densités de greffage, les résultats sont obtenus avec des chaînes courtes. Les deux lois d'échelle sont extrapolées de résultats multiples de la littérature. Des résultats obtenus avec des brosses de PMAA par Sanjuan *et al.* à pH 2 (⊗) et pH 9 (⊕) ont été ajoutés.

1-2- Hydrogels neutres de poly(*N,N*-diméthylacrylamide) et de poly(acrylamide)

Synthèse et gonflement

Des hydrogels de PDMA et de PAM ont été synthétisés à température ambiante. On mélange dans l'eau le monomère principal (*N,N*-diméthylacrylamide (DMA) ou acrylamide (AM)), le méthylène-bis-acrylamide (MBA, réticulant) et le persulfate de potassium (KPS, initiateur). Pour les gels de PDMA, on initie la réaction en ajoutant le co-amorceur N,N,N',N'-tétraméthyléthylènediamine (TEMED) sous forte agitation dans un environnement exempt d'oxygène. Le milieu réactionnel est versé dans un moule (traité hydrophobe) pendant 4 heures. Pour les gels de PAM, le milieu réactionnel désoxygéné est placé dans le moule (traité hydrophobe) sous atmosphère d'azote et chauffé à 40°C pendant 4 heures.

Le gel est ensuite retiré du moule et immergé dans l'eau pure. Post-synthèse, les analyses d'extractibles n'ont pas montré la présence de monomère résiduel et la fraction de sol n'était en général pas mesurable. L'influence des concentrations en monomère (m:w) et réticulant (x:m)[i] sur les propriétés de gonflement, sur les propriétés viscoélastiques et sur la structure des gels ont été étudiées.

L'étude des propriétés gonflement des hydrogels de PDMA a permis d'analyser les effets distincts des concentrations en monomère et en réticulant à la synthèse. Plus le gel est réticulé ou plus il est concentré en monomère, et plus son gonflement à l'équilibre Q_e est faible, comme montré sur la Figure 6-gauche. Dans les cas les plus réticulés, le gonflement à l'équilibre est plus faible que le gonflement à la synthèse Q_0. Cette étude permet de montrer que quelque soit la concentration initiale en monomère, il est possible de trouver un taux de réticulation qui permette au gel d'être synthétisé à l'équilibre de gonflement. Ce résultat, présenté simplement sur l'abaque de la Figure 7-droite est essentiel pour les propriétés d'adhésion : en effet, les tests d'adhésion sont menés sur des gels collés sur substrat et dont l'attachement ne peut être garanti que par une bonne stabilité dimensionnelle du gel.

[i] Les concentrations en monomère (m:w) et réticulant (x:m) ont été repérés par les rapports massique $(m:w) = m_{mono} / \left(m_{eau} + m_{mono}\right)$ et molaire $(x:m) = \left[MBA\right] / \left[mono\right]$, respectivement. Les gels sont repérés par un nom du type POL(m:x)x(x:m), où POL correspond à l'abréviation du polymère, PDMA ou PAM.

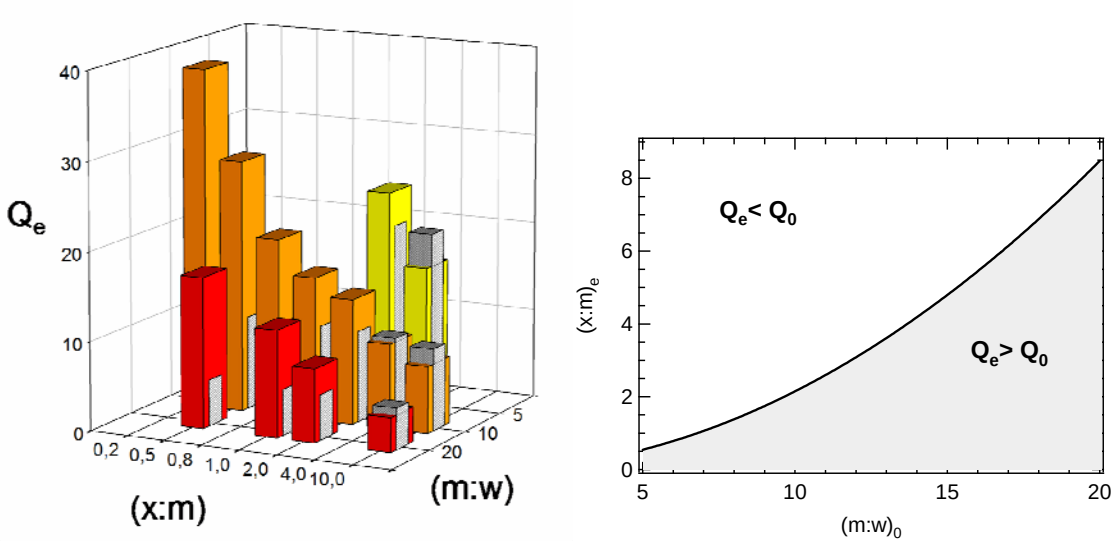

Figure 6 - Gauche : Gonflement de gels de PDMA à l'équilibre Q_e (en couleur) et à la synthèse Q_0 (gris central) en fonction des concentrations initiales en monomère et en réticulant.

Droite : Abaque permettant de déterminer, étant donnée les conditions de synthèse, si le gel sera plus ou moins gonflé à l'équilibre qu'à la synthèse.

Propriétés mécaniques

Une étude de rhéologie a clairement confirmé le caractère très élastique des hydrogels synthétisés. En effet, les modules visqueux obtenus en rhéologie sont toujours au moins un ordre de grandeur inférieurs aux modules élastiques (voir Figure 7-droite). Cette forte élasticité a été confirmée par des tests de compression dont les courbes de compression et décompression étaient très peu hystérétiques. Les mêmes variations ont été observées, c'est-à-dire que le module élastique augmente à la fois avec la concentration en monomère et avec la concentration en réticulant.

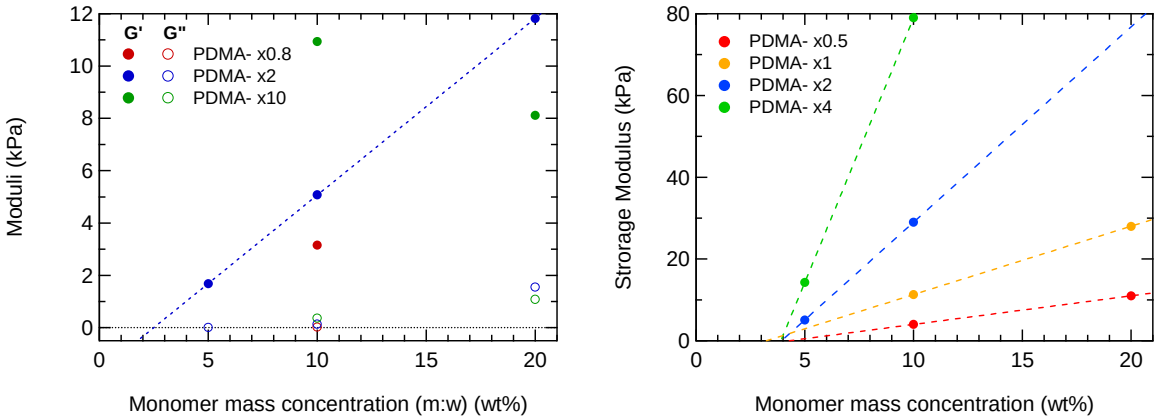

Figure 7 - Modules élastiques (●) et visqueux (○) en fonction de la concentration initiale en monomère pour des hydrogels de PDMA à différentes densité de réticulation. Les résultats sont obtenus par des mesures rhéologiques (gauche) et par des tests de compression (droite).

Cependant, de grandes différences de modules ont été observées entre les deux méthodes. Ceci peut s'expliquer par une hétérogénéité de concentration du gel entre sa masse et sa surface.

Structure et surface de gels

L'analyse de la structure des hydrogels de PDMA et PAM a été approfondie par une étude de diffusion de neutrons aux petits angles qui a révélé que la taille du blob thermique du PAM est environ deux fois plus petite que celle du PDMA et que les gels présentaient des hétérogénéités d'une taille de l'ordre de 100 Å.

Pour les tests d'adhésion, les hydrogels de PDMA ont été réalisés entre deux plaques de verre. La plaque 1 a été traitée avec un silane qui peut se lier de façon covalente à l'hydrogel au cours de la polymérisation car il porte une double liaison : le 3-methacryloxypropyl-dimethylchlorosilane. La plaque 2 a été traitée avec des silanes plus ou moins hydrophobes : soit l'octadécyltrichlorosilane (OTS), soit l'hexaméthyldisilazane (HMDZ), soit le 1H,1H,2H,2H-perfluorodecyltrichlorosilane (FTS). Celle-ci peut être retirée aisément alors que le gel est collé à la plaque 1.

Suite aux différences de propriétés mécaniques observées entre les tests de compression et la rhéologie, nous avons cherché à mesurer la concentration des hydrogels en surface. Cette analyse fine a été réalisée par réflectivité de neutrons et a mis en évidence l'effet de la nature du moule de synthèse du gel sur la concentration de surface des hydrogels. Plus le moule est hydrophobe et plus la différence de concentration en PDMA entre la masse du gel et sa surface est importante. La plus petite différence a été obtenue en utilisant des moules silanisés par phase vapeur avec le HMDZ. Néanmoins, sous compression, la concentration de surface devient quasi identique à celle en masse, ce qui correspond au cas des tests d'adhésion.

2- Complexes interpolymères en solution et aux interfaces

2-1- Complexation en solution

Polymères et méthodes

Afin de déterminer le type d'interactions impliquées dans les complexes PAA-PAM et PAA-PDMA et pour caractériser les paramètres expérimentaux qui influencent la complexation, l'association du PAA avec les homopolymères et les copolymères statistiques de l'acrylamide

(AM) et du *N,N*-diméthylacrylamide (DMA) a été étudiée en solution par une méthode de turbidimétrie. Le PAA mis à part, les homo- et co-polymères ont été synthétisés au laboratoire par des polymérisations radicalaires ; le PDMA et les copolymères ont été obtenus avec les masses molaires de 30 $kg.mol^{-1}$ et de 130 $kg.mol^{-1}$ pour le PAM. Les indices de polymolécularité sont de l'ordre de 2. Ces polymères « maison » ont été dissous à 0.25 % m/m dans une solution de PAA à la même concentration. Des diagrammes de phase pH-température ont été mesurés sur des solutions en ajustant le pH (NaOH ou HCl, 1 M) et en faisant varier la température.

Influence de l'accepteur de proton

Entre le PAA donneur de proton et le PAM accepteur de proton, des complexes ont été observés pour des pH inférieurs à 3.3 (*cf.* Figure 8-gauche) et ils se sont révélés sensibles à la température sur une gamme de pH de 1.8 à 3.3. Dans cette gamme de pH, leur transition de solubilité suit un comportement de type UCST, c'est-à-dire que la complexation faiblit à mesure que la température augmente.

Avec le PDMA, le PAA forme des complexes pour des pH inférieurs à 3.75, et pour la gamme de pH comprise entre 3.45 et 3.75, une transition de solubilité de type LCST a été observée sur une gamme de température comprise entre 0 et 60°C. La capacité du PDMA à se complexer avec le PAA est plus grande que pour le PAM, puisque ce dernier ne se complexe qu'à un pH plus faible, en présence de davantage de liaisons H possibles. Par ailleurs, la transition de type LCST suggère que les associations par liaisons H sont fortement renforcées par des effets hydrophobes.

Les résultats obtenus avec les copolymères statistiques[ii] sont intermédiaires à ceux des homopolymères : à une température donnée, la transition de solubilité peut être ajustée entre celle des deux homopolymères en jouant sur la composition du copolymère. Lorsque le copolymère statistique contient 66 mol% de DMA, la stabilité du complexe formé ne dépend plus de la température, la composante LCST de l'association du PDMA compensant exactement la composante UCST du PAM.

[ii] Les copolymères sont nommés $CopAM_x$ où x représente leur pourcentage molaire d'acrylamide dans la chaîne déterminé par RMN du proton.

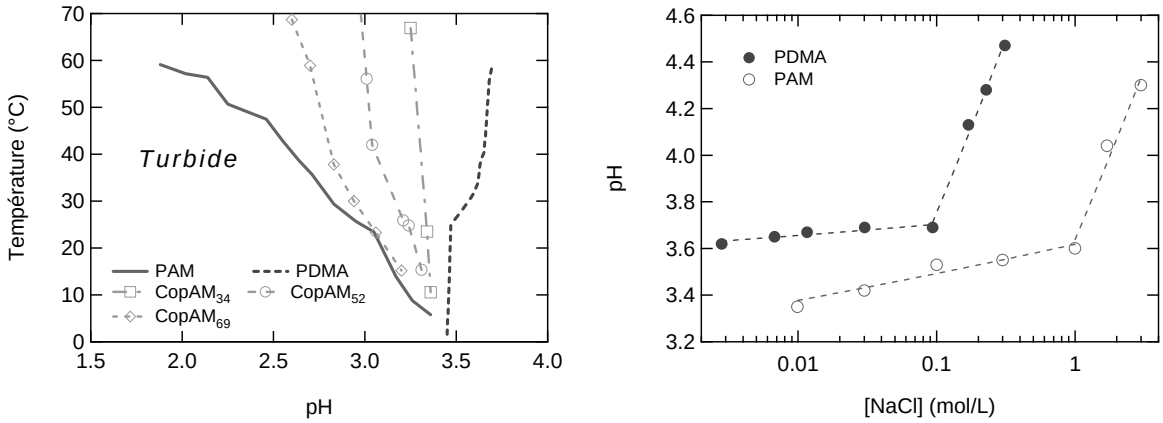

Figure 8 - Gauche : Diagramme de phase pH-température de couples de polymères de PAA et de copolymères d'acrylamide et de N,N-diméthylacrylamide à 0.25 wt% chacun en solution aqueuse. A pH élevé, le système est monophasique.

Droite : Influence de la force ionique sur le pH de transition à temperature ambiante pour les couples d'homopolymères PAA-PDMA et PAA-PAM à 0.25 wt% chacun en solution aqueuse. A force ionique élevée, le système est biphasique.

Influence de la force ionique

L'influence de la force ionique a été étudiée sur la complexation des deux couples d'homopolymères (*cf.* Figure 8-droite) par la mesure de la variation du pH de transition à l'ambiante. Dans les deux cas, l'effet de la concentration en chlorure de sodium présente deux tendances. A faible concentration en sel, le pH de transition dépend peu de la force ionique, ce qui peut être expliqué par une augmentation de l'écrantage des charges portées par le PAA qui adopte une conformation plus favorable à l'association. Au-delà d'une concentration critique, la force ionique joue un rôle majeur sur la complexation, puisque le pH de transition augmente d'une unité, probablement à cause de la détérioration de la qualité thermodynamique du solvant.

2-2- Complexation aux interfaces

L'observation des interactions à l'interface entre la brosse de PAA et les gels de PDMA et de PAM a été effectuée par une méthode à l'échelle de la brosse : nous avons mesuré le profil de densité de concentration du polymère dans la brosse par réflectivité de neutrons. Après avoir démontré qu'un gel hydrogéné gonflé dans l'eau lourde n'altérait pas la mesure du profil de la brosse de PAA, nous avons pu déterminer l'effet sur la conformation des chaînes de la brosse de l'adsorption d'un hydrogel. A pH élevé, en l'absence d'interactions spécifiques entre la brosse et le gel, la structure de la brosse est identique qu'elle soit gonflée dans l'eau ou dans

le gel. Au contraire, à pH faible et en présence d'interactions, la brosse est plus gonflée en présence du gel que dans l'eau. Cet étirement additionnel de la brosse, dû aux interactions spécifiques avec le gel, peut excéder le gonflement observé pour la même brosse à pH 9, démontrant ainsi que les interactions spécifiques étirent la chaîne similairement à la répulsion électrostatique au sein du polyélectrolyte faible. Cet effet peut s'expliquer par l'interpénétration de la brosse au sein du gel, comme représenté sur la Figure 9.

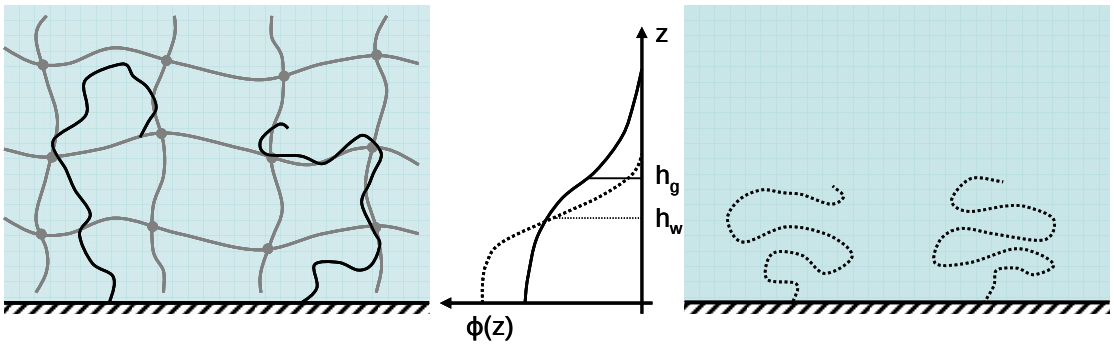

Figure 9 - Représentation schématique de l'effet de la presence du gel (PDMA ou PAM) sur la conformation des brosses de PAA en presence d'interactions spécifiques : la brosse est plus étirée.

3- Adhésion immergée

3-1- Méthode

Il existe plusieurs méthodes pour évaluer ou mesurer l'adhésion entre deux matériaux. Le test de contact plan-plan semble bien adapté pour caractériser l'adhésion de nos systèmes. En effet cette méthode permet de contrôler l'aire de contact, le temps de contact et la vitesse de décollement, tout en étant réalisable immergée (voir Figure 10). Les atouts majeurs du système que nous avons développé sont de s'affranchir des effets de tension de surface toujours présents pour des matériaux gonflés, tout en donnant la possibilité de modifier les conditions expérimentales *in situ* et en menant des observations du contact latérale et par en-dessous.

L'hydrogel d'un millimètre d'épaisseur est attaché sur un substrat de quartz. Le substrat de silicium (1 cm^2) fonctionnalisé par la brosse de PAA est collé à un poinçon plan. Il est amené à la surface du gel où une force de contact est appliquée pendant une durée prédéterminée. Puis le poinçon est retiré de la couche de gel à vitesse constante.

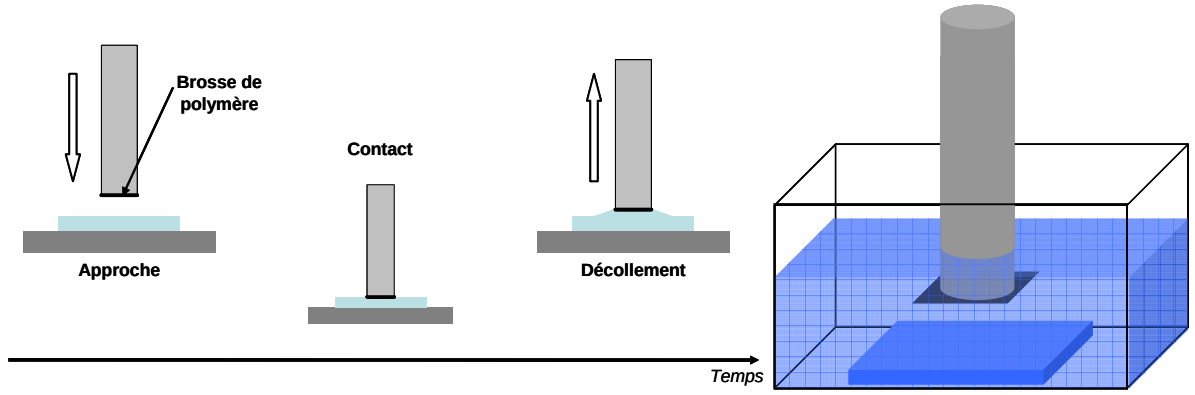

Figure 10 - Représentation schématique du test de contact plan-plan, de profil où le déroulement du test est détaillé (gauche), et en perspective (droite).

La force appliquée est mesurée pendant l'expérience et pour une géométrie plan-plan, les courbes typiques obtenues sont dessinées sur la Figure 11-gauche. Une mesure est effectuée immergée, l'autre dans l'air. Le pic d'adhésion dans l'air est bien plus fort, à cause des effets de tension de surface qui s'ajoutent lors de la séparation des deux surfaces. Dans l'eau, le pic d'adhésion mesuré n'est attribuable qu'aux forces d'interactions spécifiques. L'énergie d'adhésion est mesurée à partir de ce pic. Nous avons montré que la détermination des conditions expérimentales – que sont le temps de contact, la contrainte de contact et la vitesse de détachement – permettant d'effectuer des mesures quantitatives significatives était essentielle.

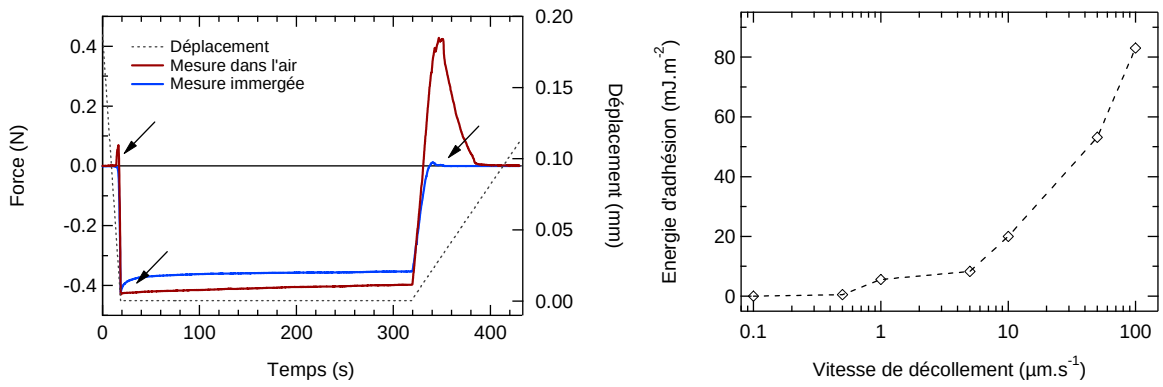

Figure 11 - Gauche : Force et déplacement mesurés en fonction du temps. Approche : le poinçon entre en contact avec le gel et le comprime. Puis le poinçon est immobilisé et le gel relaxe. Décollement : le gel restitue l'énergie de compression, puis l'adhésion est à l'origine du pic observé par la suite. Pour finir, le poinçon retourne à une force nulle.

Droite : Effet de la vitesse de décollement sur l'énergie d'adhésion.

Le temps de contact doit être de l'ordre d'au moins 100 s, durée en deçà de laquelle les interactions ne sont pas formées. La contrainte de contact doit être raisonnable pour éviter les

effets de cisaillement à l'interface entre le gel et la brosse. La vitesse de contact doit être suffisamment faible de façon à limiter les artéfacts, notamment dus aux dissipations visqueuses dans le gel et dans l'eau, et suffisamment élevée pour donner des valeurs mesurables (*cf.* Figure 11-droite). Par ailleurs, un angle de contact non nul a été employé pour faciliter l'évacuation du solvant lors de l'approche.

3-2- Résultats et discussion

Des mesures d'adhésion systématiques ont été effectuées entre les gels de PDMA et de PAM et les brosses de PAA. La réversibilité de l'adhésion en fonction du pH a été démontrée : à pH élevé, l'adhésion entre la brosse de PAA et les gels est nulle. A pH faibles, les valeurs obtenues sont de l'ordre d'énergies d'adhésion thermodynamiques. Sur les gels de PDMA, on atteint des valeurs de l'ordre de 10 $mJ.m^{-2}$ alors que l'adhésion des brosses de PAA sur les gels de PAM sont de l'ordre de 100 $mJ.m^{-2}$. Par ailleurs, les transitions de pH entre adhésion et absence d'adhésion sont plus éloignées que les transitions observées en solution, observées autour de pH 3.5.

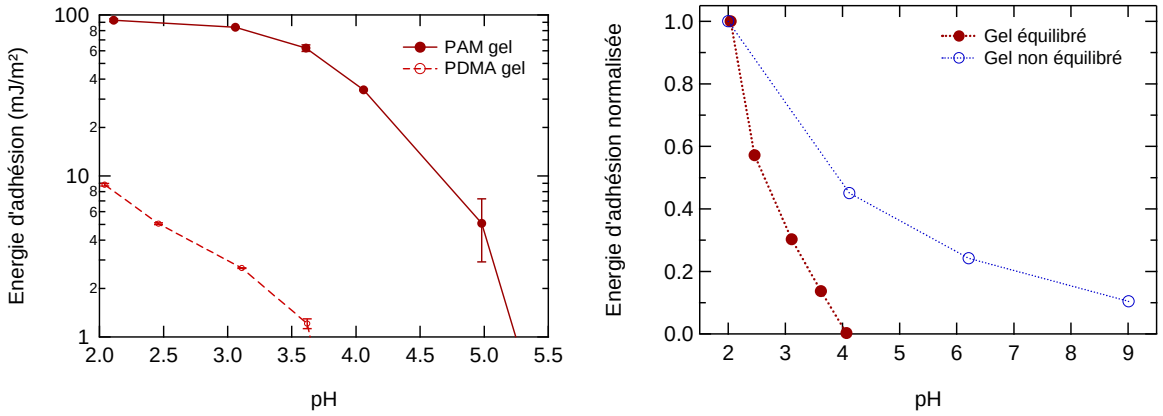

Figure 12 - Gauche : Energie d'adhésion entre un gel de PDMA ou un gel de PAM et une brose de PAA en function du pH.

Droite : Energie d'adhésion normalisée entre un gel équilibré 24 h dans la solution de test (●) et équilibré 5 min dans la solution de test (○).

Qualitativement, l'adhésion mesurée diminue avec le pH mais quantitativement, même si l'on reste sur des ordres de grandeur d'adhésion thermodynamique, la différence de magnitude observée entre des gels de PDMA et de PAM reste difficile à expliquer. Les effets cruciaux des paramètres de l'expérience, que sont le temps de contact, la vitesse de détachement ou le

temps d'équilibration du gel à un pH donné, ont été étudiés. Il a été montré qu'ils donnent accès aux cinétiques d'association et de réorganisation des complexes interfaciaux, à leur temps de vie ainsi qu'aux propriétés de diffusion du pH dans le gel. Les temps caractéristiques de diffusion dans le gel et de réorganisation des complexes sont plutôt longs, de l'ordre de la dizaine de minutes à l'heure alors que les temps de vie des liaisons sont plutôt courts. Enfin, une comparaison avec les interactions électrostatiques a été menée et a permis de montrer qu'elles renforcent de façon considérable l'adhésion par rapport aux liaisons hydrogènes.

Résumé : L'adhésion stimulable d'un hydrogel sur une surface a été étudiée de façon systématique par le jeu d'interactions spécifiques réversibles entre polymères. A cette fin, des surfaces modèles de brosses de poly(acide acrylique) (PAA) ont été obtenues par « grafting to » et leur structure, sensible au pH, a été caractérisée par réflectivité de neutrons. Parallèlement, des hydrogels neutres de poly(*N,N*-diméthylacrylamide) (PDMA) et de poly(acrylamide) (PAM) ont été synthétisés par polymérisation radicalaire conventionnelle ; leurs propriétés mécaniques, leur structure et leur gonflement ont été étudiés et variés au moyen de deux paramètres : le gonflement initial et le taux de réticulant.

En solution aqueuse, les couples de polymères PAA et PDMA ou PAA et PAM forment des complexes inter polymères dont l'apparition dépend du pH et de la température. Les associations se produisent à pH faible dans les deux cas ; et quoique relativement similaire d'un point de vue chimique, ces couples de polymères s'associent par une séparation de phase de type UCST lorsque l'accepteur de proton est le PAM, mais par une transition de type LCST avec le PDMA.

La formation de ces complexes en solution a aussi été étudiée aux interfaces entre la brosse de PAA et les hydrogels de PDMA et PAM. Une étude à l'échelle de la brosse a été menée par réflectivité de neutrons : en présence de gel, un gonflement additionnel de la brosse est observé en présence des interactions à faible pH alors que sa structure n'est pas perturbée à pH élevé. L'étude macroscopique de ces interactions aux interfaces correspond aux tests d'adhésion : un montage expérimental et des protocoles adaptés à la mesure quantitative de l'énergie d'adhésion entre matériaux immergés. Au moyen d'un contact plan-plan entre les brosses de PAA et les gels de PDMA et PAM attachés de façon covalente sur des substrats, une adhésion immergée stimulable par le pH de l'ordre de grandeur des adhésions thermodynamiques a été mise en évidence, de même que les cinétiques relativement lentes impliquées dans la formation et la rupture des complexes aux interfaces.

Mots clefs : adhésion réversible, brosses de polymère, hydrogels neutres, complexes inter polymères, interactions faibles, réflectivité de neutrons.

Abstract: The tunable adhesion of hydrogels on surfaces has systematically been studied by using specific and reversible polymer-polymer interactions. To this end, model surfaces of poly(acrylic acid) (PAA) brushes were obtained by "grafting to" and their structure, which is pH-sensitive, was characterized by neutron reflectivity. Meanwhile, neutral hydrogels of poly(*N,N*-dimethylacrylamide) (PDMA) and poly(acrylamide) (PAM) were synthesized by conventional radical polymerization, and their mechanical properties, their structure and their swelling were studied and varied by the means of two parameters: the initial swelling and the cross-linking density.

In aqueous solution, the polymeric pairs of PAA and PDMA or PAA and PAM form interpolymer complexes. Their formation depends on pH and temperature and was studied by turbidimetry. Associations occur at low pH in both cases, and even if the two polymeric pairs are chemically similar, their complexations correspond to a standard UCST-type phase transition when the the proton acceptor is PAM but to an LCST-type transition with PDMA.

The formation of these complexes in solution was also studied at the interfaces between the PAA brush and the PDMA and PAM hydrogels. The swelling behavior of the brush was investigated by neutron reflectivity: in the presence of the gel, the brush is additionally stretched in the presence of interactions at low pH and its structure remains unperturbed at high pH. A macroscopic study of these interactions at interfaces was carried out by the development of an experimental setup and protocols suitable for the quantitative measurement of the adhesion energy between immersed materials. Using a flat-flat contact test between the PAA brushes and PDMA and PAM gels covalently attached to substrates, an immersed and pH-tunable adhesion of the magnitude of thermodynamic adhesions has been demonstrated as well as the relatively slow kinetics involved in the formation and rupture of the interpolymer complexes at interfaces.

Keywords: reversible adhesion, polymer brushes, neutral hydrogels, interpolymer complexes, weak interactions, neutron reflectivity.